VERLAG DER TECHNISCHEN UNIVERSITÄT GRAZ

Mario Gobrial

Space-time Finite Element Methods for the Eddy Current Problem and Applications

CES 46

MONOGRAPHIC SERIES TU GRAZ
COMPUTATION IN ENGINEERING AND SCIENCE

Mario Gobrial

Space-time Finite Element Methods for the Eddy Current Problem and Applications

Monographic Series TU Graz
Computation in Engineering and Science

Series Edotors

Monographic Series TU Graz
Computation in Engineering and Science

Mario Gobrial

Space-time Finite Element Methods for the Eddy Current Problem and Applications

---

This work is based on the dissertation
“Space-time Finite Element Methods for the Eddy Current Problem and Applications”, presented at Graz University of Technology, Institute of Applied Mathematics in 2025.

Supervision / Assessment:

Olaf Steinbach (Graz University of Technology)
Ulrich Langer (Johannes Kepler Universität Linz)

Cover	Verlag der Technischen Universität Graz
Cover photo	Vier-Spezies-Rechenmaschine
	by courtesy of the Gottfried Wilhelm Leibniz Bibliothek
	Niedersächsische Landesbibliothek Hannover
Printed by	Buchschmiede (DATAFORM Media GmbH)

2025 Verlag der Technischen Universität Graz

www.tugraz-verlag.at

Print
ISBN 978-3-99161-048-9

E-Book
ISBN 978-3-99161-049-6
DOI 10.3217/978-3-99161-048-9

Abstract

We formulate and analyze space-time finite element methods for the numerical simulation of the eddy current approximation in Bochner spaces, derived from Maxwell's equations in the low-frequency regime. First, we examine the resulting elliptic-parabolic interface problem posed on electrically conducting and non-conducting stationary regions, providing the analysis of the unique solvability based on the Babuška-Nečas theory for the linear case and on Zarantonello's theorem as well as the principle of maximal monotone mappings for the nonlinear case. Furthermore, we address hysteresis effects in ferromagnetic materials by proposing a space-time finite element method tailored to a specific hysteretic material law. The investigation extends to moving bodies, analyzing the corresponding elliptic-parabolic interface problem for both the linear and nonlinear case based on the previously established theoretical frameworks.

The Petrov-Galerkin space-time finite element discretization is formulated on completely unstructured decompositions of the space-time cylinder into simplicial elements, which allows for an adaptive resolution of the solution both in space and time. However, it requires the solution of the overall system of algebraic equations. While the use of parallel solution algorithms seems to be mandatory, this method also allows for a parallelization in space and time simultaneously. The numerical experiments confirm related a priori error estimates and demonstrate the applicability and accuracy of the proposed approach applied to realistic problems, including the simulation of electric motors.

Zusammenfassung

Wir formulieren und analysieren Raum-Zeit Finite Elemente Methoden in Bochner-Räumen zur numerischen Simulation des Wirbelstromproblems, das sich von den Maxwell-Gleichungen im Niederfrequenzbereich ableiten lässt. Zunächst untersuchen wir das resultierende elliptisch-parabolische Transmissionsproblem, das auf elektrisch leitenden und nichtleitenden stationären Geometrien definiert wird. Für den linearen Fall beruht die Analyse der eindeutigen Lösbarkeit auf der Babuška-Nečas-Theorie, während wir für den nichtlinearen Fall den Satz von Zarantonello sowie das Prinzip maximal monotoner Abbildungen heranziehen. Darüber hinaus behandeln wir Hystereseeffekte in ferromagnetischen Materialien, wofür wir eine Raum-Zeit Finite Elemente Methode für ein bestimmtes hysteretisches Materialgesetz betrachten. Die Untersuchung wird auf bewegte Körper ausgeweitet, indem das entsprechende elliptisch-parabolische Transmissionsproblem, sowohl für den linearen als auch den nichtlinearen Fall, im Rahmen der zuvor betrachteten Theorie analysiert wird.

Die Petrov-Galerkin Raum-Zeit Finite Elemente Diskretisierung wird auf vollständig unstrukturierten Gittern des Raum-Zeit-Zylinders formuliert. Dies ermöglicht eine adaptive Auflösung der Lösung sowohl im Raum als auch in der Zeit. Allerdings erfordert diese Methode die Lösung eines Gesamtsystems von algebraischen Gleichungen. Während der Einsatz paralleler Lösungsalgorithmen als unausweichlich erscheint, erlaubt diese Methode auch eine Parallelisierung gleichzeitig in Raum und Zeit. Numerische Experimente bestätigen die zugehörigen a-priori Fehlerabschätzungen und zeigen die Anwendbarkeit sowie die Genauigkeit der Raum-Zeit Finite Elemente Methode, insbesondere an realistischen Problemen wie der Simulation von Elektromotoren.

Acknowledgments

I would like to express my deepest gratitude to my supervisor, Prof. Olaf Steinbach, for the guidance, support, and encouragement throughout this journey. His expertise and constructive feedback have been instrumental in shaping this work.

I am profoundly thankful to my family for their unwavering support and belief in me. Their encouragement has been a source of strength during the most challenging moments of this journey. Without them, I would not have come so far.

A special thank goes to my wife, Magdalena, whose patience, understanding, and sacrifices have been extraordinary. Her resilience and support, especially during the times I had to travel weekly to another town for university, made this achievement possible. Words cannot fully capture my appreciation for her love and unwavering belief in me.

This thesis would not have been possible without the contributions, and encouragement of those around me, especially my colleagues Christian, Günther, Michael and Richard. I deeply appreciated the fruitful and lengthy discussions we shared, which enriched my understanding.

I would also like to express my sincere gratitude to Uwe Iben and Markus Kraft for giving me the opportunity visiting the Bosch GmbH Research Campus in Renningen and for facilitating me a five-month stay there. The highly productive collaboration with Daniel, Iryna and Stefan greatly enriched my research experience.

Contents

1 Introduction

Almost every natural phenomena inside or even outside our planet can be described by mathematical models in form of differential equations. Their physical processes exhibit dependency across spatial and/or temporal dimensions, which can be expressed by ordinary (ODEs) or partial differential equations (PDEs). Our main focus is on solving time-dependent PDEs. Usually, such problems cannot be solved analytically, therefore we need appropriate discretization methods in order to accurately approximate the analytical solutions. The most common strategies to solve time-dependent PDEs numerically are the *method of lines* [136] and *Rothe's method* [128, 94]. The former first applies discretization in space, e.g. by the popular finite element method (FEM), see for instance [22, 24, 31, 44], and then solves the resulting semi-discretized system using time-stepping methods [38, 149]. *Rothe's method* applies those semi-discretization steps the other way round, i.e. first a time-stepping method in time, then the discretization in space. In any case, both strategies result in a series of linear systems that need to be solved efficiently. The question about efficient solvers gained a lot of interest over the last decades, for which parallel solution methods have been developed in order to solve huge linear systems divided on multiple processors, see e.g. [141, 13]. Since classical time-stepping methods suffer from the curse of sequentiality, different possibilities to employ parallelization also in time direction, so-called parallel-in-time (PinT) methods, have been investigated. We refer to the work of Gander [55] for a detailed overview of PinT methods.

However, in this thesis we will employ the idea of treating the time variable t like an additional space variable, i.e. $x_{d+1} = t$, and to construct a single $(d+1)$-dimensional space-time mesh when the spatial domain is in $\mathbb{R}^d$. This idea dates back to the late 1960s initiated by Argyris and Scharf [8], who treated the time in a variational sense. Since then, the development of space-time methods has made great progress. We refer to the paper of Steinbach and Yang [147], that gives a detailed overview of the state-of-the-art. The application of space-time methods involves many advantages, among others the parallelization [56, 134] and local adaptivity [96, 145] not only in space or time, but in the full space-time domain simultaneously. Furthermore, since time is just another variable, any uniform motion can be captured in the space-time cylinder, allowing the treatment of moving domains or moving interfaces, see e.g. [59, 60, 116]. Moreover, in the context of optimization problems with partial differential equations as constraints and involving an adjoint state, which is directed backward in time, space-time methods allow for an additional level of parallelism by

solving the coupled system for the state and the adjoint in parallel [97, 98, 101]. At first glance, the method comes with the challenge to deal with higher-dimensional linear systems, and hence an increased memory demand, as the spatial and temporal degrees of freedom (dofs) need to be solved at the same time. Nevertheless, the constantly evolving performance of processors and computer systems leads to the advancing development of parallel and efficient solvers, see e.g. [117, 134] and the references therein, which can deal with such huge systems.

In this thesis we will focus on linear and nonlinear elliptic-parabolic interface problems. While there is an extensive collection of publications for linear space-time methods of parabolic PDEs, see e.g. [6, 96, 109, 138, 144, 147], there are not so many for nonlinear parabolic problems. We mention the work of Česenek and Feistauer [27], Toulopoulos [152] and recently [26] in context of space-time methods. Elliptic-parabolic interface problems arise, when, for instance, the computational domain consists of several materials, cf. e.g. [11, 53, 87]. A widely used method to solve such types of problems is the extended finite element method (XFEM) [108] using modified or cut-off versions of the finite element basis functions. An overview of other methods are given in [57, Section 1.3]. However, since our considered space-time approach captures the deformation of the domain over time within the mesh, even if the domain is fixed, the finite elements do not overlap with the interface and standard FEM can be used. We note that Galerkin-type finite element methods on unstructured space-time meshes for the solution of linear parabolic equations in moving domains have been considered in the work of Jamet [81]. Our goal is to make use of Petrov-Galerkin finite element methods of first order for elliptic-parabolic interface problems on completely unstructured space-time meshes. Pioneered by the work of Steinbach [144], the remainder of this thesis is organized as follows.

In Chapter 2, we introduce the investigating spatially two-dimensional eddy current problem, also known as the magnetoquasistatic problem, which can be derived from the well-known Maxwell's equations and is used for low-frequency applications. Since our work also includes the study of moving bodies like rotating electric motors, the motion of the body must be incorporated into the underlying equations. Classical references, such as the book of Jackson [80] or Van Bladel [154, 155], provide the analysis of Maxwell's equations for moving bodies.

Chapter 3 is dedicated to the description of movement by means of the Eulerian coordinates and the introduction of the basic concepts about Hilbert and Sobolev spaces, as well as the Bochner and Bochner-Sobolev spaces that are used throughout this thesis. Moreover, we discuss the suitable finite-dimensional approximation spaces for the numerical treatment of the eddy current problem, for which simplicial finite elements are used. In Section 3.5, we recall the main results from the work of Steinbach [144] analyzing a Petrov-Galerkin variational formulation in Bochner spaces, which motivates the subsequent chapter. We conclude Chapter 3 with a summary of

the basic concepts of parallelization and the specification of the system and solvers that are used for the numerical experiments presented in this thesis.

The core contribution of this work appears in Chapter 4, in which we first consider the elliptic-parabolic interface problem stemming from the eddy current approximation formulated on conducting and non-conducting non-moving regions. The numerical analysis of the linear space-time variational formulation in Bochner spaces is based on the Babuška-Nečas theory [10, 114], which requires a proof of an inf-sup stability condition to ensure uniqueness, and of a surjectivity condition to ensure the existence of a solution. In context of space-time finite element methods this was done in [6, 138, 144, 153]. In Section 4.1 we extend our investigation to the nonlinear eddy current problem of elliptic-parabolic type, whose analysis is based on Zarantonello's theorem [167] for the elliptic part, and on the principle of maximal monotone mappings [167] for the parabolic part. The numerical experiments reveal linear convergence for the discretization error as well as the accuracy of the method applied to realistic applications such as the electric motor. In Section 4.2 we introduce the eddy current problem considering the rather complex behavior of hysteresis, that occurs e.g. in ferromagnetic materials. We present a space-time finite element method for a specific and widely used hysteretic material law [163]. This leads to a system of saddle point structure, for which the space-time method can be applied to solve the full system at once. Finally, we turn our focus on moving bodies in Section 4.3, and similarly analyze the derived elliptic-parabolic interface problem by means of the Babuška-Nečas theory for the linear case and by Zarantonello's theorem and the principle of maximal monotone mappings for the nonlinear case. The results of the final section are published in [59, 60], see also [26] for a further application.

Finally, in Chapter 5 we summarize and comment on ongoing and future work.

2 Physical essentials and model problem

2.1 Introduction to electric motors

Electric motors are devices that convert electrical energy into mechanical energy through the interaction of magnetic fields. They are ubiquitous in modern society, powering everything from household appliances to industrial machinery and electric vehicles. The importance and huge varieties of the different types of electric motors are justified for the countless various applications in the modern world. The flexibility of electric motors and the possibility of transferring electric power over long distances made the usage of electric motors very attractive and increasingly popular over the last decades.

In general, electric motors operate through the interaction of magnetic flux and electric current, or flow of charge. Conventionally, an electric motor consists of two primary components: the stationary part, called the stator, and the rotating part, called the rotor. Electric current is induced in the coils, which are usually contained in the stator and wounded with wire around cores, resulting in the generation of a magnetic field. Force is developed, when a conductor that carries current is placed in a magnetic field, also called the Lorentz force [20, 78, 159]. This force happens to be orthogonal to the motion of the charge and to the magnetic field. For a simple electric motor, for instance the synchronous reluctance motor, this force is already enough in order to set the rotor in motion. The direction of the rotation is given by the tendency of magnetic materials of the rotor to align themselves in a way that minimizes reluctance, i.e. the magnetic resistance [48, 78]. It quickly became clear that the mechanism for exploiting this force is of tremendous importance for the efficiency of electric motors. Strong magnetic fields are needed, that are obtained from many current driven coils, which additionally may interact with the magnetic field generated by the rotor, e.g. with permanent magnets contained in the rotor.

Electric motor technology has undergone extensive investigation and manufacturing over the past two centuries, resulting in the development of various types tailored to specific applications. In general, electric motors can be classified in two categories: DC and AC motors. DC motors operate with direct current and are commonly used in the automotive industry. AC motors on the contrary are designed to operate with alternating current power sources. They can be classified into two more types: induction motors and synchronous motors. The rotor of a synchronous electric motor

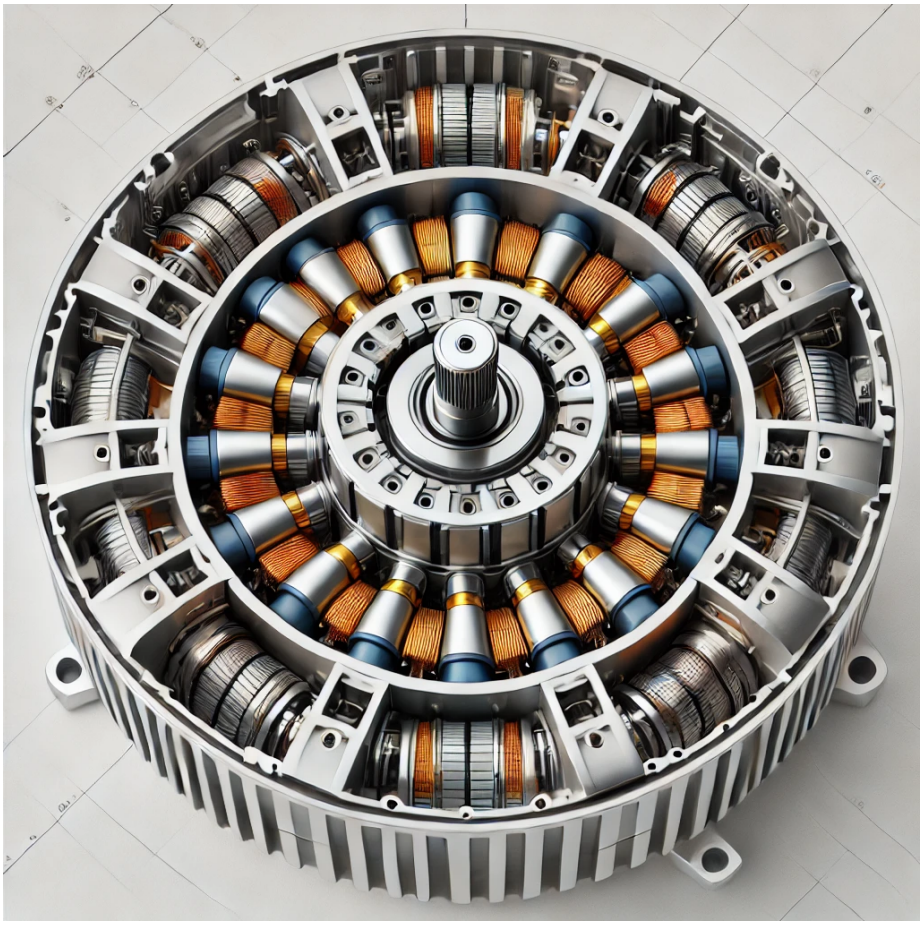

Figure 2.1: An interior permanent magnet synchronous motor[1].

rotates at a constant speed, whose magnetic field aligns with the rotating magnetic field generated by the alternating current operated in the coils. Larger industrial applications make use of this kind of motors, e.g. the permanent magnet synchronous motors (PMSM) as shown in Figure 2.1, which are used in Chapter 4 for electromagnetic simulations. Induction motors use the principle of electromagnetic induction, cf. [159, 85], where the rotating magnetic field in the stator induces current flow in the rotor causing it to rotate. They are robust, low-maintenance, widely used in industrial applications and household appliances. For an extended and detailed overview of the numerous types of electric motors and their organization and applications we refer the reader to the contributions of [16, 20, 48, 78, 159].

High performance requirements for electric machines are undoubtedly important including high torque capability, low iron losses or other losses and optimal motor

[1] OpenAI, "AI-generated image using DALL·E illustrating a design of an interior permanent magnet synchronous motor," created on December 7, 2024, with ChatGPT.

designs. Multiple methods describing the numerical computation of the torque, for instance [42, 74, 132], and the numerical realization of iron losses, see [25, 65, 92] have been developed and are still a huge topic of research. New motor designs with respect to shape optimization [61, 63, 106], or topology optimization [58, 62, 124], strive to maximize the torque, minimize the losses and lower the cost productions. Consequently, efficient and accurate numerical simulations are obligatory in order to analyze such quantities precisely. In this thesis, we will deeply investigate a space-time finite element method that will be applied to simulate electromagnetic behavior of electric motors. Our proposed method is even capable to consider hysteresis effects occurring in ferromagnetic materials, cf. Section 4.2, and to take the rotational motion of the rotor into account, see Section 4.3.

2.2 Physical model

We start this section with the introduction of the mathematical equations for electromagnetic phenomena described by Maxwell's equations. The first publication about the interaction between electric and magnetic fields was released by James Clerk Maxwell in 1862, see [104]. Albert Einstein extended Maxwell's work in his famous publication "Zur Elektrodynamik bewegter Körper" [43] in 1905, postulating that Maxwell's equation must hold in all inertial systems of moving bodies. This led to the investigation of transforming Maxwell's equation from one inertial frame to another, like for instance the Lorentz transformation, see [150, 154]. Furthermore, we derive the eddy current approximation, which is typically used as a model for the simulation of electric motors. The end of this section describes the physical properties of the occurring quantities that are relevant for the eddy current problem.

2.2.1 Maxwell's equations

Maxwell's equations in classical differential form are derived from their integral equations describing the physical background of electromagnetism. For a detailed derivation and relation to physics, we refer the reader to the work of Jackson [80], Ida and Bastos [79], Landau and Lifschitz [93] and Zaglmayr [164]. The well known set of Maxwell's equation reads as, cf. [83, 3],

$$\text{Faraday's law of induction:} \qquad \operatorname{curl} \mathbf{E} = -\frac{\partial \mathbf{B}}{\partial t}, \tag{2.1a}$$

$$\text{Ampere's law:} \qquad \operatorname{curl} \mathbf{H} = \mathbf{J} + \frac{\partial \mathbf{D}}{\partial t}, \tag{2.1b}$$

$$\text{Gauss's law:} \qquad \operatorname{div} \mathbf{D} = \rho, \tag{2.1c}$$

$$\text{Gauss's law for magnetism:} \qquad \operatorname{div} \mathbf{B} = 0. \tag{2.1d}$$

Electromagnetic quantities		
Notation	**Unit**	**Description**
$\mathbf{H}$	$\left[\frac{A}{m}\right]$	Magnetic field intensity
$\mathbf{M}$	$\left[\frac{A}{m}\right]$	Permanent magnetization
$\mathbf{B}$	$[T] = \left[\frac{kg}{A \cdot s^2}\right]$	Magnetic induction field (magnetic flux density)
$\mathbf{E}$	$\left[\frac{V}{m}\right] = \left[\frac{kg \cdot m}{A \cdot s^3}\right]$	Electric field intensity
$\mathbf{D}$	$\left[\frac{C}{m^2}\right] = \left[\frac{A \cdot s}{m^2}\right]$	Electric displacement field (electric flux density)
$\mathbf{P}$	$\left[\frac{C}{m^2}\right] = \left[\frac{A \cdot s}{m^2}\right]$	Electric polarization
$\mathbf{J}$	$\left[\frac{A}{m^2}\right]$	Current density
ρ	$\left[\frac{C}{m^3}\right] = \left[\frac{A \cdot s}{m^3}\right]$	Charge density
μ	$\left[\frac{H}{m}\right] = \left[\frac{V \cdot s}{A \cdot m}\right] = \left[\frac{kg \cdot m}{A^2 \cdot s^2}\right]$	Magnetic permeability
ν	$\left[\frac{m}{H}\right] = \left[\frac{A \cdot m}{V \cdot s}\right] = \left[\frac{A^2 \cdot s^2}{kg \cdot m}\right]$	Magnetic reluctivity
σ	$\left[\frac{S}{m}\right] = \left[\frac{A^2 \cdot s^3}{kg \cdot m^3}\right]$	Electric conductivity
ϵ	$\left[\frac{F}{m}\right] = \left[\frac{A \cdot s}{V \cdot m}\right] = \left[\frac{A^2 \cdot s^4}{kg \cdot m^3}\right]$	Electric permittivity
$\mathbf{A}$	$\left[\frac{Wb}{m}\right] = [T \cdot m] = \left[\frac{kg \cdot m}{A \cdot s^2}\right]$	Magnetic vector potential

Table 2.1: The SI units of the electromagnetic quantities as given in [30, 85]. The last unit entry describes the unit of the quantities in the SI base units ampere $[A]$, second $[s]$, meter $[m]$ and kilogram $[kg]$. The other SI units are tesla $[T]$, volt $[V]$, coulomb $[C]$, henry $[H]$, siemens $[S]$, farad $[F]$ and weber $[Wb]$, see [28].

The unknown quantities occurring in the equations (2.1a) - (2.1d) are the electric field intensity $\mathbf{E}$, the magnetic field intensity $\mathbf{H}$, the magnetic induction field (magnetic flux density) $\mathbf{B}$ and the electric displacement field (electric flux density) $\mathbf{D}$. The sources of electromagnetic fields may be electric charges described by the charge density ρ and currents described by the current density function $\mathbf{J}$. Table 2.1 describes the respective units of these quantities. Note that $\mathbf{E}, \mathbf{H}, \mathbf{B}, \mathbf{D}, \mathbf{J}$ are vector valued functions mapping from $\mathbb{R}^3 \times \mathbb{R} \to \mathbb{R}^3$, and ρ is a scalar function mapping from $\mathbb{R}^3 \times \mathbb{R} \to \mathbb{R}$, which means that all quantities depend on space and time.

Maxwell's equations for a body in uniform and much slower motion compared to the speed of light in vacuum c_0, may be described by the electromagnetic quantities in the current configuration of the moving body using the Lorentz transformation as

described in [70, 155],

$$\begin{aligned}
\mathbf{E}' &= \mathbf{E} + \mathbf{v} \times \mathbf{B}, \\
\mathbf{B}' &= \mathbf{B} - \frac{\mathbf{v} \times \mathbf{E}}{c_0^2}, \\
\mathbf{D}' &= \mathbf{D} + \frac{\mathbf{v} \times \mathbf{H}}{c_0^2}, \\
\mathbf{H}' &= \mathbf{H} - \mathbf{v} \times \mathbf{D}, \\
\mathbf{J}' &= \mathbf{J} - \rho \mathbf{v},
\end{aligned} \tag{2.2}$$

where $\mathbf{v}[m/s]$ describes the uniform velocity of the moving body. In terms of these transformed fields, Maxwell's equations take the form, see [70, 155],

$$\text{Faraday's law of induction:} \qquad \operatorname{curl} \mathbf{E}' = -\frac{\mathrm{D}\mathbf{B}}{\mathrm{D}t}, \tag{2.3a}$$

$$\text{Ampere's law:} \qquad \operatorname{curl} \mathbf{H}' = \mathbf{J}' + \frac{\mathrm{D}\mathbf{D}}{\mathrm{D}t}, \tag{2.3b}$$

$$\text{Gauss's law:} \qquad \operatorname{div} \mathbf{D} = \rho, \tag{2.3c}$$

$$\text{Gauss's law for magnetism:} \qquad \operatorname{div} \mathbf{B} = 0, \tag{2.3d}$$

where the operator $\mathrm{D}/\mathrm{D}t$ indicates the flux derivative defined as

$$\frac{\mathrm{D}\mathbf{F}}{\mathrm{D}} \coloneqq \frac{\partial \mathbf{F}}{\partial t} + \mathbf{v} \operatorname{div} \mathbf{F} - \operatorname{curl}(\mathbf{v} \times \mathbf{F}).$$

Simple calculations show, that inserting the quantities $\mathbf{E}', \mathbf{H}'$ and $\mathbf{J}'$ into (2.3a) and (2.3b) and using the definition of the flux derivative, yield the equations (2.1a) and (2.1b) in the current state of the moving body. Hence, Einstein's postulate [43] is satisfied, and we may consider (2.1a) - (2.1d) in the current configuration of the moving body. For a detailed description and derivation of the transformations (2.2) and the respective equations (2.3a) - (2.3d) we refer the reader to the work of [70, 71, 80, 154, 155, 158].

REMARK 2.1. *We want to emphasize, that the transformations* (2.2) *of the electromagnetic quantities are valid only for the case when the body is in uniform and slow motion. The motion* $\mathbf{v}$ *of the body is much smaller than the speed of light* c_0 *in vacuum, as in the case of electric motors. It is even possible, to consider such transformations for accelerated bodies, which are described in [155, 158].*

For the sake of completeness, constitutive laws are still needed. In the case of an electric motor, where certain parts are made of conducting materials and current density is driven through the coils, it is necessary to consider the generalized Ohm's law $\mathbf{J} = \mathbf{J_c} + \mathbf{J_i}$. In conducting materials the electric field $\mathbf{E}$ induces a conduction

current with density $\mathbf{J_c} = \sigma(\mathbf{E} + \mathbf{v} \times \mathbf{B})$ as a direct consequence of the Lorentz force, cf. [70, 85],

$$\mathbf{F} = \rho_e \left(\mathbf{E} + \mathbf{v} \times \mathbf{B}\right),$$

saying that an electric volume charge ρ_e moving with a velocity $\mathbf{v}$ in an electric field $\mathbf{E}$ and a magnetic field $\mathbf{B}$ experiences a force. The impressed current density $\mathbf{J_i}$ in the coils need to satisfy $\operatorname{div} \mathbf{J_i} = 0$ in any nonconducting material, see [3, 164]. The latter part $\sigma \mathbf{v} \times \mathbf{B}$ of the conduction current density $\mathbf{J}_c$ is commonly known as the motional electromotive force (emf) term, cf. [21, 85]. Together, with the relations of the electric and magnetic fields to their corresponding flux densities, the constitutive laws are

$$\mathbf{D} = \epsilon \mathbf{E} + \mathbf{P}, \tag{2.4a}$$

$$\mathbf{B} = \mu(\mathbf{H} + \mathbf{M}), \tag{2.4b}$$

$$\mathbf{J} = \sigma(\mathbf{E} + \mathbf{v} \times \mathbf{B}) + \mathbf{J_i}, \tag{2.4c}$$

where the electric permittivity ϵ, the magnetic permeability μ and the electric conductivity σ depend on the material and $\mathbf{P}$ denotes an electric polarization. The permanent magnetization $\mathbf{M}$ denotes the magnetic field intensity of permanent magnets, which may occur for instance within the rotor of an electric motor, [83, 90]. Note that the material law (2.4b) can be written in terms of the magnetic reluctivity ν, which is the inverse of the magnetic permeability μ,

$$\mathbf{H} = \nu \mathbf{B} - \mathbf{M}. \tag{2.5}$$

Usually, the material parameters $\epsilon, \mu, \sigma, \nu$ describe complex material behavior, such as anisotropy, in terms of space and time dependent tensors [23, 85]. In the context of this thesis, we only consider isotropic materials. Therefore, the material parameters become scalar fields [79]. The magnetic reluctivity ν, and hence the magnetic permeability μ, may be nonlinear, as for ferromagnetic materials, where the reluctivity depends on the magnitude of the magnetic flux density, i.e. $\nu = \nu(|\mathbf{B}|)$. Finally, in terms of the transformed quantities (2.2), the constitutive laws for a body at rest in the current configuration may be written as

$$\mathbf{D}' = \epsilon \mathbf{E}', \qquad \mathbf{B}' = \mu \mathbf{H}', \qquad \mathbf{J}' = \sigma \mathbf{E}',$$

cf. [154]. For various applications of Maxwell's equation, we refer to the classical books on electromagnetism like [79, 80, 85, 111].

2.2.2 The eddy current problem

In the sequel, we derive the eddy current approximation from Maxwell's equations, which is commonly used for the simulation of the magnetic flux density $\mathbf{B}$ for electric

motors. Low frequency applications allow the electric displacement field $\mathbf{D}$ to be neglected in Ampere's law (2.1b), see [3]. As a consequence, (2.1c) decouples from the other equations, which leads to the magnetoquasistatic problem, also called the eddy current problem. Due to Gauss's law for magnetism (2.1d), the magnetic induction field $\mathbf{B}$ is a solenoidal vector field, i.e. $\mathbf{B}$ is a divergence free vector field. Hence, in a bounded and simply connected domain $\Omega \subset \mathbb{R}^3$ and for $T > 0$, there exists a vector potential $\mathbf{A}$, such that

$$\mathbf{B} = \operatorname{curl} \mathbf{A}. \tag{2.6}$$

Using this relation and substituting into Faraday's law (2.1a) gives

$$\operatorname{curl}\left(\mathbf{E} + \frac{\partial \mathbf{A}}{\partial t}\right) = 0,$$

which implies, due to the fact that for any scalar field ϕ, $\operatorname{curl}(\nabla\phi) = 0$, that

$$\mathbf{E} = -\nabla\phi - \frac{\partial \mathbf{A}}{\partial t}.$$

The scalar field ϕ is not unique, however with so-called *gauging* techniques, e.g. the well known Coulomb gauge [164] div $\mathbf{A} = 0$, uniqueness of a solution can be enforced. We refer to [69, 85, 89] for detailed descriptions about gauging and deal with the vector potential $\mathbf{A}$, satisfying div $\mathbf{A} = 0$ and

$$\mathbf{E} = -\frac{\partial \mathbf{A}}{\partial t}. \tag{2.7}$$

Finally, we make use of the constitutive laws (2.4c) and (2.5), substitute them into Ampere's law (2.1b) and use the vector potential relation for the magnetic flux density (2.6) and for the electric field intensity (2.7), to obtain the well-known formulation of the eddy current problem [85, 103],

$$\sigma\left(\frac{\partial \mathbf{A}}{\partial t} - \mathbf{v} \times \operatorname{curl}(\mathbf{A})\right) + \operatorname{curl}(\nu \operatorname{curl}(\mathbf{A})) = \mathbf{J_i} + \operatorname{curl}(\mathbf{M}). \tag{2.8}$$

In engineering and industrial research, the so called magnetostatic problem is often considered in order to simulate the magnetic flux density $\mathbf{B}$, for example on an electric motor with a constant rotor speed. For this purpose, the electromagnetic quantities are assumed to be time independent, therefore all occurring time derivatives vanish [83],

$$\operatorname{curl}(\nu \operatorname{curl}(\mathbf{A})) = \mathbf{J_i} + \operatorname{curl}(\mathbf{M}). \tag{2.9}$$

In addition to the eddy current problem (2.8) and the magnetostatic problem (2.9), many other electromagnetic regimes may be derived from Maxwell's equations (2.1a)-(2.1d), possibly without dealing with the entire system. For a short overview, we refer

the reader to [164], whereas a detailed overview of common problem classes can be found in [80, 156].

We complete the problem formulation by imposing initial and boundary conditions, but also interface conditions between the different materials where the material parameters jump. As before, let $\Omega \subset \mathbb{R}^3$ be bounded and simply connected with outer boundary $\Gamma := \partial\Omega$ and n being the normal outward vector on Γ. In general, there are many types of boundary conditions depending on the specific application, like e.g. perfect electric conductors (PEC) or perfect magnetic conductors (PMC) [164]. Thinking about electric motors, the magnetic flux density $\mathbf{B}$ should not leave the computational domain $\Omega \times (0,T)$, hence we impose the so-called induction boundary condition, see [85],

$$\mathbf{B} \cdot n = 0 \quad \text{ on } \Gamma \times (0,T). \tag{2.10}$$

At the material interfaces where the material parameters jump, the continuity conditions need to be satisfied. Denoting the material interfaces by Γ_I, the continuity conditions read as, cf. [57, 85],

$$[\![\mathbf{B} \cdot n_{\Gamma_I}]\!] = \left(\mathbf{B}^+|_{\Gamma_I} - \mathbf{B}^-|_{\Gamma_I}\right) \cdot n_{\Gamma_I} = 0 \qquad \text{on } \Gamma_I \times (0,T), \tag{2.11}$$

$$[\![\mathbf{H} \times n_{\Gamma_I}]\!] = \left(\mathbf{H}^+|_{\Gamma_I} - \mathbf{H}^-|_{\Gamma_I}\right) \times n_{\Gamma_I} = 0 \qquad \text{on } \Gamma_I \times (0,T), \tag{2.12}$$

$$[\![\mathbf{J_c} \cdot n_{\Gamma_I}]\!] = \left(\mathbf{J_c}^+|_{\Gamma_I} - \mathbf{J_c}^-|_{\Gamma_I}\right) \cdot n_{\Gamma_I} = 0 \qquad \text{on } \Gamma_I \times (0,T), \tag{2.13}$$

which describe the jump across the interfaces Γ_I along the corresponding unit normal vector n_{Γ_I}. In fact, (2.11) and (2.13) mean that the normal components of the magnetic flux density $\mathbf{B}$ and the conduction current density $\mathbf{J}_c$ have to be continuous across the interfaces, respectively, whereas (2.12) enforces the continuity of the tangential components of the magnetic field intensity $\mathbf{H}$ across the interfaces. For the eddy current problem (2.8), the boundary condition (2.10) changes to, see [119],

$$n \times \mathbf{A} = 0 \quad \text{ on } \Gamma \times (0,T), \tag{2.14}$$

and the continuity conditions (2.11) - (2.13) change to, see [85],

$$[\![\mathbf{A} \times n_{\Gamma_I}]\!] = 0 \qquad \text{on } \Gamma_I \times (0,T), \tag{2.15}$$

$$[\![\nu \; n_{\Gamma_I} \times \text{curl } (\mathbf{A})]\!] = 0 \qquad \text{on } \Gamma_I \times (0,T), \tag{2.16}$$

$$[\![\sigma \; n_{\Gamma_I} \cdot \left(\frac{\partial \mathbf{A}}{\partial t} - \mathbf{v} \times \text{curl } (\mathbf{A})\right)]\!] = 0 \qquad \text{on } \Gamma_I \times (0,T). \tag{2.17}$$

Remark 2.2. *When we consider the magnetostatic problem* (2.9)*, the last interface continuity condition* (2.13) *or rather* (2.17) *vanishes, cf. [90].*

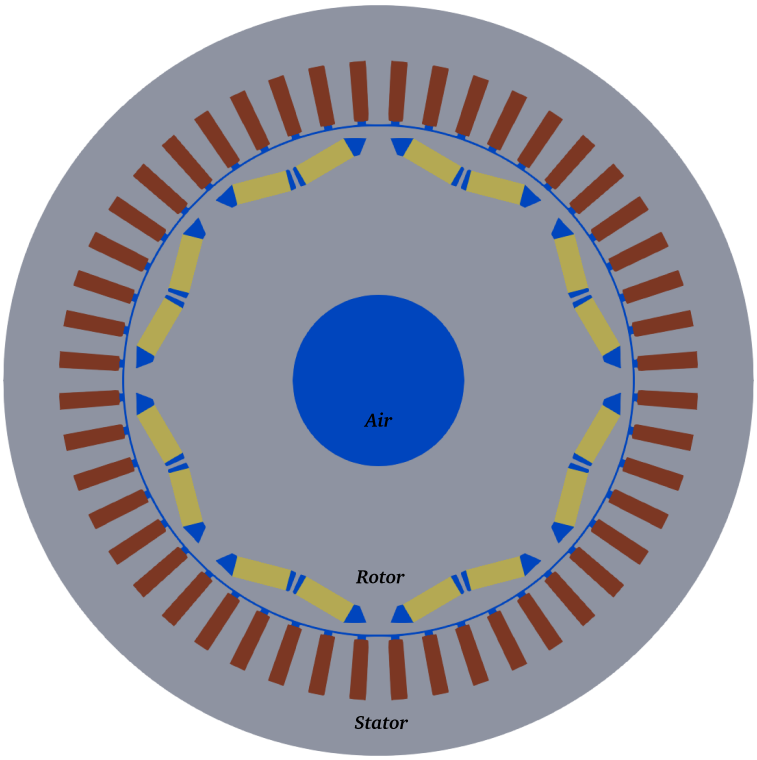

Figure 2.2: The two-dimensional cross-section of an interior permanent magnet synchronous motor [77] (property of Robert Bosch GmbH). The rotor includes 16 magnets (in yellow) with small air pockets on the magnet poles. A thin air gap separates the rotor and the stator, which contains 48 wound coils (in brown). In the middle of the electric motor there is an air hole, in which a shaft is used to be attached.

The initial condition is simply given by a known function $\mathbf{A_0}$ at time $t = 0$, i.e.

$$\mathbf{A}(\mathbf{x}, 0) = \mathbf{A_0} \quad \text{for } \mathbf{x} \in \Omega,$$

where we most often consider homogeneous initial conditions in the remainder of this thesis.

2.2.3 The 2D eddy current problem

The numerical simulation of the eddy current problem for electric motors is a widely investigated research topic, for which various of methods has been developed to solve this problem. One particular simplification is the reduction to a 2D model assuming that one dimension of the computational domain is much larger than the others and that the geometry is invariant in this direction, see [57, 119]. In the

case of an electric motor the problem is posed on the cross-section of the device as visualized in Figure 2.2. Many comparisons for different motor types have been done between the 2D and 3D model, analyzing relevant quantities like the torque, the magnetic flux density and energy losses as eddy current or iron losses, see for instance [47, 110, 113, 118]. The coinciding results show that the reduction to the 2D model is a good approximation to the 3D model and deliver the same universally good results. Hence, we want to formulate the eddy current problem (2.8) in the two-dimensional plane. For this purpose, we assume that the given data $\mathbf{J_i}$, $\mathbf{M}$ and $\mathbf{v}$ as well as the magnetic field intensity $\mathbf{H}$ are constant with respect to the third spatial coordinate x_3, see [57], and of the form

$$\mathbf{J_i}(\mathbf{x},t) = \begin{pmatrix} 0 \\ 0 \\ J_3(x_1,x_2,t) \end{pmatrix}, \ \mathbf{M}(\mathbf{x},t) = \begin{pmatrix} M_1(x_1,x_2,t) \\ M_2(x_1,x_2,t) \\ 0 \end{pmatrix}, \ \mathbf{v}(\mathbf{x},t) = \begin{pmatrix} v_1(x_1,x_2,t) \\ v_2(x_1,x_2,t) \\ 0 \end{pmatrix},$$

and

$$\mathbf{H}(\mathbf{x},t) = \begin{pmatrix} H_1(x_1,x_2,t) \\ H_2(x_1,x_2,t) \\ 0 \end{pmatrix}.$$

It immediately follows that $\mathbf{J_i}$ is divergence free and the magnetic flux density $\mathbf{B}$ has the same form as the magnetic field intensity $\mathbf{H}$ due to the constitutive relation (2.4b). Since relation (2.6) holds for the magnetic flux density $\mathbf{B}$, the third component reads

$$0 = B_3(x_1,x_2,t) = \frac{\partial A_1}{\partial x_2} - \frac{\partial A_2}{\partial x_1},$$

which can be achieved when choosing

$$\mathbf{A}(\mathbf{x},t) = \begin{pmatrix} 0 \\ 0 \\ u(x_1,x_2,t) \end{pmatrix}. \tag{2.18}$$

Note that this approach yields, that the Coulomb gauge div $\mathbf{A} = 0$ is always satisfied, hence the uniqueness of this vector potential is always given, cf. [85]. Inserting the form (2.18) into (2.6) gives

$$\mathbf{B}(\mathbf{x},t) = \operatorname{curl} \mathbf{A}(\mathbf{x},t) = \begin{pmatrix} \frac{\partial}{\partial x_2} u(x_1,x_2,t) \\ -\frac{\partial}{\partial x_1} u(x_1,x_2,t) \\ 0 \end{pmatrix} = \begin{pmatrix} B_1(x_1,x_2,t) \\ B_2(x_1,x_2,t) \\ 0 \end{pmatrix}.$$

Hence, it follows that $|\mathbf{B}| = |\nabla_x u|$, where ∇_x denotes the gradient with respect to the first two spatial coordinates and $|\cdot|$ the Euclidean norm. A simple calculation

shows that

$$\begin{aligned}\mathbf{v} \times \operatorname{curl}(\mathbf{A}) &= \begin{pmatrix} 0 \\ 0 \\ -v_1(x_1,x_2,t)\frac{\partial}{\partial x_1}u(x_1,x_2,t) - v_2(x_1,x_2,t)\frac{\partial}{\partial x_2}u(x_1,x_2,t) \end{pmatrix} \\ &= \begin{pmatrix} 0 \\ 0 \\ -\widetilde{v}\cdot\nabla_x u \end{pmatrix},\end{aligned}$$

when using (2.18) for $\mathbf{A}$, where $\widetilde{v}(x_1,x_2,t) = \begin{pmatrix} v_1(x_1,x_2,t) \\ v_2(x_1,x_2,t) \end{pmatrix}$. Furthermore, we obtain with (2.18) that

$$\operatorname{curl}(\nu \operatorname{curl}(\mathbf{A})) = \operatorname{curl}\left(\nu \operatorname{curl}\left(\begin{pmatrix} 0 \\ 0 \\ u(x_1,x_2,t) \end{pmatrix}\right)\right) = -\operatorname{div}_x(\nu\nabla_x u(x_1,x_2,t)),$$

and

$$\operatorname{curl}(\mathbf{M}) = \operatorname{curl}\left(\begin{pmatrix} M_1(x_1,x_2,t) \\ M_2(x_1,x_2,t) \\ 0 \end{pmatrix}\right) = -\operatorname{div}\left(\begin{pmatrix} -M_2(x_1,x_2,t) \\ M_1(x_1,x_2,t) \\ 0 \end{pmatrix}\right) = -\operatorname{div}_x\left(M^{\perp}\right),$$

where $M^{\perp} = (-M_2, M_1)^{\top}$ and div_x denotes the divergence with respect to the first two spatial coordinates. Finally, considering all assumptions above, the 2D eddy current problem reads as

$$\sigma\left(\frac{\partial u}{\partial t} + \widetilde{v}\cdot\nabla_x u\right) - \operatorname{div}_x(\nu\nabla_x u) = J_3 - \operatorname{div}_x(M^{\perp}) \qquad \text{in } \Omega\times(0,T), \tag{2.19}$$

where Ω denotes a two-dimensional, bounded and simply connected domain, for instance the cross-section of the electric motor, and $(0,T)$ the considered time span for a terminal time $T>0$. The occurring time derivative in equation (2.19) is referred as the material or total time derivative [41, 140], denoted by

$$\frac{d}{dt}u(x_1,x_2,t) \coloneqq \frac{\partial}{\partial t}u(x_1,x_2,t) + \widetilde{v}(x_1,x_2,t)\cdot\nabla_x u(x_1,x_2,t). \tag{2.20}$$

Hence, the eddy current equation (2.19) may be additionally read as

$$\sigma\frac{d}{dt}u - \operatorname{div}_x(\nu\nabla_x u) = J_3 - \operatorname{div}_x(M^{\perp}) \qquad \text{in } \Omega\times(0,T). \tag{2.21}$$

The eddy current equation (2.19) or rather (2.21) is complemented with the homogeneous Dirichlet boundary condition

$$u(x,t) = 0 \qquad \text{for } (x,t)\in\partial\Omega\times(0,T),\ x=(x_1,x_2),$$

and the interface conditions

$$\begin{aligned} [\![u]\!] &= 0 \qquad \text{on } \Gamma_I \times (0,T), \\ [\![\nu \nabla_x u \cdot n_{\Gamma_I}]\!] &= 0 \qquad \text{on } \Gamma_I \times (0,T), \end{aligned}$$

inherited from the induction boundary condition (2.14) and the interface conditions (2.15) - (2.16), respectively, where now Γ_I denotes the interface of the two-dimensional domain Ω with its corresponding outer unit normal vector n_{Γ_I}. Note that, the interface condition (2.17) is always satisfied for the two-dimensional case, since

$$\sigma \; n_{\Gamma_I} \cdot \left(\frac{\partial \mathbf{A}}{\partial t} - \mathbf{v} \times \text{curl } (\mathbf{A}) \right) = \sigma \begin{pmatrix} n_1 \\ n_2 \\ 0 \end{pmatrix} \cdot \left(\begin{pmatrix} 0 \\ 0 \\ \partial_t u \end{pmatrix} - \begin{pmatrix} v_1 \\ v_2 \\ 0 \end{pmatrix} \times \begin{pmatrix} \partial_{x_2} \\ -\partial_{x_1} \\ 0 \end{pmatrix} \right) = 0.$$

The homogeneous initial condition is

$$u(x,0) = 0 \qquad \text{for } x = (x_1, x_2) \in \Omega.$$

Remark 2.3. *As mentioned in Section 2.2.1, in the context of electric motors the reluctivity ν for ferromagnetic materials is nonlinear and depends on the magnitude of the magnetic flux density, i.e. $\nu = \nu(|\mathbf{B}|)$. As previously derived, it holds that $|\mathbf{B}| = |\nabla_x u|$, therefore the nonlinear reluctivity for the 2D eddy current problem reads as $\nu = \nu(|\nabla_x u|)$, which will be further investigated in Section 2.3.*

The 2D magnetostatic problem is introduced as in the three-dimensional case (2.9) by omitting the total time derivative in the eddy current equation (2.21) giving

$$-\text{div}_x(\nu \nabla_x u) = J_3 - \text{div}_x(M^{\perp}) \qquad \text{in } \Omega \times (0,T), \tag{2.22}$$

with the homogeneous Dirichlet boundary condition $u(x,t) = 0$ for $x = (x_1, x_2) \in \partial\Omega$, $t \in (0,T)$, the interface conditions

$$\begin{aligned} [\![u]\!] &= 0 \qquad \text{on } \Gamma_I \times (0,T), \\ [\![\nu \nabla_x u \cdot n_{\Gamma_I}]\!] &= 0 \qquad \text{on } \Gamma_I \times (0,T), \end{aligned}$$

and the homogeneous initial condition $u(x,0) = 0$ for $x = (x_1, x_2) \in \Omega$, see [57].

Remark 2.4. *The eddy current approximations, i.e. equation* (2.8) *for the three-dimensional case and equation* (2.21) *for the two-dimensional case, respectively, consider the movement of the domain, therefore the velocity field representing the deformation of the body has been taken into account. However, in terms of the electric motor, non-moving parts like the stator need to be modeled without any movement. In this case, Ohm's law* (2.4c) *changes to,*

$$\mathbf{J} = \sigma \mathbf{E} + \mathbf{J_i},$$

hence, in the same manner of Section 2.2.2, the eddy current equation can be derived as, see [142],

$$\sigma \frac{\partial \mathbf{A}}{\partial t} + \operatorname{curl}(\nu \operatorname{curl}(\mathbf{A})) = \mathbf{J_i} + \operatorname{curl}(\mathbf{M}). \tag{2.23}$$

With the same assumptions as in Section 2.2.3, the reduction of (2.23) *to the two-dimensional case leads to the equation, cf. [142],*

$$\sigma \frac{\partial u}{\partial t} - \operatorname{div}_x(\nu \nabla_x u) = J_3 - \operatorname{div}_x(M^{\perp}). \tag{2.24}$$

2.3 Physical properties of the B-H-curve and related quantities

For the derivation of the eddy current equations (2.8) and (2.21), or rather the magnetostatic approximations (2.9) and (2.22), the constitutive law (2.5) is essential. It describes the material dependent relation between the magnetic field intensity $\mathbf{H}$ and the magnetic flux density $\mathbf{B}$ via the magnetic reluctivity ν. The inverse relation of (2.5) is the constitutive law (2.4b) describing the relation between $\mathbf{H}$ and $\mathbf{B}$ via the magnetic permeability μ. In general, the magnetic permeability μ, and hence the magnetic reluctivity ν, are rank two tensors (3×3 matrices) and describe the magnetic property of a material that differs in each axial direction, see [88]. Such materials are called anisotropic materials. However, in our applications we deal with so-called isotropic materials, which means that a material has the same magnetic property in every axial direction, cf. [72]. Consequently, the magnetic field intensity $\mathbf{H}$ and the magnetic flux density $\mathbf{B}$ are parallel and the coefficients μ and ν reduce to scalar values, cf. [80, 85, 120],

$$\mu = \mu_0 \mu_r, \qquad \nu = \frac{1}{\mu}, \tag{2.25}$$

where $\mu_0 = 4\pi \cdot 10^{-7}[V \cdot s \cdot A^{-1} \cdot m^{-1}]$ is the permeability in vacuum and μ_r the dimensionless relative permeability characterizing the magnetic material. In general, the magnitude $B \coloneqq |\mathbf{B}|$ of the magnetic flux density depends on the magnitude $H \coloneqq |\mathbf{H}|$ of the magnetic field intensity and on the material properties, cf. [120].

Basically, there are two types of magnetic materials, namely soft magnetic materials and hard magnetic materials, see [15, 85]. Soft magnetic materials can be classified into diamagnetic, paramagnetic and ferromagnetic materials, while hard magnetic materials are typically permanent magnets. In the context of electric motors, copper, of which coils may be fabricated, belongs to the group of diamagnetic materials, whose relative permeability μ_r is slightly smaller than 1, meaning that such a material is

repelled by an external magnetic field. In practice, the relative permeability μ_r of those materials is chosen to be equal to 1. This means, that the relation in (2.4b) is linear, from which we conclude that $\mathbf{B} = \mu_0 \mathbf{H}$. Conversely, the stator and the rotor are usually made of iron, which is associated to the group of ferromagnetic materials. Such materials possess a relative permeability μ_r much larger than 1, meaning that they respond strongly to an external magnetic field, and the relation between the magnitudes B and H is nonlinear, characterized by its corresponding B-H-curve, cf. [84],

$$f : \mathbb{R}_0^+ \to \mathbb{R}_0^+ : H \mapsto B = f(H),$$

where $\mathbb{R}_0^+$ represents the non-negative real numbers. Based on this notation, the magnetic permeability μ and the magnetic reluctivity ν for ferromagnetic materials, respectively, are defined as

$$\mu(s) \coloneqq f(s)/s, \qquad \text{and} \qquad \nu(s) \coloneqq f^{-1}(s)/s,$$

for $s \in \mathbb{R}_0^+$, relating the two parallel fields in the following way,

$$\mathbf{B} = \mu(|\mathbf{H}|)\mathbf{H}, \qquad \text{and} \qquad \mathbf{H} = \nu(|\mathbf{B}|)\mathbf{B}.$$

Last but not least, permanent magnets correspond to hard magnetic materials, that create their own persistent magnetic field and retain a significant remanent flux density B_r after removing the external magnetic field. The relative permeability μ_r of permanent magnets is usually constant, which leads to a linear behavior of (2.4b) or rather (2.5), see [73]. For a more detailed description about the different material properties we refer the reader to [15, 85].

Remark 2.5. *Usually, ferromagnetic materials are subject to realistic physical B-H-curve models that take the phenomenon of hysteresis into account. Hysteresis models are relatively complex, since the magnetic behavior of the material depends on its magnetic past. In Section 4.2 we consider a specific hysteresis model and refer to [157] for other different models. However, in this section we neglect the effect of hysteresis for the investigated B-H-curves.*

Ferromagnetic materials have commonly a typical shaped B-H-curve, as visualized in Figure 2.3a. Small magnitudes of the electric field intensity H strongly amplify the magnitude of the magnetic flux density B, whereas increasing values of H reduce the amplification of B until so-called saturation occurs. This behavior is reflected in the permeability μ and reluctivity ν, whose curves saturate to their respective values in vacuum $\mu_0 = 4\pi \cdot 10^{-7} [V \cdot s \cdot A^{-1} \cdot m^{-1}]$ and $\nu_0 = 10^7/(4\pi) [A \cdot m \cdot V^{-1} \cdot s^{-1}]$, as depicted in Figure 2.3c and Figure 2.3b. These physical properties can be summarized in the following assumptions on the B-H-curve f, that does not consider any hysteresis effects, cf. [120].

ASSUMPTION 2.6. *The B-H-curve $f : \mathbb{R}_0^+ \to \mathbb{R}_0^+$ fulfills the following assumptions.*

(A1) *f is continuously differentiable in $\mathbb{R}_0^+$,*

(A2) *$f(0) = 0$,*

(A3) *$f'(s) \geq \mu_0$ for $s \in \mathbb{R}_0^+$,*

(A4) *$\lim_{s\to\infty} f'(s) = \mu_0$.*

From the statements in Assumption 2.6 it immediately follows that the B-H-curve f is strongly monotone, continuously differentiable, Lipschitz continuous and bounded, and that the reluctivity function ν satisfies important properties, as summed up in the next lemma.

LEMMA 2.7. *Let Assumption 2.6 hold. Then, the following statements for the B-H-curve $f : \mathbb{R}_0^+ \to \mathbb{R}_0^+$ and the reluctivity function $\nu : \mathbb{R}_0^+ \to \mathbb{R}_0^+$ are valid.*

(i) *f is strongly monotone with monotonicity constant μ_0, i.e.*

$$(f(s) - f(t))\,(s - t) \geq \mu_0 (s - t)^2 \quad \text{for all } s, t \in \mathbb{R}_0^+.$$

(ii) *f is continuously differentiable on $\mathbb{R}_0^+$ satisfying*

$$0 < \mu_0 \leq f'(s) \leq \overline{L} \coloneqq \sup_{s\in\mathbb{R}_0^+} f'(s) < \infty \quad \text{for all } s \in \mathbb{R}_0^+.$$

(iii) *f is Lipschitz continuous with Lipschitz constant $\overline{L} > 0$, i.e.*

$$|f(s) - f(t)| \leq \overline{L}|s - t| \quad \text{for all } s, t \in \mathbb{R}_0^+.$$

(iv) *The image of f is $\mathrm{Im}(f) = \mathbb{R}_0^+$ and the inverse function $f^{-1} : \mathbb{R}_0^+ \to \mathbb{R}_0^+$ exists.*

(v) *f^{-1} is continuously differentiable on $\mathbb{R}_0^+$ satisfying*

$$0 < \frac{1}{\overline{L}} \leq (f^{-1})'(s) \leq \nu_0 = \frac{1}{\mu_0} < \infty \quad \text{for all } s \in \mathbb{R}_0^+.$$

(vi) *ν is well-defined, continuous on $\mathbb{R}_0^+$, bounded with constants*

$$\frac{1}{\overline{L}} \leq \nu(s) \leq \nu_0 \quad \text{for all } s \in \mathbb{R}_0^+,$$

$\lim_{s\to\infty} \nu(s) = \nu_0$ and $\nu(0) = (f^{-1})'(0)$.

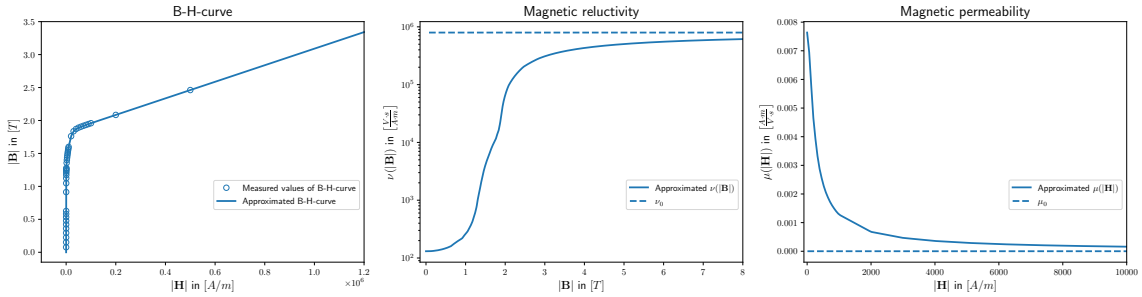

a) b) c)

Figure 2.3: a): The B-H-curve approximated by a quadratic B-spline, which is generated from measured values given in Table 5.1 and linearly continued based on the last two entries.
b): The magnetic reluctivity ν with logarithmic scale on the $\nu(|\mathbf{B}|)$-axis.
c): The magnetic permeability μ.

(vii) $\nu(\cdot)\cdot = f^{-1}$ *is strongly monotone with monotonicity constant* $\frac{1}{L}$ *and Lipschitz continuous with Lipschitz constant* ν_0*, i.e.*

$$\begin{aligned} (\nu(s)s - \nu(t)t)\,(s-t) &\geq \frac{1}{L}(s-t)^2 \\ |\nu(s)s - \nu(t)t| &\leq \nu_0 |s-t| \end{aligned} \quad \text{for all } s,t \in \mathbb{R}_0^+, \tag{2.26}$$

(viii) ν *is continuously differentiable on* $(0,\infty)$ *and* $\lim_{s\to\infty} \nu'(s) = 0$.

Proof. The proof is given in [119, Chapter 2]. □

Obviously, the properties in (2.26) also hold, when the magnetic reluctivity $\nu = \nu_0$ is constant. Therefore, the global reluctivity function $\nu(x, |\mathbf{B}|)$ defined on a body with multiple materials like an electric motor, fulfills (2.26) as well, i.e. the mapping $s \mapsto \nu(x,s)s$ is strongly monotone and Lipschitz continuous with the same constants $1/L$ and ν_0, independent of the spatial position $x \in \Omega$, see [57]. In Section 4.1.3 and Section 4.3.3 we will see that the properties in (2.26) are essential in order to make statements about the existence of a solution for the variational formulation of the boundary value problem (2.21).

Lastly, we would like to point out that the B-H-curve for ferromagnetic materials is not known analytically in advance. In practice, the values of the B-H-curve are obtained from experimental measurements, e.g. [68] or [168], and need to be approximated with suitable methods. Particularly, all these methods must ensure that the properties in (2.26) remain fulfilled, even if the values have inaccuracies due to the measurements. Different approaches for monotonicity preserving interpolation of

discrete data are given for instance in [7, 52, 102, 120]. In the scope of this thesis, we use a quadratic B-spline as given in [121] or [133], that is provided by the free finite element software Netgen/NGSolve [137] in order to create a monotone, Lipschitz continuous and differentiable B-H-curve, as visualized in Figure 2.3a. A B-spline curve $b(s)$ of order $p+1$ is an affine combination of some control points (b_i),

$$b(s) = \sum_i b_i B_i^p(s),$$

where every $B_i^p(s)$ is a piecewise polynomial function of degree p defined by a sequence of given knots (a_i) with $a_i < a_{i+1}$, minimal support and certain continuity conditions, i.e.

$$B_i^0(s) = \begin{cases} 1 & \text{if } s \in [a_i, a_{i+1}), \\ 0 & \text{otherwise,} \end{cases}$$

and

$$B_i^n(s) = \frac{s - a_i}{a_{i+n} - a_i} B_i^{n-1}(s) + \frac{a_{i+n+1} - s}{a_{i+n+1} - a_{i+1}} B_{i+1}^{n-1}(s).$$

Thus, quadratic B-splines are of order 3 (degree 2) and continuously differentiable, cf. [121]. In this sense, the B-H-curve can be approximated by a quadratic B-spline curve, whose control points are the measured values for magnetic flux density B and the list of knots is the list of the measured values of the magnetic field intensity H. In Table 5.1 a list of measured values for B and H is given, that was kindly provided by Robert Bosch GmbH and used in Section 4.3.4 for the electromagnetic simulation of a permanent magnet synchronous motor. This applies not only for the B-H-curve, but also for the magnetic permeability μ and magnetic reluctivity ν, whose control points are given by the values B/H and H/B and the knots are given by the list of H and B, respectively.

Remark 2.8. *In general, a B-spline curve does not pass through its control points. However, repeating knot values at the beginning or end of the knot list, will cause the B-spline curve to pass through some of its control points, see [121].*

3 Preliminaries

In this chapter, we briefly introduce the notations, the function spaces and the finite element method (FEM), that are used throughout this thesis. Furthermore, we recall the theory for the unique solvability of a parabolic initial boundary value problem (IBVP) in so-called Bochner spaces, and conclude this chapter with the description of parallel computation methods, which are used to solve the linear systems of the presented numerical experiments in this work.

We start with the introduction of some important notations, that accompany us throughout the entire work. For a function $u : \mathbb{R}^d \times \mathbb{R} \to \mathbb{R}$, we introduce the spatial gradient

$$\nabla_y u(y,t) = (\partial_{y_1} u(y,t), \dots, \partial_{y_d} u(y,t))^\top = \left(\frac{\partial}{\partial y_1} u(y,t), \dots, \frac{\partial}{\partial y_d} u(y,t) \right)^\top,$$

and the spatial Laplacian

$$\Delta_y u(y,t) = \operatorname{div}_y \nabla_y u(y,t) = \sum_{i=1}^{d} \frac{\partial^2}{\partial y_i^2} u(y,t),$$

where the spatial divergence of vector-valued functions $\mathbf{v} : \mathbb{R}^d \times \mathbb{R} \to \mathbb{R}^d$ is given by

$$\operatorname{div}_y \mathbf{v}(y,t) = \sum_{i=1}^{d} \frac{\partial}{\partial y_i} v_i(y,t).$$

Since in all our applications, the time is just an additional spatial component, i.e. $y_{d+1} = t$, we bear in mind that

$$\partial_t u(y,t) = \frac{\partial}{\partial t} u(y,t) = \frac{\partial}{\partial y_{d+1}} u(y, y_{d+1}),$$

hence the space-time gradient is given as

$$\nabla u(y,t) = \nabla_{(y,t)} u(y,t) = \begin{pmatrix} \nabla_y u(y,t) \\ \partial_t u(y,t) \end{pmatrix}.$$

3.1 Description of moving domains

In what follows next, $\Omega \subset \mathbb{R}^d$, $d = 1, 2, 3$, is an open, non-empty and connected set, i.e. a domain, that is bounded and Lipschitz, see [39]. For a non-moving domain, the (open) space-time cylinder is defined as $Q := \Omega \times (0, T) \subset \mathbb{R}^{d+1}$, where $T > 0$ denotes the terminal time. The boundary ∂Q of the space-time cylinder Q is divided into the lateral boundary $\Sigma := \partial\Omega \times (0, T)$, the bottom $\Sigma_0 := \Omega \times \{0\}$ and the top $\Sigma_T := \Omega \times \{T\}$. However, when the body undergoes a motion, or deformation, $\varphi : \mathbb{R}^d \times [0, T] \to \mathbb{R}^d$ that is known a priori, we can describe the position of a material point $x \in \Omega_0 \subset \mathbb{R}^d$ in an initial domain Ω_0 at time $t \in (0, T)$ as

$$y = \varphi(x, t) \quad \text{or} \quad y_i = \varphi_i(x, t) \quad \text{for } i = 1, ..., d. \tag{3.1}$$

The coordinates y_i are referred as Eulerian coordinates, cf. [17, 41]. The mapping $\varphi(\cdot, t)$ maps the initial configuration $\Omega_0 \subset \mathbb{R}^d$ to the current configuration $\Omega(t)$ at time t, i.e.

$$\Omega(t) := \left\{ y = \varphi(x, t) \in \mathbb{R}^d |\ x \in \Omega_0 \right\} \subset \mathbb{R}^d,$$

and need to satisfy the following natural assumptions, see [17, 41].

ASSUMPTION 3.1. *The motion, or deformation, $\varphi : \overline{\Omega}_0 \times [0, T] \to \mathbb{R}^d$ of a domain Ω_0 in initial state fulfills the following assumptions.*

(A1) $\varphi(\overline{\Omega}_0, 0) = \overline{\Omega}_0$, *i.e.* $\varphi(x, 0) = x$ *for all* $x \in \overline{\Omega}_0$.

(A2) The motion φ is continuously differentiable.

(A3) For every $t \in [0, T]$ the mapping $\varphi(\cdot, t) : \overline{\Omega}_0 \to \overline{\Omega(t)}$ is invertible.

(A4) The Jacobian determinant $J_\varphi(x, t) := \det(\nabla_x \varphi(x, t)) > 0$ for all $x \in \Omega_0$ and $t \in [0, T]$.

From Assumption $(A3)$ we deduce, that for a fixed t, we can follow back the motion of a point $y \in \Omega(t)$ in the current configuration to arrive at its starting point $x = \varphi^{-1}(y) \in \Omega_0$. Furthermore, we describe the velocity field $\mathbf{w}(x, t) : \Omega_0 \times (0, T) \to \mathbb{R}^d$ at which the body moves by

$$\mathbf{w}(x, t) = \frac{\partial}{\partial t} \varphi(x, t),$$

and we assume that the velocity field is continuously differentiable. The velocity field in terms of the spatial, or Eulerian, coordinates, i.e. $\mathbf{v}(y, t) : \Omega(t) \times (0, T) \to \mathbb{R}^d$, is hence defined as, see [41],

$$\mathbf{v}(y, t) = \mathbf{v}(\varphi(x, t), t) = \frac{\partial}{\partial t} \varphi(\varphi^{-1}(y), t) = \mathbf{w}(x, t). \tag{3.2}$$

Moreover, the trajectory of a material point is given as the solution of

$$\begin{cases} \frac{\partial}{\partial t}\varphi(x,t) & = \mathbf{v}(\varphi(x,t),t), \\ \varphi(x,0) & = x, \end{cases} \quad \text{for } x \in \Omega_0. \tag{3.3}$$

For a physical quantity $u(y,t)$, e.g. the temperature or the last coordinate of the magnetic vector potential (2.18), that is described in Eulerian coordinates, the time derivative plays a crucial role and when using the chain rule and (3.2), we obtain

$$\begin{aligned} \frac{\partial}{\partial t}\Big(u(\varphi(x,t),t)\Big) &= \frac{\partial}{\partial t}u(\varphi(x,t),t) + \nabla_y u(y,t)\Big|_{y=\varphi(x,t)} \cdot \frac{\partial}{\partial t}\varphi(x,t) \\ &= \frac{\partial}{\partial t}u(y,t) + \nabla_y u(y,t)\cdot \mathbf{v}(y,t). \end{aligned}$$

This leads to the definition of the material or total time derivative, which was already mentioned in Section 2.2.3 in context of moving domains.

Definition 3.2 ([17, 41]). *The material or total time derivative of* $u : \Omega(t)\times(0,T) \to \mathbb{R}$ *is given as*

$$\frac{d}{dt}u(y,t) = \frac{\partial}{\partial t}u(y,t) + \mathbf{v}(y,t)\cdot\nabla_y u(y,t).$$

An associated important result, which will be essential in Section 4.3 in order to make a statement about a unique solution for equation (2.21), is Reynolds' transport theorem.

Theorem 3.3 (Reynolds's transport theorem). *Let the motion* $\varphi : \overline{\Omega}_0 \times [0,T] \to \mathbb{R}^d$ *fulfills Assumption 3.1, and let the velocity field* $\mathbf{v}(y,t)$ *and the function* $u(y,t)$ *be continuously differentiable. Then,*

$$\begin{aligned} \frac{d}{dt}\int_{\Omega(t)} u(y,t)dy &= \int_{\Omega(t)} \left[\frac{\partial}{\partial t}u(y,t) + \operatorname{div}_y\left(u(y,t)v(y,t)\right)\right] dy \\ &= \int_{\Omega(t)} \left[\frac{\partial}{\partial t}u(y,t) + \mathbf{v}(y,t)\cdot\nabla_y u(y,t) + u(y,t)\operatorname{div}_y\mathbf{v}(y,t)\right] dy \\ &= \int_{\Omega(t)} \left[\frac{d}{dt}u(y,t) + u(y,t)\operatorname{div}_y\mathbf{v}(y,t)\right] dy. \end{aligned} \tag{3.4}$$

Proof. The proof is given in [17, Section 3.5.3] and [41, Theorem 5.4]. □

Now, we are able to define the (open) space-time cylinder Q for a moving domain starting from the bounded Lipschitz domain Ω_0, whose movement is described by

the motion φ, where $\Omega(t)$ is also bounded and Lipschitz for every $t \in (0,T)$, in the following way,

$$Q \coloneqq \left\{(y,t) \in \mathbb{R}^{d+1} |\ y = \varphi(x,t) \in \Omega(t),\ x \in \Omega_0,\ t \in (0,T)\right\}. \tag{3.5}$$

The bottom and the top of Q are denoted by $\Sigma_0 \coloneqq \Omega(0) \times \{0\} = \Omega_0 \times \{0\}$ and $\Sigma_T \coloneqq \Omega(T) \times \{T\}$, respectively, whereas the lateral boundary is defined as

$$\Sigma \coloneqq \left\{(y,t) \in \mathbb{R}^{d+1} |\ y = \varphi(x,t),\ x \in \partial\Omega_0,\ t \in (0,T)\right\}, \tag{3.6}$$

giving all together the whole boundary ∂Q of the space-time cylinder.

Remark 3.4. *In the case of a non-moving body, the deformation is simply the identity in space, i.e.*

$$y = \mathrm{Id}_x(x,t) = x, \tag{3.7}$$

hence, the velocity field $\mathbf{v} = \frac{\partial}{\partial t}\mathrm{Id}_x = 0$ *and consequently the total time derivative* $\frac{d}{dt}$ *reduces to the partial time derivative* $\frac{\partial}{\partial t}$.

3.2 Domains with moving and non-moving regions

In association with electric motors, the entire domain is composed of moving and non-moving parts. Therefore, a motion φ needs to be defined, that satisfies Assumption 3.1 for every part of the device. Particularly this means considering the electric motor of Figure 2.2, that the moving parts of the electric motor undergo a rotational movement, whereas the fixed parts can be simply described by the identity (3.7). However, the motion of the air gap Ω_{gap}, which have on one side an interface with the rotor and on the other side an interface with the stator, needs to be chosen in such a way that φ is continuously differentiable and $\varphi(\Omega_{gap}) = \Omega_{gap}$.

The two-dimensional rotation

We now consider the two-dimensional cross-section $\Omega_0 \subset \mathbb{R}^2$ of the electric motor from Figure 2.2, which has its center in the origin. The rotor, the magnets as well as the air pockets at the magnet poles experience a counter-clockwise constant rotational motion about the origin, that is described by

$$\varphi_{R_\alpha}(x,t) = R_{\alpha(t)} \begin{pmatrix} x_1 \\ x_2 \end{pmatrix} \quad \text{for } x = (x_1, x_2)^\top \in \Omega_0, \tag{3.8}$$

with

$$R_\alpha = \begin{pmatrix} \cos\alpha(t) & -\sin\alpha(t) \\ \sin\alpha(t) & \cos\alpha(t) \end{pmatrix} \quad \text{and} \quad \alpha(t) = \phi\frac{t}{T} \quad \text{for } \phi \in [0, 2\pi],$$

where $\alpha(t)$ represents the angle through which the rotating parts have turned at time t, and ϕ denotes the angle at the final rotated position at time T, cf. [17]. The stator and the coils are fixed, therefore the motion in these domains is simply represented by the identity (3.7). In order to describe the motion jointly in all parts of the motor, we use polar coordinates $(x_1, x_2)^\top = r(\cos\psi, \sin\psi)^\top \in \Omega_0$ for $\psi \in [0, 2\pi)$ and $r \in (0, R)$, where R is the exterior radius of the motor as visualized in Figure 3.1. Similar to [60], when using

$$\Psi(r) = \begin{cases} \dfrac{r}{r_1} & \text{for } r \in (0, r_1), \\ 1 & \text{for } r \in (r_1, r_2), \\ \dfrac{r_3 - r}{r_3 - r_2} & \text{for } r \in (r_2, r_3), \\ 0 & \text{for } r \in (r_3, R), \end{cases}$$

and (3.8) with $\alpha(t) = \phi\ \Psi(r)\frac{t}{T}$, where r_1, r_2 and r_3 are the different radii of the motor as outlined in Figure 3.1, we can introduce the continuous motion

$$y = \varphi(x,t) = \begin{pmatrix} y_1 \\ y_2 \end{pmatrix} = R_\alpha\ r \begin{pmatrix} \cos\psi \\ \sin\psi \end{pmatrix} = \begin{pmatrix} r\left(\cos\alpha(t)\cos\psi - \sin\alpha(t)\sin\psi\right) \\ r\left(\sin\alpha(t)\cos\psi + \cos\alpha(t)\sin\psi\right) \end{pmatrix}.$$

With the help of the well known trigonometric identities

$$\begin{aligned} \sin(\alpha \pm \beta) &= \sin\alpha\cos\beta \pm \cos\alpha\sin\beta, \\ \cos(\alpha \pm \beta) &= \cos\alpha\cos\beta \mp \sin\alpha\sin\beta, \end{aligned}$$

we finally obtain

$$y = \varphi(x,t) = \begin{pmatrix} y_1 \\ y_2 \end{pmatrix} = r \begin{pmatrix} \cos(\psi + \alpha(t)) \\ \sin(\psi + \alpha(t)) \end{pmatrix} \in \Omega(t) \text{ for } t \in (0, T). \tag{3.9}$$

Thus, the velocity field of this motion is given as

$$\widetilde{v}(y,t) = \begin{pmatrix} \widetilde{v}_1(y,t) \\ \widetilde{v}_2(y,t) \end{pmatrix} = \frac{\partial\alpha(t)}{\partial t}\ r \begin{pmatrix} -\sin(\psi + \alpha(t)) \\ \cos(\psi + \alpha(t)) \end{pmatrix} = \frac{\phi\ \Psi(r)}{T} \begin{pmatrix} -y_2 \\ y_1 \end{pmatrix},$$

where $\partial_t\alpha(t)$ is usually known as the angular velocity [17]. Moreover, when using the chain rule, recall $r = \sqrt{y_1^2 + y_2^2}$, we obtain

$$\frac{\partial}{\partial y_1}\widetilde{v}_1(y,t) = -\frac{\phi\ \Psi'(r)y_2}{T}\frac{y_1}{\sqrt{y_1^2 + y_2^2}} \quad \text{and} \quad \frac{\partial}{\partial y_2}\widetilde{v}_2(y,t) = \frac{\phi\ \Psi'(r)y_1}{T}\frac{y_2}{\sqrt{y_1^2 + y_2^2}},$$

which yields, that the velocity field $\widetilde{v}$ is divergence free, i.e.

$$\operatorname{div}_y \widetilde{v}(y,t) = 0. \tag{3.10}$$

As a result, using (3.10) and the total time derivative (2.20), Reynolds transport theorem (3.4) becomes to

$$\begin{aligned}\frac{d}{dt}\int_{\Omega(t)} u(y,t)dy &= \int_{\Omega(t)} \left[\frac{\partial}{\partial t}u(y,t) + \widetilde{v}(y,t)\cdot\nabla_y u(y,t) + u(y,t)\operatorname{div}_y\widetilde{v}(y,t)\right] dy \\ &= \int_{\Omega(t)} \frac{d}{dt}u(y,t)dy, \end{aligned}\tag{3.11}$$

which will be an essential ingredient, when it comes to prove the existence of a unique solution for IBVPs in Section 4.3. In order to verify whether $J_\varphi(x,t) > 0$, we write

$$\begin{aligned}\varphi(x,t) &= \begin{pmatrix} r\cos\alpha(t)\cos\psi - r\sin\alpha(t)\sin\psi \\ r\sin\alpha(t)\cos\psi + r\cos\alpha(t)\sin\psi \end{pmatrix} = \begin{pmatrix} \cos\alpha(t)x_1 - \sin\alpha(t)x_2 \\ \sin\alpha(t)x_1 + \cos\alpha(t)x_2 \end{pmatrix} \\ &= \begin{pmatrix} \cos\left(\phi\,\Psi(r)\frac{t}{T}\right)x_1 - \sin\left(\phi\,\Psi(r)\frac{t}{T}\right)x_2 \\ \sin\left(\phi\,\Psi(r)\frac{t}{T}\right)x_1 + \cos\left(\phi\,\Psi(r)\frac{t}{T}\right)x_2 \end{pmatrix},\end{aligned}$$

and use $r = \sqrt{x_1^2 + x_2^2}$ and the chain rule to obtain

$$\begin{aligned}\frac{\partial}{\partial x_1}\varphi_1(x,t) =& -\sin\left(\phi\,\Psi(r)\frac{t}{T}\right)\phi\,\Psi'(r)\frac{t}{T}\frac{x_1^2}{\sqrt{x_1^2+x_2^2}} + \cos\left(\phi\,\Psi(r)\frac{t}{T}\right) \\ &- \cos\left(\phi\,\Psi(r)\frac{t}{T}\right)\phi\,\Psi'(r)\frac{t}{T}\frac{x_1x_2}{\sqrt{x_1^2+x_2^2}}, \\ \frac{\partial}{\partial x_2}\varphi_1(x,t) =& -\sin\left(\phi\,\Psi(r)\frac{t}{T}\right)\phi\,\Psi'(r)\frac{t}{T}\frac{x_1x_2}{\sqrt{x_1^2+x_2^2}} - \sin\left(\phi\,\Psi(r)\frac{t}{T}\right) \\ &- \cos\left(\phi\,\Psi(r)\frac{t}{T}\right)\phi\,\Psi'(r)\frac{t}{T}\frac{x_2^2}{\sqrt{x_1^2+x_2^2}}, \\ \frac{\partial}{\partial x_1}\varphi_2(x,t) =& \cos\left(\phi\,\Psi(r)\frac{t}{T}\right)\phi\,\Psi'(r)\frac{t}{T}\frac{x_1^2}{\sqrt{x_1^2+x_2^2}} + \sin\left(\phi\,\Psi(r)\frac{t}{T}\right) \\ &- \sin\left(\phi\,\Psi(r)\frac{t}{T}\right)\phi\,\Psi'(r)\frac{t}{T}\frac{x_1x_2}{\sqrt{x_1^2+x_2^2}}, \\ \frac{\partial}{\partial x_2}\varphi_2(x,t) =& \cos\left(\phi\,\Psi(r)\frac{t}{T}\right)\phi\,\Psi'(r)\frac{t}{T}\frac{x_1x_2}{\sqrt{x_1^2+x_2^2}} + \cos\left(\phi\,\Psi(r)\frac{t}{T}\right) \\ &- \sin\left(\phi\,\Psi(r)\frac{t}{T}\right)\phi\,\Psi'(r)\frac{t}{T}\frac{x_2^2}{\sqrt{x_1^2+x_2^2}}.\end{aligned}$$

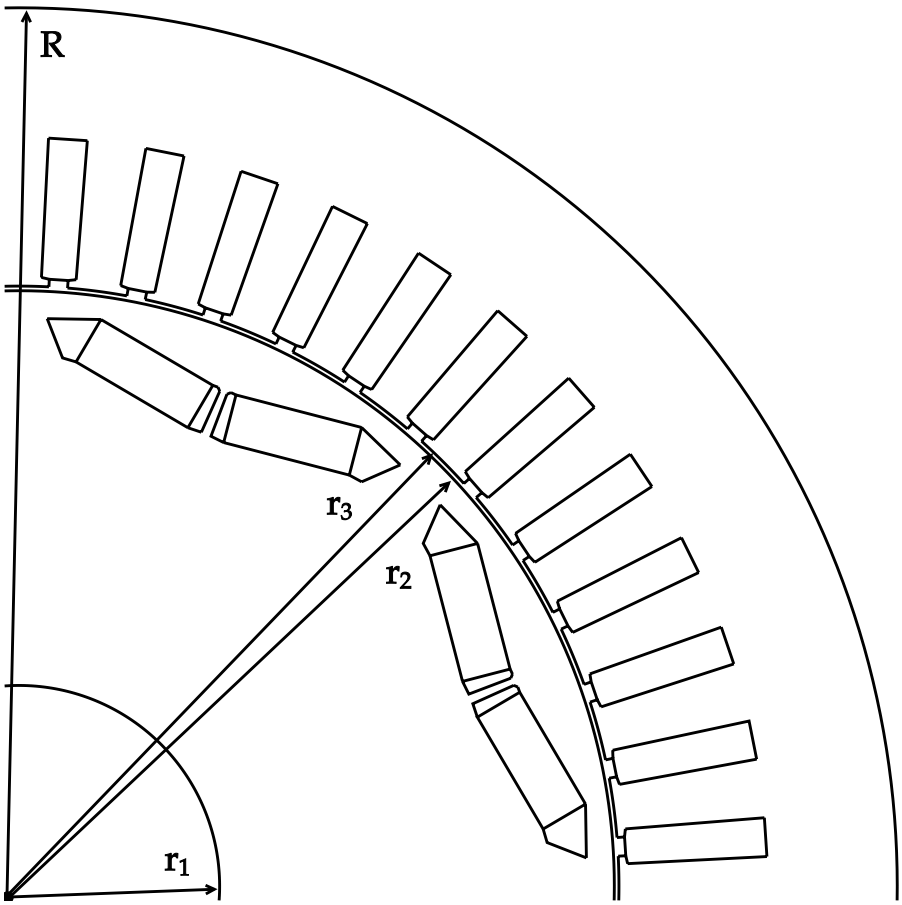

Figure 3.1: An enlarged section of the geometry of the interior PMSM from Figure 2.2. The motor has its center in the origin, from which the different radii are measured. The interior and exterior radii of the motor are denoted by $r_1 = 26.5$ $[mm]$ and $R = 116$ $[mm]$, respectively. The respective inner and outer radii of the air gap are $r_2 = 78.632$ $[mm]$ and $r_3 = 79.242$ $[mm]$.

The result after a slightly longer but simple calculation is

$$J_\varphi(x,t) = \det\left(\nabla_x \varphi(x,t)\right) = \cos^2\left(\phi\, \Psi(r)\frac{t}{T}\right) + \sin^2\left(\phi\, \Psi(r)\frac{t}{T}\right) = 1.$$

Finally, the space-time cylinder Q and its boundary for the specific motion (3.9) are defined in the exact same way as in (3.5).

Remark 3.5. *Even though we have discussed the particular case of a two-dimensional rotation* (3.9)*, that only describes rotational movement in combination with*

no movement, more general uniform motions φ, e.g. rotations and translations, satisfying Assumption 3.1 and $\varphi(\Omega_{gap}) = \Omega_{gap}$ with the associated velocity field $\mathbf{v}(y,t) = \partial_t\varphi(\varphi^{-1}(y),t)$, shall not create additional difficulties in further analysis.

3.3 Function spaces

In order to introduce Bochner spaces, which form the basis of our mathematical analysis in the remainder of this thesis, we first need to briefly recall some important function spaces in the real space. The theory presented in this section is mainly based on the work of [1, 39], however other extensive contributions may be found e.g. in [45, 67, 99]. We denote the space of continuous functions on $\Omega \subset \mathbb{R}^d$, whose derivatives up to order k are also continuous in Ω, by $C^k(\Omega)$. For the case $k = 0$, we shortly write $C(\Omega)$. In addition, the space of infinitely differentiable functions is defined as $C^\infty(\Omega) = \bigcap_{k=0}^{\infty} C^k(\Omega)$. The spaces of functions in $C^k(\Omega)$ and $C^\infty(\Omega)$ with compact support, i.e.

$$\operatorname{supp}(u) \coloneqq \overline{\{y \in \Omega : u(y) \neq 0\}} \quad \text{for } u : \Omega \to \mathbb{R},$$

is compact, are denoted by $C_0^k(\Omega)$ and $C_0^\infty(\Omega)$, respectively. Since Ω is an open set, the spaces $C^k(\Omega)$ contain unbounded functions. Hence, we describe the space of bounded and uniformly continuous functions on $\overline{\Omega}$, whose derivatives up to order k are bounded and uniformly continuous on Ω, as $C^k(\overline{\Omega})$. Note that both, $C_0^k(\Omega)$ and $C^k(\overline{\Omega})$, are subspaces of $C^k(\Omega)$. Moreover, when we define the norm

$$\|u\|_{C^k(\overline{\Omega})} \coloneqq \max_{|\beta|\leq k} \sup_{y\in\Omega} |D^\beta u(y)|,$$

where $\beta = (\beta_1, \ldots, \beta_d)$ is the multi-index with $\beta_i \geq 0$ for $i = 1, \ldots, d$,

$$|\beta| \coloneqq \sum_{i=1}^{d} \beta_i \quad \text{and} \quad D^\beta u(y) \coloneqq \frac{\partial^{|\beta|}}{\partial y_1^{\beta_1} \cdots \partial y_d^{\beta_d}} u(y),$$

then the space $C^k(\overline{\Omega})$ equipped with this norm is a Banach space, see [39, Theorem 2.41].

3.3.1 Lebesgue- and Sobolev spaces

Now, let $1 \leq p < \infty$ and let us define the space of Lebesgue measurable and $p-$integrable functions on Ω as

$$L^p(\Omega) \coloneqq \left\{ u : \Omega \to \mathbb{R} \mid \|u\|_{L^p(\Omega)} < \infty \right\}$$

with the corresponding norm

$$\|u\|_{L^p(\Omega)} \coloneqq \left(\int_\Omega |u(y)|^p \, dy \right)^{1/p}.$$

For the case $p = \infty$, the norm is defined for essential bounded functions, cf. [39, Definition 4.15], which is denoted by $\|\cdot\|_{L^\infty(\Omega)}$. Note that the Lebesgue spaces $L^p(\Omega)$ equipped with the corresponding norm $\|\cdot\|_{L^p(\Omega)}$ for $1 \leq p \leq \infty$ are Banach spaces, see e.g. [39, Theorem 4.17]. For our purpose, the particular case $p = 2$, i.e. the space of square-integrable functions $L^2(\Omega)$, is of special interest, which even defines a Hilbert space endowed with the inner product [39, Corollary 4.18]

$$(u, v)_{L^2(\Omega)} \coloneqq \int_\Omega u(y)v(y) \, dy \quad \text{for all } u, v \in L^2(\Omega).$$

As a matter of fact, the space of infinitely differentiable functions with compact support $C_0^\infty(\Omega)$ is dense in $L^p(\Omega)$ for $1 \leq p < \infty$, see [39, Theorem 4.23], which allows an equivalent definition of the Lebesgue spaces, $L^p(\Omega) = \overline{C_0^\infty(\Omega)}^{\|\cdot\|_{L^p(\Omega)}}$. Moreover, we say a function $u : \Omega \to \mathbb{R}$ is locally integrable on Ω, if $u \in L^1(U)$ for every open set U that is compactly embedded in Ω, i.e. $\overline{U} \subset \mathbb{R}^d$ is a compact subset and $\overline{U} \subset \Omega$, cf. [1, Definition 1.58]. The space of locally integrable functions on Ω is denoted by $L^1_{\text{loc}}(\Omega)$.

Now, let us consider the concept of weak derivatives in order to formulate the IBVPs in a suitable way for the mathematical analysis.

Definition 3.6 ([1], [39, Definition 5.3]). *Let $u \in L^1_{\text{loc}}(\Omega)$ and β be a multi-index. We say that u has a β^{th}-weak partial derivative in Ω, if there exists a $u_\beta \in L^1_{\text{loc}}(\Omega)$, such that*

$$\int_\Omega u(y) D^\beta \phi(y) \, dy = (-1)^{|\beta|} \int_\Omega u_\beta(y)\phi(y) \, dy$$

for all test functions $\phi \in C_0^\infty(\Omega)$.

A function that is differentiable in the classical sense, is also weakly differentiable, cf. [39, Lemma 5.4], and, since the weak partial derivative is unique if it exists, we do not distinguish between classical and weak partial derivative anymore and write $D^\beta u$ instead of u_β. This leads us to the introduction of Sobolev spaces.

Definition 3.7 ([1], [39, Definition 5.9]). *Let $m \geq 0$ and $1 \leq p \leq \infty$. The Sobolev space $W^{m,p}(\Omega)$ consists of all functions $u \in L^p(\Omega)$, whose weak partial derivatives up to order m are also in $L^p(\Omega)$, i.e.*

$$\begin{aligned} W^{m,p}(\Omega) &\coloneqq \left\{ u \in L^p(\Omega) : D^\beta u \in L^p(\Omega) \text{ for } 0 \leq |\beta| \leq m \right\} \\ &= \left\{ u \in L^p(\Omega) : \|u\|_{W^{m,p}(\Omega)} < \infty \right\}, \end{aligned}$$

with the Sobolev norm

$$\|u\|_{W^{m,p}(\Omega)} = \left(\sum_{0 \le |\beta| \le m} \|D^\beta u\|^p_{L^p(\Omega)} \right)^{1/p}.$$

For the special case $p = \infty$, we refer to [39, Definition 5.9].

Particularly, every Sobolev space $W^{m,p}(\Omega)$ for $1 \le p \le \infty$ and $m \ge 0$ is a Banach space, [39, Theorem 5.10], and the famous result of Meyers and Serrin [107] in 1964 holds for $1 \le p < \infty$, which states that $C^\infty(\Omega) \cap W^{m,p}(\Omega)$ is dense in $W^{m,p}(\Omega)$, allowing the alternative definition

$$W^{m,p}(\Omega) \coloneqq \overline{C^\infty(\Omega)}^{\|\cdot\|_{W^{m,p}(\Omega)}} \quad \text{and} \quad W_0^{m,p}(\Omega) \coloneqq \overline{C_0^\infty(\Omega)}^{\|\cdot\|_{W^{m,p}(\Omega)}},$$

see also [1, Theorem 3.17, Definition 6.9] or [39, Theorem 5.16]. This result yields the validity of the chain and product rule for functions in Sobolev spaces, cf. [39, Section 5.4]. Under stronger assumptions, when the domain Ω has a continuous boundary, it is even possible to prove that $C_0^\infty(\mathbb{R}^d)$ is dense in $W^{m,p}(\Omega)$, [1, Theorem 3.22] and [39, Theorem 6.7].

In order to handle the boundary conditions of IBVPs we need to introduce the rather important boundary traces, since function evaluations of functions in Sobolev spaces are in general not well-defined. The next theorem offers a remedy with the help of the so-called trace operator.

Theorem 3.8 (Trace theorem). *Let Ω be bounded and Lipschitz, and $1 \le p < \infty$. Then there exists a bounded linear operator $\gamma_0 : W^{1,p}(\Omega) \to L^p(\partial\Omega)$ such that*

(i) $\gamma_0 u = u|_{\partial\Omega}$ for $u \in C^\infty(\overline{\Omega})$, and

(ii) $\|\gamma_0 u\|_{L^p(\partial\Omega)} \le c\|u\|_{W^{1,p}(\Omega)}$, with a constant c depending on p and Ω.

Proof. The proof is given in [1, Chapter 5] and [39, Theorem 6.15]. □

Remark 3.9. *Note that from now on we always mean by $u = 0$ on $\partial\Omega$ that the trace $\gamma_0 u = 0$ on $\partial\Omega$. In terms of the boundary traces it is possible to characterize the space $W_0^{1,p}(\Omega)$ in the following way, cf. [1, Theorem 5.37],*

$$W_0^{1,p}(\Omega) \coloneqq \left\{ u \in W^{1,p}(\Omega) : u = 0 \text{ on } \partial\Omega \right\}.$$

As mentioned before, the main interest in this thesis lies in the special case of $p = 2$ for which we use the notation

$$H^m(\Omega) \coloneqq W^{m,2}(\Omega) \quad \text{and} \quad H_0^1(\Omega) \coloneqq W_0^{1,2}(\Omega).$$

Moreover, the spaces $H^m(\Omega)$ endowed with the inner product

$$(u,v)_{H^m(\Omega)} \coloneqq \sum_{0\leq|\beta|\leq m} (D^\beta u, D^\beta v)_{L^2(\Omega)}$$

form Hilbert spaces, see [39, Corollary 5.11] and [1, Theorem 3.6]. In particular, for $m = 1$ the inner product can be written as

$$(u,v)_{H^1(\Omega)} = \int_\Omega (u(y)v(y) + \nabla_y u(y) \cdot \nabla_y v(y))\, dy,$$

and the subspace $H_0^1(\Omega) \subset H^1(\Omega)$ incorporates homogenous boundary conditions, i.e.

$$H_0^1(\Omega) = \{u \in H^1(\Omega) : u = 0 \text{ on } \partial\Omega\}.$$

Particularly,

$$|u|^2_{H^1(\Omega)} \coloneqq \int_\Omega |\nabla_y u(y)|^2\, dy \quad \text{and} \quad (u,v)_{H_0^1(\Omega)} \coloneqq \int_\Omega \nabla_y u(y) \cdot \nabla_y v(y)\, dy,$$

define an equivalent norm and inner product on $H_0^1(\Omega)$, respectively, which follow from Friedrichs's inequality, often called as Friedrichs-Poincaré inequality,

$$\|u\|_{L^2(\Omega)} \leq c_F(\Omega)\|\nabla_y u\|_{L^2(\Omega)} \quad \text{for all } u \in H_0^1(\Omega), \tag{3.12}$$

see [1, Theorem 6.30] and [1, Corollary 6.31]. Furthermore, the boundary traces $\gamma_0 u$ belong to the space $H^{1/2}(\partial\Omega) \subset L^2(\partial\Omega)$ and can be categorized as fractional order or broken Sobolev spaces, cf. [1, Chapter 7] and [39, Section 6.11].

The dual space of $H_0^1(\Omega)$, denoted by $H^{-1}(\Omega)$, is characterized as the completion of $L^2(\Omega)$ with respect to the norm

$$\|f\|_{H^{-1}(\Omega)} \coloneqq \sup_{0\neq v\in H_0^1(\Omega)} \frac{|\langle f, v\rangle_\Omega|}{\|v\|_{H_0^1(\Omega)}}, \tag{3.13}$$

where $\langle\cdot,\cdot\rangle_\Omega$ is the duality pairing as extension of the inner product in $L^2(\Omega)$, see [1].

Remark 3.10. *Note that for moving domains as described in Section 3.2 the domain $\Omega(t)$ is considered to be time-dependent. Since the deformation φ does not change the shape or topology of the domain, and for a specific time point $t \in (0,T)$, $\Omega(t)$ can be identified as a fixed domain, i.e. $\Omega(t) = \Omega$, with respect to its variable in the current configuration, i.e. $y = \varphi(x,t)$, the definitions and results of this section apply also for the domain $\Omega(t)$.*

3.3.2 Bochner spaces

We are now in the stage to introduce the Bochner spaces in order to pose IBVPs in the weak sense on the full space-time cylinder Q. We refer to [1, Chapter 7], [35, Chapter XVIII], [45, Section 5.9.2], [67, Section 5.1.1], [100], [165, Section 2.4 and Section 2.6] and [166, Chapter 23] for a detailed description of Bochner spaces. Now, let $0 < T < \infty$, and Q be the open space-time cylinder as defined in (3.5). Also, let V be a real Banach space with norm $\|\cdot\|_V$, then we can define the space of measurable and integrable functions on $(0,T)$ with values in V and finite norm as

$$L^p(0,T;V) \coloneqq \left\{ v : (0,T) \to V \mid \|v\|_{L^p(0,T;V)} < \infty \right\}, \tag{3.14}$$

where

$$\|v\|_{L^p(0,T;V)} \coloneqq \left(\int_0^T \|v(t)\|_V^p \, dt \right)^{1/p} \quad \text{for } 1 \leq p < \infty.$$

In the case of $p = 2$ and when V is a separable real Hilbert space, then the Bochner space $L^2(0,T;V)$ becomes also a Hilbert space with respect to the inner product

$$(u,v)_{L^2(0,T;V)} \coloneqq \int_0^T (u(t), v(t))_V \, dt \quad \text{for } u, v \in L^2(0,T;V),$$

see [100]. Additionally, the dual space $[L^2(0,T;V)]^\star$ and the space $L^2(0,T;V^\star)$ are isometric [166, Section 23.3, Convention 23.8] with respect to the duality pairing

$$\langle f, v \rangle_{L^2(0,T;V^\star),L^2(0,T;V)} = \int_0^T \langle f(t), v(t) \rangle_{V^\star,V} \, dt,$$

where $V^\star$ denotes the dual space of V and $\langle \cdot, \cdot \rangle_{V^\star,V}$ the usual duality pairing in V. In general, the Bochner-Sobolev space for $m \in \mathbb{N}_0$ is defined as

$$H^m(0,T;V) \coloneqq \{ v \in L^2(0,T;V) : (\partial t)^k v \in L^2(0,T;V) \text{ for } 0 \leq k \leq m \},$$

where $v = (\partial t)^k u$ denotes the k^{th}-weak derivative of $u \in H^m(0,T;V)$ with respect to time, i.e.

$$\int_0^T \frac{\partial^k}{\partial t^k} \phi(t) u(t) \, dt = (-1)^k \int_0^T \phi(t) v(t) \, dt \quad \text{for all } \phi \in C_0^\infty(0,T), \tag{3.15}$$

cf. [165, Section 2.4], which is again a Hilbert space, when equipped with the corresponding inner product

$$(u,v)_{H^m(0,T;V)} \coloneqq \sum_{0 \leq k \leq m} \int_0^T \left((\partial t)^k u(t), (\partial t)^k v(t) \right)_V \, dt.$$

For the specific case $m = 1$, it can be shown that $H^1(0,T;V)$ is embedded in $C([0,T];V)$, where $C([0,T];V)$ comprises all continuous functions $v : [0,T] \to V$ with

$$\|v\|_{C([0,T];V)} = \max_{0\le t\le T} \|v(t)\|_V < \infty,$$

see [45, Section 5.9.2, Theorem 2]. In particular, this embedding yields, that the expression $u(\cdot,0) = 0$ has a precise meaning, hence the spaces

$$\begin{aligned} H^1_{0,}(0,T;V) &\coloneqq \left\{ v \in H^1(0,T;V) : v(0) = 0 \right\}, \\ H^1_{,0}(0,T;V) &\coloneqq \left\{ v \in H^1(0,T;V) : v(T) = 0 \right\}, \end{aligned}$$

are well-defined and closed subspaces of $H^1(0,T;V)$. Finally, in view of the upcoming analysis we will need the Bochner-Sobolev space

$$\begin{aligned} W(0,T;V,V^\star) &\coloneqq \left\{ v \in L^2(0,T;V) : \partial_t v \in L^2(0,T;V^\star) \right\} \\ &= L^2(0,T;V) \cap H^1(0,T;V^\star), \end{aligned}$$

which is a Hilbert space equipped with the norm

$$\|u\|^2_{W(0,T;V,V^\star)} = \|u\|^2_{L^2(0,T;V)} + \|\partial_t u\|^2_{L^2(0,T;V^\star)} = \int_0^T \left[\|u(t)\|^2_V + \|\partial_t u(t)\|^2_{V^\star} \right] \, dt$$

see [35, Chapter XVIII, Paragraph 1, Sec. 2, Prop. 6]. For the case $V = H^1_0(\Omega)$, we introduce the notation

$$W(Q) \coloneqq L^2(0,T;H^1_0(\Omega)) \cap H^1(0,T;H^{-1}(\Omega)), \tag{3.16}$$

where $W(Q)$ forms a Hilbert space with respect to the inner product

$$(u,v)_{W(Q)} \coloneqq \int_0^T \int_\Omega \nabla_y u(y,t) \cdot \nabla_y v(y,t) \, dy \, dt + \int_0^T (\partial_t u(\cdot,t), \partial_t v(\cdot,t))_{H^{-1}(\Omega)} \, dt, \tag{3.17}$$

see [161, Theorem 25.4], and the norm defined as

$$\|v\|_{W(Q)} \coloneqq \left(\int_0^T \int_\Omega |\nabla_y u(y,t)|^2 \, dy \, dt + \int_0^T \|\partial_t u(\cdot,t)\|^2_{H^{-1}(\Omega)} \, dt \right)^{1/2},$$

where the norm in the dual space $H^{-1}(\Omega)$ is given as in (3.13) by

$$\|\partial_t u(\cdot,t)\|_{H^{-1}(\Omega)} = \sup_{0\neq v\in H^1_0(\Omega)} \frac{|\langle \partial_t u(\cdot,t), v\rangle_\Omega|}{|v|_{H^1(\Omega)}},$$

and the abstract inner product $(\cdot,\cdot)_{H^{-1}(\Omega)}$ induces the norm $\|\cdot\|_{H^{-1}(\Omega)} = \sqrt{(\cdot,\cdot)_{H^{-1}(\Omega)}}$. Moreover, the space $W(Q)$ is continuously embedded in $C([0,T];L^2(\Omega))$, i.e. there exists a constant c_{em} such that for every $u \in W(Q)$

$$\max_{t\in[0,T]} \|u(\cdot,t)\|_{L^2(\Omega)} = \max_{t\in[0,T]} \left(\int_\Omega |u(y,t)|^2 \, dy \right)^{1/2} \leq c_{em} \|u\|_{W(Q)},$$

cf. [166, Proposition 23.23]. Due to this continuous embedding, the initial condition

$$u(\cdot,0) = u_0 \quad \text{in } L^2(\Omega)$$

has a precise meaning, which leads to the fact that the subspace

$$W_{0,}(Q) \coloneqq \{v \in W(Q) : v(\cdot,0) = 0\} \subset W(Q) \tag{3.18}$$

incorporating the initial condition, is again a Hilbert space with respect to the inner product (3.17) of $W(Q)$.

Remark 3.11. *We want to point out, that the continuous embedding of $W(Q)$ into $C([0,T];L^2(\Omega))$ is related to the so-called evolution triple*

$$H_0^1(\Omega) \subset L^2(\Omega) \subset H^{-1}(\Omega),$$

or, in general, if H and V are real separable Hilbert spaces, then $V \subset H \subset V^\star$, where V is dense in H and H is identified by its dual $H^\star$, which is used in most literature, e.g. [35, 44, 166].

Remark 3.12. *Note that in the definition of the space $W(Q)$ in* (3.16)*, the Hilbert space V does not depend on time as desired for our applications. In order to adjust the space for our purpose, we need to define*

$$\begin{aligned} W(Q) &\coloneqq \left\{ v \in L^2(0,T;H_0^1(\Omega(t))) : \frac{d}{dt} v \in L^2(0,T;H_0^1(\Omega(t))^\star) \right\} \\ &= L^2(0,T;H_0^1(\Omega(t))) \cap H^1(0,T;H^{-1}(\Omega(t))), \end{aligned} \tag{3.19}$$

where now $\frac{d}{dt}$ denotes the weak total derivative as in (3.15)*, i.e. $\frac{d}{dt}u = v$ for*

$$\int_0^T \frac{d}{dt}\phi(t)u(t) \, dt = -\int_0^T \phi(t)v(t) \, dt \quad \text{for all } \phi \in C_0^\infty(0,T).$$

To the best of our knowledge, no analysis has been carried out for the spaces in (3.19) *using time dependent spaces $V = H_0^1(\Omega(t))$ so far. The first considerations of such*

spaces are given in [59] and [60], assuming $W(Q)$ is a Hilbert space with respect to the inner product

$$(u,v)_{W(Q)} := \int_Q \nabla_y u(y,t)\cdot\nabla_y v(y,t)\;dy\;dt + \int_0^T \left(\frac{d}{dt}u(\cdot,t),\frac{d}{dt}v(\cdot,t)\right)_{H^{-1}(\Omega(t))} dt,$$

and norm

$$\|v\|_{W(Q)} := \left(\int_Q |\nabla_y u(y,t)|^2\;dy\;dt + \int_0^T \|\frac{d}{dt}u(\cdot,t)\|^2_{H^{-1}(\Omega(t))}\;dt\right)^{1/2},$$

where

$$\|\frac{d}{dt}u(\cdot,t)\|_{H^{-1}(\Omega(t))} = \sup_{0\neq z\in H_0^1(\Omega(t))} \frac{|\langle \frac{d}{dt}u(\cdot,t),z\rangle_{\Omega(t)}|}{|z|_{H^1(\Omega(t))}},$$

and $\|\cdot\|_{H^{-1}(\Omega(t))} = \sqrt{(\cdot,\cdot)_{H^{-1}(\Omega(t))}}$ is induced by the abstract inner product $(\cdot,\cdot)_{H^{-1}(\Omega(t))}$. We want to highlight, that the proofs of these statements are very technical, however they are assumed to be similarly transferable from [45], [100] or [166]. Another treatment of the space $W(Q)$ for moving domains $\Omega(t)$ has been recently considered in [26], where a transformation to the initial state enables the usual definition of the space $W(Q)$.

3.4 Space-time approximation spaces by simplicial finite elements

In general, in the field of computational mathematics we approximate the solution of partial differential equations by numerical schemes, so also of IBVPs. A widely popular scheme is the Finite Element Method (FEM), which will be used for all numerical examples throughout this thesis. In this section, we recall the basic notations of the finite element discretization and refer to [22, 24, 44, 143] for further details.

Let $\Omega(t) \subset \mathbb{R}^d$ be bounded and Lipschitz for every $t \in [0,T]$. For simplicity, we assume that $\Omega(t)$ is an interval for $d = 1$, or polygonal for $d = 2$, or polyhedral for $d = 3$. Then, the space-time cylinder $Q \subset \mathbb{R}^{d+1}$ as defined in (3.5) is polygonal for $d = 1$, or polyhedral for $d = 2$, or polychoral for $d = 3$. Further, let $\{\mathcal{T}_h\}_{h>0}$ be a sequence of decompositions (triangulations or meshes) with

$$\overline{Q} = \overline{\mathcal{T}_h} = \bigcup_{\ell=1}^N \overline{\tau_\ell}, \tag{3.20}$$

where $\mathcal{T}_h = \{\tau_\ell\}_{\ell=1}^N$ is a decomposition of Q into non-overlapping, simplicial space-time elements $\tau_\ell \subset \mathbb{R}^{d+1}$, $\ell = 1, \dots, N$, i.e. $\tau_\ell \cap \tau_k = \emptyset$ for all $\ell \neq k$. A simplicial element, or simplex, is defined as the convex hull of $\{(\tilde{y}_0, \tilde{t}_0), \dots, (\tilde{y}_{d+1}, \tilde{t}_{d+1})\}$, where $\{(\tilde{y}_i, \tilde{t}_i)\}_{i=0}^{d+1}$ is a family of points in $\mathbb{R}^{d+1}$, also called vertices of the simplex, for which the vectors $\{(\tilde{y}_1, \tilde{t}_1) - (\tilde{y}_0, \tilde{t}_0), \dots, (\tilde{y}_{d+1}, \tilde{t}_{d+1}) - (\tilde{y}_0, \tilde{t}_0)\}$ are linearly independent, see [44, Section 1.2.3]. The set of all vertices, denoted by $\{(y_k, t_k)\}_{k=1}^M$, generates the nodes of the decomposition $\mathcal{T}_h$ and $h = h_{\max} = \max_{\ell=1,\dots,N} h_\ell$ is the global mesh size, where the local mesh sizes h_ℓ are defined by the volumes Δ_ℓ of the finite elements τ_ℓ as

$$h_\ell = \Delta_\ell^{1/(d+1)} = \left(\int_{\tau_\ell} dydt \right)^{1/(d+1)} \qquad \text{for } \ell = 1, \dots, N, \tag{3.21}$$

while $h_{\min} = \min_{\ell=1,\dots,N} h_\ell$ is the minimal local mesh size, cf. [143, Section 9.1]. We will always assume that the decomposition (3.20) is

- admissible, i.e. two neighboring elements join either an edge ($d = 1, 2, 3$), a face ($d = 2, 3$), or a tetrahedron ($d = 3$), or equivalently speaking, we avoid hanging nodes, cf. [115]; and
- shape regular, i.e. there exists a constant c_F independent of the decomposition $\mathcal{T}_h$, such that

$$d_\ell \leq c_F r_\ell \quad \text{for all } \ell = 1, \dots, N, \tag{3.22}$$

  where

$$d_\ell = \sup_{(y_1,t_1),(y_2,t_2) \in \tau_\ell} |(y_1, t_1) - (y_2, t_2)|$$

  is the diameter of the element τ_ℓ and

$$r_\ell = \arg\max\{r > 0 : B_r((y,t)) \subset \tau_\ell, \text{ for any } (y,t) \in \tau_\ell\}$$

  is the radius of the largest ball that can be inscribed in τ_ℓ, see [143, Section 9.1].

We say the family of decompositions $\{\mathcal{T}_h\}_{h>0}$ consists of shape regular simplicial finite elements, if there is a constant $c_F > 0$ independent of every $\mathcal{T}_h$, such that (3.22) holds for all $\mathcal{T}_h$. Moreover, $\{\mathcal{T}_h\}_{h>0}$ is called locally quasi-uniform, if

$$\frac{h_\ell}{h_k} \leq c_L$$

for all neighboring elements $\overline{\tau_\ell} \cap \overline{\tau_k} \neq \emptyset$ and a constant $c_L > 0$ independent of h. Furthermore, any simplicial finite element τ_ℓ can be transformed to the reference element

$$\tau = \left\{ \xi = (\xi_1, \ldots, \xi_d, \xi_{d+1} = \hat{t}\,)^\top \in \mathbb{R}^{d+1} : \xi_i > 0 \text{ for } i = 1, \ldots, d+1, \sum_{i=1}^{d+1} \xi_i < 1 \right\},$$

which is a simplex with one vertex at the origin and one vertex at each axis, by using the bijective affine linear mapping (local parametrization) $y_\tau : \tau \to \tau_\ell$,

$$y_\tau(\xi) = \begin{pmatrix} \tilde{y}_0 \\ \tilde{t}_0 \end{pmatrix} + \sum_{i=1}^{d+1} \xi_i \left(\begin{pmatrix} \tilde{y}_i \\ \tilde{t}_i \end{pmatrix} - \begin{pmatrix} \tilde{y}_0 \\ \tilde{t}_0 \end{pmatrix} \right) = \begin{pmatrix} \tilde{y}_0 \\ \tilde{t}_0 \end{pmatrix} + J_\tau \xi,$$

where $(\tilde{y}_0, \tilde{t}_0)$ is the vertex of τ_ℓ to which the origin is mapped, and $J_\tau = \frac{\partial y_\tau}{\partial \xi} \in \mathbb{R}^{d+1} \times \mathbb{R}^{d+1}$ is the Jacobian of the map. Specifically, when using (3.21), we obtain that

$$h_\ell^{d+1} = \int_{\tau_\ell} dydt = \int_\tau |\mathrm{det} J_\tau| \, d\xi = |\mathrm{det} J_\tau| \int_\tau d\xi = |\mathrm{det} J_\tau| |\tau|, \tag{3.23}$$

cf. [143, Section 9.1] or [144], with

$$|\tau| = \begin{cases} \frac{1}{2} & \text{for } d = 1, \\ \frac{1}{6} & \text{for } d = 2, \\ \frac{1}{24} & \text{for } d = 3. \end{cases}$$

Now, let us define the approximation space of piecewise linear and globally continuous functions as

$$S_h^1(\mathcal{T}_h) \coloneqq \mathrm{span}\{\phi_k\}_{k=1}^M \subset H^1(Q), \tag{3.24}$$

where $\{\phi_k\}_{k=1}^M$ denotes the nodal basis given by

$$\phi_k(y,t) \coloneqq \begin{cases} 1 & \text{for } (y,t) = (y_k, t_k), \\ 0 & \text{for } (y,t) = (y_j, t_j), j \neq k, \\ \text{linear} & \text{elsewhere.} \end{cases}$$

Those functions, which are associated to the global degrees of freedom (dofs), are defined locally by using suitable form functions. In our case, using Lagrangian finite elements of first order, the global dofs are equal to the number of vertices of the space-time mesh (3.20). Hence, any function $v_h \in S_h^1(\mathcal{T}_h)$ admits the representation

$$v_h(y,t) = \sum_{k=1}^M v_k \phi_k(y,t) \quad \text{for } (y,t) \in \overline{Q},$$

where the coefficient vector $\mathbf{v}_h \in \mathbb{R}^M$ with $\mathbf{v}_h[k] = v_k$ gives an alternative representation of v_h, see [143, Section 9.3]. The space-time interpolation operator $I_h : C(\overline{Q}) \to S_h^1(\mathcal{T}_h)$ is given by

$$I_h v(y,t) = \sum_{k=1}^{M} v(y_k, t_k)\phi_k(y,t) \quad \text{for } (y,t) \in \overline{Q}.$$

Note that with the help of the Sobolev embedding theorem [24, Theorem 1.4.6], i.e. the Sobolev space $H^m(Q)$ is embedded into $C(\overline{Q})$ for $2m > (d+1)$, the following local interpolation error estimate holds true for $d = 1, 2$ assuming smooth solutions in $H^2(Q)$.

THEOREM 3.13. *Let $\mathcal{T}_h = \{\tau_\ell\}_{\ell=1}^N$ be a locally quasi-uniform decomposition of the space-time cylinder $Q \subset \mathbb{R}^{d+1}$ for $d = 1, 2$ and let $v|_{\tau_\ell} \in H^2(\tau_\ell)$ for $l = 1, \dots, N$. Then, the local error estimate*

$$\|v - I_h v\|_{L^2(\tau_\ell)} \leq c h_\ell^2 |v|_{H^2(\tau_\ell)}$$

holds for $I_h : H^2(\tau_\ell) \to S_h^1(\mathcal{T}_h)$ with a constant $c > 0$ independent of the mesh size h.

Proof. The proof is given in [143, Theorem 9.9]. □

As a direct consequence, the global interpolation error estimate

$$\|v - I_h v\|_{L^2(\mathcal{T}_h)} \leq c h^2 |v|_{H^2(\mathcal{T}_h)} \quad \text{for } v \in H^2(\mathcal{T}_h), \tag{3.25}$$

applies for $I_h : H^2(\mathcal{T}_h) \to S_h^1(\mathcal{T}_h)$, and, in the same way as in Theorem 3.13, the following error estimates are valid,

$$\begin{aligned} \|\nabla_{(y,t)}(v - I_h v)\|_{L^2(\tau_\ell)} \leq \|v - I_h v\|_{H^1(\tau_\ell)} \leq c h_\ell |v|_{H^2(\tau_\ell)} \quad &\text{for } v|_{\tau_\ell} \in H^2(\tau_\ell), \\ \|\nabla_{(y,t)}(v - I_h v)\|_{L^2(\mathcal{T}_h)} \leq \|v - I_h v\|_{H^1(\mathcal{T}_h)} \leq c h |v|_{H^2(\mathcal{T}_h)} \quad &\text{for } v \in H^2(\mathcal{T}_h). \end{aligned} \tag{3.26}$$

For $d = 3$, the Sobolev embedding theorem does not hold for functions in $H^2(Q)$, indicating that the nodal interpolation is not well-defined for those functions. A remedy offers the so-called quasi-interpolation operator, see e.g. [29] introduced by Clément or [139] by Scott and Zhang, or, in context of space-time discretization methods, e.g. [101] and [134]. However, we only consider problems of dimension $d = 1, 2$ in this work and refer to the mentioned references as well as [143, Section 9.4] for an extensive analysis of other interpolation operators.

Furthermore, we briefly introduce projection operators which allow us to weaken the global continuity assumption required for the application of the interpolation

operator. The global space-time L^2-projection $Q_h : L^2(\mathcal{T}_h) \to S_h^1(\mathcal{T}_h)$ is defined as the unique solution of the variational problem

$$(Q_h u, v_h)_{L^2(\mathcal{T}_h)} := \sum_{\ell=1}^{N} \int_{\tau_\ell} Q_h u(y,t) v_h(y,t)\, dydt = (u, v_h)_{L^2(\mathcal{T}_h)} \tag{3.27}$$

for all $v_h \in S_h^1(\mathcal{T}_h)$, and the global H^1-projection $P_h : H^1(\mathcal{T}_h) \to S_h^1(\mathcal{T}_h)$ is defined as the unique solution of

$$\begin{aligned}(P_h u, v_h)_{H^1(\mathcal{T}_h)} :=& (Q_h u, v_h)_{L^2(\mathcal{T}_h)} + (\nabla_{(y,t)} Q_h u, \nabla_{(y,t)} v_h)_{L^2(\mathcal{T}_h)} \\ =& (u, v_h)_{L^2(\mathcal{T}_h)} + (\nabla_{(y,t)} u, \nabla_{(y,t)} v_h)_{L^2(\mathcal{T}_h)}\end{aligned} \tag{3.28}$$

for all $v_h \in S_h^1(\mathcal{T}_h)$. When choosing $v_h = Q_h u$ and $v_h = P_h u$ in (3.27) and (3.28), respectively, we deduce the stability estimates

$$\begin{aligned}\|Q_h u\|_{L^2(\mathcal{T}_h)} &\le \|u\|_{L^2(\mathcal{T}_h)} \quad \text{for all } u \in L^2(\mathcal{T}_h), \\ \|P_h u\|_{H^1(\mathcal{T}_h)} &\le \|u\|_{H^1(\mathcal{T}_h)} \quad \text{for all } u \in H^1(\mathcal{T}_h),\end{aligned}$$

see [143, Section 9.3]. Additionally, making use of the Galerkin orthogonalities

$$\begin{aligned}(u - Q_h u, v_h)_{L^2(\mathcal{T}_h)} &= 0 \quad \text{for all } v_h \in L^2(\mathcal{T}_h), \\ (u - P_h u, v_h)_{H^1(\mathcal{T}_h)} &= 0 \quad \text{for all } v_h \in H^1(\mathcal{T}_h),\end{aligned}$$

the error of the L^2-projection (3.27) and the H^1-projection (3.28), respectively, can be estimated by the interpolation errors (3.25) and (3.26) considering enough regularity, i.e. for $u \in H^2(\mathcal{T}_h)$ we have

$$\begin{aligned}\|u - Q_h u\|_{L^2(\mathcal{T}_h)} &\le \|u - I_h u\|_{L^2(\mathcal{T}_h)} \le c h^2 |u|_{H^2(\mathcal{T}_h)}, \\ \|u - P_h u\|_{H^1(\mathcal{T}_h)} &\le \|u - I_h u\|_{H^1(\mathcal{T}_h)} \le c h |u|_{H^2(\mathcal{T}_h)}.\end{aligned}$$

We can summarize the latter to obtain the approximation property of the space-time approximation space $S_h^1(\mathcal{T}_h)$ of piecewise linear and continuous functions.

THEOREM 3.14. *Let $\mathcal{T}_h = \{\tau_\ell\}_{\ell=1}^N$ be a locally quasi-uniform decomposition of the space-time cylinder $Q \subset \mathbb{R}^{d+1}$ for $d = 1, 2$, and let $u \in H^m(\mathcal{T}_h)$ for $m = \sigma, \dots, 2$ and $\sigma = 0, 1$. Then,*

$$\inf_{v_h \in S_h^1(\mathcal{T}_h)} \|u - v_h\|_{H^\sigma(\mathcal{T}_h)} \le c h^{m-\sigma} |u|_{H^m(\mathcal{T}_h)},$$

with a constant $c > 0$ independent of the mesh size h.

Proof. Cf. [143, Theorem 9.10]. For the case $d = 3$ a similar estimate in terms of the quasi-interpolation operator is given, see e.g. [101, Theorem 2.35]. □

Finally, we introduce the rather important inverse inequalities, which play an important role in the finite element error analysis and are based on the equivalence of norms in finite-dimensional spaces.

THEOREM 3.15. *Let $\mathcal{T}_h = \{\tau_\ell\}_{\ell=1}^N$ be a decomposition and $v_h \in S_h^1(\mathcal{T}_h)$. Then, there holds the local inverse inequality*

$$\|\nabla_{(y,t)} v_h\|_{L^2(\tau_\ell)} \leq c_I h_\ell^{-1} \|v_h\|_{L^2(\tau_\ell)}$$

for a positive constant c_I. Moreover, it holds true that

$$\|\nabla_{(y,t)} v_h\|_{L^2(\mathcal{T}_h)}^2 \leq c_I \sum_{\ell=1}^N h_\ell^{-2} \|v_h\|_{L^2(\tau_\ell)}^2.$$

Proof. The proof is given in [143, Lemma 9.6 and Lemma 9.8]. □

REMARK 3.16. *At this point we want to highlight, that the triangulation* (3.20) *already considers the moving domain, since the motion is known in advance. However, although the domain $\Omega(t)$ is moving, i.e. it analytically depends on time, and so also the space-time cylinder Q, the decomposition is fixed but completely unstructured capturing the motion, hence the used elements are the standard simplicial finite elements in space. For more details about different finite elements, e.g. higher order elements, curved elements or prismatic elements, we refer for instance to the classical books by Braess [22] or Ern and Guermond [44].*

3.5 Space-time variational methods in Bochner spaces

3.5.1 Solvability analysis

In this section we recall the theory about the existence of a unique solution and the finite element discretization for IBVPs in the setting of Bochner spaces. We summarize the method proposed by Steinbach [144], considering a Petrov-Galerkin variational formulation of IBVPs. Pioneered by this work, the goal is to extend the analysis in [144] to linear and nonlinear elliptic-parabolic interface problems posed on stationary and moving domains, which will be the aim of Chapter 4. The eddy current equation (2.24) is a special form of the more general parabolic evolution equation (heat equation) considered in [144],

$$\begin{aligned} c_H \frac{\partial}{\partial t} u(x,t) - \operatorname{div}_x [A(x,t) \nabla_x u(x,t)] &= f(x,t) && \text{for } (x,t) \in Q \coloneqq \Omega \times (0,T), \\ u(x,t) &= 0 && \text{for } (x,t) \in \partial\Omega \times (0,T), \\ u(x,0) &= u_0(x) && \text{for } x \in \Omega, \end{aligned} \tag{3.29}$$

where $\Omega \subset \mathbb{R}^d$ for $d = 1, 2, 3$, is bounded and Lipschitz, $c_H > 0$ is the positive heat capacity constant and $A(x,t) \in \mathbb{R}^{d\times d}$ is a symmetric and uniformly positive definite coefficient matrix in Q, i.e. there exist constants $\underline{c}^A, \overline{c}^A > 0$, such that

$$0 < \underline{c}^A \|\xi\|^2 \leq \xi^\top A(x,t)\xi \leq \overline{c}^A \|\xi\|^2 \quad \text{for all } \xi = \{\xi_1, \ldots, \xi_{d+1}\} \in \mathbb{R}^{d+1}\backslash\{0\}.$$

In many cases and for all of our applications, the coefficient matrix $A(x,t)$ is constant in time, hence we can write $A(x,t) = A(x)$. Furthermore, $f \in L^2(0,T;H^{-1}(\Omega))$ is a given source term, and we assume that $u_0 \in L^2(\Omega)$. We start with the case of homogeneous initial conditions, i.e. $u_0 = 0$. Recalling the Bochner spaces (3.14), (3.16) and (3.18), the Petrov-Galerkin space-time variational formulation of (3.29) with homogenous initial conditions is to find $u \in W_{0,}(Q)$, such that

$$a(u,v) = l(v) \quad \text{for all } v \in L^2(0,T;H_0^1(\Omega)), \tag{3.30}$$

where

$$\begin{aligned} a(u,v) &= \int_0^T \int_\Omega \left[c_H \frac{\partial}{\partial t} u(x,t)v(x,t) + [A(x)\nabla_x u(x,t)] \cdot \nabla_x v(x,t) \right] \, dxdt \\ l(v) &= \int_0^T \int_\Omega f(x,t)v(x,t) \, dxdt. \end{aligned}$$

The following central theorem guarantees the existence of a unique solution of space-time variational formulations with different trial and test spaces.

THEOREM 3.17 (Banach-Nečas-Babuška). *Let X be a real Banach space and Y a real, reflexive Banach space. Further, let $a : X \times Y \to \mathbb{R}$ be a bilinear form and $l \in Y^\star$ a continuous linear form. Then the variational problem: Find $u \in X$, such that*

$$a(u,v) = l(v) \quad \textit{for all } v \in Y,$$

has a unique solution if and only if the following conditions hold.

(BNB1) *(Continuity).* $\exists c_2^a > 0 : \quad |a(u,v)| \leq c_2^a \|u\|_X \|v\|_Y \quad \forall u \in X, v \in Y.$

(BNB2) *(Inf-sup condition).* $\exists c_1^a > 0 : \quad \inf_{0\neq u\in X} \sup_{0\neq v\in Y} \frac{a(u,v)}{\|u\|_X\|v\|_Y} \geq c_1^a.$

(BNB3) *(Surjectivity).* $\forall v \in Y\backslash\{0\} : \exists u \in X : \quad a(u,v) \neq 0.$

In addition, the following a priori estimate is satisfied,

$$\|u\|_X \leq \frac{1}{c_1^a} \|l\|_{Y^\star}.$$

Proof. The proof is given in [22, Theorem 3.6] and [44, Theorem 2.6]. □

REMARK 3.18. *The continuous, linear operator $A : X \to Y^\star$, associated with the bilinear form $a : X \times Y \to \mathbb{R}$, is bijective and its inverse $A^{-1} : Y^\star \to X$ is continuous, i.e. A is an isomorphism, which is equivalent to the conditions (BNB1) - (BNB3). In particular, the surjectivity in (BNB3) is equivalent to the injectivity of the inverse operator A^{-1}.*

As in [144], we first consider for given $u(x,t)$ the elliptic Dirichlet boundary value problem

$$\begin{aligned} -\mathrm{div}_x\left[A(x)\nabla_x w_u(x,t)\right] &= c_H \frac{\partial}{\partial t} u(x,t) \quad \text{for } (x,t) \in Q, \\ w_u(x,t) &= 0 \qquad\qquad\qquad\quad \text{for } (x,t) \in \partial\Omega \times (0,T), \end{aligned} \tag{3.31}$$

whose related variational formulation is to find $w_u \in Y = L^2(0,T;H_0^1(\Omega))$, such that

$$\int_0^T \int_\Omega \left[A(x)\nabla_x w_u(x,t)\right] \cdot \nabla_x v(x,t)\; dxdt = \int_0^T \int_\Omega c_H \frac{\partial}{\partial t} u(x,t) v(x,t)\; dxdt \tag{3.32}$$

for all $v \in Y$, where $\partial_t u \in Y^\star = L^2(0,T;H^{-1}(\Omega))$. Since the coefficient matrix is uniformly positive definite, the norm

$$\|v\|_Y := \sqrt{\int_0^T \int_\Omega \left[A(x)\nabla_x v(x,t)\right] \cdot \nabla_x v(x,t)\; dxdt}$$

is an equivalent norm in $L^2(0,T;H_0^1(\Omega))$. Hence, the unique solvability of (3.32) follows due to the lemma of Lax-Milgram [22, Theorem 2.5], and we conclude that

$$\|w_u\|_Y = \|c_H \partial_t u\|_{Y^\star},$$

where the dual norm is defined in terms of the duality pairing,

$$\|c_H \partial_t u\|_{Y^\star} := \sup_{0 \neq v \in Y} \frac{|\langle c_H \partial_t u, v\rangle_Q|}{\|v\|_Y}.$$

The related energy norm (graph norm) in $X = W_{0,}(Q) \subset Y$ is defined as

$$\|u\|_X := \sqrt{\|u\|_Y + \|c_H \partial_t u\|_{Y^\star}} = \sqrt{\|u\|_Y + \|w_u\|_Y},$$

where $w_u \in Y$ is the unique solution of (3.32).

Note that the variational formulation (3.30) and the related elliptic Dirichlet boundary value problem (3.32) require homogenous initial data. In order to incorporate an inhomogeneous initial condition as given in (3.29), we need to apply homogenization, i.e. $u = \widetilde{u} + \widetilde{u}_0$, where $u, \widetilde{u}_0 \in W(Q)$, $\widetilde{u} \in W_{0,}(Q)$ and $\widetilde{u}_0 = Eu_0$ is a continuous and linear extension of $u_0 \in L^2(\Omega)$. Thus, we are in position to state the solvability result of the homogenized variational formulation of (3.29), which is to find $\widetilde{u} \in X$, such that

$$a(\widetilde{u}, v) = l(v) - a(\widetilde{u}_0, v) \quad \text{for all } v \in Y. \tag{3.33}$$

Now, applying Theorem 3.17 we are able to derive the unique solvability of (3.33).

THEOREM 3.19. *Let $f \in L^2(0,T;H^{-1}(\Omega))$ be a given right-hand side. Further, let $\widetilde{u}_0 \in W(Q)$ be some extension of the given initial datum $u_0 \in H_0^1(\Omega)$. Then there exists a unique solution $\widetilde{u} \in X$ of (3.33) satisfying*

$$\|\widetilde{u}\|_X \leq \|f\|_{L^2(0,T;H^{-1}(\Omega))} + \sqrt{2}\|\widetilde{u}_0\|_X.$$

Proof. The three properties (BNB1) - (BNB3) of Theorem 3.17 have to be verified in order to conclude unique solvability of the variational problem (3.33). Note that the inclusion $X \subset Y$ is essential for the verification of (BNB2) and (BNB3), however this is naturally given due to the definition of the spaces. A general proof is given in [44, Theorem 6.6], the proof with the specific constants in [144, Corollary 2.3] and [165, Theorem 3.2.4]. In particular, it holds the continuity (BNB1)

$$|a(\widetilde{u}, v)| \leq \sqrt{2}\|\widetilde{u}\|_X \|v\|_Y \quad \text{for all } \widetilde{u} \in X \text{ and } v \in Y,$$

and the inf-sup condition (BNB2) [144, Theorem 2.1], [91]

$$\inf_{0 \neq \widetilde{u} \in X} \sup_{0 \neq v \in Y} \frac{a(\widetilde{u}, v)}{\|\widetilde{u}\|_X \|v\|_Y} \geq 1,$$

from which the above stability estimate follows. The surjectivity (BNB3) can be obtained for $0 \neq v \in Y$ by choosing

$$\widehat{u}(x,t) = \int_0^t v(x,\tau)\, d\tau, \quad \frac{\partial}{\partial t}\widehat{u}(x,t) = v(x,t) \quad \text{for } x \in \Omega, t \in [0,T].$$

By definition, we have $\widehat{u} \in X$, cf. [97], and we deduce that

$$\begin{aligned} a(\widehat{u}, v) &= \int_0^T \int_\Omega \left[c_H \frac{\partial}{\partial t}\widehat{u}(x,t) v(x,t) + [A(x)\nabla_x \widehat{u}(x,t)] \cdot \nabla_x v(x,t) \right] dxdt \\ &= \int_0^T \int_\Omega \left[c_H [\frac{\partial}{\partial t}\widehat{u}(x,t)]^2 + [A(x)\nabla_x \widehat{u}(x,t)] \cdot \nabla_x \frac{\partial}{\partial t}\widehat{u}(x,t) \right] dxdt \\ &\geq c_H \|\partial_t \widehat{u}\|^2_{L(Q)} + \frac{1}{2}\, \underline{c}^A \|\nabla_x \widehat{u}(T)\|^2_{L^2(\Omega)} > 0, \end{aligned}$$

where the last estimate follows from the chain rule

$$\begin{aligned}
&\int_0^T \int_\Omega [A(x)\nabla_x \widehat{u}(x,t)]\cdot\nabla_x \frac{\partial}{\partial t}\widehat{u}(x,t)\; dxdt \\
&\qquad = \int_0^T \int_\Omega \frac{1}{2}\frac{\partial}{\partial t}\Big([A(x)\nabla_x \widehat{u}(x,t)]\cdot\nabla_x \widehat{u}(x,t)\Big)\; dxdt \\
&\qquad \geq \frac{1}{2}\,\underline{c}^A \int_0^T \int_\Omega \frac{\partial}{\partial t}[\nabla_x \widehat{u}(x,t)]^2\; dxdt \\
&\qquad = \frac{1}{2}\,\underline{c}^A \int_\Omega [\nabla_x \widehat{u}(x,T)]^2\; dx > 0,
\end{aligned} \tag{3.34}$$

with $\widehat{u}(x,0) = 0$ for $x \in \Omega$.

When using the triangle inequality for $u \in W(Q)$, another similar stability estimate

$$\|u\|_X \leq \Big[\|f\|_{L^2(0,T;H^{-1}(\Omega))} + \sqrt{2}\|\widetilde{u}_0\|_X\Big] + \|\widetilde{u}_0\|_X,$$

can be obtained, see [165, Theorem 3.2.4]. □

Remark 3.20. *Note that, the inf-sup constant $c_1^a = 1$ [91] is an improvement of the constant $c_1^a = \frac{1}{2\sqrt{2}}$ given in [144] and $c_1^a = \frac{1}{\sqrt{2}}$ given in [148]. In Section 4.1 we will investigate these conditions (BNB1) - (BNB3) in more detail.*

3.5.2 Space-time finite element discretization

Let $X_h \subset X$ and $Y_h \subset Y$ be finite-dimensional spaces assuming $X_h \subset Y_h$ as in the continuous case $X \subset Y$. The discretization of the Petrov-Galerkin space-time variational formulation (3.33) reads as, find $\widetilde{u}_h \in X_h$, such that

$$a(\widetilde{u}_h, v_h) = l(v_h) - a(\widetilde{u}_0, v_h) \quad \text{for all } v_h \in Y_h. \tag{3.35}$$

Similar to the continuous case, we first consider for $\widetilde{u} \in X$ the unique solution $w_{u,h} \in Y_h$ to the discrete variational problem of (3.32), which is to find $w_{u,h} \in Y_h$, such that

$$\int_0^T \int_\Omega [A(x)\nabla_x w_{u,h}(x,t)]\cdot\nabla_x v_h(x,t)\; dxdt = \int_0^T \int_\Omega c_H \frac{\partial}{\partial t}\widetilde{u}(x,t)v_h(x,t)\; dxdt, \tag{3.36}$$

for all $v_h \in Y_h$. For a conformal discretization $Y_h \subset Y$, it is convenient to use (3.36) and (3.32) as in [144], in order to obtain

$$\|w_{u,h}\|_Y \leq \|w_u\|_Y,$$

and hence, we can define the mesh dependent energy norm

$$\|\widetilde{u}\|_{X_h}^2 \coloneqq \|\widetilde{u}\|_Y^2 + \|w_{u,h}\|_Y^2 \leq \|\widetilde{u}\|_Y^2 + \|w_u\|_Y^2 = \|\widetilde{u}\|_X^2 \quad \text{for all } \widetilde{u} \in X.$$

Correspondingly, for $\widetilde{u}_h \in X_h$ we define $w_{u_h,h} \in Y_h$ as the unique solution of (3.36) in order to prove the discrete inf-sup condition

$$\|\widetilde{u}_h\|_{X_h} \leq \sup_{0 \neq v_h \in Y_h} \frac{a(\widetilde{u}_h, v_h)}{\|v_h\|_Y} \quad \text{for all } \widetilde{u}_h \in X_h, \tag{3.37}$$

when repeating the same steps as in the continuous case with the particular choice $v_h = \widetilde{u}_h + w_{u_h,h} \in Y_h$ due to $X_h \subset Y_h$. As a result, the unique solvability of the discrete space-time variational problem (3.35) follows from (3.37), and, due to the Galerkin orthogonality

$$a(\widetilde{u} - \widetilde{u}_h, v_h) = 0 \quad \text{for all } v_h \in Y_h,$$

where $\widetilde{u} \in X$ and $\widetilde{u}_h \in X_h$ are the unique solutions of (3.33) and (3.35), respectively, we obtain for arbitrary $v_h \in Y_h$, that

$$\begin{aligned}
\|\widetilde{u}_h - v_h\|_{X_h} &\leq \sup_{0 \neq z_h \in Y_h} \frac{a(\widetilde{u}_h - v_h, z_h)}{\|z_h\|_Y} \\
&= \sup_{0 \neq z_h \in Y_h} \frac{a(\widetilde{u}_h - \widetilde{u}, z_h) + a(\widetilde{u} - v_h, z_h)}{\|z_h\|_Y} \\
&= \sup_{0 \neq z_h \in Y_h} \frac{a(\widetilde{u} - v_h, z_h)}{\|z_h\|_Y} \leq \sqrt{2}\|\widetilde{u} - v_h\|_X.
\end{aligned}$$

Hence, we deduce the a priori error estimate

$$\|\widetilde{u} - \widetilde{u}_h\|_{X_h} \leq \|\widetilde{u} - v_h\|_{X_h} + \|v_h - \widetilde{u}_h\|_{X_h} \leq \left(1 + \sqrt{2}\right) \|\widetilde{u} - v_h\|_X$$

for all $v_h \in Y_h$, i.e. we derived Céa's lemma

$$\|\widetilde{u} - \widetilde{u}_h\|_{X_h} \leq \left(1 + \sqrt{2}\right) \inf_{v_h \in Y_h} \|\widetilde{u} - v_h\|_X.$$

REMARK 3.21. *For finite-dimensional spaces X_h and Y_h, where* $\dim(X_h) = \dim(Y_h)$, *it is sufficient to prove only the continuity (BNB1) and the discrete inf-sup condition* (3.37) *for $\widetilde{u}_h \in X_h$ and $v_h \in Y_h$ in order to conclude a unique solution of the discrete variational formulation* (3.35)*, see [36, Theorem 4.1.2].*

For our specific purpose, we consider the conforming space-time discretization

$$X_h = Y_h = S_h^1(Q_h) \cap X$$

of piecewise linear and globally continuous basis functions as defined in (3.24) with respect to some admissible and locally quasi-uniform decomposition $\overline{Q_h} = \bigcup_{\ell=1}^{N} \overline{\tau}_\ell$ of the space-time cylinder Q into shape regular simplicial finite elements τ_ℓ. Obviously, the discrete inf-sup condition (3.37) holds for this particular choice of the finite element spaces X_h and Y_h, and we conclude the following a priori estimate.

THEOREM 3.22. *Let $\widetilde{u} \in X$ and $\widetilde{u}_h \in X_h$ be the unique solutions of the variational problems* (3.33) *and* (3.35)*, respectively, and assume $\widetilde{u} \in H^2(Q)$. Then, the following energy error estimate holds with a constant $c > 0$ independent of the mesh size h,*

$$\|\widetilde{u} - \widetilde{u}_h\|_Y \leq ch|\widetilde{u}|_{H^2(Q)}.$$

Proof. The proof is given in [144, Theorem 3.3]. □

REMARK 3.23. *The finite element spaces $X_h \subset Y_h$ may also be spanned by continuous form functions of higher order $p > 1$. In this case, assuming $\widetilde{u} \in H^s(Q)$ for some $s = 2, \ldots, p+1$, the energy error estimate becomes*

$$\|\widetilde{u} - \widetilde{u}_h\|_Y \leq ch^{s-1}|\widetilde{u}|_{H^s(Q)}.$$

For numerical examples and the validation of the estimates we refer to [144, 145, 146, 147].

3.6 Parallelization

In this section, we will describe the space-time parallel computing, which is used in this work to solve all occurring linear systems. At the beginning of this chapter we already mentioned, that we treat the time t for parabolic partial differential equations as an additional spatial variable $x_{d+1} = t$, when the spatial domain is in $\mathbb{R}^d$. This has the effect that we need to construct a $(d+1)$-dimensional mesh and to deal with the computation of higher dimensional linear systems. However, using space-time methods result in the solving of only one single linear system, for which parallel computing techniques can be applied. Particularly this means, that parallel solving of these systems is associated to the parallelization of space and time at once, whereas for classical time-stepping methods [149] the right balance of parallelism between the spatial and temporal semi-discretization must be chosen. Due to the inherently sequential behavior of time-stepping, so-called parallel-in-time (PinT) methods have been developed in order to overcome the challenge of the time parallelization. For a comprehensive overview of the history of PinT methods we refer to the work of Gander [55].

Another capability that space-time methods offer is the convenient treatment of (partly) moving domains, since the movement can be easily captured by the space-time mesh. The moving boundaries and interfaces are handled more naturally, as they can seamlessly accommodate shifts in the domain over time without requiring complex remeshing or adjustments, e.g. as arbitrary Lagrangian Eulerian (ALE) schemes [40], mortaring methods [18] or unfitted finite element methods [12]. As before, we end up with a single linear system, that we want to solve by space-time parallel computing.

In terms of space-time finite element methods, parallelization means to split the large problem into smaller ones and solve each reduced problem parallel at the same time. On the one hand, the shared memory model allow the concurrent tasks to interact by reading and writing shared objects in the memory, e.g. OpenMP [32]. On the other hand, the distributed memory model distribute the work load on different nodes, where every single node has its own local memory. However, all nodes are connected to an interconnection network in order to interact with each other by message passing (MP). Different implementations of the Message Passing Interface (MPI) provide different realizations of the communication between the nodes, e.g. OpenMPI [54] or MPICH [66]. Hybrid parallelization techniques combine both models, such that the problem is distributed on several nodes, but on each node a shared memory model is used.

For our purpose, it is convenient to use the distributed memory model, since the resulting system to solve may get extremely large, which is very likely to happen with three- or four-dimensional meshes. The expensive parts of the finite element scheme are the assembling of the linear system and the solving of the linear system to obtain the solution. However, before assembling, the initial decomposition of the mesh need to be distributed to the chosen amount of nodes in a suitable way. A graph partitioning algorithm assigns each node a part of the mesh, in which the information of the shared vertices needs to be restored for further communication between the nodes. Hence, the element-wise assembly of the linear system and the right-hand side can be done independently on each node taking into account the information about the shared degrees of freedom. Nowadays, many finite element libraries have implemented the parallel assembly. However, only a bunch of them can deal with four-dimensional meshes. In the scope of this work we only obtain two- or three-dimensional space-time meshes and refer to [115] and [134] for the treatment of next higher dimensional meshes.

The other expensive part of finite element methods is the solving of the linear system. We distinguish between sparse direct solvers and iterative solvers. In many cases the system matrix of the finite element discretization is sparse, hence efficient parallel direct solvers can be implemented, see for instance the fast parallel sparse direct solvers

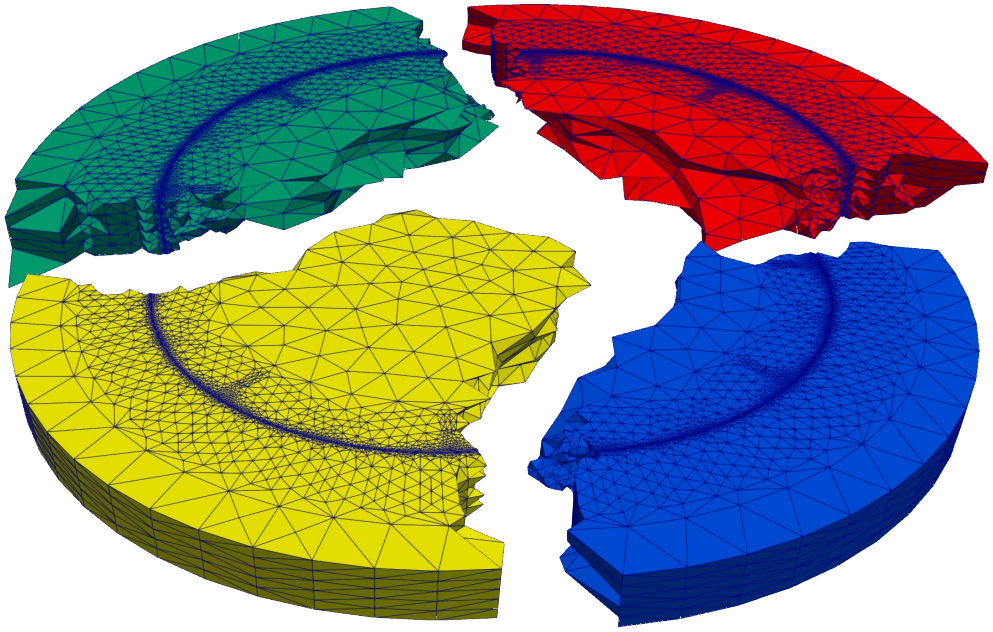

Figure 3.2: A mesh of the PMSM divided into 4 parts by METIS.

PARDISO [135] or MUMPS [4, 5]. The main drawback of such solvers is their enormous memory demand that strongly depend on the sparsity pattern of the system matrix. A remedy to the high memory consumption offers iterative solvers, e.g. the Conjugate Gradient (CG) method [76] or the Generalized Minimal Residual (GMRES) method [131], which usually can be easily parallelized, since they rely mostly on matrix-vector and vector-vector products. Speaking about iterative solvers, also (parallel) preconditioners need to be chosen wisely in order to effectively reduce the number of iterations. Many parallel linear algebra libraries provide a huge set of different direct and iterative solvers, as well as a great variety of preconditioners. For a detailed overview we refer to the book of Saad [130] and the work of Langer and Neumüller [95], as well as the references therein.

3.6.1 Software libraries

For all of our numerical experiments we have used the high performance multiphysics finite element software Netgen/NGSolve [137]. It is a C++ software implementation with a user-friendly Python interface and provides many functionalities including mesh generation, a set of (parallel) solvers and preconditioners, and a visualization tool. We use the Python interface mpi4py [127, 33] to issue OpenMPI [54] calls from Python, which causes a parallel distributed memory execution of Netgen/NGSolve. The *master* process distributes the mesh within the group of processes by the graph

partitioning algorithm METIS [86] and assigns each process a part of the mesh. Then, the finite element space, the bilinear form and the right-hand side are defined in Netgen/NGSolve considering the distributed degrees of freedom, which follow the distribution of the mesh. An example of how the mesh distribution by METIS may look like for the permanent magnet synchronous motor from Figure 2.2 is visualized in Figure 3.2. For the mesh generation we have used the open source 3D finite mesh generator GMSH [64]. Finally, the solving of the resulting linear systems is done by the parallel numerical software library PETSc [14, 34]. The Netgen/NGSolve data structures are converted into the PETSc data structures, for which we use the provided direct solver MUMPS or the iterative solver GMRES with the BoomerAMG preconditioner [129] from the hypre library [46] to obtain the solution to the linear system. We use the default settings for the BoomerAMG[1] preconditioner, that is an $\ell 1$-Gauss-Seidel smoother [13] using a forward solve on the down cycle and a backward solve on the up-cycle.

3.6.2 Hardware specification

At the Institute of Applied Mathematics at TU Graz, Austria, there is a local workstation called Babbage, on which we execute all numerical examples in this thesis. It has a 384 GiB RAM and two 16-core Intel Xeon Gold 5218 processors.

[1] `https://hypre.readthedocs.io/en/latest/solvers-boomeramg.html`

4 Space-time eddy current problem

This chapter forms the main part of this work and focuses mainly on the analysis of the space-time variational formulation in the setting of Bochner spaces and its conforming discretization for parabolic evolution problems considering fixed domains as well as uniformly and slowly moving domains, i.e. the movement is much slower than the speed of light c_0. The model problem of interest is the eddy current problem (2.21) with homogenous Dirichlet boundary and initial conditions defined on a (partly) moving domain,

$$\begin{aligned} \sigma(y)\frac{d}{dt}u(y,t) - \operatorname{div}_y(\nu(y)\nabla_y u(y,t)) &= J_3(y,t) - \operatorname{div}_y(M^{\perp}(y,t)) \text{ for } (y,t) \in Q, \\ u(y,t) &= 0 \qquad \text{for } (y,t) \in \Sigma, \\ u(x,0) &= 0 \qquad \text{for } \varphi(x,0) = x \in \Omega_0, \end{aligned} \tag{4.1}$$

where the open space-time cylinder Q is defined as in (3.5), the lateral boundary Σ of Q as in (3.6), and $\Omega_0 \in \mathbb{R}^d$, $d = 1, 2, 3$, is bounded and Lipschitz and the initial state of the domain at time $t = 0[s]$. Furthermore, the electric conductivity σ and the magnetic reluctivity ν are material dependent constant coefficients, and J_3 and $M^{\perp}$ are given source terms denoting the current density and the magnetization, respectively. Note that the partial differential equation (4.1) is posed on both conducting ($\sigma > 0$) and non-conducting ($\sigma = 0$) materials, making it to an elliptic-parabolic type, and considers fixed parts of the domain ($\widetilde{v} = 0$) and moving regions. Hence, the occurring time derivative is the total time derivative as defined in (2.20). Additionally, we also consider realistic applications, where the magnetic reluctivity $\nu(y, |\nabla_y u|)$ is nonlinear for ferromagnetic material. The IBVP (4.1) usually takes interface conditions into account, if the domain consists of multiple materials, i.e. the material coefficients jump across the interfaces. Although the interface conditions

$$\begin{aligned} [\![u]\!] &= 0 \qquad \text{on } \Gamma_I(t) \times (0,T), \\ [\![\nu\nabla_x u \cdot n_{\Gamma_I}]\!] &= 0 \qquad \text{on } \Gamma_I(t) \times (0,T), \end{aligned}$$

are not explicitly stated in (4.1), they always hold true as a result of Theorem 4.17.

First, we extend the evolution problem (3.29) to a coupled elliptic-parabolic interface problem for non-moving domains and analyze the unique solvability of its space-time variational formulation in Bochner spaces in Section 4.1. Here, the linear as well as the nonlinear case will be investigated. In Section 4.2, we address a specific

material law that accounts for hysteresis, resulting in a modified equation, for which the proposed method is still applicable. Furthermore, we obtain the eddy current problem (4.1) for moving domains as an extension to the problem in Section 4.1, for which we also examine the unique solvability of the corresponding variational formulation for the linear and nonlinear case in Section 4.3. Numerical results will be given for each problem in order to verify either the related error estimate of Section 3.5.2, or to illustrate the applicability of the proposed method to an electric motor. We refer the reader to the pioneering work of Steinbach [144], which serves as the essentials for this chapter. Other related contributions considering the space-time variational formulation of evolution problems in Bochner spaces are for instance [6, 138, 153].

4.1 Eddy current problem for conducting and non-conducting regions

This section starts with the formulation of a Bochner-type space-time variational problem for the elliptic-parabolic interface eddy current equation posed on non-moving domains. We first address the unique solvability of the linear case using Theorem 3.17 and introduce a space-time finite element discretization, accompanied by corresponding numerical examples. For the nonlinear case, unique solvability is established using results from monotone operator theory [167], with numerical examples presented at the end of this section.

4.1.1 Linear eddy current problem

Space-time variational formulation

Recalling the evolution equation (3.29), for which we now assume that the coefficient matrix $A(x,t)$ is a diagonal matrix with the same diagonal entry $\nu(x) \in L^\infty(\Omega)$, such that $0 < \underline{\nu} \leq \nu(x) \leq \nu_0$ as in Lemma 2.7, and $\sigma(x) \geq 0$ is piecewise constant, we deduce the following elliptic-parabolic evolution problem, also referred as the two-dimensional eddy current problem.

$$\begin{aligned} \sigma(x)\frac{\partial}{\partial t}u(x,t) - \operatorname{div}_x(\nu(x)\nabla_x u(x,t)) &= J_3(x,t) - \operatorname{div}_x(M^\perp(x,t)) \text{ for } (x,t) \in Q, \\ u(x,t) &= 0 \qquad \text{for } (x,t) \in \partial\Omega \times (0,T), \\ u(x,0) &= 0 \qquad \text{for } x \in \Omega \backslash \Omega_{non}, \end{aligned}$$

where $Q = \Omega \times (0,T)$ is the space-time cylinder for a terminal time $T > 0$, the fixed domain Ω ($\widetilde{v} = 0$) is composed of conducting regions Ω_{con} ($\sigma > 0$) and non-conducting

regions Ω_{non} ($\sigma = 0$), and the current density J_3 as well as the magnetization $M^{\perp}$ are given sources. As in Section 3.5, we use the notation $Y := L^2(0,T;H_0^1(\Omega))$ for the Bochner space covering homogenous Dirichlet boundary conditions, equipped with the equivalent norm

$$\|v\|_Y := \left(\int_0^T \int_\Omega \nu(x) |\nabla_x v(x,t)|^2 \, dxdt \right)^{1/2},$$

and

$$X := \{u \in Y : \sigma \frac{\partial}{\partial t} u \in Y^\star, u(x,0) = 0 \in \Omega_{con}\} \subset Y \tag{4.2}$$

for the trial space with the corresponding graph norm

$$\|u\|_X^2 := \|u\|_Y^2 + \|\sigma \frac{\partial}{\partial t} u\|_{Y^\star}^2 = \|u\|_Y^2 + \|w_u\|_Y^2,$$

where $w_u \in Y$ is the unique solution of the variational problem

$$\int_0^T \int_\Omega \nu(x) \nabla_x w_u(x,t) \cdot \nabla_x v(x,t) \, dxdt = \int_0^T \int_\Omega \sigma(x) \frac{\partial}{\partial t} u(x,t) v(x,t) \, dxdt \tag{4.3}$$

for all $v \in Y$. Indeed, the variational problem (4.3) admits a unique solution due to the lemma of Lax-Milgram. The related space-time variational formulation is to find $u \in X$, such that

$$a(u,v) = l(v) \quad \text{for all } v \in Y, \tag{4.4}$$

where

$$\begin{aligned} a(u,v) &= \int_0^T \int_\Omega \left[\sigma(x) \frac{\partial}{\partial t} u(x,t) v(x,t) + \nu(x) \nabla_x u(x,t) \cdot \nabla_x v(x,t) \right] dxdt, \\ l(v) &= \int_0^T \int_\Omega \left[J_3(x,t) v(x,t) + M^{\perp}(x,t) \cdot \nabla_x v(x,t) \right] dxdt. \end{aligned}$$

In order to prove the unique solvability of (4.4), we need to verify the conditions (BNB1) - (BNB3) of Theorem 3.17. The continuity follows immediately from the duality, the Cauchy-Schwarz and the Hölder inequality, i.e.

$$\begin{aligned} |a(u,v)| &\leq \|\sigma \frac{\partial}{\partial t} u\|_{Y^\star} \|v\|_Y + \|u\|_Y \|v\|_Y = \left[\|\sigma \frac{\partial}{\partial t} u\|_{Y^\star} + \|u\|_Y \right] \|v\|_Y \\ &\leq \sqrt{2} \sqrt{\|\sigma \frac{\partial}{\partial t} u\|_{Y^\star}^2 + \|u\|_Y^2} \|v\|_Y = \sqrt{2} \|u\|_X \|v\|_Y, \end{aligned}$$

for all $u \in X$ and $v \in Y$. Similar to Section 3.5, we want to derive an inf-sup stability condition for the bilinear form in (4.4). For this purpose, let $w_u \in Y$ be the unique solution of the variational formulation (4.3) for a given $u \in X$. Since $X \subset Y$, we can consider $v_u = u + w_u \in Y$ and (4.3) in order to obtain

$$\begin{aligned} a(u, v_u) &= a(u, u + w_u) \\ &= \int_0^T \int_\Omega \sigma \frac{\partial}{\partial t} u (u + w_u) \, dxdt + \int_0^T \int_\Omega \nu \nabla_x u \cdot \nabla_x (u + w_u) \, dxdt \\ &= \int_0^T \int_\Omega \nu \nabla_x w_u \cdot \nabla_x (u + w_u) \, dxdt + \int_0^T \int_\Omega \nu \nabla_x u \cdot \nabla_x (u + w_u) \, dxdt \\ &= \int_0^T \int_\Omega \nu \nabla_x (u + w_u) \cdot \nabla_x (u + w_u) \, dxdt \\ &= \|u + w_u\|_Y^2 = \|v_u\|_Y^2. \end{aligned}$$

On the other hand, we obtain that

$$\begin{aligned} \|v_u\|_Y^2 &= \|u + w_u\|_Y^2 \\ &= \int_0^T \int_\Omega \nu |\nabla_x u|^2 \, dxdt + \int_0^T \int_\Omega \nu |\nabla_x w_u|^2 \, dxdt + 2 \int_0^T \int_\Omega \nu \nabla_x u \cdot \nabla_x w_u \, dxdt \\ &= \|u\|_Y^2 + \|w_u\|_Y^2 + 2 \int_0^T \int_\Omega \sigma \frac{\partial}{\partial t} u \; u \, dxdt \\ &\geq \|u\|_Y^2 + \|w_u\|_Y^2 = \|u\|_X^2 \end{aligned}$$

where we have used the chain rule

$$\begin{aligned} \int_0^T \int_\Omega 2\sigma \frac{\partial}{\partial t} u \; u \, dxdt &= \int_0^T \int_\Omega \sigma \frac{\partial}{\partial t} [u]^2 \, dxdt = \int_0^T \frac{\partial}{\partial t} \int_\Omega \sigma [u]^2 \, dxdt \\ &= \int_\Omega \sigma(x) [u(x,t)]^2 \, dx \Big|_0^T = \int_{\Omega_{con}} \sigma(x) [u(x,T)]^2 \, dx > 0 \end{aligned}$$

with $u(x, 0) = 0$ for $x \in \Omega \backslash \Omega_{non}$. Therefore, the inf-sup stability condition reads as

$$\|u\|_X \leq \sup_{0 \neq v \in Y} \frac{a(u, v)}{\|v\|_Y} \quad \text{for all } u \in X. \tag{4.5}$$

Lastly, we want to prove the surjectivity (BNB3) of the bilinear form $a(\cdot, \cdot)$ in (4.4). However, since we deal with an elliptic-parabolic interface problem, the verification of the surjectivity is more involved compared to the parabolic case (3.33) and needs the application of the so-called Steklov-Poincaré operator, see e.g. [125] or [143, Section 6.6.3]. The proof is given in the following lemma, cf. [60].

LEMMA 4.1. *For all $v \in Y\backslash\{0\}$ there exists a $\widehat{u} \in X$ such that*

$$a(\widehat{u}, v) \neq 0.$$

Proof. For a given $v \in Y\backslash\{0\}$ we first define

$$\widehat{u}(x,t) = \int_0^t v(x,\tau)\ d\tau, \quad \frac{\partial}{\partial t}\widehat{u}(x,t) = v(x,t) \quad \text{for } x \in \Omega_{con}, t \in [0,T].$$

By definition, we have $\widehat{u} \in X$ satisfying the initial condition $u(x,0) = 0$ for $x \in \Omega_{con}$ and

$$\begin{aligned} a(\widehat{u}, v) &= \int_0^T \int_\Omega \left[\sigma(x)\frac{\partial}{\partial t}\widehat{u}(x,t)v(x,t) + \nu(x)\nabla_x\widehat{u}(x,t)\cdot\nabla_x v(x,t)\right]\ dxdt \\ &= \int_0^T \int_{\Omega_{con}} \sigma(x)[v(x,t)]^2\ dxdt + \int_0^T \int_\Omega \nu(x)\nabla_x\widehat{u}(x,t)\cdot\nabla_x\frac{\partial}{\partial t}\widehat{u}(x,t)\ dxdt \\ &= \int_0^T \int_{\Omega_{con}} \sigma(x)[v(x,t)]^2\ dxdt + \int_0^T \int_{\Omega_{con}\cup\Omega_{non}} \nu(x)\nabla_x\widehat{u}(x,t)\cdot\nabla_x\frac{\partial}{\partial t}\widehat{u}(x,t)\ dxdt. \end{aligned}$$

Obviously, the first expression is positive as well as the second expression when using the chain rule (3.34) in the conducting regions. Hence, it follows that

$$a(\widehat{u}, v) \geq \int_0^T \int_{\Omega_{con}} \sigma(x)[v(x,t)]^2\ dxdt + \int_0^T \int_{\Omega_{non}} \nu(x)\nabla_x\widehat{u}(x,t)\cdot\nabla_x\frac{\partial}{\partial t}\widehat{u}(x,t)\ dxdt.$$

It remains to define $\widehat{u} \in X$ for the non-conducting regions in a suitable way. In any non-conducting subregion we can use Gauss's divergence theorem to write

$$\begin{aligned} \int_0^T \int_{\Omega_{non}} \nu(x)\nabla_x\widehat{u}(x,t)\cdot\nabla_x v(x,t)\ dxdt &= \int_0^T \int_{\Omega_{non}} -\mathrm{div}[\nu(x)\nabla_x\widehat{u}(x,t)]v(x,t)\ dxdt \\ &\quad + \int_0^T \int_{\partial\Omega_{non}} \gamma_0[\nu(x)\nabla_x\widehat{u}(x,t)]\cdot n_x\ \gamma_0 v(x,t)\ ds_x dt \\ &= \int_0^T \int_{\Omega_{non}} [v(x,t)]^2\ dxdt + \int_0^T \int_{\partial\Omega_{non}} \gamma_0[\nu(x)\nabla_x\widehat{u}(x,t)]\cdot n_x\ \gamma_0 v(x,t)\ ds_x dt, \end{aligned}$$

where γ_0 is the trace operator as defined in Theorem 3.8, n_x is the spatial unit outward normal vector and $\widehat{u}$ is a solution of the elliptic Dirichlet boundary value problem

$$-\mathrm{div}[\nu(x)\nabla_x\widehat{u}(x,t)] = v(x,t) \quad \text{for } x \in \Omega_{non}, t \in (0,T). \tag{4.6}$$

To ensure $\widehat{u} \in Y$, we formulate the boundary conditions

$$\begin{aligned} \widehat{u}_{|\Omega_{non}} &= \widehat{u}_{|\Omega_{con}} \qquad \text{on } \partial\Omega_{non} \cap \partial\Omega_{con}, \\ \widehat{u}_{|\Omega_{non}} &= 0 \qquad\qquad \text{on } \partial\Omega_{non} \cap \partial\Omega. \end{aligned}$$

The solution of the elliptic Dirichlet boundary value problem (4.6) implies the Dirichlet to Neumann map

$$\gamma_0 \left[\nu(x)\nabla_x \widehat{u}(x,t)\right] \cdot n_x = (S\gamma_0\widehat{u})(x,t) \quad \text{for } x \in \partial\Omega_{non}, t \in [0,T],$$

with the Steklov-Poincaré operator $S : H^{1/2}(\partial\Omega) \to H^{-1/2}(\partial\Omega)$. Since S is self-adjoint and positive semi-definite, we can factorize S and use the chain rule in order to write

$$\begin{aligned} \int_0^T \int_{\partial\Omega_{non}} (S\gamma_0\widehat{u})(x,t)\ \gamma_0 v(x,t)\ ds_x dt &= \int_0^T \int_{\partial\Omega_{non}} (S^{1/2}\gamma_0\widehat{u})(x,t)(S^{1/2}\gamma_0 v)(x,t)\ ds_x dt \\ &= \int_0^T \int_{\partial\Omega_{non}} (S^{1/2}\gamma_0\widehat{u})(x,t)\frac{\partial}{\partial t}(S^{1/2}\gamma_0\widehat{u})(x,t)\ ds_x dt \\ &= \frac{1}{2}\int_0^T \frac{\partial}{\partial t} \int_{\partial\Omega_{non}} \left[(S^{1/2}\gamma_0\widehat{u})(x,t)\right]^2 ds_x dt \\ &= \frac{1}{2}\int_{\partial\Omega_{non}} \left[(S^{1/2}\gamma_0\widehat{u})(x,T)\right]^2\ ds_x \geq 0. \end{aligned}$$

Therefore, we deduce that

$$\int_0^T \int_{\Omega_{non}} \nu(x)\nabla_x \widehat{u}(x,t) \cdot \nabla_x v(x,t) \geq \int_0^T \int_{\Omega_{non}} [v(x,t)]^2\ dxdt,$$

which finally gives

$$a(\widehat{u}, v) \geq \int_0^T \int_{\Omega_{con}} \sigma(x)[v(x,t)]^2\ dxdt + \int_0^T \int_{\Omega_{non}} [v(x,t)]^2\ dxdt > 0.$$

This concludes the proof. □

Summarizing the latest results yield the following theorem.

THEOREM 4.2. *Let $J_3 \in L^2(0,T;H^{-1}(\Omega))$ and $M^\perp \in [L^2(Q)]^d$ be given. Then there exists a unique solution $u \in X$ of (4.4) satisfying*

$$\|u\|_X \leq \|J_3\|_{L^2(0,T;H^{-1}(\Omega))} + c\|M^\perp\|_{L^2(Q)}.$$

Proof. The unique solvability of (4.4) follows from the Banach-Nečas-Babuška Theorem 3.17. The stability estimate is deduced from the inf-sup condition, i.e.

$$\begin{aligned}\|u\|_X &\leq \sup_{0\neq v\in Y} \frac{a(u,v)}{\|v\|_Y} = \sup_{0\neq v\in Y} \frac{l(v)}{\|v\|_Y} \\ &\leq \sup_{0\neq v\in Y} \frac{\|J_3\|_{L^2(0,T;H^{-1}(\Omega))}\|v\|_Y + \|M^\perp\|_{L^2(Q)}\|\nabla_x v\|_{L^2(Q)}}{\|v\|_Y} \\ &\leq \|J_3\|_{L^2(0,T;H^{-1}(\Omega))} + \sqrt{L}\ \|M^\perp\|_{L^2(Q)},\end{aligned}$$

where the last estimate follows from the fact that

$$\sqrt{\frac{1}{L}}\|\nabla_x v\|_{L^2(Q)} \leq \|v\|_Y \leq \sqrt{\nu_0}\|\nabla_x v\|_{L^2(Q)},$$

due to Theorem 2.7. □

Remark 4.3. *A more general alternative to prove the unique solvability of parabolic linear evolution problems gives the main theorem on first-order linear evolution equations [166, Section 23.7] considering the linear, continuous and strongly monotone operator $A : Y \to Y^\star$ with $\langle Au, v\rangle := a_e(u,v)$, where*

$$a_e(u,v) := \int_0^T \int_\Omega \nu(x)\nabla_x u(x,t)\cdot\nabla_x v(x,t)\ dxdt \quad \text{for } u,v \in Y.$$

Under these assumptions and for $l \in Y^\star$, the initial value problem

$$\begin{aligned}\frac{\partial}{\partial t}u + Au &= l \quad \text{in } Y^\star, \\ u(0) &= 0,\end{aligned}$$

which is equivalent to (3.33)*, admits a unique solution $u \in Y$ with the weak derivative $\partial_t u \in Y^\star$, see [166, Theorem 23.A and Corollary 23.24]. In terms of this theorem, a statement about the existence of a unique solution for the elliptic-parabolic interface problem* (4.4) *can be given in the following way. Suppose the solution u_{con} in the conducting region Ω_{con} is known. Then the interface conditions together with the boundary conditions provide the necessary boundary conditions for the elliptic problem in the non-conducting region Ω_{non}. By the lemma of Lax-Milgram a unique solution $u_{non}(u_{con})$ depending on u_{con} exists, i.e. the solution in the conducting region Ω_{con} uniquely determines the solution in the non-conducting region Ω_{non}. Since the parabolic problem in the conducting region Ω_{con} has a solution u_{con} by the above theorem, the full eddy current problem is uniquely solvable when using the relation $u_{non}(u_{con})$. The authors of [11] and [87] have taken advantage of this idea in order to*

show unique solvability for the nonlinear eddy current problem as well as [90] for the linear case. The numerical treatment of such interface problems leads to the popular domain decomposition methods [126, 151]. Within each subdomain the corresponding problems can be formulated, i.e.

$$\begin{aligned} \frac{\partial}{\partial t} u_{con} + A u_{con} &= l \quad \text{in } \Omega_{con}, \\ A u_{non} &= l \quad \text{in } \Omega_{non}, \end{aligned}$$

and are coupled through the subdomain interface, i.e. $u_{con} = u_{non}$ *and* $\frac{\partial u_{con}}{\partial n_A} = \frac{\partial u_{non}}{\partial n_A}$ *on* $\partial\Omega_{con} \cap \partial\Omega_{non}$.

Space-time finite element discretization

For the space-time finite element scheme we introduce conforming finite dimensional spaces $X_h \subset X$ and $Y_h \subset Y$, where we assume as in the continuous case that $X_h \subset Y_h$. For our specific purpose we even consider

$$X_h = Y_h \coloneqq S_h^1(\mathcal{T}_h) \cap X = \operatorname{span}\{\phi_k\}_{k=1}^M, \tag{4.7}$$

where the space $S_h^1(\mathcal{T}_h)$ of piecewise linear and globally continuous functions ϕ_k is defined as in (3.24) with respect to some admissible and locally quasi-uniform decomposition $\mathcal{T}_h = \{\tau_\ell\}_{\ell=1}^N$ of the space-time cylinder Q into shape regular simplicial finite elements τ_ℓ of mesh size h_ℓ, cf. Section 3.4. The Galerkin space-time finite element discretization of the variational formulation (4.4) is to find $u_h \in X_h$, such that

$$a(u_h, v_h) = l(v_h) \quad \text{for all } v_h \in Y_h. \tag{4.8}$$

In order to guarantee the existence of a unique solution for the discrete variational problem (4.8), we proceed as in the continuous case. First, for any $u \in X$ we define $w_{u,h} \in Y_h$ as the unique solution of the Galerkin variational formulation

$$\int_0^T \int_\Omega \nu(x) \nabla_x w_{u,h}(x,t) \cdot \nabla_x v_h(x,t) \, dxdt = \int_0^T \int_\Omega \sigma(x) \frac{\partial}{\partial t} u(x,t) v_h(x,t) \, dxdt, \tag{4.9}$$

for all $v_h \in Y_h$. Consequently, we define the discrete energy norm as

$$\|u\|_{X_h}^2 \coloneqq \|u\|_Y^2 + \|w_{u,h}\|_Y^2 \leq \|u\|_Y^2 + \|w_u\|_Y^2 = \|u\|_X^2 \quad \text{for all } u \in X, \tag{4.10}$$

where $w_u \in Y$ is the unique solution of the variational formulation (4.3), and due to the conformal discretization $Y_h \subset Y$ we have $\|w_{u,h}\|_Y \leq \|w_u\|_Y$, cf. [144]. Similarly, we define $w_{u_h,h} \in Y_h$ as the unique solution of (4.9) for $u_h \in X_h$ in the right-hand

side. Hence, we can consider the particular test function $v_{u_h,h} = u_h + w_{u_h,h}$ due to $X_h \subset Y_h$, in order to conclude

$$a(u_h, v_{u_h,h}) = a(u_h, u_h + w_{u_h,h}) = \|u_h + w_{u_h,h}\|_Y^2 = \|v_{u_h,h}\|_Y^2$$

and

$$\|v_{u_h,h}\|_Y^2 = \|u_h + w_{u_h,h}\|_Y^2 \geq \|u_h\|_Y^2 + \|w_{u_h,h}\|_Y^2 = \|u_h\|_{X_h}^2$$

as in the continuous case, which finally gives the discrete inf-sup stability condition

$$\|u_h\|_{X_h} \leq \sup_{0 \neq v_h \in Y_h} \frac{a(u_h, v_h)}{\|v_h\|_Y} \quad \text{for all } u_h \in X_h. \tag{4.11}$$

From (4.11) we deduce unique solvability of the Galerkin space-time variational formulation (4.8). Furthermore, if $u \in X$ and $u_h \in X_h$ are the unique solutions of the variational problems (4.4) and (4.8), respectively, we obtain with the help of the Galerkin orthogonality

$$a(u - u_h, v_h) = 0 \quad \text{for all } v_h \in Y_h,$$

and due to

$$\|u_h\|_{X_h} \leq \sup_{0 \neq v_h \in Y_h} \frac{a(u_h, v_h)}{\|v_h\|_Y} = \sup_{0 \neq v_h \in Y_h} \frac{a(u, v_h)}{\|v_h\|_Y} \leq \sqrt{2}\|u\|_X,$$

the boundedness of the Galerkin projection $u_h = G_h u$, i.e.

$$\|G_h u\|_{X_h} = \|u_h\|_{X_h} \leq \sqrt{2}\|u\|_X \quad \text{for } u \in X.$$

In the same way as in Section 3.5.2, we can derive Céa's lemma

$$\|u - u_h\|_{X_h} \leq \left(1 + \sqrt{2}\right) \inf_{v_h \in Y_h} \|u - v_h\|_X,$$

and the a priori error estimate in the energy norm as given in Theorem 3.22,

$$\|u - u_h\|_Y \leq ch|u|_{H^2(Q)},$$

if $u \in H^2(Q)$.

4.1.2 Numerical examples

In this section we provide some numerical results in order to illustrate the applicability and accuracy of the proposed approach. We define the finite element spaces Y_h

and X_h as in (4.7), which are spanned by piecewise linear and globally continuous functions ϕ_k, cf. (3.24). Hence, for all $v_h \in Y_h$ we can find the representation

$$v_h(x,t) = \sum_{k=1}^{M} v_k \phi_k(x,t), \quad \text{with } v_k = v_h(x_k, t_k), \tag{4.12}$$

that defines the finite element isomorphism $v_h \leftrightarrow \mathbf{v}_h \in \mathbb{R}^M$, where $\mathbf{v}_h[k] = v_k$, for $k = 1, \ldots, M$. The discrete space-time variational formulation (4.8) is then equivalent to the linear system

$$(A_h + K_h)\mathbf{u}_h = \mathbf{l}_h, \tag{4.13}$$

where $A_h \in \mathbb{R}^{M\times M}$ and the stiffness matrix $K_h \in \mathbb{R}^{M\times M}$ are given as

$$A_h[i,j] = \int_0^T \int_\Omega \sigma(x) \frac{\partial}{\partial t} \phi_j(x,t) \phi_i(x,t) \; dxdt,$$
$$K_h[i,j] = \int_0^T \int_\Omega \nu(x) \nabla_x \phi_j(x,t) \cdot \nabla_x \phi_i(x,t) \; dxdt,$$

for $i, j = 1, \ldots, M$, and the load vector $\mathbf{l}_h$ has the entries

$$\mathbf{l}_h[i] = \int_0^T \int_\Omega [J_3(x,t)\phi_i(x,t) + M^\perp(x,t) \cdot \nabla_x \phi_i(x,t)] \; dxdt,$$

for $i = 1, \ldots, M$. We solve the resulting non-symmetric linear system (4.13) in parallel with the methods described in Section 3.6.1. On the one hand we use the parallel direct solver MUMPS, and on the other hand we use the parallel iterative solver GMRES with the BoomerAMG preconditioner. Both solvers are provided by PETSc, where we use the preconditioner from the hypre library for the iterative solver. The following examples will show the computational times of these two solvers and the expected convergence rate as stated in Theorem 3.22.

We start with an example for $d = 1$, for which we consider an interval $\Omega = (0,1)$, such that $\overline{\Omega} = \overline{\Omega}_{con} \cup \overline{\Omega}_{non}$ with $\Omega_{con} = (0, 0.5)$ and $\Omega_{non} = (0.5, 1)$, where each half is made of a different material, i.e. the electric conductivity σ and magnetic reluctivity ν have different values on each half of the interval and jump across the interface. Furthermore, the interval Ω is extruded in time with $T = 1$, which defines the space-time cylinder $Q = (0,1)^2 \in \mathbb{R}^2$ as depicted in Figure 4.1. Considering the manufactured solution

$$u(x,t) = x(1-x)t,$$

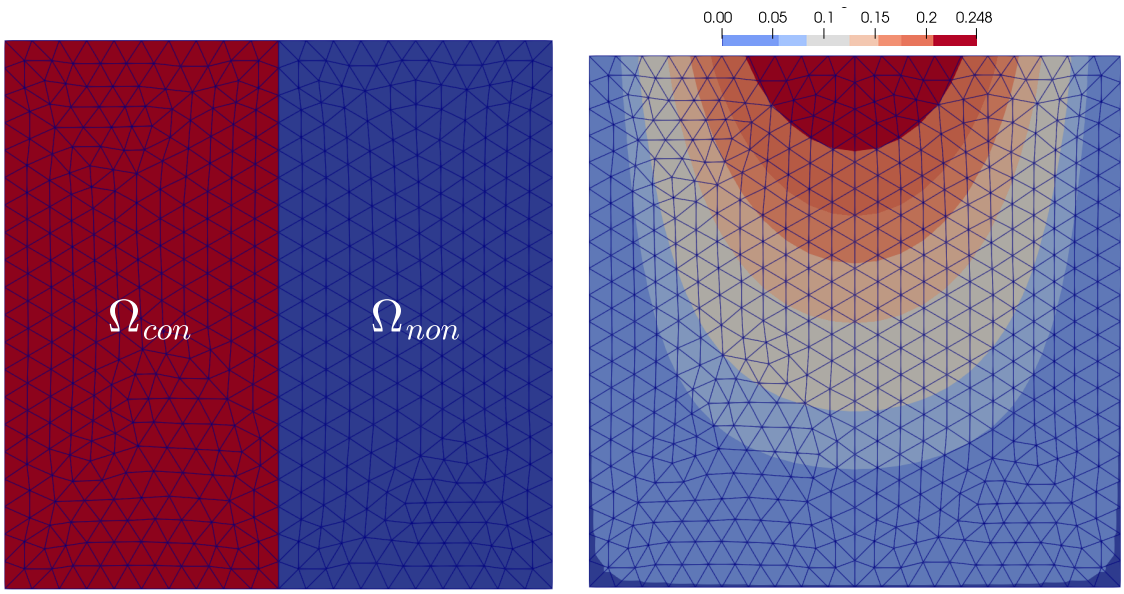

Figure 4.1: Left: An unstructured mesh of the space-time cylinder $Q = (0, 1)^2$, consisting of the conducting region Ω_{con} (red) and the non-conducting region Ω_{non} (blue). The visualized mesh has 549 nodes (degrees of freedom) and 1015 elements. Right: The approximate solution u_h of (4.8) computed on this mesh.

L	dofs	$\|u - u_h\|_Y$	EOC
1	13	0.13582	
2	41	0.06868	0.983
3	145	0.03468	0.986
4	545	0.01745	0.991
5	2,113	0.00875	0.996
6	8,321	0.00438	0.999
7	33,025	0.00219	0.999
8	131,585	0.00109	1
9	525,313	0.00055	1
10	2,099,201	0.00027	1
11	8,392,705	0.00014	1

Table 4.1: The discretization error in the energy norm, which indicates linear convergence when using the parallel direct solver as well as the iterative solver on 16 cores for a uniform mesh refinement. The number of GMRES iterations increases in each refinement step, ending up with a maximum of 3000 iterations.

Number of cores	1	2	4	8	16
MUMPS	9.09	8.30	7.67	7.33	7.26
GMRES	147.16	99.15	36.92	19.59	10.12
iterations	215	192	160	176	171

Table 4.2: Computational times in seconds for solving the linear system (4.13) with MUMPS and preconditioned GMRES with the BoomerAMG preconditioner on a mesh with 525,313 nodes (dofs) and 262,144 elements.

that satisfies the homogenous boundary and initial condition, and the material parameters

$$\sigma(x) = \begin{cases} 1 & \text{for } x \in \Omega_{con}, \\ 0 & \text{for } x \in \Omega_{non}, \end{cases} \quad \text{and} \quad \nu(x) = \begin{cases} 2 & \text{for } x \in \Omega_{con}, \\ 1 & \text{for } x \in \Omega_{non}, \end{cases}$$

we deduce the right-hand side

$$l(v_h) = \int_0^T \int_\Omega J_3(x,t) v_h(x,t) \, dxdt, \quad \text{with } J_3 = \begin{cases} x(1-x) + 4t & \text{for } x \in \Omega_{con}, \\ 2t & \text{for } x \in \Omega_{non}. \end{cases}$$

Figure 4.1 depicts the approximate solution u_h of (4.8), and Table 4.1 shows the expected linear convergence as stated in Theorem 3.22. Here, we used a relative error tolerance of 10^{-8} for the parallel iterative solver GMRES. Hence, the errors in Table 4.1 are almost the same as for the direct solver MUMPS. In Table 4.2 the computational times are given with respect to the number of cores. Note that the computational times relate purely to the time for solving the system (4.13), i.e. the assembly and the converting of the data types between Netgen/NGSolve and PETSc are not measured. Obviously, the parallel direct solver MUMPS is very efficient for the spatially one-dimensional case.

Our next numerical experiment considers a spatially two-dimensional problem with $\Omega = (0,1)^2$, which consists of the non-conducting region $\Omega_{non} = (0.25, 0.75)^2$ and the conducting region $\Omega_{con} = \Omega \backslash \overline{\Omega}_{non}$. The domain is extruded in time with $T = 1$, hence the space-time cylinder Q is defined as $Q = (0,1)^3$, see Figure 4.2. We consider the manufactured solution

$$u(x_1, x_2, t) = \sin(x_1(1-x_1)\pi) \sin(x_2(1-x_2)\pi) t^2,$$

and the material parameters

$$\sigma(x) = \begin{cases} 0.1 & \text{for } x \in \Omega_{con}, \\ 0 & \text{for } x \in \Omega_{non}, \end{cases} \quad \text{and} \quad \nu(x) = \begin{cases} x_1 x_2 & \text{for } x \in \Omega_{con}, \\ x_1 x_2 & \text{for } x \in \Omega_{non}. \end{cases}$$

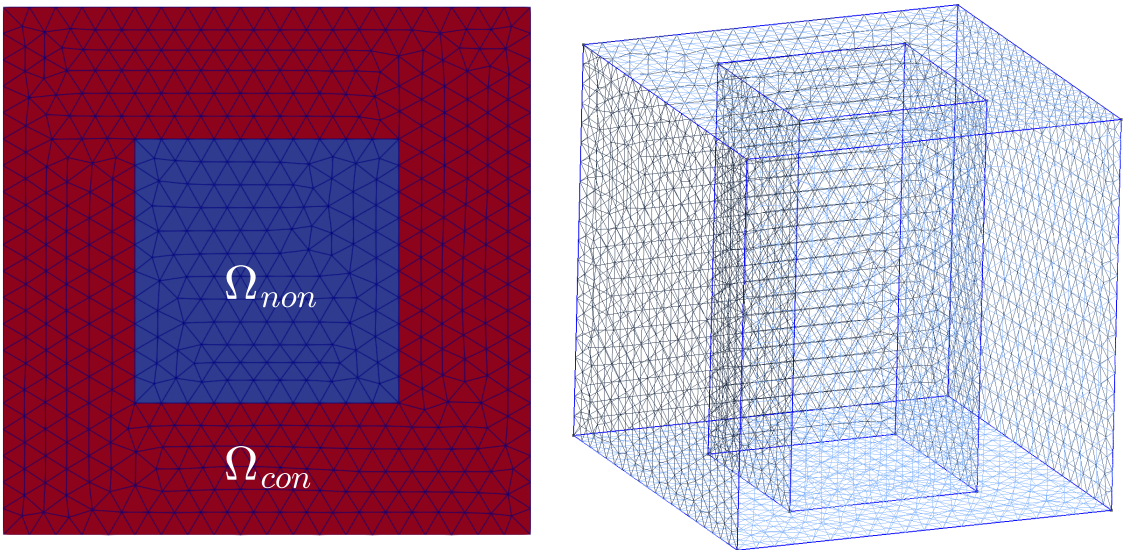

Figure 4.2: Left: The domain Ω showing the non-conducting region Ω_{non} (blue) in the middle surrounded by the conducting region Ω_{con} (red). Right: An unstructured mesh of the space-time cylinder $Q = (0,1)^3$, which is extruded vertically in time and has 7,539 nodes (degrees of freedom) and 37,642 elements.

The right-hand side J_3 is computed by using the underlying partial differential equation, i.e.

$$J_3(x,t) = \sigma(x)\frac{\partial}{\partial t}u(x,t) - \mathrm{div}_x(\nu(x)\nabla_x u(x,t)).$$

The approximate solution u_h is displayed for different time points in Figure 4.3 and indicates the expected linear convergence in the energy norm in Table 4.3. As before, we use a relative error tolerance of 10^{-8} for the parallel iterative solver GMRES. Furthermore, the computational times for solving the linear system (4.13) with respect to the number of cores are given in Table 4.4. Again, the measured times relate purely to the solving of the linear systems.

4.1.3 Nonlinear eddy current problem

Space-time variational formulation

As already mentioned, in realistic applications the magnetic reluctivity ν additionally depends on the magnitude of the magnetic flux density, which leads to the following

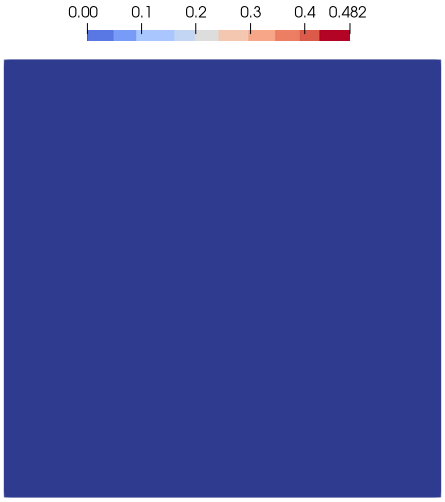

Solution u_h at time $t = 0.0[s]$.

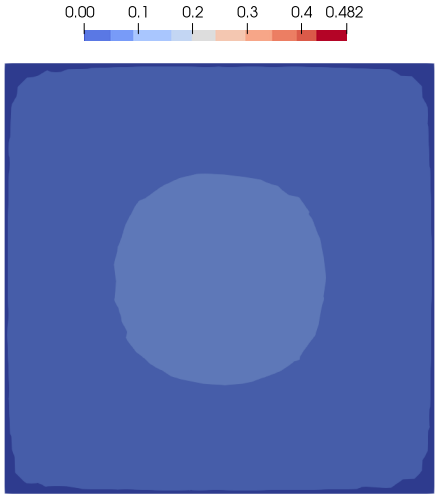

Solution u_h at time $t = 0.35[s]$.

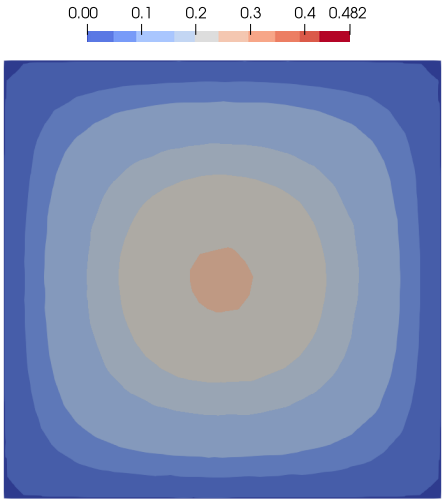

Solution u_h at time $t = 0.7[s]$.

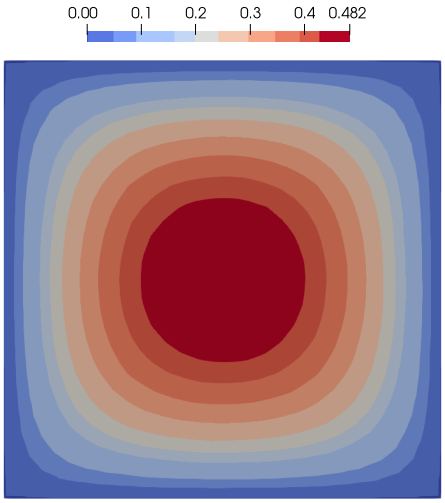

Solution u_h at time $t = 1.0[s]$.

Figure 4.3: The approximate solution u_h of (4.8) for different time points computed on the mesh from Figure 4.2.

L	dofs	$\|u - u_h\|_Y$	EOC
1	26	0.15976	
2	143	0.11193	0.513
3	941	0.06559	0.771
4	6,809	0.03541	0.889
5	51,761	0.01830	0.952
6	403,553	0.00928	0.980
7	3,186,881	0.00467	0.991

Table 4.3: The discretization error in the energy norm, which indicates linear convergence when using the parallel direct solver as well as the iterative solver on 16 cores for a uniform mesh refinement. The number of GMRES iterations increases in each refinement step, ending up with a maximum of 80 iterations.

Number of cores	1	2	4	8	16
MUMPS	58.83	44.62	35.89	26.15	20.03
GMRES	67.32	46.14	24.45	15.96	9.61
iterations	34	33	34	34	32

Table 4.4: Computational times in seconds for solving the linear system (4.13) with MUMPS and preconditioned GMRES with the BoomerAMG preconditioner on a mesh with 403,553 nodes (dofs) and 2,359,296 elements.

nonlinear evolution problem,

$$\begin{aligned} \sigma\frac{\partial}{\partial t}u - \operatorname{div}_x(\nu(x,|\nabla_x u|)\nabla_x u) = J_3 - \operatorname{div}_x(M^{\perp}) \qquad & \text{in } Q, \\ u(x,t) = 0 \qquad & \text{for } (x,t) \in \partial\Omega \times (0,T), \\ u(x,0) = 0 \qquad & \text{for } x \in \Omega\backslash\Omega_{non}. \end{aligned} \tag{4.14}$$

As before, the fixed domain Ω consists of conducting regions $\Omega_{con}(\sigma > 0)$ and non-conducting regions $\Omega_{non}(\sigma = 0)$, and we keep the same notations $Y = L^2(0,T;H_0^1(\Omega))$ and X as in (4.2). The nonlinear space-time variational formulation is to find $u \in X$, such that

$$a(u,v) = l(v) \quad \text{for all } v \in Y, \tag{4.15}$$

where

$$a(u,v) = \int_0^T \int_\Omega \left[\sigma(x) \frac{\partial}{\partial t} u(x,t) v(x,t) + \nu(x, |\nabla_x u|) \nabla_x u(x,t) \cdot \nabla_x v(x,t) \right] \, dxdt,$$

$$l(v) = \int_0^T \int_\Omega \left[J_3(x,t) v(x,t) + M^\perp(x,t) \cdot \nabla_x v(x,t) \right] \, dxdt.$$

In order to make a statement about the unique solvability of the variational formulation (4.15), we first need to recall some general results for nonlinear problems, see e.g. [167, Chapter 25, Chapter 30-32]. We start with the well-known Theorem of Zarantonello [167], that yields the existence of a unique solution for nonlinear elliptic problems in a Hilbert space, whose operator satisfies certain monotonicity and continuity conditions.

THEOREM 4.4 (Zarantonello [167, Theorem 25.B]). *Let $(H, \|\cdot\|_H)$ be a real Hilbert space and let the operator $A : H \to H^\star$ be strongly monotone and Lipschitz continuous, i.e. there exists a constant $c_M > 0$, such that*

$$\langle Au - Av, u - v \rangle_{H^\star, H} \geq c_M \|u - v\|_H^2 \quad \text{for all } u, v \in H,$$

and there exists a constant $L > 0$, such that

$$\|Au - Av\|_{H^\star} \leq L \|u - v\|_H \quad \text{for all } u, v \in H.$$

Then, for each $b \in H^\star$, the operator equation $A(u) = b$ has a unique solution $u \in H$. The solution u depends continuously on the data b. More precisely, for the solutions $u_1, u_2 \in H$ of $Au_i = b_i$, $i = 1, 2$, with respective $b_1, b_2 \in H^\star$, it holds

$$\|u_1 - u_2\|_H \leq c_M^{-1} \|b_1 - b_2\|_{H^\star}.$$

With this theorem, we can prove the following lemma about the unique solvability of the rather general elliptic boundary value problem

$$\begin{aligned} -\operatorname{div}\left(\nu(|B^\top(x) \nabla \overline{u}(x)|) B(x) B^\top(x) \nabla \overline{u}(x) \right) &= f(x) && \text{for } x \in \Omega, \\ \overline{u}(x) &= g(x) && \text{for } x \in \partial\Omega, \end{aligned}$$

whose variational formulation reads as to find $u = \overline{u} - \widetilde{g} \in H_0^1(\Omega)$, such that

$$a_e(u,v) = \int_\Omega f(x) v(x) \, dx \quad \text{for all } v \in H_0^1(\Omega), \tag{4.16}$$

where $\widetilde{g} \in H^1(\Omega)$ such that $\widetilde{g}|_{\partial\Omega} = g$ and

$$a_e(u,v) \coloneqq \int_\Omega \nu(|B^\top(x) \nabla (u(x) + \widetilde{g}(x))|) B(x) B^\top(x) \nabla (u(x) + \widetilde{g}(x)) \cdot \nabla v(x) \, dx.$$

Note that the product $B(x)B^\top(x)$ is usually a decomposition of the coefficient matrix $A(x) = B(x)B^\top(x)$ as given in (3.29). Additionally, we can define the related operator $A : H_0^1(\Omega) \to H^{-1}(\Omega)$ by the relation

$$\langle Au, v\rangle_\Omega = a_e(u, v),$$

which allow rewriting (4.16) as an operator equation in the dual space, i.e.

$$Au = f \qquad \text{in } H^{-1}(\Omega).$$

LEMMA 4.5. *Let $\Omega \in \mathbb{R}^d$ be bounded and Lipschitz and let $\nu : \mathbb{R}_0^+ \to \mathbb{R}_0^+$ be a function satisfying* (2.26)*. Furthermore, let $B \in C^\infty(\overline{\Omega}; \mathbb{R}^{d\times d})$ be a matrix-valued function, such that $B(x)$ is invertible for all $x \in \overline{\Omega}$. Then for all $f \in H^{-1}(\Omega)$ and $g \in H^{1/2}(\partial\Omega)$, the variational problem* (4.16) *has a unique solution, which continuously depends on the data f and g, i.e. for the solutions $u_1, u_2 \in H_0^1(\Omega)$ of* (4.16) *with respective $(f_1, g_1), (f_2, g_2) \in H^{-1}(\Omega) \times H^{1/2}(\partial\Omega)$, it holds for a constant $c > 0$, that*

$$\|u_1 - u_2\|_{H_0^1(\Omega)} \le c\Big(\|f_1 - f_2\|_{H^{-1}(\Omega)} + \|g_1 - g_2\|_{H^{1/2}(\partial\Omega)}\Big). \tag{4.17}$$

Proof. A related proof is given in [26, Lemma B.2]. Here we will sketch the main idea, hence let $\widetilde{g} \in H^1(\Omega)$, such that $\widetilde{g}|_{\partial\Omega} = g$. Further, let $u_1, u_2 \in H_0^1(\Omega)$ be arbitrary functions and introduce $U_i = B^\top(\nabla u_i + \nabla\widetilde{g}) \in L^2(\Omega)^d$ for $i = 1, 2$. Then, since the reluctivity function maps to the non-negative real numbers, we obtain

$$\begin{aligned}
\langle Au_1 - Au_2, u_1 - u_2\rangle_\Omega &= \int_\Omega (\nu(|U_1|)BU_1 - \nu(|U_2|)BU_2) \cdot \nabla(u_1 - u_2)\, dx \\
&= \int_\Omega B\,(\nu(|U_1|)U_1 - \nu(|U_2|)U_2) \cdot \nabla(u_1 - u_2)\, dx \\
&= \int_\Omega (\nu(|U_1|)U_1 - \nu(|U_2|)U_2) \cdot B^\top\nabla(u_1 - u_2)\, dx \\
&= \int_\Omega (\nu(|U_1|)U_1 - \nu(|U_2|)U_2)\,(U_1 - U_2)\, dx. \\
&= \underline{\nu}\int_\Omega |U_1 - U_2|^2\, dx \\
&\quad + \int_\Omega \Big[(\nu(|U_1|)U_1 - \nu(|U_2|)U_2)\,(U_1 - U_2) - \underline{\nu}|U_1 - U_2|^2\Big]\, dx \\
&= \underline{\nu}\int_\Omega |U_1 - U_2|^2\, dx \\
&\quad + \int_\Omega \Big[(\nu(|U_1|) - \underline{\nu})U_1 - (\nu(|U_2|) - \underline{\nu})U_2\Big](U_1 - U_2)\, dx.
\end{aligned}$$

In order to obtain the strong monotonicity of the operator A, we further use the Cauchy-Schwarz inequality and (2.26) to derive

$$\begin{aligned}
&\langle Au_1 - Au_2, u_1 - u_2\rangle_\Omega \\
&\quad = \underline{\nu}\int_\Omega |U_1 - U_2|^2 \, dx + \int_\Omega \Big[(\nu(|U_1|) - \underline{\nu})U_1 - (\nu(|U_2|) - \underline{\nu})U_2\Big](U_1 - U_2) \, dx \\
&\quad = \underline{\nu}\int_\Omega |U_1 - U_2|^2 \, dx + \int_\Omega \Big[(\nu(|U_1|) - \underline{\nu})|U_1|^2 + (\nu(|U_2|) - \underline{\nu})|U_2|^2\Big] \, dx \\
&\qquad - \int_\Omega (\nu(|U_1|) + \nu(|U_2|) - 2\underline{\nu})U_1 \cdot U_2 \, dx \\
&\quad \geq \underline{\nu}\int_\Omega |U_1 - U_2|^2 \, dx + \int_\Omega \Big[(\nu(|U_1|) - \underline{\nu})|U_1|^2 + (\nu(|U_2|) - \underline{\nu})|U_2|^2\Big] \, dx \\
&\qquad - \int_\Omega (\nu(|U_1|) + \nu(|U_2|) - 2\underline{\nu})|U_1||U_2| \, dx \\
&\quad = \underline{\nu}\int_\Omega |U_1 - U_2|^2 \, dx + \int_\Omega \Big[\nu(|U_1|)|U_1| - \nu(|U_2|)|U_2|\Big](|U_1| - |U_2|) \, dx \\
&\qquad - \underline{\nu}\int_\Omega ||U_1| - |U_2||^2 \, dx \\
&\quad \geq \underline{\nu}\int_\Omega |U_1 - U_2|^2 \, dx + \underline{\nu}\int_\Omega ||U_1| - |U_2||^2 \, dx - \underline{\nu}\int_\Omega ||U_1| - |U_2||^2 \, dx \\
&\quad = \underline{\nu}\|U_1 - U_2\|^2_{L^2(\Omega)},
\end{aligned}$$

where the last estimate follows from the monotonicity of the reluctivity (2.26). By the definition of U_1 and U_2, we deduce

$$\begin{aligned}
\|U_1 - U_2\|^2_{L^2(\Omega)} &= \int_\Omega B^\top(\nabla u_1 - \nabla u_2) \cdot B^\top(\nabla u_1 - \nabla u_2) \, dx \\
&= \int_\Omega BB^\top(\nabla u_1 - \nabla u_2) \cdot (\nabla u_1 - \nabla u_2) \, dx \\
&\geq \underline{\gamma}_B \|\nabla u_1 - \nabla u_2\|^2_{L^2(\Omega)} = \underline{\gamma}_B |u_1 - u_2|^2_{H^1_0(\Omega)},
\end{aligned}$$

where the last estimate follows due to the fact that for invertible and smooth matrix-valued functions B, the symmetric matrix $BB^\top$ is uniformly bounded, see e.g. [133], i.e. there exist constants $\underline{\gamma}_B, \overline{\gamma}_B > 0$, such that

$$\underline{\gamma}_B|\xi|^2 < B(x)B^\top(x)\xi \cdot \xi < \overline{\gamma}_B|\xi|^2 \quad \text{for all } x \in \Omega, \xi \in \mathbb{R}^d. \tag{4.18}$$

This finally gives the strong monotonicity of the operator A with constant $c_m = \underline{\nu}\underline{\gamma}_B$.

For the Lipschitz continuity of A, we first realize that the Lipschitz constant ν_0 is an upper bound for the reluctivity function $\nu : \mathbb{R}_0^+ \to \mathbb{R}_0^+$, since

$$\nu(s)s = |\nu(s)s - \nu(0)0| \leq \nu_0|s - 0| = \nu_0 s \quad \text{for } s \in \mathbb{R}_0^+,$$

when using (2.26), which yields $\nu(s) \leq \nu_0$ for all $s \in \mathbb{R}_0^+$ as given in Lemma 2.7. Hence, with U_1 and U_2 as above, we have

$$\begin{aligned}
|\langle Au_1 - Au_2, v\rangle| &\leq \int_\Omega \Big|\Big(\nu(|U_1|)U_1 - \nu(|U_2|)U_2\Big) \cdot B^\top \nabla v\Big| \; dx \\
&= \int_\Omega \Big|\Big[\nu(|U_1|)(U_1 - U_2) + \Big(\nu(|U_1|) - \nu(|U_2|)\Big)U_2\Big] \cdot B^\top \nabla v\Big| \; dx \\
&\leq \int_\Omega \Big|\nu(|U_1|)(U_1 - U_2) + \Big(\nu(|U_1|) - \nu(|U_2|)\Big)U_2\Big| \Big|B^\top \nabla v\Big| \; dx \\
&\leq \int_\Omega \Big[\nu(|U_1|)|U_1 - U_2| + \Big|\Big(\nu(|U_1|) - \nu(|U_2|)\Big)|U_2|\Big|\Big] \Big|B^\top \nabla v\Big| \; dx.
\end{aligned}$$

We further observe with the boundedness of the reluctivity function that

$$\begin{aligned}
\Big|\Big(\nu(|U_1|) - \nu(|U_2|)\Big)|U_2|\Big| &= \Big|\nu(|U_1|)(|U_2| - |U_1|) + \nu(|U_1|)|U_1| - \nu(|U_2|)|U_2|\Big| \\
&\leq \nu(|U_1|)\Big||U_2| - |U_1|\Big| + \Big|\nu(|U_1|)|U_1| - \nu(|U_2|)|U_2|\Big| \\
&\leq \nu(|U_1|)|U_1 - U_2| + \Big|\nu(|U_1|)|U_1| - \nu(|U_2|)|U_2|\Big| \\
&\leq \nu_0|U_1 - U_2| + \nu_0\Big||U_1| - |U_2|\Big| \\
&\leq 2\nu_0|U_1 - U_2|,
\end{aligned}$$

which yields

$$\begin{aligned}
|\langle Au_1 - Au_2, v\rangle| &\leq \int_\Omega \Big[\nu(|U_1|)|U_1 - U_2| + \Big|\Big(\nu(|U_1|) - \nu(|U_2|)\Big)|U_2|\Big|\Big] \Big|B^\top \nabla v\Big| \; dx \\
&\leq \int_\Omega \Big[\nu_0|U_1 - U_2| + 2\nu_0|U_1 - U_2|\Big] \Big|B^\top \nabla v\Big| \; dx \\
&\leq 3\nu_0 \|U_1 - U_2\|_{L^2(\Omega)} \|B^\top \nabla u\|_{L^2(\Omega)} \\
&\leq 3\nu_0 \overline{\gamma}_B \|u_1 - u_2\|_{H_0^1(\Omega)} \|v\|_{H_0^1(\Omega)},
\end{aligned}$$

where the last estimate follows from (4.18). Finally, we conclude that

$$\begin{aligned}
\|Au_1 - Au_2\|_{H^{-1}(\Omega)} &= \sup_{0 \neq v \in H_0^1(\Omega)} \frac{|\langle Au_1 - Au_2, v\rangle|}{\|v\|_{H_0^1(\Omega)}} \\
&\leq 3\nu_0 \overline{\gamma}_B \sup_{0 \neq v \in H_0^1(\Omega)} \frac{\|u_1 - u_2\|_{H_0^1(\Omega)} \|v\|_{H_0^1(\Omega)}}{\|v\|_{H_0^1(\Omega)}} \\
&= 3\nu_0 \overline{\gamma}_B \|u_1 - u_2\|_{H_0^1(\Omega)},
\end{aligned}$$

with the constant $L = 3\nu_0\overline{\gamma}_B$. It follows from Theorem 4.4 that the variational formulation (4.16) has a unique solution, with a Lipschitz continuous dependence on the data given by the constant $c = \frac{3\nu_0\overline{\gamma}_B}{\underline{\nu\gamma}_B}$. □

After presenting the unique solvability of nonlinear elliptic problems, we now turn our focus on the well-posedness of nonlinear evolution problems, for which we use the principle of maximal monotone mappings, see e.g. [167, Chapter 32]. For our purpose, we summarize the important results in the following theorem.

THEOREM 4.6. *Let the operator $A(t) : H_0^1(\Omega) \to H^{-1}(\Omega)$ be strongly monotone and Lipschitz continuous for each $t \in (0,T)$, whose monotonicity and Lipschitz constant are independent of time. Then, $A : Y \to Y^\star$ defines a strongly monotone and Lipschitz continuous operator, whose monotonicity and Lipschitz constant are as well independent of time, and the space-time operator formulation*

$$\begin{aligned} \frac{\partial}{\partial t}u + Au &= f \quad \text{in } Y^\star, \\ u(0) &= 0, \end{aligned}$$

admits a unique solution $u \in \{u \in Y : \partial_t u \in Y^\star\}$ for every $f \in Y^\star$.

Proof. A proof for the linear and time dependent operator is given in [167, Theorem 30.A]. The extension to the nonlinear time dependent case is the combination of Theorem 32.D and Theorem 30.12 in [167]. Further investigations are done in [167, Chapter 30-32]. □

Lastly, the following lemma is another important ingredient in order to prove the unique solvability of (4.15), and it is based on Sobolev's norm equivalence theorem [143, Theorem 2.6].

LEMMA 4.7. *Let $u \in H^1(\Omega_{con})$, where $\Omega_{con} = \Omega\backslash\overline{\Omega_{non}} \subset \mathbb{R}^d$. Then, the norm*

$$\|u\|^2_{H^1(\Omega_{con}),H^{1/2}(\partial\Omega_{con})} \coloneqq \|\nabla_x u\|^2_{L^2(\Omega_{con})} + \|\gamma_0 u\|^2_{H^{1/2}(\partial\Omega_{con})}$$

defines an equivalent norm in the space $H^1(\Omega_{con})$, i.e.

$$\underline{c}_P\|u\|_{H^1(\Omega_{con})} \le \|u\|_{H^1(\Omega_{con}),H^{1/2}(\partial\Omega_{con})} \le \overline{c}_P\|u\|_{H^1(\Omega_{con})},$$

where γ_0 is the trace operator as defined in Theorem 3.8.

Proof. This lemma is a result of Sobolev's norm equivalence theorem [143, Theorem 2.6], for which we need to prove that the mapping $u \to \|\gamma_0 u\|_{H^{1/2}(\partial\Omega_{con})}$ is bounded and satisfies

$$\begin{aligned} \|\alpha\gamma_0 u\|_{H^{1/2}(\partial\Omega_{con})} &= |\alpha|\|\gamma_0 u\|_{H^{1/2}(\partial\Omega_{con})} && \text{for all } u \in H^1(\Omega_{con}),\ \alpha \in \mathbb{R}, \\ \|\gamma_0(u+v)\|_{H^{1/2}(\partial\Omega_{con})} &\le \|\gamma_0 u\|_{H^{1/2}(\partial\Omega_{con})} + \|\gamma_0 v\|_{H^{1/2}(\partial\Omega_{con})} && \text{for all } u, v \in H^1(\Omega_{con}). \end{aligned}$$

Furthermore, we have to show that, if $\|\alpha\|_{H^{1/2}(\partial\Omega_{con})} = 0$ for $\alpha \in \mathbb{R}$, then it must hold that $\alpha = 0$.

The mapping $u \to \|\gamma_0 u\|_{H^{1/2}(\partial\Omega_{con})}$ is bounded due to the trace inequality in Theorem 3.8, i.e.

$$\|\gamma_0 u\|_{H^{1/2}(\partial\Omega_{con})} \leq c_{tr}\|u\|_{H^1(\Omega_{con})}.$$

Obviously, $\|\gamma_0 u\|_{H^{1/2}(\partial\Omega_{con})}$ satisfies the remaining conditions, since it defines a norm in the space $H^{1/2}(\partial\Omega_{con})$. □

Finally, we are now in the position to state the well-posedness of the nonlinear elliptic-parabolic variational problem (4.15) by using Lemma 4.5, Theorem 4.6 and Lemma 4.7.

THEOREM 4.8. *Let $l \in Y^\star$, then the space-time variational formulation* (4.15) *has a unique solution $u \in X$, which has a Lipschitz dependence on l, i.e. there exists a constant $c > 0$, such that*

$$\|u_1 - u_2\|^2_{L^2(0,T;H^1_0(\Omega))} + \|\sigma\frac{\partial}{\partial t}(u_1 - u_2)\|^2_{L^2(0,T;H^{-1}(\Omega))} \leq c\|l_1 - l_2\|^2_{L^2(0,T;H^{-1}(\Omega))},$$

where $u_1, u_2 \in X$ are the solutions of (4.15) *associated to the respective sources $l_1, l_2 \in Y^\star$.*

Proof. We will proceed in the following way. First, we assume there exists a solution $u \in X$ to the space-time variational problem (4.15) and consider an equivalent problem (4.20), for which Theorem 4.6 is applicable. Indeed, the solution is unique if it exists. Finally, we construct a solution for (4.15) from the solution of (4.20) in order to conclude the proof.

Assume that $u \in X$ is the solution to the space-time variational problem (4.15). We can equivalently rewrite (4.15) to the variational problem, that is to find $u \in X$, such that for almost all $t \in (0, T)$

$$\int_\Omega \left[\sigma(x)\frac{\partial}{\partial t}u(x,t)v(x) + \nu(x, |\nabla_x u|)\nabla_x u(x,t) \cdot \nabla_x v(x)\right] dx = \widetilde{l}(x,t) \tag{4.19}$$

for all $v \in H^1_0(\Omega)$, see [167, Section 30.4 and Chapter 32], where

$$\widetilde{l}(x,t) = \int_\Omega \left[J_3(x,t)v(x) + M^\perp(x,t) \cdot \nabla_x v(x)\right] dx.$$

Hence, the solution $u \in X$ to (4.15) is also a solution to (4.19), and (4.19) is still of elliptic-parabolic type, recalling that σ vanishes in Ω_{non}. When using test functions v with compact support inside $\Omega \backslash \overline{\Omega_{con}}$ in (4.19), we see that u satisfies the equation

$$-\mathrm{div}_x\Big(\nu(x, |\nabla_x u|)\nabla_x u(x,t)\Big) = J_3(x,t) \quad \text{for } x \in \Omega\backslash\overline{\Omega_{con}},$$

assuming $M^\perp = 0$ in Ω_{non}. Now, when we consider the spatial restriction of $u(\cdot,t)$ to Ω_{con}, denoted by $u_c(\cdot,t)$, spatial integration by parts on $\Omega\backslash\overline{\Omega_{con}}$ reveals that u_c satisfies the variational problem

$$\begin{aligned}\sigma_{con} \int\limits_{\Omega_{con}} \frac{\partial}{\partial t} u_c(x,t)v(x)\,dx + \nu_{con} \int\limits_{\Omega_{con}} \nabla_x u_c(x,t)\cdot\nabla_x v(x)\,dx \\ - \int\limits_{\partial\Omega_{con}} \gamma_0\Big(\nu(x, |\nabla_x \mathcal{L}_t u_c|)\nabla_x \mathcal{L}_t u_c(x,t)\Big)\cdot n(x)\gamma_0 v(x)\,ds_x = \widetilde{l}(x,t)\end{aligned} \tag{4.20}$$

for all $v \in H^1(\Omega_{con})$, where $\widetilde{l}(\cdot,t)$ is defined on Ω_{con}, σ_{con} and ν_{con} are constants in Ω_{con}, γ_0 is the trace operator as defined in Theorem 3.8, n is the outward unit normal vector of Ω_{con}, and for $u_c(\cdot,t) \in H^1(\Omega_{con})$, we define $\mathcal{L}_t u_c(\cdot,t) \in H^1(\Omega\backslash\overline{\Omega_{con}})$ as the unique solution of the Dirichlet boundary value problem

$$\begin{aligned} -\mathrm{div}_x\Big(\nu(x, |\nabla_x \mathcal{L}_t u_c|)\nabla_x \mathcal{L}_t u_c(x,t)\Big) &= J_3(x,t) && \text{for } x \in \Omega\backslash\overline{\Omega_{con}}, \\ \mathcal{L}_t u_c(x,t) &= \gamma_0 u_c(x,t) && \text{for } x \in \partial\Omega_{con}, \\ \mathcal{L}_t u_c(x,t) &= 0 && \text{for } x \in \partial\Omega. \end{aligned} \tag{4.21}$$

We want to prove that u_c is indeed a unique solution to the variational problem (4.20). For this purpose, we introduce the linear operator $\mathcal{A} : H^1(\Omega_{con}) \to H^1(\Omega_{con})^\star$ and the nonlinear operator $\mathcal{B} : H^1(\Omega_{con}) \to H^1(\Omega_{con})^\star$, which are defined by

$$\begin{aligned}\langle \mathcal{A}u, v\rangle_{H^1(\Omega_{con})^\star, H^1(\Omega_{con})} &= \nu_{con} \int\limits_{\Omega_{con}} \nabla_x u(x,t)\cdot\nabla_x v(x)\,dx, \\ \langle \mathcal{B}u, v\rangle_{H^1(\Omega_{con})^\star, H^1(\Omega_{con})} &= -\int\limits_{\partial\Omega_{con}} \gamma_0\Big(\nu(x, |\nabla_x \mathcal{L}_t u|)\nabla_x \mathcal{L}_t u(x,t)\Big)\cdot n(x)\gamma_0 v(x)\,ds_x,\end{aligned}$$

for $u(\cdot,t), v \in H^1(\Omega_{con})$. Hence, we can write (4.20) shortly as

$$\sigma_{con} \int\limits_{\Omega_{con}} \frac{\partial}{\partial t} u_c(x,t)v(x)\,dx + \langle \mathcal{A}u_c + \mathcal{B}u_c, v\rangle_{H^1(\Omega_{con})^\star, H^1(\Omega_{con})} = \widetilde{l}(x,t)$$

for all $v \in H^1(\Omega_{con})$. We start to analyze the linear operator $\mathcal{A}$ and easily obtain

that $\mathcal{A}$ is Lipschitz continuous, i.e. for all $u_1, u_2 \in H^1(\Omega_{con})$ it holds

$$\begin{aligned}\|\mathcal{A}u_1 - \mathcal{A}u_2\|_{H^1(\Omega_{con})^\star} &= \sup_{0\neq v\in H^1(\Omega_{con})} \frac{|\langle \mathcal{A}u_1 - \mathcal{A}u_2, v\rangle_{H^1(\Omega_{con})^\star, H^1(\Omega_{con})}|}{\|v\|_{H^1(\Omega_{con})}} \\ &\leq \sup_{0\neq v\in H^1(\Omega_{con})} \frac{\nu_{con}\|\nabla_x(u_1-u_2)\|_{L^2(\Omega_{con})}\|\nabla_x v\|_{L^2(\Omega_{con})}}{\|v\|_{H^1(\Omega_{con})}} \\ &\leq \nu_{con}\|u_1-u_2\|_{H^1(\Omega_{con})}.\end{aligned}$$

Furthermore, the linear operator $\mathcal{A}$ is monotone, since for all $u_1, u_2 \in H^1(\Omega_{con})$ it holds

$$\langle \mathcal{A}u_1 - \mathcal{A}u_2, u_1 - u_2\rangle_{H^1(\Omega_{con})^\star, H^1(\Omega_{con})} = \nu_{con}\|\nabla_x(u_1-u_2)\|^2_{L^2(\Omega_{con})} \geq 0.$$

We now focus on the nonlinear operator $\mathcal{B}$, for which we fist introduce the linear extension operator $\mathcal{E} : H^1(\Omega_{con}) \to H^1(\Omega)$, such that $\|\mathcal{E}v\|_{H^1(\Omega)} \leq c_E\|v\|_{H^1(\Omega_{con})}$, cf. [1], in order to obtain when using integration by parts, that

$$\begin{aligned}\langle \mathcal{B}u, v\rangle_{H^1(\Omega_{con})^\star, H^1(\Omega_{con})} &= -\int_{\partial\Omega_{con}} \gamma_0\Big(\nu(x,|\nabla_x\mathcal{L}_t u|)\nabla_x\mathcal{L}_t u(x,t)\Big)\cdot n(x)\gamma_0 v(x)\; ds_x \\ &= \int_{\Omega\setminus\overline{\Omega_{con}}} \nu(x,|\nabla_x\mathcal{L}_t u|)\nabla_x\mathcal{L}_t u(x,t)\cdot\nabla_x\mathcal{E}v(x)\; dx \\ &\qquad - \int_{\Omega\setminus\overline{\Omega_{con}}} \mathrm{div}_x(\nu(x,|\nabla_x\mathcal{L}_t u|)\nabla_x\mathcal{L}_t u(x,t))\mathcal{E}v(x)\; dx \\ &= \int_{\Omega\setminus\overline{\Omega_{con}}} \nu(x,|\nabla_x\mathcal{L}_t u|)\nabla_x\mathcal{L}_t u(x,t)\cdot\nabla_x\mathcal{E}v(x)\; dx \\ &\qquad + \int_{\Omega\setminus\overline{\Omega_{con}}} J_3(x,t)\mathcal{E}v(x)\; dx,\end{aligned}$$

for $u, v \in H^1(\Omega_{con})$, where $\mathcal{L}_t u$ satisfies the boundary value problem (4.21). Hence, for $u_1, u_2 \in H^1(\Omega_{con})$ satisfying (4.21), we have

$$\begin{aligned}\langle \mathcal{B}u_1 - \mathcal{B}u_2, v\rangle_{H^1(\Omega_{con})^\star, H^1(\Omega_{con})} &= \int_{\Omega\setminus\overline{\Omega_{con}}} \nu(x,|\nabla_x\mathcal{L}_t u_1|)\nabla_x\mathcal{L}_t u_1(x,t)\cdot\nabla_x\mathcal{E}v(x)\; dx \\ &\qquad - \int_{\Omega\setminus\overline{\Omega_{con}}} \nu(x,|\nabla_x\mathcal{L}_t u_2|)\nabla_x\mathcal{L}_t u_2(x,t)\cdot\nabla_x\mathcal{E}v(x)\; dx,\end{aligned}$$

where the application of Lemma 4.5 to the operator $\mathcal{L}_t : H^1(\Omega_{con}) \to H^1(\Omega\setminus\overline{\Omega_{con}})$

with $B = I$ gives

$$\begin{aligned}\|Bu_1 - Bu_2\|_{H^1(\Omega_{con})^\star} &= \sup_{v\in H^1(\Omega_{con})} \frac{|\langle \mathcal{B}u_1 - \mathcal{B}u_2, v\rangle_{H^1(\Omega_{con})^\star, H^1(\Omega_{con})}|}{\|v\|_{H^1(\Omega_{con})}} \\ &\leq 3\nu_0 c_E \|\nabla_x \mathcal{L}_t u_1 - \nabla_x \mathcal{L}_t u_2\|_{L^2(\Omega\setminus\overline{\Omega_{con}})} \\ &\leq 3\nu_0 c_E \|\mathcal{L}_t u_1 - \mathcal{L}_t u_2\|_{H^1(\Omega\setminus\overline{\Omega_{con}})}.\end{aligned}$$

According to Lemma 4.5, $\mathcal{L}_t u_1$ and $\mathcal{L}_t u_2$ are the unique solutions to (4.21) for the given boundary data u_1 and u_2, respectively, but the same right-hand side J_3, hence the continuity estimate (4.17) holds, and we deduce

$$\begin{aligned}\|Bu_1 - Bu_2\|_{H^1(\Omega_{con})^\star} &\leq 3\nu_0 c_E \|\mathcal{L}_t u_1 - \mathcal{L}_t u_2\|_{H^1(\Omega\setminus\overline{\Omega_{con}})} \\ &\leq 3\nu_0 c_E c_{\mathcal{L}_t} \|\gamma_0(u_1 - u_2)\|_{H^{1/2}(\partial\Omega_{con})} \\ &\leq 3\nu_0 c_E c_{\mathcal{L}_t} c_{tr} \|u_1 - u_2\|_{H^1(\Omega_{con})},\end{aligned}$$

where the last estimate follows from the trace inequality. Hence, we conclude the Lipschitz continuity of the operator $\mathcal{B}$.

Moreover, for $u_1, u_2 \in H^1(\Omega_{con})$ satisfying (4.21) we obtain with the same calculations as before that

$$\begin{aligned}&\langle \mathcal{B}u_1 - \mathcal{B}u_2, u_1 - u_2\rangle_{H^1(\Omega_{con})^\star, H^1(\Omega_{con})} \\ &\quad = \int_{\Omega\setminus\overline{\Omega_{con}}} \nu(x, |\nabla_x \mathcal{L}_t u_1|)\nabla_x \mathcal{L}_t u_1(x,t) \cdot (\nabla_x \mathcal{L}_t u_1(x,t) - \nabla_x \mathcal{L}_t u_2(x,t))\, dx \\ &\qquad - \int_{\Omega\setminus\overline{\Omega_{con}}} \nu(x, |\nabla_x \mathcal{L}_t u_2|)\nabla_x \mathcal{L}_t u_2(x,t) \cdot (\nabla_x \mathcal{L}_t u_1(x,t) - \nabla_x \mathcal{L}_t u_2(x,t))\, dx.\end{aligned}$$

Using the same steps as in the proof of Lemma 4.5, we deduce

$$\langle \mathcal{B}u_1 - \mathcal{B}u_2, u_1 - u_2\rangle_{H^1(\Omega_{con})^\star, H^1(\Omega_{con})} \geq \underline{\nu} \|\nabla_x \mathcal{L}_t u_1 - \nabla_x \mathcal{L}_t u_2\|^2_{L^2(\Omega\setminus\overline{\Omega_{con}})}.$$

Due to Friedrichs's inequality (3.12), the norms $\|\nabla_x u\|_{L^2(\Omega\setminus\overline{\Omega_{con}})}$ and $\|u\|_{H^1(\Omega\setminus\overline{\Omega_{con}})}$ are equivalent on the space $H^1_{0,\partial\Omega}(\Omega\setminus\overline{\Omega_{con}}) := \{u \in H^1(\Omega\setminus\overline{\Omega_{con}}) : \gamma_0 u = 0 \text{ on } \partial\Omega\}$, hence it follows that

$$\begin{aligned}\langle \mathcal{B}u_1 - \mathcal{B}u_2, u_1 - u_2\rangle_{H^1(\Omega_{con})^\star, H^1(\Omega_{con})} &\geq c\underline{\nu} \|\mathcal{L}_t u_1 - \mathcal{L}_t u_2\|^2_{H^1(\Omega\setminus\overline{\Omega_{con}})} \\ &\geq c c_{tr}^2 \underline{\nu} \|\gamma_0(u_1 - u_2)\|^2_{H^{1/2}(\partial\Omega_{con})},\end{aligned}$$

where the last estimate follows from the trace inequality.

Finally, we can combine both operators $\mathcal{A} + \mathcal{B}$ to conclude the Lipschitz continuity,

$$\|(\mathcal{A} + \mathcal{B})u_1 - (\mathcal{A} + \mathcal{B})u_2\|_{H^1(\Omega_{con})^\star} \leq L\|u_1 - u_2\|_{H^1(\Omega_{con})},$$

with $L = \max(\nu_{con}, 3\nu_0 c_E c_{\mathcal{L}_t} c_{tr})$, and the strong monotonicity,

$$\begin{aligned}\langle(\mathcal{A}+\mathcal{B})u_1 - (\mathcal{A}+\mathcal{B})u_2, u_1 - u_2\rangle_{H^1(\Omega_{con})^\star, H^1(\Omega_{con})} \\ \geq \nu_{con}\|\nabla_x(u_1-u_2)\|^2_{L^2(\Omega_{con})} + cc_{tr}^2\underline{\nu}\|\gamma_0(u_1-u_2)\|^2_{H^{1/2}(\partial\Omega_{con})} \\ \geq C\|u_1-u_2\|^2_{H^1(\Omega_{con}),H^{1/2}(\partial\Omega_{con})} \geq \underline{c}_P^2 C\|u_1-u_2\|^2_{H^1(\Omega_{con})}\end{aligned}$$

with $C = \min(\nu_{con}, cc_{tr}^2\underline{\nu})$, where we have used the norm as defined in Lemma 4.7 and its application. Therefore, it follows from Theorem 4.6 that the variational problem (4.20) has a unique solution $u_c \in L^2(0,T;H^1(\Omega_{con}))$, such that $u_c(x,0) = 0$ for $x \in \Omega_{con}$. This almost implies that the solution $u \in X$ of the original space-time variational formulation (4.15) is unique, when it exists. In fact, let $u_1, u_2 \in X$ be two solutions of (4.15) and let $u_{c,1}(\cdot,t), u_{c,2}(\cdot,t)$ be their restrictions on $H^1(\Omega_{con})$, respectively, then we conclude as a result from the previous steps that $u_{c,1}, u_{c,2}$ belong to $L^2(0,T;H^1(\Omega_{con}))$ and satisfy the variational problem (4.20) with the homogenous initial condition $u_{c,1}(x,0) = u_{c,2}(x,0) = 0$ for $x \in \Omega_{con}$. As a consequence of Theorem 4.6, $u_{c,1}(\cdot,t) = u_{c,2}(\cdot,t)$ on Ω_{con} for almost all $t \in [0,T]$, hence $u_1(\cdot,t)$ and $u_2(\cdot,t)$ coincide on Ω_{con} for almost all $t \in [0,T]$. Moreover, since $u_1(\cdot,t)|_{\Omega\setminus\overline{\Omega_{con}}} = \mathcal{L}_t u_{c,1}(\cdot,t)$ and $u_2(\cdot,t)|_{\Omega\setminus\overline{\Omega_{con}}} = \mathcal{L}_t u_{c,2}(\cdot,t)$ on $\Omega\setminus\overline{\Omega_{con}}$, it immediately follows that $u_1 = u_2$ in $L^2(0,T;H_0^1(\Omega))$. This means, that there exists at most one solution $u \in X$ of (4.20).

In the final step, we need to construct a solution $u \in X$ to (4.20), which essentially relies on the previous steps. Let $u_c \in L^2(0,T;H^1(\Omega_{con}))$ be the unique solution of (4.20) satisfying the homogenous initial condition $u_c(x,t) = 0$ for $x \in \Omega_{con}$. Particularly, $u_c(\cdot,t)$ is a function in $H^1(\Omega_{con})$ for almost all $t \in [0,T]$, hence we can introduce the unique solution $u_{c,ext}(\cdot,t) = \mathcal{L}_t u_c(\cdot,t) \in H^1(\Omega\setminus\overline{\Omega_{con}})$ to the version of (4.21) featuring Dirichlet data $\gamma_0 u_c(\cdot,t)$ on $\partial\Omega_{con}$. This leads to the definition of $u(\cdot,t) \in H_0^1(\Omega)$, that is

$$u(x,t) = \begin{cases} u_c(x,t) & \text{for } x \in \Omega_{con}, \\ u_{c,ext}(x,t) & \text{for } x \in \Omega\setminus\overline{\Omega_{con}}. \end{cases}$$

By construction, $u \in L^2(0,T;H_0^1(\Omega))$ is one solution of (4.19). Furthermore, it can be seen that $\sigma\frac{\partial}{\partial t}u \in L^2(0,T;H^{-1}(\Omega))$, since $\frac{\partial}{\partial t}u_c \in L^2(0,T;H^1(\Omega_{con})^\star)$, and for almost all $t \in [0,T]$ and for any test function $v \in H_0^1(\Omega)$, we have

$$\langle\sigma\frac{\partial}{\partial t}u, v\rangle_{H^{-1}(\Omega),H_0^1(\Omega)} = \sigma_{con}\langle\frac{\partial}{\partial t}u_c, v\rangle_{H^1(\Omega_{con})^\star,H^1(\Omega_{con})}.$$

We conclude that $u \in X$ is a solution to (4.19), hence also to (4.15), for which the Lipschitz dependence on the data follows from the Lipschitz dependence of the solutions to the problems (4.20) and (4.21). This ends the proof. □

Space-time finite element discretization

As for the linear case, we introduce the conforming finite-dimensional spaces $X_h \subset X$ and $Y_h \subset Y$, such that $X_h \subset Y_h$. Particularly, we even consider $X_h = Y_h$ as in (4.7) for our purpose. Hence, the discrete problem reads to find $u_h \in X_h$, such that

$$a(u_h, v_h) = l(v_h) \quad \text{for all } v_h \in Y_h, \tag{4.22}$$

where $a(\cdot,\cdot)$ and $l(\cdot)$ are defined as in (4.15). The existence of a unique solution $u_h \in X_h$ follows from Theorem 4.8, since the properties of $a(\cdot,\cdot)$ are inherited from the continuous problem. We apply Newton's method [37] to solve the nonlinear problem (4.22). Therefor, we introduce the operator $A_e : Y_h \to Y_h^\star$, such that

$$\langle A_e(u_h), v_h\rangle = \int_0^T \int_\Omega \nu(x, |\nabla_x u_h|)\nabla_x u_h(x,t) \cdot \nabla_x v_h(x,t)\; dxdt,$$

hence we can rewrite (4.22) as an operator equation

$$\langle \sigma \frac{\partial}{\partial t} u_h, v_h\rangle + \langle A_e(u_h), v_h\rangle = l(v_h).$$

Furthermore, we need to compute the Fréchet derivative of the operator $A_e(u_h)$ in a direction w_h, which is

$$\begin{aligned}\langle D_{w_h}(A_e(u_h)), v_h\rangle &= \lim_{\delta\to 0}\frac{1}{\delta}\Big[\langle A_e(u_h+\delta w_h), v_h\rangle - \langle A_e(u_h), v_h\rangle\Big] \\ &= \int_0^T \int_\Omega \lim_{\delta\to 0}\frac{1}{\delta}\Big[\nu(|\nabla_x u_h + \delta\nabla_x w_h|)(\nabla_x u_h + \delta\nabla_x w_h) - \nu(|\nabla_x u_h|)\nabla_x u_h\Big]\cdot\nabla_x v_h\; dxdt.\end{aligned}$$

We set $p = \nabla_x u_h$ and $q = \nabla_x w_h$ in order to obtain with the Taylor expansion for $p \neq 0$ that

$$\nu(|p+\delta q|) = \nu(|p|) + \delta\nu'(|p|)\frac{p}{|p|}\cdot q + \mathcal{O}(\delta|q|).$$

Hence, we get

$$\nu(|p+\delta q|)(p+\delta q) - \nu(|p|)p = \delta\nu(|p|)q + \delta\frac{\nu'(|p|)}{|p|}(p\cdot q)p + \mathcal{O}(\delta|q|).$$

For $p = 0$ we deduce

$$\lim_{\delta\to 0}\frac{\nu(|\delta q|)tq - \nu(0)0}{\delta - 0} = \lim_{\delta\to 0}\nu(|\delta q|)tq = \nu(0)q.$$

Now, using $p = \nabla_x u_h$ and $q = \nabla_x w_h$, we get the Fréchet derivative of $A_e(u_h)$ in direction w_h

$$\langle D_{w_h}(A_e(u_h)), v_h\rangle = \int_0^T \int_\Omega \nu(|\nabla_x u_h|)\nabla_x w_h \cdot \nabla_x v_h + \frac{\nu'(|\nabla_x u_h|)}{|\nabla_x u_h|}(\nabla_x u_h \cdot \nabla_x w_h)(\nabla_x u_h \cdot \nabla_x v_h)\; dxdt,$$

for $\nabla_x u_h \neq 0$, and

$$\langle D_{w_h}(A_e(u_h)), v_h\rangle = \int_0^T \int_\Omega \nu(0)\nabla_x w_h \cdot \nabla_x v_h\; dxdt,$$

for $\nabla_x u_h = 0$. Hence, we can define the Newton operator $A'_e(u_h) \in \mathcal{L}(Y_h, Y_h^\star)$ as

$$\langle A'_e(u_h)w_h, v_h\rangle \coloneqq \langle D_{w_h}(A_e(u_h)), v_h\rangle. \tag{4.23}$$

In fact, $D_{w_h}(A_e(u_h))$ is linear and bounded in w_h. For a deeper analysis of the Newton operator $A'_e(u_h)$, also in the continuous setting, with respect to the eddy current problem we refer to [57, 119]. A more general approach is provided by the book of Deuflhard [37]. Note that the above derivation of the Newton operator is also valid in the continuous case.

We use the finite element isomorphism (4.12) in order to derive the equivalent nonlinear Galerkin system, which is to find $\underline{u}_h \in \mathbb{R}^M$, such that

$$A(\underline{u}_h) = \underline{l}, \tag{4.24}$$

where

$$A(\underline{u}_h) = \Big(a(u_h, \phi_i)\Big)_{i=1}^M, \qquad \underline{l} = \Big(l(\phi_i)\Big)_{i=1}^M,$$

cf. [44]. Note that the operator A in (4.24) considers also the time derivative of $\underline{u}_h$. However, the time derivative is linear with respect to $\underline{u}_h$, hence we can write

$$\langle A'(\underline{u}_h)\underline{w}_h, \underline{v}_h\rangle = \langle \sigma \frac{\partial}{\partial t}\underline{w}_h, \underline{v}_h\rangle + \langle A'_e(\underline{u}_h)\underline{w}_h, \underline{v}_h\rangle.$$

We use Newton's method [37] with an adapted backtracking line search method in order to solve the system (4.24). For this reason we write our problem as to find $\underline{u}_h$, such that

$$A(\underline{u}_h) - \underline{l} = 0,$$

for which we apply Newton's method with damping [37]

$$\underline{u}_{k+1} = \underline{u}_k - \tau \left[A'(\underline{u}_k)\right]^{-1} \left(A(\underline{u}_k) - \underline{l}\right), \tag{4.25}$$

for a starting vector $\underline{u}_0$ and a damping factor $\tau > 0$. We solve (4.25) in the following way. First, we compute $\underline{w}_k$ as the solution of the linear system

$$A'(\underline{u}_k)\underline{w}_k = (A(\underline{u}_k) - \underline{l}), \tag{4.26}$$

and we use the solution $\underline{w}_k$ to compute the next approximate solution via the line search

$$\widetilde{\underline{u}}_k = \underline{u}_k - \tau \underline{w}_k \quad \text{for } \tau \in \{1, 0.5, 0.25, \dots 2^{-j}\}.$$

We stop the line search if $\|A(\widetilde{\underline{u}}_k) - \underline{l}\| < \|A(\underline{u}_k) - \underline{l}\|$ or $\tau > 2^{-j}$ for $j \in \mathbb{N}$, and update

$$\underline{u}_{k+1} = \widetilde{\underline{u}}_k.$$

The method stops when a given error tolerance is reached, i.e. $(\underline{w}_k, A(\widetilde{\underline{u}}_k) - \underline{l}) < TOL$. Note that, the described method is applied efficiently with respect to the number of operations and the memory usage, and we refer to [37] for a detailed analysis of Newton's method.

4.1.4 Numerical examples

First, we again consider the space-time cylinder $Q = (0,1)^2$ as given in Figure 4.1 and the manufactured solution

$$u(x,t) = x(1-x)t.$$

For the nonlinear variational formulation (4.15) we use the material parameters

$$\sigma(x) = \begin{cases} 1 & \text{for } x \in \Omega_{con}, \\ 0 & \text{for } x \in \Omega_{non}, \end{cases} \quad \text{and} \quad \nu(x, |\partial_x u|) = \begin{cases} 2 & \text{for } x \in \Omega_{con}, \\ 1 + |\partial_x u|^2 & \text{for } x \in \Omega_{non}. \end{cases}$$

Hence, we obtain for the right-hand side that $M^{\perp} = 0$ and

$$J_3(x,t) = \begin{cases} x(1-x) + 4t & \text{for } x \in \Omega_{con}, \\ 2t(1 + 3t^2(1-2x)^2) & \text{for } x \in \Omega_{non}, \end{cases}$$

We compute the solution of (4.22) by using the finite element isomorphism (4.12) in order to deduce the system (4.24) and apply Newton's method (4.25) with damping. The occurring linear system (4.26) is solved by the parallel direct solver MUMPS and iterative solver GMRES with the BoomerAMG preconditioner as described in Section 3.6.1. We use a relative error tolerance of 10^{-8} for the stop criterion of Newton's method as well as for the parallel iterative solver GMRES. In Table 4.5 we

L	dofs	$\|\nabla_x(u-u_h)\|_{L^2(Q)}$	EOC
1	13	0.11216	
2	41	0.05656	0.988
3	145	0.02855	0.986
4	545	0.01436	0.991
5	2,113	0.00720	0.996
6	8,321	0.00360	0.999
7	33,025	0.00180	0.999
8	131,585	0.00090	1
9	525,313	0.00045	1
10	2,099,201	0.00023	1

Table 4.5: The discretization error, which indicates linear convergence when using the parallel direct solver as well as the iterative solver on 16 cores for a uniform mesh refinement. The number of GMRES iterations increases in each refinement step, ending up with a maximum of 1973 iterations.

Number of cores	1	2	4	8	16
MUMPS	109.24	79.25	62.85	53.12	49.78
GMRES	914.89	615.59	244.32	119.48	65.90
iterations	274	196	186	177	171

Table 4.6: Computational times in seconds for solving the nonlinear problem (4.24) with MUMPS and preconditioned GMRES with the BoomerAMG preconditioner on a mesh with 525,313 nodes (degrees of freedom) and 262,144 elements. The solvers required 5 Newton iterations and the number of GMRES iterations gives the most needed iterations of all Newton steps.

obtain a linear convergence behavior of the error in the semi-norm. In each refinement level mostly 6 Newton iterations were needed. Furthermore, the computational times for solving the nonlinear problem (4.24) with respect to the number of cores are given in Table 4.6. Note that the measured times include the linearization of A in order to obtain A' in (4.26) and the converting of the data types between the software Netgen/NGSolve and PETSc in each Newton iteration.

As our next example we consider the realistic application of an electric motor stated in the TEAM24 benchmark [2]. The geometry is similar to a Switched Reluctance Motor with two poles. The rotor is rotated to a specific point but standing still at this location. The 350-turn coils are located above the stator and excited by a step voltage. Figure 4.5 displays the geometry of the motor, whose dimensions are given in [2]. The stator and the rotor are made of steel and the magnetic reluctivity ν_{fe}

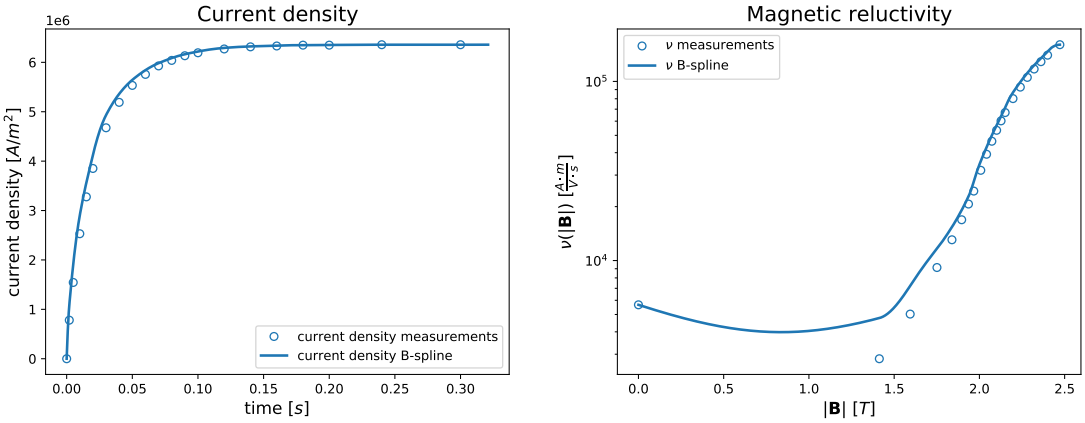

Figure 4.4: Left: The current density J_3 approximated by a cubic B-spline. Right: The magnetic reluctivity ν_{fe} of steel approximated by a cubic B-spline.

of this steel is approximated by a cubic B-Spline based on measured values from [2], see Figure 4.4 and Section 2.3. Similarly, the current density J_3, calculated by

$$J_3(x,t) = \frac{I(x,t)\omega}{A},$$

where I is the given current excitation, ω the number of turns of the coils and A the area of one coil, is approximated by a cubic B-Spline as displayed in Figure 4.4. The direction of the current passing through the coils is denoted by the signs in Figure 4.5. The material parameters are given as

$$\sigma(x) = \begin{cases} 0 & \text{for } x \in \Omega_{non}, \\ 4.54 \cdot 10^6 & \text{for } x \in \Omega_{con}, \end{cases} \quad \text{and} \quad \nu(x, |\nabla_x u|) = \begin{cases} 10^7/(4\pi) & \text{for } x \in \Omega_{non}, \\ \nu_{fe}(|\nabla_x u|) & \text{for } x \in \Omega_{con}, \end{cases}$$

where Ω_{con} describes the rotor and the stator and Ω_{non} consists of the coils and air. The mesh of the space-time cylinder Q is depicted in Figure 4.5, which has 21 time slices according to the time points of measurements in [2]. This points out another advantage of this space-time method, which is the possibility to construct desired graded meshes in order to obtain better resolutions in time for specific time spans. In Figure 4.5 it can be seen, that from the bottom of the mesh the time slices are very close to each other, so the mesh is quite fine in temporal direction, whereas towards the top of the mesh the distances between the time slices become larger. As before, the finite element isomorphism (4.12) is used to derive the nonlinear system (4.24) and to compute the solution of (4.22) by Newton's method (4.25) with a relative error tolerance of 10^{-10}. In each Newton step, the occurring linear system (4.26) is solved by the parallel direct solver MUMPS and the iterative solver GMRES with the BoomerAMG preconditioner with a relative error tolerance of 10^{-8}, cf. Section 3.6.1.

Number of cores	1	2	4	8	16
MUMPS	267.75	177.08	126.49	97.75	81.03
GMRES	2993	1876	1033	577	355
iterations	649	637	642	596	599

Table 4.7: Computational times in seconds for solving the nonlinear problem (4.24) with MUMPS and preconditioned GMRES with the BoomerAMG preconditioner. The solvers required 4 Newton iterations and the number of GMRES iterations gives the most needed iterations of all Newton steps.

The computational times with respect to the number of cores is given in Table 4.7, from which we obtain the good performance of the direct solver, whereas the iterative solver need to be improved, i.e. still a suitable preconditioner need to be found for rather complicated problems like this example. Note that the measured times include the linearization of A in order to obtain A' in (4.26) and the converting of the data types between the software Netgen/NGSolve and PETSc in each Newton iteration. The solution of (4.22) at the bottom and the top of the space-time cylinder Q is visualized in Figure 4.6, and the comparison of the second component of the magnetic flux density B_2 between the simulation and the measured values in the hall probe from [2] is depicted in Figure 4.7, where we have used

$$\mathbf{B} = \begin{pmatrix} B_1(x_1, x_2, t) \\ B_2(x_1, x_2, t) \end{pmatrix} = \begin{pmatrix} \partial_{x_2} u(x_1, x_2, t) \\ -\partial_{x_1} u(x_1, x_2, t) \end{pmatrix}. \tag{4.27}$$

Furthermore, we solved (4.22) on a uniformly refined mesh of the one from Figure 4.5, for which we obtain for the magnetic flux density better correspondence to the measurements compared to the simulation on the coarse mesh.

4.2 Eddy current problem including hysteresis

The goal of this section is to extend our investigating eddy current problem (4.14) to an evolution equation, which takes the effects of hysteresis into account. We have considered the constitutive law (2.5) so far, that is nonlinear for ferromagnetic materials as described in Section 2.3. However, there the considered B-H-curve neglects hysteretic effects, cf. Remark 2.5, since hysteresis models are usually relatively complex and requires a lot of computational effort. Although it is sufficient to use such B-H-curves in many applications, hysteresis models are still of great interest and an ongoing research topic. Basically, hysteresis in a ferromagnetic material describes the dependence of the magnetic behavior on its magnetic past. If an external magnetic field is applied to a ferromagnetic material, the atomic domain aligns itself with it.

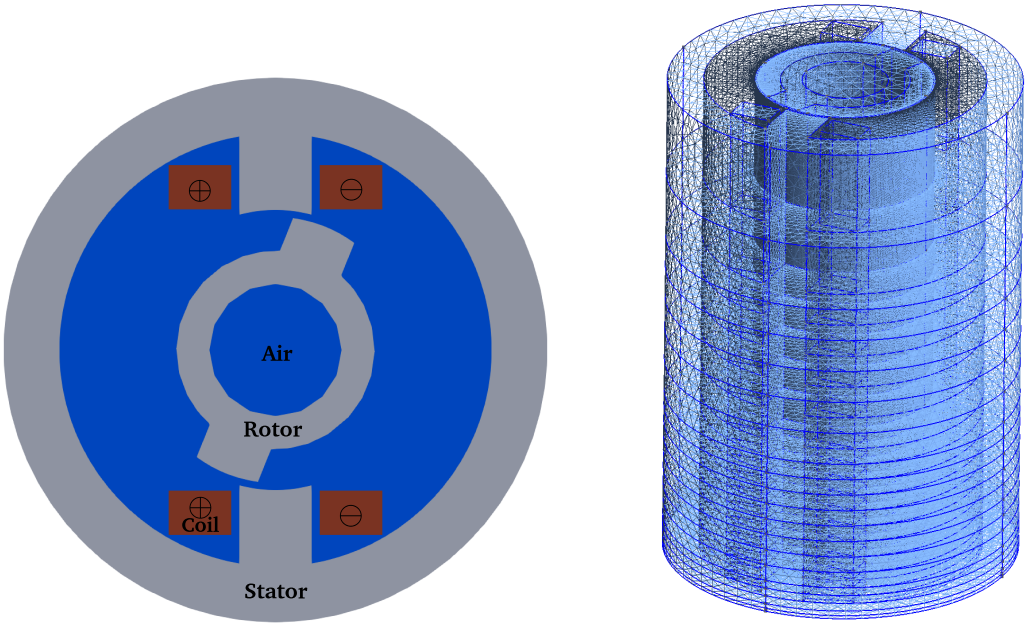

Figure 4.5: Left: A cross-section of the motor showing the non-conducting region Ω_{non} consisting of air (blue) and the coils (brown), as well as the conducting region Ω_{con}, which is made of iron (gray). Right: An unstructured graded mesh of the space-time cylinder Q, which is extruded vertically in time containing 21 time slices and has 451,624 nodes (degrees of freedom) and 2,692,370 elements.

Some parts of the magnetized state retain, even when the external field is removed, see e.g. [19, 105, 157, 160]. Hysteretic behavior becomes visible in the B-H-curve when the so-called hysteresis loop appears, see Figure 4.8. In general, many models have been developed in order to describe the complex behavior of hysteresis. Most popular and widely used models are the so-called Preisach [122] or Jiles-Atherton [82] models, which belong to the group of empirical models. Other more natural vectorial approaches attempt to describe the material behavior up to the atomic structure very accurately using suitable equations, which lead to highly complex equations, see e.g. [50, 157, 162]. A specific approach is based on the optimization of the parameters of parametric algebraic models in order to match measured hysteresis curves. Particularly, we consider the PAM (Pragmatic Algebraic Model) as our hysteresis model, which uses six real parameters $p_0, \ldots, p_5 > 0$ in one algebraic equation in order to describe hysteretic effects, cf. [75, 163]. In contrast to other hysteresis models, the efficiency of PAM lies into its formulation by one algebraic equation, which reduces the computational effort and takes the static and the dynamic effects into account. The main task of this model is the identification of appropriate parameters by minimizing the least squares approximation error with respect to the measurements as

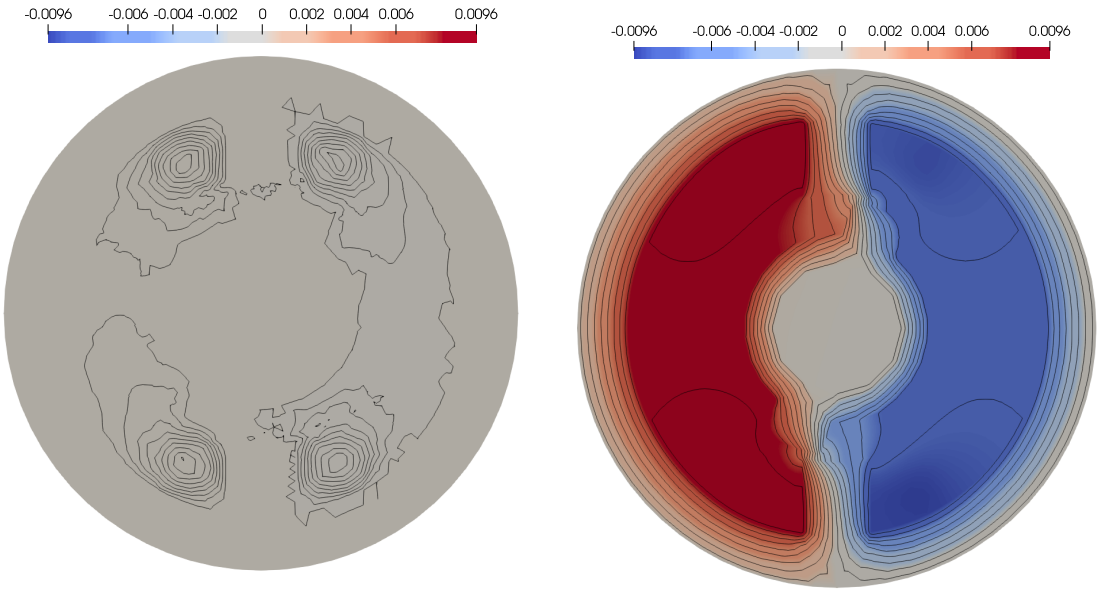

Solution u_h at time $t = 0.0[s]$. Solution u_h at time $t = 0.3[s]$.

Figure 4.6: The approximate solution u_h of (4.22) at the bottom and the top of the space-time cylinder Q.

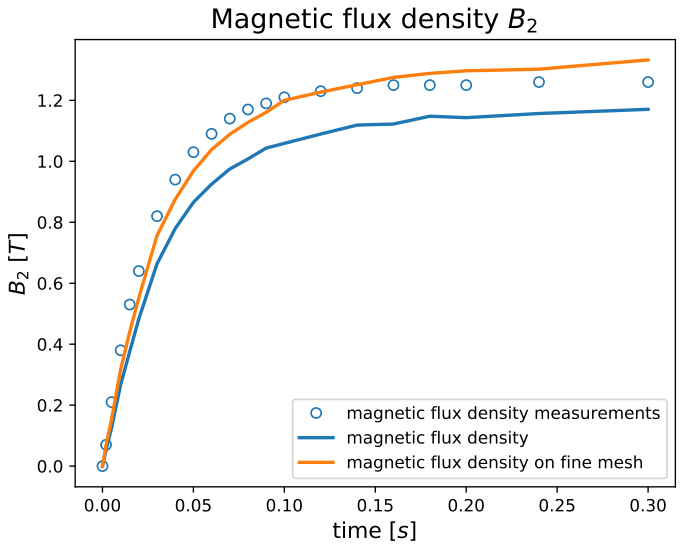

Figure 4.7: The comparison of the second component of the magnetic flux density **B** between the simulations and the measured values from [2]. The blue line shows B_2 computed from the simulation on the mesh from Figure 4.5, whereas the orange line shows B_2 computed from the simulation on the uniformly refined mesh with 3,606,387 nodes (dofs) and 23,803,016 elements.

described in [75, 123].

4.2.1 Hysteresis model

The PAM considers the isotropic constitutive law

$$\mathbf{H} = f(|\mathbf{B}|)\mathbf{B} + g(|\dot{\mathbf{B}}|)\dot{\mathbf{B}} - \mathbf{M}, \tag{4.28}$$

where

$$\begin{aligned} f(|\mathbf{B}|) &= p_0 + p_1|\mathbf{B}|^{2p_2}, \\ g(|\dot{\mathbf{B}}|) &= p_3 + \frac{p_4}{\sqrt{p_5^2 + |\dot{\mathbf{B}}|^2}}, \end{aligned}$$

and $\dot{\mathbf{B}}$ denotes the time derivative of the magnetic flux density $\mathbf{B}$. The first expression $f(|\mathbf{B}|)$ in (4.28) describes the anhysteretic part, which is in fact similar to the magnetic reluctivity ν, which reflects the BH-curve relation described by (2.5). The parameters p_0, p_1, p_2 can be fitted in order to obtain the same behavior as ν. The second expression $g(|\dot{\mathbf{B}}|)$ describes on the one hand the macroscopic eddy currents by the parameter p_3, and on the other hand the hysteresis effects, that are considered by p_4 and p_5, cf. [163]. As before, $\mathbf{M}$ is the permanent magnetization of occurring permanent magnets. Now, when using the constitutive law (4.28) instead of (2.5) and repeating the same computations of Section 2.2.2, the underlying eddy current equation considering hysteresis, reads as

$$\sigma\frac{\partial \mathbf{A}}{\partial t} + \operatorname{curl}\left(f\Big(|\operatorname{curl}(\mathbf{A})|\Big)\operatorname{curl}(\mathbf{A}) + g\Big(|\operatorname{curl}\dot{(\mathbf{A})}|\Big)\operatorname{curl}\dot{(\mathbf{A})}\right) = \mathbf{J_i} + \operatorname{curl}(\mathbf{M}). \tag{4.29}$$

The reduction to the spatially two-dimensional case requires the same assumptions as in Section 2.2.3, i.e. we can write

$$\mathbf{H}(\mathbf{x},t) = \begin{pmatrix} H_1(x_1,x_2,t) \\ H_2(x_1,x_2,t) \\ 0 \end{pmatrix},\ \mathbf{J_i}(\mathbf{x},t) = \begin{pmatrix} 0 \\ 0 \\ J_3(x_1,x_2,t) \end{pmatrix},\ \mathbf{M}(\mathbf{x},t) = \begin{pmatrix} M_1(x_1,x_2,t) \\ M_2(x_1,x_2,t) \\ 0 \end{pmatrix},$$

hence the vector potential $\mathbf{A}$ has the same form as in (2.18), and we can rewrite (4.29) as

$$\sigma(x)\frac{\partial}{\partial t}u(x,t) - \operatorname{div}_x\left(f(|\nabla_x u|)\nabla_x u(x,t) + g(|\partial_t \nabla_x u|)\frac{\partial}{\partial t}\nabla_x u(x,t)\right) = l(x,t), \tag{4.30}$$

for $(x,t) \in \Omega \times (0,T)$, where $\Omega \subset \mathbb{R}^2$ and

$$l(x,t) = J_3(x,t) - \operatorname{div}_x(M^{\perp}(x,t)).$$

In addition to the partial differential equation (4.30) we consider homogenous Dirichlet boundary conditions $u = 0$ on $\partial\Omega \times (0,T)$, which implies the induction boundary condition $B \cdot n = 0$ on $\partial\Omega \times (0,T)$ and the initial condition $u(x,0) = 0$ for $x \in \Omega$.

REMARK 4.9. *Note that the constitutive law* (4.28) *reflects hysteretic behavior in ferromagnetic materials. If the full domain* Ω *consists of multiple materials, the functions* f *and* g *depend also on the spatial variable* x*, i.e.* $f(x, |\nabla_x u|)$ *and* $g(x, |\partial_t \nabla_x u|)$*, like the magnetic reluctivity* ν*. For the sake of brevity, we often use the notations* $f(|\nabla_x u|)$ *and* $g(|\partial_t \nabla_x u|)$ *in place of* $f(x, |\nabla_x u|)$ *and* $g(x, |\partial_t \nabla_x u|)$*, respectively.*

REMARK 4.10. *The Pragmatic Algebraic Model can be extended to a two-dimensional vector hysteresis model [112], so that the characterization of anisotropic materials may be taken into account. This leads to the identification of the set of parameters* $p_{0,i}, \dots, p_{5,i}$ *for each axial direction* $i = 1, \dots, d$*.*

In order to formulate the weak formulation of (4.30), we use the same notation for the Bochner space $Y := L^2(0,T; H_0^1(\Omega))$ and the corresponding norm $\|\cdot\|_Y$ as introduced in Section 4.1.1. For the trial space, we define the space

$$Z = H^1_{0,}(0,T; H_0^1(\Omega)) := \Big\{ u \in Y : \partial_t u \in Y,\ u(x,0) = 0 \text{ for } x \in \Omega \Big\} \subset Y,$$

equipped with the norm

$$\|u\|_Z := \|\partial_t \nabla_x u\|_{L^2(Q)}.$$

In fact, this norm is equivalent to the norm $\|\cdot\|_{H^1(0,T;H_0^1(\Omega))}$ as defined in Section 3.3.2, since

$$\|u\|^2_{H^1(0,T;H_0^1(\Omega))} = \|u\|^2_Y + \|\partial_t u\|^2_Y \le (c_F^2 + 1)\|\partial_t u\|^2_Y = (c_F^2 + 1)\|u\|^2_Z,$$

which follows from Friedrichs's inequality applied to the time derivative satisfying the homogenous initial condition. Thus, the related space-time variational formulation reads as to find $u \in Z$, such that

$$b(u,v) = l(v) \quad \text{for all } v \in Y, \tag{4.31}$$

where

$$\begin{aligned} b(u,v) = \int_0^T \int_\Omega \Big[\sigma(x) \frac{\partial}{\partial t} u(x,t) v(x,t) + f(|\nabla_x u|) \nabla_x u(x,t) \cdot \nabla_x v(x,t) \\ + g(|\partial_t \nabla_x u|) \frac{\partial}{\partial t} \nabla_x u(x,t) \cdot \nabla_x v(x,t) \Big] \, dx dt \\ l(v) = \int_0^T \int_\Omega \Big[J_3(x,t) v(x,t) + M^\perp(x,t) \cdot \nabla_x v(x,t) \Big] \, dx dt. \end{aligned}$$

We first consider the simplified linear version of (4.31). Usually, the material parameters are uniformly bounded, i.e. $\overline{\sigma} > \sigma(x) \geq \sigma_0 > 0$, $\overline{f} > f(|\nabla_x u|) \geq f_0 > 0$ and $\overline{g} > g(|\partial_t \nabla_x u|) \geq g_0 > 0$. Hence, we obtain the linear space-time variational formulation to find $u \in Z$, such that

$$b_l(u, v) = l(v) \quad \text{for all } v \in Y, \tag{4.32}$$

where

$$b_l(u, v) = \int_0^T \int_\Omega \Big[\sigma_0 \frac{\partial}{\partial t} u(x,t) v(x,t) + f_0 \nabla_x u(x,t) \cdot \nabla_x v(x,t) + g_0 \frac{\partial}{\partial t} \nabla_x u(x,t) \cdot \nabla_x v(x,t)\Big] \, dxdt.$$

As a matter of fact, the bilinear form $b_l(\cdot, \cdot)$ is bounded, since

$$\begin{aligned} |b_l(u,v)| &\leq \sigma_0 \|\partial_t u\|_{L^2(Q)} \|v\|_{L^2(Q)} + f_0 \|\nabla_x u\|_{L^2(Q)} \|\nabla_x v\|_{L^2(Q)} \\ &\quad + g_0 \|\partial_t \nabla_x u\|_{L^2(Q)} \|\nabla_x v\|_{L^2(Q)} \\ &\leq c_F^2 \sigma_0 \|\nabla_x \partial_t u\|_{L^2(Q)} \|\nabla_x v\|_{L^2(Q)} + c_{F,t} f_0 \|\partial_t \nabla_x u\|_{L^2(Q)} \|\nabla_x v\|_{L^2(Q)} \\ &\quad + g_0 \|\partial_t \nabla_x u\|_{L^2(Q)} \|\nabla_x v\|_{L^2(Q)} \\ &\leq \max(c_F^2 \sigma_0, c_{F,t} f_0, g_0) \|u\|_Z \|v\|_Y, \end{aligned}$$

which follows from Friedrichs's inequality applied to the spatial gradient as well as to the time derivative. Furthermore, we want to show the inf-sup stability condition, i.e. there exists a constant $c_1^b > 0$, such that

$$c_1^b \|u\|_Z \leq \sup_{0 \neq v \in Y} \frac{b_l(u,v)}{\|v\|_Y} \quad \text{for all } u \in Z. \tag{4.33}$$

For this purpose, we choose $v = \partial_t u$ for each $u \in Z$ to obtain

$$b_l(u,v) = b_l(u, \partial_t u) = \sigma_0 \|\partial_t u\|_{L^2(Q)}^2 + f_0 \langle \nabla_x u, \partial_t \nabla_x u \rangle_{L^2(Q)} + g_0 \|\partial_t \nabla_x u\|_{L^2(Q)}^2. \tag{4.34}$$

We further deduce when using the chain rule that

$$\begin{aligned} \langle \nabla_x u, \partial_t \nabla_x u \rangle_{L^2(Q)} &= \int_0^T \int_\Omega \nabla_x u(x,t) \cdot \frac{\partial}{\partial t} \nabla_x u(x,t) \, dxdt = \frac{1}{2} \int_0^T \int_\Omega \frac{\partial}{\partial t} [\nabla_x u(x,t)]^2 \, dxdt \\ &= \frac{1}{2} \int_\Omega [\nabla_x u(x,t)]^2 \, dx \Big|_0^T = \frac{1}{2} \int_\Omega [\nabla_x u(x,T)]^2 \, dx > 0, \end{aligned}$$

where the initial condition $u(x,0) = 0$ for $x \in \Omega$ also gives $\nabla_x u(x,0) = 0$ for $x \in \Omega$. Together with $\|\partial_t u\|_{L^2(Q)}^2 \geq 0$, we can estimate (4.34) by

$$b_l(u,v) = b_l(u, \partial_t u) \geq g_0 \|\partial_t \nabla_x u\|_{L^2(Q)}^2,$$

which yields the inf-sup stability condition (4.33) with $c_1^b = g_0$. Lastly, we want to examine the surjectivity of the bilinear form $b_l(\cdot,\cdot)$. Therefore, for a given $v \in Y\backslash\{0\}$ we define

$$\widehat{u}(x,t) = \int_0^t v(x,\tau)d\tau, \quad \frac{\partial}{\partial t}\widehat{u}(x,t) = v(x,t) \quad \text{for } x \in \Omega, t \in [0,T].$$

Hence,

$$b_l(\widehat{u},v) = \sigma_0\|\partial_t\widehat{u}\|^2_{L^2(Q)} + f_0\langle\nabla_x\widehat{u},\partial_t\nabla_x\widehat{u}\rangle_{L^2(Q)} + g_0\|\partial_t\nabla_x\widehat{u}\|^2_{L^2(Q)},$$

for which we make the same calculations as for the inf-sup stability condition before in order to obtain

$$b_l(\widehat{u},v) \neq 0.$$

Thus, all three conditions (BNB1) - (BNB3) of Theorem 3.17 are verified and the existence of a unique solution $u \in Z$ for (4.32) follows.

Our goal is to use a conforming space-time finite element discretization with finite-dimensional spaces spanned by piecewise linear and globally continuous functions as described in Section 3.5.2. However, second order derivatives occur in the variational formulation (4.31), which usually requires conforming approximation spaces constructed by finite elements of higher smoothness. A remedy offers the introduction of an auxiliary function $p = \partial_t u \in Y$. Making use of this substitution, we can equivalently rewrite (4.31) to the system, to find $(u,p) \in W_{0,}(Q) \times Y$, such that

$$\begin{aligned} b_1(u,p,v) &:= \int_0^T\int_\Omega \big[\sigma(x)\frac{\partial}{\partial t}u(x,t)v(x,t) + f(|\nabla_x u|)\nabla_x u(x,t)\cdot\nabla_x v(x,t) \\ &\qquad + g(|\nabla_x p|)\nabla_x p(x,t)\cdot\nabla_x v(x,t)\big]\, dxdt = l(v), \qquad (4.35) \\ b_2(u,p,q) &:= \int_0^T\int_\Omega \frac{\partial}{\partial t}u(x,t)q(x,t)\, dxdt - \int_0^T\int_\Omega p(x,t)q(x,t)\, dxdt = 0, \end{aligned}$$

for all $(v,q) \in Y \times L^2(Q)$, where the space $W_{0,}(Q)$ is defined as in (3.18). Although this method requires to solve an enlarged linear system, it allows for a parallelization [59] and adaptivity [147] for both unknowns at once in space and time simultaneously.

Remark 4.11. *Note that, another possibility would be to choose the auxiliary function* $\underline{p} = \nabla_x u$*, for which we deduce the equivalent system to* (4.31)*, that is to find*

$(u, \underline{p}) \in W_{0,}(Q) \times [Y]^2$, *such that*

$$\int_0^T \int_\Omega \Big[\sigma(x)\frac{\partial}{\partial t}u(x,t)v(x,t) + f(|\nabla_x u|)\nabla_x u(x,t)\cdot\nabla_x v(x,t) + g(|\partial_t \underline{p}|)\frac{\partial}{\partial t}\underline{p}(x,t)\cdot\nabla_x v(x,t)\Big]\, dxdt = l(v),$$

$$\int_0^T \int_\Omega \underline{p}(x,t)\cdot\underline{q}(x,t)\, dxdt = \int_0^T \int_\Omega \nabla_x u(x,t)\cdot\underline{q}(x,t)\, dxdt,$$

for all $(v, \underline{q}) \in Y \times [L^2(Q)]^2$. *However, this approach forces us to set an initial condition for the auxiliary function* $\underline{p}$ *and enlarges the system even more than the variational problem* (4.35). *Numerical experiments have shown that the solving of the resulting system with respect to the substitution* $\underline{p} = \nabla_x u$ *comes with computational difficulties and unstable solutions.*

For the space-time finite element discretization of (4.35) we again introduce the finite-dimensional spaces $X_h \subset W_{0,}(Q)$ and $Y_h \subset Y$, such that $X_h \subset Y_h$. As usual, our particular choice is even $X_h = Y_h$ as in (4.7), hence the discrete space-time variational formulation is to find $(u_h, p_h) \in X_h \times Y_h$, such that

$$\begin{aligned} b_1(u_h, p_h, v_h) &= l(v_h), \qquad \text{for all } v_h \in Y_h, \\ b_2(u_h, p_h, q_h) &= 0, \qquad \text{for all } q_h \in Y_h. \end{aligned} \tag{4.36}$$

We apply Newton's method [37] to solve the nonlinear system (4.36). Therefore we introduce the operator $B_e : Y_h \times Y_h \to Y_h$, such that

$$\langle B_e(u_h, p_h), v_h\rangle_{Y_h} = \int_0^T \int_\Omega \Big[f(|\nabla_x u_h|)\nabla_x u_h(x,t)\cdot\nabla_x v_h(x,t) + g(|\nabla_x p_h|)\nabla_x p_h(x,t)\cdot\nabla_x v_h(x,t)\Big]\, dxdt,$$

hence we can rewrite (4.36) as a system of operator equations

$$\begin{aligned} \langle\sigma\frac{\partial}{\partial t}u_h, v_h\rangle_{Y_h} + \langle B_e(u_h, p_h), v_h\rangle_{Y_h} &= l(v), \\ \langle\frac{\partial}{\partial t}u_h, q_h\rangle_{Y_h} - \langle p_h, q_h\rangle_{Y_h} &= 0. \end{aligned}$$

Similar to Section 4.1.3, we compute the Fréchet derivative of the operator $B_e(u_h, p_h)$

in a direction w_h, which reads as

$$\begin{aligned}\langle D_{w_h}(B_e(u_h,p_h)),v_h\rangle_{Y_h} &= \\ \int_0^T\int_\Omega \Big[f(|\nabla_x u_h|)\nabla_x w_h\cdot\nabla_x v_h + \frac{f'(|\nabla_x u_h|)}{|\nabla_x u_h|}(\nabla_x u_h\cdot\nabla_x w_h)(\nabla_x u_h\cdot\nabla_x v_h) \\ + g(|\nabla_x p_h|)\nabla_x w_h\cdot\nabla_x v_h + \frac{g'(|\nabla_x p_h|)}{|\nabla_x p_h|}(\nabla_x p_h\cdot\nabla_x w_h)(\nabla_x p_h\cdot\nabla_x v_h)\Big]\,dxdt,\end{aligned}$$

for $\nabla_x u_h \neq 0$ and $\nabla_x p_h \neq 0$, and

$$\langle D_{w_h}(B_e(u_h,p_h)),v_h\rangle_{Y_h} = \int_0^T\int_\Omega \Big[f(0)\nabla_x w_h\cdot\nabla_x v_h + g(0)\nabla_x w_h\cdot\nabla_x v_h\Big]\,dxdt,$$

for $\nabla_x u_h = 0$ and $\nabla_x p_h = 0$. Hence, we can define the Newton operator $B_e'(u_h,p_h)$ as

$$\langle B_e'(u_h,p_h)w_h, v_h\rangle_{Y_h} \coloneqq \langle D_{w_h}(B_e(u_h,p_h)),v_h\rangle_{Y_h},$$

and refer to [37] for an extensive analysis of Newton's method applied to systems.

We use the finite element isomorphism (4.12) in order to derive the equivalent nonlinear Galerkin system, which is to find $(\underline{u}_h,\underline{p}_h)\in\mathbb{R}^M\times\mathbb{R}^M$, such that

$$B(\underline{u}_h,\underline{p}_h) = \underline{l}, \tag{4.37}$$

where

$$B(\underline{u}_h,\underline{p}_h) = \begin{pmatrix} b_1(u_h,p_h,\phi_i)\\ b_2(u_h,p_h,\phi_j)\end{pmatrix}_{i,j=1}^{M}, \qquad \underline{l} = \begin{pmatrix} l(\phi_i)\\ 0\end{pmatrix}_{i=1}^{M},$$

for which we obtain the Newton operator

$$\langle B'(\underline{u}_h,\underline{p}_h)\begin{pmatrix}\underline{w}_{h,1}\\ \underline{w}_{h,2}\end{pmatrix},\begin{pmatrix}\underline{v}_h\\ \underline{q}_h\end{pmatrix}\rangle = \begin{pmatrix}\langle\sigma\frac{\partial}{\partial t}\underline{w}_{h,1},\underline{v}_h\rangle + \langle B_e'(\underline{u}_h,\underline{p}_h)\underline{w}_{h,1},\underline{v}_h\rangle\\ \langle\frac{\partial}{\partial t}\underline{w}_{h,2},\underline{q}_h\rangle - \langle\underline{w}_{h,2},\underline{q}_h\rangle\end{pmatrix},$$

for $\underline{v}_h,\underline{q}_h,\underline{w}_{h,1},\underline{w}_{h,2}\in\mathbb{R}^M$. We apply Newton's method with the backtracking line search method as described in Section 4.1.3 in order to solve (4.37). Starting with an arbitrary initial guess $\underline{u}_0,\underline{p}_0$ (in many cases the zero vector), Newton's strategy with damping is

$$\begin{pmatrix}\underline{u}_{k+1}\\ \underline{p}_{k+1}\end{pmatrix} = \begin{pmatrix}\underline{u}_k\\ \underline{p}_k\end{pmatrix} - \tau\left[B'(\underline{u}_k,\underline{p}_k)\right]^{-1}\left(B(\underline{u}_k,\underline{p}_k)-\underline{l}\right), \tag{4.38}$$

for a damping factor $\tau > 0$. To solve (4.38), we first compute $(\underline{w}_{k,1}, \underline{w}_{k,2})^\top$ as the solution of the linear system

$$B'(\underline{u}_k, \underline{p}_k) \begin{pmatrix} \underline{w}_{k,1} \\ \underline{w}_{k,2} \end{pmatrix} = \left(B(\underline{u}_k, \underline{p}_k) - \underline{l} \right), \tag{4.39}$$

and use this solution to determine the next approximate solution via the line search

$$\begin{pmatrix} \widetilde{\underline{u}}_k \\ \widetilde{\underline{p}}_k \end{pmatrix} = \begin{pmatrix} \underline{u}_k \\ \underline{p}_k \end{pmatrix} - \tau \begin{pmatrix} \underline{w}_{k,1} \\ \underline{w}_{k,2} \end{pmatrix} \quad \text{for } \tau \in \{1, 0.5, 0.25, \dots 2^{-j}\}.$$

We stop the line search if $\|B(\widetilde{\underline{u}}_k, \widetilde{\underline{p}}_k) - \underline{l}\| < \|B(\underline{u}_k, \underline{p}_k) - \underline{l}\|$ or $\tau > 2^{-j}$ for $j \in \mathbb{N}$, and update

$$\begin{pmatrix} \underline{u}_{k+1} \\ \underline{p}_{k+1} \end{pmatrix} = \begin{pmatrix} \widetilde{\underline{u}}_k \\ \widetilde{\underline{p}}_k \end{pmatrix}.$$

The method stops when a given error tolerance $\langle (\underline{w}_{k,1}, \underline{w}_{k,2})^\top, B(\widetilde{\underline{u}}_k, \widetilde{\underline{p}}_k) - \underline{l} \rangle < TOL$ is reached.

4.2.2 Numerical examples

In this section we provide numerical results in order to illustrate the applicability of the introduced space-time method for the hysteresis model (4.28). The first example considers a two-dimensional spatial domain $\Omega = (0,1)^2$, which consists of two different materials $\Omega_{cu} = (0.25, 0.75)$, through which the excitation J_3 passes, and $\Omega_{fe} = \Omega \backslash \overline{\Omega_{cu}}$, in which the hysteresis model holds true. The terminal time is given as $T = 1.25$, hence the decomposition of the space-time cylinder $Q = \Omega \times (0,T)$ is similar to the visualized unstructured mesh in Figure 4.2. However, we consider a mesh with 100 time slices in temporal direction, 53,530 nodes and 293,400 elements. Furthermore, we use the following parameters,

$$\sigma(x) = \begin{cases} 0.01 & \text{in } \Omega_{cu}, \\ 0.01 & \text{in } \Omega_{fe}, \end{cases} \qquad f(|\nabla_x u|) = \begin{cases} \frac{10^7}{4\pi} & \text{in } \Omega_{cu}, \\ p_0 + p_1 |\nabla_x u|^{2p_2} & \text{in } \Omega_{fe}, \end{cases}$$

$$J_3(x,t) = \begin{cases} 2000 \sin(2\pi t) & \text{in } \Omega_{cu}, \\ 0 & \text{in } \Omega_{fe}, \end{cases} \qquad g(|\nabla_x p|) = \begin{cases} 0 & \text{in } \Omega_{cu}, \\ p_3 + \frac{p_4}{\sqrt{p_5^2 + |\nabla_x p|^2}} & \text{in } \Omega_{fe}, \end{cases}$$

where $p_0 = 75.6$, $p_1 = 0.0223$, $p_2 = 11.47$, $p_3 = 0.0001$, $p_4 = 65.8$, $p_5 = 25$. Note that no permanent magnets occur, therefore $M^\perp = (0,0)^\top$. We solve (4.36) by Newton's method (4.38) with damping. For the occurring linear system (4.39) we use the parallel direct solver MUMPS as described in Section 3.6.1. The relative

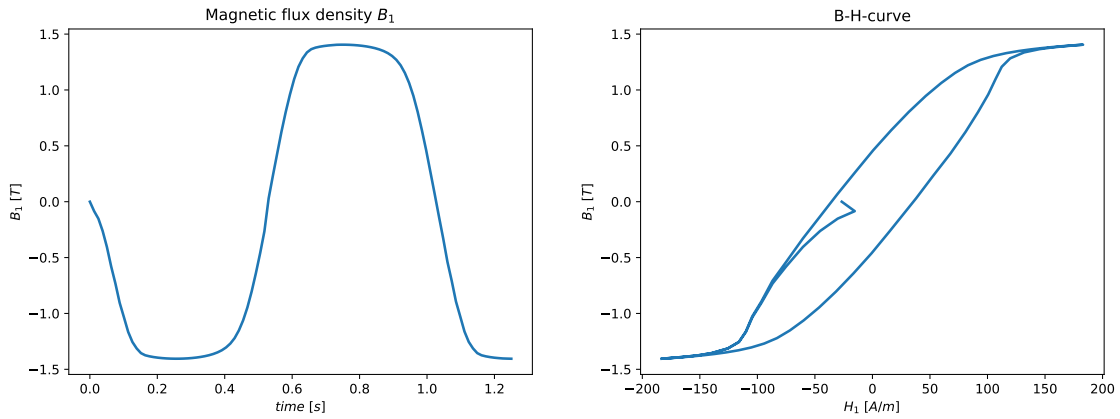

Figure 4.8: Left: The first component of the magnetic flux density B_1 over time. Right: The B-H-curve in the first component indicating the expected hysteretic behavior.

Number of cores	1	2	4	8	16
MUMPS	307.72	184.22	123.44	84.28	66.83

Table 4.8: Computational times in seconds for solving the nonlinear problem (4.36) with the parallel direct solver MUMPS. The solver required 20 Newton iterations for 107,060 degrees of freedom.

error tolerance of Newton's method is 10^{-11}. Figure 4.8 displays the first component of the magnetic flux density B_1 as well as the B-H curve in the first component indicating the hysteresis loop, both evaluated in the spatial reference point $(0.5, 0.8)$ in each time slice, where the magnetic flux density is computed as in (4.27). The solver required 20 Newton iterations and Table 4.8 shows the computational times with respect to the number of processes. Note that the measured times include the linearization of B in order to obtain B' in (4.39) and the converting of the data types between the software Netgen/NGSolve and PETSc in each Newton iteration.

The second and more realistic example is the application of a Switched Reluctance Motor of the Team24 benchmark [2]. The description of the motor is given in Section 4.1.4. We consider a similar decomposition of the space-time cylinder Q to Figure 4.5, which has 40 equidistant time slices in temporal direction with $T = 0.1$, 222,448 nodes and 1,303,241 elements. However, we denote the rotor and the stator by Ω_{con}, the coils by Ω_{cu} and air by Ω_a. Furthermore, we consider the parameters

$$J_3(x,t) = \begin{cases} 5 \cdot 10^6 \sin(2\pi t/T) & \text{in } \Omega_{cu}, \\ 0 & \text{in } \Omega_{con} \cup \Omega_a, \end{cases} \qquad \sigma(x) = \begin{cases} 0.1 & \text{in } \Omega_{con}, \\ 0 & \text{in } \Omega_{cu} \cup \Omega_a, \end{cases}$$

Number of cores	1	2	4	8	16
MUMPS	633.33	421.15	304.68	210.55	171.47

Table 4.9: Computational times in seconds for solving the nonlinear problem (4.36) with the parallel direct solver MUMPS. The solver required 8 Newton iterations for 444,896 degrees of freedom.

and

$$f(|\nabla_x u|) = \begin{cases} \frac{10^7}{4\pi} & \text{in } \Omega_{cu} \cup \Omega_a, \\ p_0 + p_1 |\nabla_x u|^{2p_2} & \text{in } \Omega_{con}, \end{cases}$$

$$g(|\nabla_x p|) = \begin{cases} 0 & \text{in } \Omega_{cu} \cup \Omega_a, \\ p_3 + \frac{p_4}{\sqrt{p_5^2 + |\nabla_x p|^2}} & \text{in } \Omega_{con}, \end{cases}$$

with $p_0 = 181.88232$, $p_1 = 0.267053$, $p_2 = 8.999565$, $p_3 = 0.0001$, $p_4 = 80$, $p_5 = 50$. Since no permanent magnets occur, $M^\perp = (0,0)^\top$. We solve (4.36) by Newton's method (4.38) with damping. For the occurring linear system (4.39) we use the parallel direct solver MUMPS as described in Section 3.6.1. The relative error tolerance of Newton's method is 10^{-11}. Figure 4.9 displays the second component of the magnetic flux density B_2 as well as the B-H curve in the second component indicating the hysteresis loop, both evaluated in the spatial reference point $(0.0129906, 0.0535091)^\top$ in each time slice, where the magnetic flux density is computed as in (4.27). The solver required 8 Newton iterations and Table 4.9 shows the computational times with respect to the number of processes. Note that the measured times include the linearization of B in order to obtain B' in (4.39) and the converting of the data types between the software Netgen/NGSolve and PETSc in each Newton iteration.

4.3 Eddy current problem in moving domains

We now analyze the eddy current problem (4.1) in moving domains, where we assume a smooth movement φ satisfying Assumption 3.1 and the corresponding velocity field $\widetilde{v}$, which is considered in the total time derivative (2.20), see [60]. Hence, the open space-time cylinder Q is given as in (3.5), which already captures the movement of the domain within the mesh. The variational formulation is obtained when applying integration by parts with respect to the transformed spatial variable, and when recalling the spaces $X = W(Q)$ from (3.19) and $Y = L^2(0,T; H_0^1(\Omega(t)))$, it reads as to find $u \in X$, such that

$$a(u,v) = l(v) \quad \text{for all } v \in Y, \tag{4.40}$$

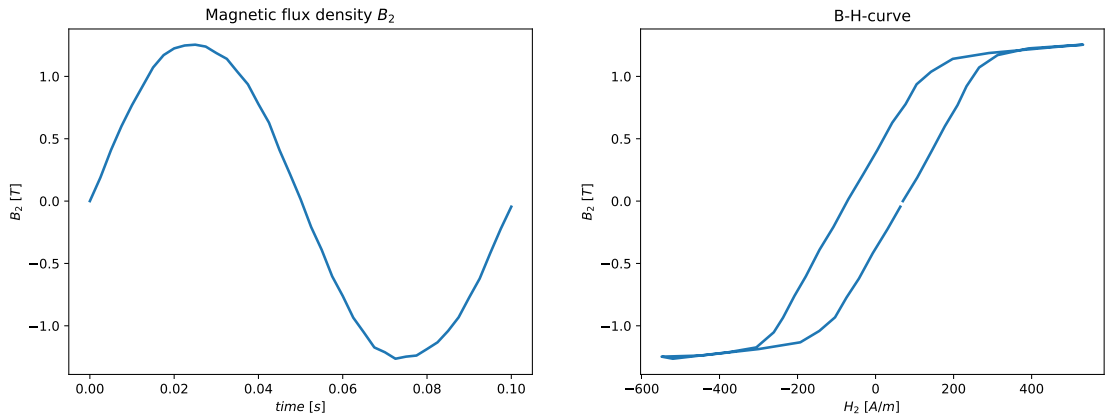

Figure 4.9: Left: The second component of the magnetic flux density B_2 over time. Right: The B-H-curve in the second component indicating the expected hysteretic behavior.

where

$$a(u,v) = \int_0^T \int_{\Omega(t)} \left[\sigma(y) \frac{d}{dt} u(y,t) v(y,t) + \nu(y, |\nabla_y u|) \nabla_y u(y,t) \cdot \nabla_y v(y,t) \right] \, dy dt,$$
$$l(v) = \int_0^T \int_{\Omega(t)} \left[J_3(y,t) v(y,t) + M^{\perp}(y,t) \cdot \nabla_y v(y,t) \right] \, dy dt.$$

The spatial partial integration with respect to the transformed variable $y = \varphi(x,t)$ for $x \in \Omega_0$ and $t \in (0,T)$ can be verified when using the integral transform to the initial domain Ω_0 according to [49, Chapter 9 and Chapter 10, Theorem 4], that is

$$\begin{aligned} \int_{\Omega(t)} u(y,t) \, dy &= \int_{\Omega_0} u(\varphi(x,t),t) |\det \nabla_x \varphi(x,t)| \, dx, \\ \int_{\Omega(t)} \nabla_y u(y,t) \, dy &= \int_{\Omega_0} (\nabla_x \varphi^{-1}(x,t))^{\top} \nabla_x u(\varphi(x,t),t) |\det \nabla_x \varphi(x,t)| \, dx. \end{aligned} \tag{4.41}$$

We define the smooth matrix valued function $B : \Omega_0 \times (0,T) \to C^{\infty}(\overline{\Omega_0}; \mathbb{R}^{d \times d})$ by

$$B(x,t) = \nabla_x \varphi^{-1}(x,t), \tag{4.42}$$

and obtain in terms of the integral transform (4.41) and (4.42), that the total time derivative becomes

$$\begin{aligned}\int_{\Omega(t)} \frac{d}{dt}u(y,t)\ dy &= \int_{\Omega(t)} \left[\frac{\partial}{\partial t}u(y,t) + \widetilde{v}(y,t)\cdot\nabla_y u(y,t)\right]\ dy \\ &= \int_{\Omega_0} \left[\frac{\partial}{\partial t}u(\varphi(x,t),t) + \widetilde{v}(\varphi(x,t),t)\cdot B^\top(x,t)\nabla_x u(\varphi(x,t),t)\right]|B^{-1}|\ dx.\end{aligned}$$

Furthermore, it holds that

$$\begin{aligned}&\int_{\Omega(t)} \operatorname{div}_y\Big(\nu(y,|\nabla_y u|)\nabla_y u(y,t)\Big)v(x,t)\ dy \\ &\quad= \int_{\Omega_0} \operatorname{div}_x\Big(\nu(\varphi(x,t),|B^\top\nabla_x u|)B(x,t)B^\top(x,t)\nabla_x u(\varphi(x,t),t)\Big)v(\varphi(x,t),t)|B^{-1}|\ dy \\ &\quad= \int_{\Omega_0} \nu(\varphi(x,t),|B^\top\nabla_x u|)B(x,t)B^\top(x,t)\nabla_x u(\varphi(x,t),t)\cdot\nabla_x v(\varphi(x,t),t)|B^{-1}|\ dy \\ &\quad= \int_{\Omega_0} \nu(\varphi(x,t),|B^\top\nabla_x u|)B^\top(x,t)\nabla_x u(\varphi(x,t),t)\cdot B^\top(x,t)\nabla_x v(\varphi(x,t),t)|B^{-1}|\ dy \\ &\quad= \int_{\Omega(t)} \nu(y,|\nabla_y u|)\nabla_y u(y,t)\cdot\nabla_y v(y,t)\ dy.\end{aligned}$$

Hence, starting from the partial differential equation in (4.1) and using the above identities due to the integral transform (4.41) as well as (4.42), we deduce the integration by parts' formula with respect to the transformed variable y, i.e.

$$\begin{aligned}&\int_{\Omega(t)} \Big[\sigma(y)\frac{d}{dt}u(y,t) - \operatorname{div}_y(\nu(y,|\nabla_y u|)\nabla_y u(y,t))\Big]v(y)\ dy \\ &\quad= \int_{\Omega_0}\sigma(\varphi(x,t))\frac{\partial}{\partial t}u(\varphi(x,t),t)v(\varphi(x,t),t)|B^{-1}|\ dx \\ &\qquad+ \int_{\Omega_0} \widetilde{v}(\varphi(x,t),t)\cdot B^\top(x,t)\nabla_x u(\varphi(x,t),t)v(\varphi(x,t),t)|B^{-1}|\ dx \\ &\qquad+ \int_{\Omega_0} \nu(\varphi(x,t),|B^\top\nabla_x u|)B^\top\nabla_x u(x,t))\cdot B^\top\nabla_x v(\varphi(x,t),t)|B^{-1}|\ dx \\ &\quad= \int_{\Omega(t)} \left[\sigma(y)\frac{d}{dt}u(y,t)v(y,t) + \nu(y,|\nabla_y u|)\nabla_y u(y,t)\cdot\nabla_y v(y,t)\right]\ dy.\end{aligned}$$

As in Section 4.1 we first consider the linear case of (4.40), hence $\nu(y,|\nabla_y u|) = \nu(y)$, for which we state the unique solvability similar to Section 4.1.1. We proceed with the

investigation of the nonlinear problem (4.40) and conclude this section with numerical examples of academic and practical interest for both the linear and nonlinear case.

4.3.1 Linear eddy current problem in moving domains

Space-time variational formulation

In this section we consider the linear eddy current problem posed on a moving or partly moving body, whose space-time variational formulation is given as in (4.40) with $\nu(y, |\nabla_y u|) = \nu(y)$. We recall the open space-time cylinder Q as given in (3.5), which already considers partly moving domains as well as conducting ($\sigma > 0$) and non-conducting ($\sigma = 0$) materials denoted by $\Omega_{con}(t)$ and $\Omega_{non}(t)$, respectively. Moreover, the Bochner space $Y = L^2(0, T; H_0^1(\Omega(t)))$ covering homogenous Dirichlet boundary conditions on moving domains can be equipped with the norm

$$\|v\|_Y^2 = \int_0^T \int_{\Omega(t)} \nu(y) |\nabla_y v(y,t)|^2 \, dydt,$$

where $\nu \in L^\infty(\Omega(t))$, and the trial space

$$X = \{u \in Y : \sigma \frac{d}{dt} u \in Y^\star, u(x,0) = 0 \text{ for } x \in \Omega_{con}(0)\} \subset Y, \tag{4.43}$$

covering homogenous initial and boundary conditions can be equipped with the graph norm

$$\|u\|_X^2 = \|u\|_Y^2 + \|\sigma \frac{d}{dt} u\|_{Y^\star}^2 = \|u\|_Y^2 + \|w_u\|_Y^2,$$

where $w_u \in Y$ is the unique solution of the variational problem

$$\int_0^T \int_{\Omega(t)} \nu(y) \nabla_y w_u(y,t) \cdot \nabla_y v(y,t) \, dydt = \int_0^T \int_{\Omega(t)} \sigma(y) \frac{d}{dt} u(y,t) v(y,t) \, dydt \tag{4.44}$$

for all $v \in Y$, cf. [60] and [144]. As in Section 4.1.1, we conclude that the bilinear form $a(\cdot, \cdot)$ is bounded, since

$$\begin{aligned} |a(u,v)| &\leq \|\sigma \frac{d}{dt} u\|_{Y^\star} \|v\|_Y + \|u\|_Y \|v\|_Y = \left[\|\sigma \frac{d}{dt} u\|_{Y^\star} + \|u\|_Y \right] \|v\|_Y \\ &= \sqrt{2} \sqrt{\|\sigma \frac{d}{dt} u\|_{Y^\star}^2 + \|u\|_Y^2} \|v\|_Y = \sqrt{2} \|u\|_X \|v\|_Y, \end{aligned}$$

due to the duality, the Cauchy-Schwarz and the Hölder inequality. Furthermore, the inf-sup stability condition holds, since for a given $u \in X$ and the associated unique solution $w_u \in Y$ of (4.44), we can choose $v_u = u + w_u \in Y$ in order to obtain

$$\begin{aligned}
a(u, v_u) &= a(u, u + w_u) \\
&= \int_0^T \int_{\Omega(t)} \sigma \frac{d}{dt} u(u + w_u) \; dydt + \int_0^T \int_{\Omega(t)} \nu \nabla_y u \cdot \nabla_y (u + w_u) \; dydt \\
&= \int_0^T \int_{\Omega(t)} \nu \nabla_y w_u \cdot \nabla_y (u + w_u) \; dydt + \int_0^T \int_{\Omega(t)} \nu \nabla_y u \cdot \nabla_y (u + w_u) \; dydt \\
&= \int_0^T \int_{\Omega(t)} \nu |\nabla_y (u + w_u)|^2 \; dydt \\
&= \|u + w_u\|_Y^2 = \|v_u\|_Y^2.
\end{aligned}$$

On the other hand, we obtain that

$$\begin{aligned}
\|v_u\|_Y^2 &= \|u + w_u\|_Y^2 \\
&= \int_0^T \int_{\Omega(t)} \nu |\nabla_y u|^2 \; dydt + \int_0^T \int_{\Omega(t)} \nu |\nabla_y w_u|^2 \; dydt + 2 \int_0^T \int_{\Omega(t)} \nu \nabla_y u \cdot \nabla_y w_u \; dydt \\
&= \|u\|_Y^2 + \|w_u\|_Y^2 + 2 \int_0^T \int_{\Omega(t)} \sigma \frac{d}{dt} uu \; dydt \\
&\geq \|u\|_Y^2 + \|w_u\|_Y^2 = \|u\|_X^2,
\end{aligned}$$

where the last estimate follows when using the chain rule, Reynolds transport theorem (3.11) with $\operatorname{div}_y \widetilde{v} = 0$ and the fact that the electric conductivity σ is constant in time, i.e.

$$\begin{aligned}
2 \int_0^T \int_{\Omega(t)} \sigma(y) \frac{d}{dt} u(y,t) u(y,t) \; dydt &= \int_0^T \int_{\Omega(t)} \sigma(y) \frac{d}{dt} [u(y,t)]^2 \; dydt \\
&= \int_0^T \frac{d}{dt} \int_{\Omega(t)} \sigma(y) [u(y,t)]^2 \; dydt \\
&= \int_{\Omega(t)} \sigma(y) [u(y,t)]^2 \; dy \Big|_0^T \\
&= \int_{\Omega_{con}(T)} \sigma(y) [u(y,T)]^2 \; dy > 0,
\end{aligned}$$

with $u(y,0) = 0$ for $y \in \Omega_{con}(0)$. Therefore, the inf-sup stability conditions reads as

$$\|u\|_X \leq \sup_{0 \neq v \in Y} \frac{a(u,v)}{\|v\|_Y} \quad \text{for all } u \in X. \tag{4.45}$$

REMARK 4.12. *Note that the inf-sup constant has been improved compared to the constant $c_1^a = \frac{1}{\sqrt{2}}$ recently given in [60].*

More involved, and not as simple as in the case of fixed domains as in Section 4.1.1, is the validation of the surjectivity for the bilinear form in (4.40). Again, the application of the Steklov-Poincaré operator [143] is needed for the treatment of the elliptic-parabolic interface problem. However, for the proof of the surjectivity we recall that the movement of the domain is uniform, which means that for all of our applications we consider translations and rotations in time. The following lemma states the surjectivity of (4.40), where the underlying domains are assumed to be a moving interval (in 1D) and an electric motor with rotating and fixed parts (in 2D) as visualized in Figure 3.1.

LEMMA 4.13. *For all $v \in Y \backslash \{0\}$ there exists a $\widehat{u} \in X$ such that*

$$a(\widehat{u}, v) \neq 0.$$

Proof. We prove this statement for the case of uniformly moving bodies in the spatially one-dimensional and two-dimensional case. Uniform motion in 1D makes sense, if it is considered to be a translation in time. For the latter, translations and rotations are the underlying movements. We consider the domain

$$\Omega(t) = (\Omega_s \cap \Omega_{con}) \cup (\Omega_r(t) \cap \Omega_{con}(t)) \cup \Omega_{non}(t), \tag{4.46}$$

that consists of the moving regions $\Omega_r(t)$ and fixed regions Ω_s, where both of them may contain conducting parts Ω_{con} and non-conducting parts Ω_{non}. For a given $v \in Y \backslash \{0\}$ we first define

$$\widehat{u}(y,t) = \widehat{u}(\varphi(x,t),t) \coloneqq \int_0^t v(\varphi(x,s),s)\, ds,$$

such that

$$\frac{d}{dt}\widehat{u}(y,t) = v(y,t) \quad \text{for } y \in \Omega_{con}(t),\ t \in (0,T).$$

By definition, we have $\widehat{u} \in X$ satisfying the initial condition $\widehat{u}(y,0) = 0$ for every $y \in \Omega_{con}(0)$ and

$$\begin{aligned} a(\widehat{u}, v) &= \int_0^T \int_{\Omega(t)} \sigma(y) \frac{d}{dt}\widehat{u}(y,t) v(y,t) \; dydt + \int_0^T \int_{\Omega(t)} \nu(y) \nabla_y \widehat{u}(y,t) \cdot \nabla_y v(y,t) \; dydt \\ &= \int_0^T \int_{\Omega_{con}(t)} \sigma(y) [v(y,t)]^2 \; dydt + \int_0^T \int_{\Omega(t)} \nu(y) \nabla_y \widehat{u}(y,t) \cdot \nabla_y \frac{d}{dt}\widehat{u}(y,t) \; dydt. \end{aligned} \tag{4.47}$$

The first term is obviously positive, hence it remains to consider the second term of (4.47). For the non-moving regions Ω_s of the domain, $\varphi(x,t) = x$ and $v(y,t) = 0$, therefore

$$\begin{aligned} &\int_0^T \int_{\Omega_s \cap \Omega_{con}} \nu(y) \nabla_y \widehat{u}(y,t) \cdot \nabla_y \frac{d}{dt}\widehat{u}(y,t) \; dydt \\ &\qquad = \int_0^T \int_{\Omega_s \cap \Omega_{con}} \nu(x) \nabla_x \widehat{u}(x,t) \cdot \nabla_x \frac{\partial}{\partial t}\widehat{u}(x,t) \; dxdt \\ &\qquad = \int_0^T \int_{\Omega_s \cap \Omega_{con}} \frac{1}{2}\frac{\partial}{\partial t} \left[\nu(x) |\nabla_x \widehat{u}(x,t)|^2\right] \; dxdt \\ &\qquad = \frac{1}{2} \int_0^T \frac{\partial}{\partial t} \int_{\Omega_s \cap \Omega_{con}} \nu(x) |\nabla_x \widehat{u}(x,t)|^2 \; dxdt \\ &\qquad = \frac{1}{2} \int_{\Omega_s \cap \Omega_{con}} \nu(x) |\nabla_x \widehat{u}(x,T)|^2 \; dx \geq 0. \end{aligned} \tag{4.48}$$

For the moving regions, we start with the one-dimensional case, where the motion is a translation, i.e.

$$\varphi(x,t) = x + \alpha \frac{t}{T} \quad \text{for } x \in \Omega_0 \subset \mathbb{R}, \; \alpha > 0,$$

where α denotes the constant velocity within the time span $(0,T)$. The velocity field is given as

$$\widetilde{v}(y,t) = \frac{\partial}{\partial t}\varphi(x,t) = \alpha \frac{1}{T}.$$

Furthermore, it is divergence free, i.e. $\operatorname{div}_y \widetilde{v}(y,t) = 0$, and we obtain that

$$\nabla_y \frac{d}{dt}\widehat{u}(y,t) = \frac{\partial}{\partial y_1}\frac{d}{dt}\widehat{u}(y_1,t) = \frac{\partial}{\partial y_1}\left[\frac{\partial}{\partial t}\widehat{u}(y_1,t) + \alpha \frac{1}{T}\frac{\partial}{\partial y_1}\widehat{u}(y_1,t)\right] = \frac{d}{dt}\frac{\partial}{\partial y_1}\widehat{u}(y_1,t),$$

which means that we can change the gradient and the total time derivative in the second expression of (4.47). The same result is also needed for the two-dimensional case, for which we may consider e.g. the domain of the electric motor as visualized in Figure 3.1. The domain $\Omega(t)$ is defined as in (4.46), where Ω_s denotes the stator including the coils, and $\Omega_r(t)$ denotes the rotor including the magnets. In the stator domain Ω_s, i.e. for $r \in (r_3, R)$, we have $y(x,t) = x$ for all $t \in (0,T)$ and $v(y,t) = 0$, hence we obtain similarly to (4.48) that

$$\int_0^T \int_{\Omega_s \cap \Omega_{con}} \nu(y) \nabla_y \widehat{u}(y,t) \cdot \nabla_y \frac{d}{dt} \widehat{u}(y,t) \, dy dt = \frac{1}{2} \int_{\Omega_s \cap \Omega_{con}} \nu(x) |\nabla_x \widehat{u}(x,T)|^2 \, dx \geq 0. \tag{4.49}$$

Next, we consider the moving regions and generally obtain for the total time derivative that

$$\begin{aligned} \frac{d}{dt} \widehat{u}(y,t) &= \frac{\partial}{\partial t} \widehat{u}(y,t) + \widetilde{v}(y,t) \cdot \nabla_y \widehat{u}(y,t) \\ &= \frac{\partial}{\partial t} \widehat{u}(y,t) + \widetilde{v}_1(y,t) \frac{\partial}{\partial y_1} \widehat{u}(y,t) + \widetilde{v}_2(y,t) \frac{\partial}{\partial y_2} \widehat{u}(y,t). \end{aligned}$$

To compute the spatial gradient of the total time derivative, we now consider for $i = 1, 2$,

$$\begin{aligned} \frac{\partial}{\partial y_i} \frac{d}{dt} \widehat{u}(y,t) &= \frac{\partial}{\partial y_i} \left[\frac{\partial}{\partial t} \widehat{u}(y,t) + \widetilde{v}_1(y,t) \frac{\partial}{\partial y_1} \widehat{u}(y,t) + \widetilde{v}_2(y,t) \frac{\partial}{\partial y_2} \widehat{u}(y,t) \right] \\ &= \frac{\partial}{\partial y_i} \frac{\partial}{\partial t} \widehat{u}(y,t) + \frac{\partial}{\partial y_i} \widetilde{v}_1(y,t) \frac{\partial}{\partial y_1} \widehat{u}(y,t) + \widetilde{v}_1(y,t) \frac{\partial^2}{\partial y_i \partial y_1} \widehat{u}(y,t) \\ &\quad + \frac{\partial}{\partial y_i} \widetilde{v}_2(y,t) \frac{\partial}{\partial y_2} \widehat{u}(y,t) + \widetilde{v}_2(y,t) \frac{\partial^2}{\partial y_i \partial y_2} \widehat{u}(y,t), \end{aligned}$$

in order to derive

$$\begin{aligned} \nabla_y \widehat{u}(y,t) \cdot \nabla_y \frac{d}{dt} \widehat{u}(y,t) &= \nabla_y \widehat{u}(y,t) \cdot \nabla_y \left(\frac{\partial}{\partial t} \widehat{u}(y,t) + \widetilde{v}(y,t) \cdot \nabla_y \widehat{u}(y,t) \right) \\ &= \nabla_y \widehat{u}(y,t) \cdot \nabla_y \frac{\partial}{\partial t} \widehat{u}(y,t) + \nabla_y \widehat{u}(y,t) \nabla_y \Big(\widetilde{v}(y,t) \cdot \nabla_y \widehat{u}(y,t) \Big) \\ &= \nabla_y \widehat{u}(y,t) \cdot \nabla_y \frac{\partial}{\partial t} \widehat{u}(y,t) + \sum_{i=1}^{2} \frac{\partial}{\partial y_i} \widehat{u}(y,t) \frac{\partial}{\partial y_i} \Big(\widetilde{v}(y,t) \cdot \nabla_y \widehat{u}(y,t) \Big) \\ &= \nabla_y \widehat{u}(y,t) \cdot \left[\frac{\partial}{\partial t} \nabla_y \widehat{u}(y,t) + \begin{pmatrix} \widetilde{v}_1 \frac{\partial^2}{\partial y_1^2} \widehat{u}(y,t) + \widetilde{v}_2 \frac{\partial^2}{\partial y_1 \partial y_2} \widehat{u}(y,t) \\ \widetilde{v}_1 \frac{\partial^2}{\partial y_1 \partial y_2} \widehat{u}(y,t) + \widetilde{v}_2 \frac{\partial^2}{\partial y_2^2} \widehat{u}(y,t) \end{pmatrix} \right] + R(\widehat{u}) \\ &= \nabla_y \widehat{u}(y,t) \cdot \frac{d}{dt} \nabla_y \widehat{u}(y,t) + R(\widehat{u}), \end{aligned}$$

where the rest term $R(\widehat{u})$ is given as

$$R(\widehat{u}) = \frac{\partial}{\partial y_1}\widetilde{v}_1(y,t)\frac{\partial^2}{\partial y_1^2}\widehat{u}(y,t) + \frac{\partial}{\partial y_1}\widetilde{v}_2(y,t)\frac{\partial^2}{\partial y_1 \partial y_2}\widehat{u}(y,t) + \frac{\partial}{\partial y_2}\widetilde{v}_2(y,t)\frac{\partial^2}{\partial y_1 \partial y_2}\widehat{u}(y,t) + \frac{\partial}{\partial y_2}\widetilde{v}_2(y,t)\frac{\partial^2}{\partial y_2^2}\widehat{u}(y,t).$$

To receive the desired result, we need to assure that $R(\widehat{u}) = 0$. When we consider the rotor domain Ω_r, i.e. $r \in (r_1, r_2)$, which rotates according to the velocity field as described in Section 3.2, recall $\Psi(r) = 1$ for $r \in (r_1, r_2)$, hence

$$\widetilde{v}(y,t) = \frac{\phi}{T}\begin{pmatrix} -y_2 \\ y_1 \end{pmatrix},$$

and

$$\frac{\partial}{\partial y_1}\widetilde{v}_1(y,t) = 0, \quad \frac{\partial}{\partial y_2}\widetilde{v}_1(y,t) = -\frac{\phi}{T}, \quad \frac{\partial}{\partial y_1}\widetilde{v}_2(y,t) = \frac{\phi}{T}, \quad \frac{\partial}{\partial y_2}\widetilde{v}_2(y,t) = 0.$$

This yields that $R(\widehat{u}) = 0$ for a uniform rotation. Summarizing, it follows for the one-dimensional as well as for the two-dimensional case, that

$$\begin{aligned}
&\int_0^T \int_{\Omega_r(t)\cap\Omega_{con}(t)} \nu(y)\nabla_y \widehat{u}(y,t) \cdot \nabla_y \frac{d}{dt}\widehat{u}(y,t)\; dydt \\
&\qquad = \int_0^T \int_{\Omega_r(t)\cap\Omega_{con}(t)} \nu(y)\nabla_y \widehat{u}(y,t) \cdot \frac{d}{dt}\nabla_y \widehat{u}(y,t)\; dydt \\
&\qquad = \int_0^T \int_{\Omega_r(t)\cap\Omega_{con}(t)} \frac{1}{2}\nu(y)\frac{d}{dt}|\nabla_y \widehat{u}(y,t)|^2\; dydt \\
&\qquad = \frac{1}{2}\int_0^T \frac{d}{dt} \int_{\Omega_r(t)\cap\Omega_{con}(t)} \nu(y)|\nabla_y \widehat{u}(y,t)|^2\; dydt \\
&\qquad = \frac{1}{2} \int_{\Omega_r(T)\cap\Omega_{con}(T)} \nu(y)|\nabla_y \widehat{u}(y,T)|^2\; dy \;\geq 0.
\end{aligned} \tag{4.50}$$

Using (4.48), (4.49) and (4.50), we can estimate (4.47) for both cases as follows,

$$a(\widehat{u}, v) \geq \int_0^T \int_{\Omega_{con}(t)} \sigma(y)[v(y,t)]^2\; dydt + \int_0^T \int_{\Omega_{non}(t)} \nu(y)\nabla_y \widehat{u}(y,t) \cdot \nabla_y v(y,t)\; dydt.$$

It remains to define $\widehat{u}$ in the non-conduction regions in a suitable way. In any non-conducting subregion we can write

$$\int_0^T \int_{\Omega_{non}(t)} \nu(y)\nabla_y \widehat{u}(y,t) \cdot \nabla_y v(y,t)\; dydt$$
$$= \int_0^T \int_{\Omega_{non}(t)} [v(y,t)]^2\; dydt + \int_0^T \int_{\partial\Omega_{non}(t)} n_y \cdot [\nu(y)\nabla_y \widehat{u}(y,t)] v(y,t)\; dydt,$$

where n_y is the spatial unit outward normal vector and $\widehat{u}$ is a solution of the Dirichlet boundary value problem

$$\begin{aligned} -\mathrm{div}_y[\nu(y)\nabla_y \widehat{u}(y,t)] &= v(y,t) && \text{for } y \in \Omega_{non}(t), \\ \widehat{u}_{|\Omega_{non}(t)} &= \widehat{u}_{|\Omega_{con}(t)} && \text{on } \partial\Omega_{non}(t) \cap \partial\Omega_{con}(t), \\ \widehat{u}_{|\Omega_{non}(t)} &= 0 && \text{on } \partial\Omega_{non}(t) \cap \partial\Omega(t), \end{aligned}$$

for all $t \in (0,T)$, and, due to the choice of these boundary conditions, it follows that $\widehat{u} \in Y$. The solution of this Dirichlet boundary value problem implies the Dirichlet to Neumann map

$$n_y \cdot [\nu(y)\nabla_y \widehat{u}(y,t)] = (S\widehat{u})(y,t) \quad \text{for } y \in \partial\Omega_{non}(t),\ t \in (0,T),$$

with the Steklov-Poincaré operator $S : H^{1/2}(\partial\Omega_{non}(t)) \to H^{-1/2}(\partial\Omega_{non}(t))$. Since the shape of $\Omega_{non}(t)$ is fixed, S does not depend on time. On the other hand, since S is self-adjoint and positive semi-definite, we can factorize S to write

$$\begin{aligned} \int_0^T \int_{\partial\Omega_{non}(t)} (S\widehat{u})(y,t) v(y,t)\; ds_y dt &= \int_0^T \int_{\partial\Omega_{non}(t)} (S^{1/2}\widehat{u})(y,t)(S^{1/2}v)(y,t)\; ds_y dt \\ &= \int_0^T \int_{\partial\Omega_{non}(t)} (S^{1/2}\widehat{u})(y,t) \frac{d}{dt}(S^{1/2}\widehat{u})(y,t)\; ds_y dt \\ &= \frac{1}{2}\int_0^T \frac{d}{dt} \int_{\partial\Omega_{non}(t)} \left[(S^{1/2}\widehat{u})(y,t)\right]^2\; ds_y dt \\ &= \frac{1}{2} \int_{\partial\Omega_{non}(T)} \left[(S^{1/2}\widehat{u})(y,T)\right]^2\; ds_y \geq 0. \end{aligned}$$

Hence, it follows that

$$\int_0^T \int_{\Omega_{non}(t)} \nu(y)\nabla_y \widehat{u}(y,t) \cdot \nabla_y v(y,t)\; dydt \geq \int_0^T \int_{\Omega_{non}(t)} [v(y,t)]^2\; dydt,$$

which finally gives

$$a(\widehat{u},v) \geq \int_0^T \int_{\Omega_{con}(t)} \sigma(y)[v(y,t)]^2 \, dydt + \int_0^T \int_{\Omega_{non}(t)} [v(y,t)]^2 \, dydt > 0.$$

This concludes the proof. □

Remark 4.14. *Note that for the spatially two-dimensional case also translations with respect to time of the form*

$$\varphi(x,t) = x + \alpha\frac{t}{T} \in \Omega_0 \subset \mathbb{R}^2, \ t \in (0,T), \quad \text{and} \quad \widetilde{v}(y,t) = \frac{\alpha}{T},$$

fulfill the requirement of the rest term $R(\widehat{u}) = 0$. Similar results are valid for uniform motion in the spatially three-dimensional case. Furthermore, the proof of this lemma still holds true, if the whole body is moving. In [60] the proof has been carried out for a periodic behavior of the solution, which is also reflected in the trial space by using the definition

$$X = \left\{ u \in Y : \sigma\frac{d}{dt}u \in Y^\star, u(x,T) = u(x,0) \text{ for } x \in \Omega_{con}(0) \right\} \subset Y.$$

Theorem 4.15. *Let $J_3 \in L^2(0,T;H^{-1}(\Omega(t)))$ and $M^\perp \in [L^2(Q)]^d$ be given. Then there exists a unique solution $u \in X$ of (4.40) with $\nu(y,|\nabla_y u|) = \nu(y)$ satisfying*

$$\|u\|_X \leq \|J_3\|_{L^2(0,T;H^{-1}(\Omega))} + c\|M^\perp\|_{L^2(Q)}.$$

Proof. Since the inf-sup condition (4.45) and the surjectivity due to Lemma 4.13 hold, we deduce the unique solvability of (4.40) with $\nu(y,|\nabla_y u|) = \nu(y)$ from Theorem 3.17. The estimate follows from the inf-sup stability condition (4.45). □

Space-time finite element discretization

For the space-time finite element discretization of the linear variational formulation (4.40) with $\nu(y,|\nabla_y u|) = \nu(y)$ we introduce the conforming finite-dimensional spaces $X_h \subset X$ and $Y_h \subset Y$, where we assume as in the continuous case that $X_h \subset Y_h$. For our specific purpose we even consider

$$X_h = Y_h \coloneqq S_h^1(\mathcal{T}_h) \cap X = \operatorname{span}\{\phi_k\}_{k=1}^M, \tag{4.51}$$

where the space $S_h^1(\mathcal{T}_h)$ of piecewise linear and globally continuous functions ϕ_k is defined as in (3.24) with respect to some admissible and locally quasi-uniform decomposition $\mathcal{T}_h = \{\tau_\ell\}_{\ell=1}^N$ of the space-time cylinder Q into shape regular simplicial

finite elements τ_ℓ of mesh size h_ℓ, cf. Section 3.4. The Galerkin space-time finite element discretization of the variational formulation (4.40) is to find $u_h \in X_h$, such that

$$a(u_h, v_h) = l(v_h) \quad \text{for all } v_h \in Y_h. \tag{4.52}$$

In order to guarantee the existence of a unique solution for the discrete variational problem (4.52), we proceed as in the continuous case. First, for any $u \in X$ we define $w_{u,h} \in Y_h$ as the unique solution of the Galerkin variational formulation

$$\int_0^T \int_{\Omega(t)} \nu(y) \nabla_y w_{u,h}(y,t) \cdot \nabla_y v_h(y,t) \, dydt = \int_0^T \int_{\Omega(t)} \sigma(y) \frac{d}{dt} u(y,t) v_h(y,t) \, dydt, \tag{4.53}$$

for all $v_h \in Y_h$. Consequently, we define the discrete energy norm as in (4.10), where $w_u \in Y$ is the unique solution of the variational formulation (4.44), and due to the conformal discretization $Y_h \subset Y$ we have $\|w_{u,h}\|_Y \leq \|w_u\|_Y$, cf. [144]. Similarly, we define $w_{u_h,h} \in Y_h$ as the unique solution of (4.53) for $u_h \in X_h$ in the right-hand side. Hence, we can consider the particular test function $v_{u_h,h} = u_h + w_{u_h,h}$ due to $X_h \subset Y_h$, in order to conclude

$$a(u_h, v_{u_h,h}) = a(u_h, u_h + w_{u_h,h}) = \|u_h + w_{u_h,h}\|_Y^2 = \|v_{u_h,h}\|_Y^2$$

and

$$\|v_{u_h,h}\|_Y^2 = \|u_h + w_{u_h,h}\|_Y^2 \geq \|u_h\|_Y^2 + \|w_{u_h,h}\|_Y^2 = \|u_h\|_{X_h}^2$$

as in the continuous case, which finally gives the discrete inf-sup stability condition

$$\|u_h\|_{X_h} \leq \sup_{0 \neq v_h \in Y_h} \frac{a(u_h, v_h)}{\|v_h\|_Y} \quad \text{for all } u_h \in X_h. \tag{4.54}$$

From (4.54) we deduce the unique solvability of the Galerkin space-time variational formulation (4.52). Similar to Section 4.1.1, we can derive Céa's lemma

$$\|u - u_h\|_{X_h} \leq \left(1 + \sqrt{2}\right) \inf_{v_h \in Y_h} \|u - v_h\|_X,$$

and the a priori error estimate in the energy norm as given in Theorem 3.22,

$$\|u - u_h\|_Y \leq ch|u|_{H^2(Q)},$$

if $u \in H^2(Q)$, where $u \in X$ and $u_h \in X_h$ are the solutions of the variational problems (4.40) and (4.52), respectively.

4.3.2 Numerical examples

In this section we provide some numerical results in order to illustrate the applicability and accuracy of the proposed approach. We define the finite element spaces Y_h and X_h as in (4.51), which are spanned by piecewise linear and globally continuous functions ϕ_k, cf. (3.24). Hence, for all $v_h \in Y_h$ we can find the representation

$$v_h(y,t) = \sum_{k=1}^{M} v_k \phi_k(y,t), \quad \text{with } v_k = v_h(y_k, t_k), \tag{4.55}$$

that defines the finite element isomorphism $v_h \leftrightarrow \mathbf{v}_h \in \mathbb{R}^M$, where $\mathbf{v}_h[k] = v_k$, for $k = 1, \ldots, M$. The discrete space-time variational formulation (4.52) is then equivalent to the linear system

$$(A_h + K_h)\mathbf{u}_h = \mathbf{l}_h, \tag{4.56}$$

where $A_h \in \mathbb{R}^{M\times M}$ and the stiffness matrix $K_h \in \mathbb{R}^{M\times M}$ are given as

$$A_h[i,j] = \int_0^T \int_{\Omega(t)} \sigma(y) \frac{d}{dt}\phi_j(y,t)\phi_i(y,t)\, dydt,$$

$$K_h[i,j] = \int_0^T \int_{\Omega(t)} \nu(y) \nabla_y \phi_j(y,t) \cdot \nabla_y \phi_i(y,t)\, dydt,$$

for $i, j = 1, \ldots, M$, and the load vector $\mathbf{l}_h$ has the entries

$$\mathbf{l}_h[i] = \int_0^T \int_{\Omega(t)} \left[J_3(y,t)\phi_i(y,t) + M^{\perp}(y,t) \cdot \nabla_y \phi_i(y,t) \right] dydt,$$

for $i = 1, \ldots, M$. We solve the resulting non-symmetric linear system (4.56) in parallel with the methods described in Section 3.6.1.

We start with an example that considers a moving interval $\Omega(t)$, where the initial domain $\Omega(0) = (0,1)$, consisting of the conducting region $\Omega_{con}(0) = (0, 0.5)$ and the non-conducting region $\Omega_{non}(0) = (0.5, 1)$, is uniformly translated in time for $T = 1$ with $\varphi(x,t) = x+t$ for $x \in \Omega(0)$, hence $\widetilde{v} = 1$. The space-time cylinder Q is defined as in (3.5), which is depicted in Figure 4.10. We consider the manufactured solution

$$u(y,t) = (y-t)(1-y+t)t$$

satisfying the homogenous boundary and initial conditions, and the material parameters

$$\sigma(y) = \begin{cases} 1 & \text{for } y \in \Omega_{con}(t), \\ 0 & \text{for } y \in \Omega_{non}(t), \end{cases} \quad \text{and} \quad \nu(y) = \begin{cases} 2 & \text{for } y \in \Omega_{con}(t), \\ 1 & \text{for } y \in \Omega_{non}(t), \end{cases}$$

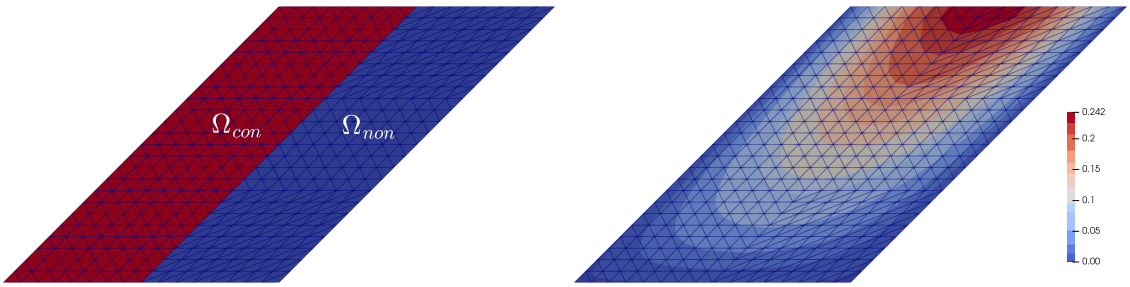

Figure 4.10: Left: An unstructured mesh of the space-time cylinder Q, consisting of the conducting region $\Omega_{con}(t)$ (red) and the non-conducting region $\Omega_{non}(t)$ (blue). The visualized mesh has 425 nodes (degrees of freedom) and 768 elements. Right: The approximate solution u_h of (4.52) computed on this mesh.

L	dofs	$\|u - u_h\|_Y$	EOC
1	153	0.04682	
2	561	0.02367	0.984
3	2,145	0.01190	0.992
4	8,385	0.00596	0.997
5	331,53	0.00298	0.999
6	131,841	0.00149	1
7	525,825	0.00075	1
8	2,100,225	0.00037	1
9	8,394,753	0.00019	1

Table 4.10: The discretization error in the energy norm, which indicates linear convergence when using the parallel direct solver MUMPS on 16 cores for a uniform mesh refinement.

Number of cores	1	2	4	8	16
MUMPS	7.11	6.62	6.13	5.81	5.32
GMRES	61.36	306.55	61.36	52.83	22.33
iterations	178	1158	513	705	526

Table 4.11: Computational times in seconds for solving the linear system (4.56) with MUMPS and preconditioned GMRES with the BoomerAMG preconditioner on a mesh with 394,497 nodes (dofs) and 786,432 elements.

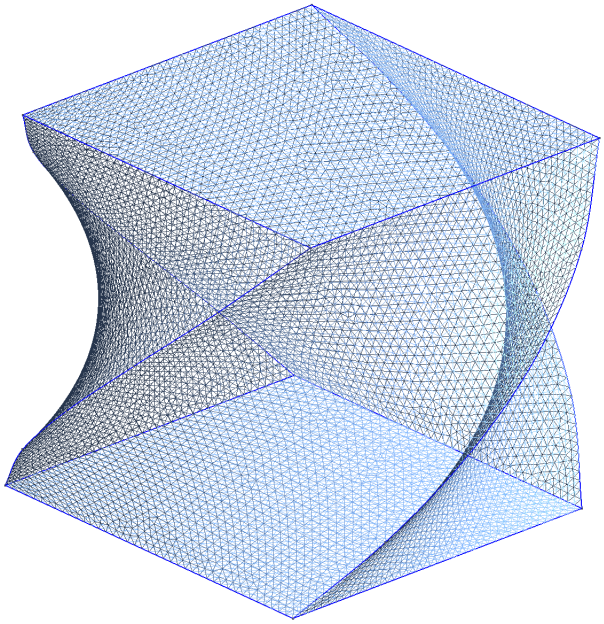

Figure 4.11: An unstructured mesh of the space-time cylinder Q, which is extruded vertically in time considering a counterclockwise rotational motion of $\Omega(0)$ and has 49,928 nodes (degrees of freedom) and 274,439 elements.

hence we deduce for the right-hand side in (4.56) that

$$J_3(y,t) = \begin{cases} (1-y+t)(y-t)+4t & \text{for } y \in \Omega_{con}(t), \\ 2t & \text{for } y \in \Omega_{non}(t). \end{cases}$$

Figure 4.10 visualizes the approximate solution u_h of (4.52), and Table 4.10 shows the expected linear convergence as stated in Theorem 3.22. In Table 4.11 the computational times are given with respect to the number of cores. Here, we used a relative error tolerance of 10^{-5} for the parallel iterative solver GMRES. Note that the computational times relate purely to the time for solving the system (4.56), i.e. the assembly and the converting of the data types between Netgen/NGSolve and PETSc are not measured. Obviously, the parallel direct solver MUMPS is very efficient for the spatially one-dimensional case, whereas the iterative solver seems to have troubles depending on the number of processes, highlighting the question of a suitable preconditioner.

For the next example, we consider a spatially two-dimensional moving domain $\Omega(t) \subset \mathbb{R}^2$ made of one material, whose initial domain $\Omega(0) = (0,1)^2$ rotates 90-degree counterclockwise in temporal direction around the midpoint $x_M = (0.5, 0.5)^\top$ of $\Omega(t)$

Solution u_h at time $t = 0.0[s]$.

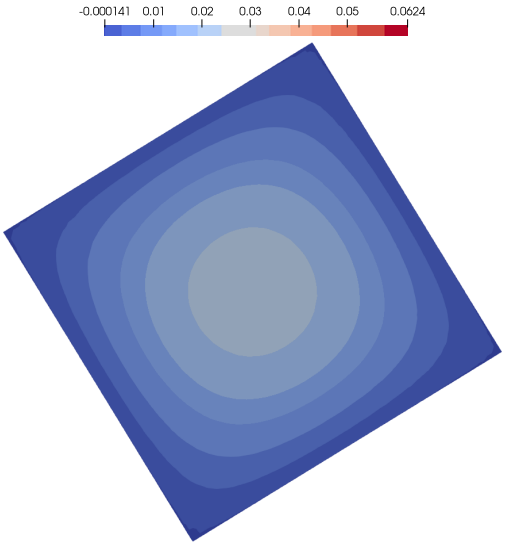

Solution u_h at time $t = 0.35[s]$.

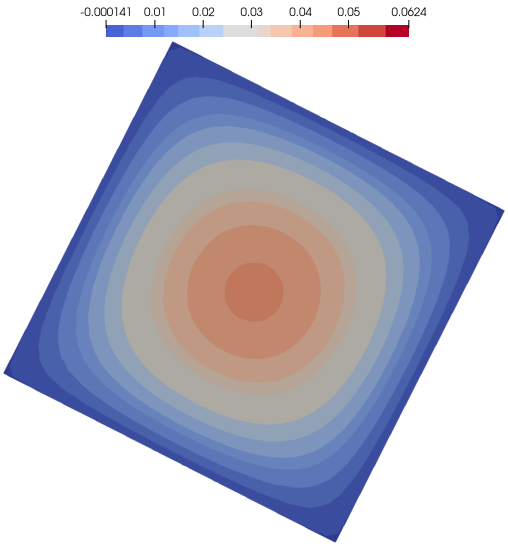

Solution u_h at time $t = 0.7[s]$.

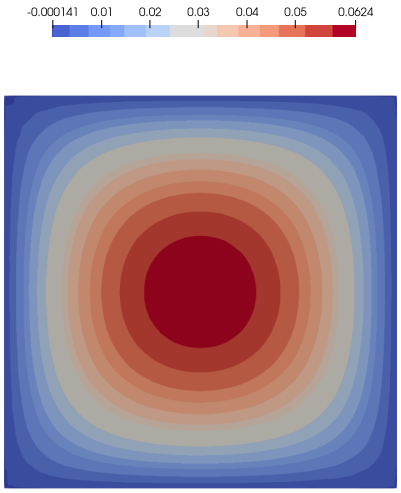

Solution u_h at time $t = 1.0[s]$.

Figure 4.12: The approximate solution u_h of (4.52) for different time points computed on the mesh from Figure 4.11.

within a time span of $(0, T)$ with $T = 1$. The rotation is given as

$$\varphi(x,t) = \begin{pmatrix} 0.5 \\ 0.5 \end{pmatrix} + \begin{pmatrix} \cos\alpha(t) & -\sin\alpha(t) \\ \sin\alpha(t) & \cos\alpha(t) \end{pmatrix} \begin{pmatrix} x_1 - 0.5 \\ x_2 - 0.5 \end{pmatrix} \quad \text{with} \quad \alpha(t) = \frac{\pi t}{2},$$

for $x \in \Omega(0)$, for which we deduce the velocity field $\widetilde{v} = \frac{\pi}{2}(-y_2 - 0.5, y_1 - 0.5)^\top$, cf. Section 3.2. As before, the space-time cylinder Q is defined as in (3.5) and is visualized in Figure 4.11. We consider the rotating manufactured solution

$$u(\widehat{y}_1, \widehat{y}_2, t) = \widehat{y}_1(1 - \widehat{y}_1)\widehat{y}_2(1 - \widehat{y}_2)t,$$

where

$$\begin{aligned} \widehat{y}_1 &= (y_1 - 0.5)\cos(\alpha(t)) + (y_2 - 0.5)\sin(\alpha(t)) + 0.5, \\ \widehat{y}_2 &= (y_2 - 0.5)\cos(\alpha(t)) - (y_1 - 0.5)\sin(\alpha(t)) + 0.5, \end{aligned}$$

and the material parameters

$$\sigma(y) = 10 \quad \text{for } y \in \Omega(t), \qquad \text{and} \qquad \nu(y) = y_1^2 + y_2^2 \quad \text{for } y \in \Omega(t).$$

The right-hand side J_3 is computed by using the underlying partial differential equation, i.e.

$$J_3(y,t) = \sigma(y)\frac{d}{dt}u(y,t) - \operatorname{div}_y(\nu(y)\nabla_y u(y,t)).$$

The approximate solution u_h of (4.52) is displayed for different time points in Figure 4.12 and indicates the expected linear convergence in the energy norm as given in Table 4.12. Furthermore, the computational times for solving the linear system (4.13) with respect to the number of cores are given in Table 4.13. Again, the measured times relate purely to the solving of the linear systems. Here, we used a relative error tolerance of 10^{-5} for the parallel iterative solver GMRES. Obviously, the iterative solver does not scale well and a suitable preconditioner for this class of problems need to be constructed.

4.3.3 Nonlinear eddy current problem in moving domains

Space-time variational formulation

Finally, we turn our focus to the nonlinear eddy current problem (4.40) for moving or partly moving domains. As already mentioned, in realistic applications the magnetic reluctivity ν additionally depends on the magnitude of the magnetic flux

L	dofs	$\|u - u_h\|_Y$	EOC
1	41	0.05745	
2	207	0.03087	0.896
3	1,269	0.01586	0.961
4	8,777	0.00803	0.982
5	65,041	0.00403	0.992
6	500,257	0.00202	0.997
7	3,923,009	0.00101	0.999

Table 4.12: The discretization error in the energy norm, which indicates linear convergence when using the parallel direct solver MUMPS on 16 cores for a uniform mesh refinement.

Number of cores	1	2	4	8	16
MUMPS	40.66	29.72	24.54	17.94	14.66
GMRES	2127.76	1389.31	757.22	108.24	5.74
iterations	1704	1897	1818	515	10

Table 4.13: Computational times in seconds for solving the linear system (4.56) with MUMPS and preconditioned GMRES with the BoomerAMG preconditioner on a mesh with 373,063 nodes (dofs) and 2,190,940 elements.

density, which causes the evolution problem to be nonlinear. As before, we distinguish between the conducting ($\sigma > 0$) and non-conducting ($\sigma = 0$) regions denoted by $\Omega_{con}(t)$ and $\Omega_{non}(t)$, respectively, and recall the definition of the space-time domain Q in (3.5). Furthermore, we keep the notations for the Bochner space $Y = L^2(0,T; H_0^1(\Omega(t)))$ and the space X as defined in (4.43). We proceed as in Section 4.1.3, where we make use Theorem 4.4, Lemma 4.5 and Theorem 4.6 in order to conclude the existence of a unique solution for the nonlinear space-time variational formulation (4.40), as summarized in the next theorem.

THEOREM 4.16. *Let the motion $\varphi : \Omega(0) \times (0,T) \to \mathbb{R}$ satisfy Assumption 3.1 and let $l \in Y^\star$. Then the space-time variational formulation* (4.40) *has a unique solution $u \in X$, which has a Lipschitz dependence on l, i.e. there exists a constant $c > 0$, such that*

$$\|u_1 - u_2\|^2_{L^2(0,T;H_0^1(\Omega(t)))} + \|\sigma \frac{d}{dt}(u_1 - u_2)\|^2_{L^2(0,T;H^{-1}(\Omega(t)))} \leq c\|l_1 - l_2\|^2_{L^2(0,T;H^{-1}(\Omega(t)))},$$

where $u_1, u_2 \in X$ are the solutions of (4.40) *associated to the respective sources $l_1, l_2 \in Y^\star$.*

Proof. This proof has been first investigated by [26]. We will proceed similar to the proof from Theorem 4.8. First, we assume there exists a solution $u \in X$ to the space-time variational problem (4.40) and consider an equivalent problem (4.61), for which Theorem 4.6 is applicable. The solution is unique if it exists, from which we construct a solution for (4.40) in order to conclude the proof.

Assume that (4.40) has a solution $u \in X$. We can equivalently rewrite (4.40) to the variational problem, to find $u \in X$, such that for almost all $t \in (0,T)$

$$\int_{\Omega(t)} \left[\sigma(y)\frac{d}{dt}u(y,t)v(y) + \nu(y,|\nabla_y u|)\nabla_y u(y,t)\cdot\nabla_y v(y)\right] dy = \widetilde{l}(y,t), \tag{4.57}$$

for all $v \in H_0^1(\Omega(t))$, where

$$\widetilde{l}(y,t) = \int_{\Omega(t)} \left[J_3(y,t)v(y) + M^{\perp}(y,t)\cdot\nabla_y v(y)\right] dy.$$

Hence, the solution $u \in X$ of (4.40) also satisfies (4.57) for all $v \in H_0^1(\Omega(t))$, which is still of elliptic-parabolic type. We use the notation $\Omega = \Omega(0)$ for the initial state of the domain, as well as $\Omega_{con} = \Omega_{con}(0)$ for the conducting region and introduce the transported function $\overline{u} \in L^2(0,T;H_0^1(\Omega))$ defined as

$$\overline{u}(x,t) \coloneqq u(\varphi(x,t),t) \quad \text{for } t \in [0,T] \text{ and } x \in \Omega.$$

When considering test functions of the form $v = \overline{v} \circ \varphi$, $v \in H_0^1(\Omega)$, the integral transform (4.41) with respect to the transformed variable $y = \varphi(x,t)$ in (4.57) yields, for almost all $t \in (0,T)$

$$\begin{aligned} &\int_{\Omega} \sigma(\varphi(x,t))\frac{\partial}{\partial t}\overline{u}(x,t)v(x)\,dx \\ &\quad + \int_{\Omega} \nu(\varphi(x,t),|B^{\top}\nabla_x\overline{u}|)B^{\top}(x,t)\nabla_x\overline{u}(x,t)\cdot B^{\top}(x,t)\nabla_x v(x)\,dx = \widetilde{l}(\varphi(x,t),t), \end{aligned} \tag{4.58}$$

for all $v \in H_0^1(\Omega)$, where B is a smooth matrix-valued function as defined in (4.42) satisfying (4.18), and for our purpose the uniform motion fulfills

$$|\det\nabla_x\varphi(x,t)| = 1.$$

The material parameters σ and ν do not depend on time and are isotropic, i.e. the orientation of the material has no effect on the parameters, which verify the identities

$$\sigma(y) = \sigma(x), \qquad \nu(y,|\nabla_y u|) = \nu(x,|B^{\top}\nabla_x\overline{u}|). \tag{4.59}$$

Using the material parameter identities (4.59) in (4.58), we obtain that $u \in X$ satisfies for almost all $t \in (0,T)$

$$\int_\Omega \sigma(x)\frac{\partial}{\partial t}\overline{u}(x,t)v(x)\,dx + \int_\Omega \nu(x,|B^\top \nabla_x \overline{u}|)B(x,t)B^\top(x,t)\nabla_x\overline{u}(x,t)\cdot\nabla_x v(x)\,dx = \widetilde{l}(\varphi(x,t),t), \tag{4.60}$$

for all $v \in H_0^1(\Omega)$. From now on, we can proceed as in the proof of Theorem 4.8. When using test functions v with compact support inside $\Omega\backslash\overline{\Omega_{con}}$ in (4.60), we see that $\overline{u}$ satisfies the equation

$$-\mathrm{div}_x\Big(\nu(x,|B^\top\nabla_x\overline{u}|)B(x,t)B^\top(x,t)\nabla_x\overline{u}(x,t)\Big) = J_3(\varphi(x,t),t) \quad \text{in } \Omega\backslash\overline{\Omega_{con}},$$

assuming $M^\perp = 0$ in Ω_{non}. Now, when we consider the spatial restriction of $\overline{u}(\cdot,t)$ to Ω_{con}, denoted by $\overline{u}_c(\cdot,t)$, spatial integration by parts on $\Omega\backslash\overline{\Omega_{con}}$ reveals that $\overline{u}_c$ satisfies the variational problem

$$\begin{aligned}&\sigma_{con}\int_{\Omega_{con}}\frac{\partial}{\partial t}\overline{u}_c(x,t)v(x)\,dx + \nu_{con}\int_{\Omega_{con}} B(x,t)B^\top(x,t)\nabla_x\overline{u}_c(x,t)\cdot\nabla_x v(x)\,dx\\ &-\int_{\partial\Omega_{con}}\gamma_0\Big(\nu(x,|B^\top\nabla_x\mathcal{L}_t\overline{u}_c|)B(x,t)B^\top(x,t)\nabla_x\mathcal{L}_t\overline{u}_c(x,t)\Big)\cdot n(x)\gamma_0 v(x)\,ds_x\\ &=\widetilde{l}(\varphi(x,t),t),\end{aligned} \tag{4.61}$$

for all $v \in H^1(\Omega_{con})$, where $\widetilde{l}(\varphi(\cdot,t),t)$ is defined on Ω_{con}, σ_{con} and ν_{con} are constants in Ω_{con}, γ_0 is the trace operator as defined in Theorem 3.8, n is the outward unit normal vector of Ω_{con}, and for $\overline{u}_c(\cdot,t) \in H^1(\Omega_{con})$, we define $\mathcal{L}_t\overline{u}_c(\cdot,t) \in H^1(\Omega\backslash\overline{\Omega_{con}})$ as the unique solution of Dirichlet boundary problem

$$\begin{aligned}-\mathrm{div}_x\Big(\nu(x,|B^\top\nabla_x\mathcal{L}_t\overline{u}_c|)B(x,t)B^\top(x,t)\nabla_x\mathcal{L}_t\overline{u}_c(x,t)\Big) &= J_3(\varphi(x,t),t) \quad \text{in } \Omega\backslash\overline{\Omega_{con}},\\ \mathcal{L}_t\overline{u}_c(x,t) &= \overline{u}_c(x,t) \quad \text{on } \partial\Omega_{con},\\ \mathcal{L}_t\overline{u}_c(x,t) &= 0 \quad \text{on } \partial\Omega.\end{aligned} \tag{4.62}$$

We want to prove that $\overline{u}_c$ is indeed a unique solution to the variational problem (4.61). For this purpose, we introduce the linear operator $\mathcal{A} : H^1(\Omega_{con}) \to H^1(\Omega_{con})^\star$ and the nonlinear operator $\mathcal{B} : H^1(\Omega_{con}) \to H^1(\Omega_{con})^\star$, which are defined by

$$\begin{aligned}\langle \mathcal{A}u, v\rangle_{H^1(\Omega_{con})^\star, H^1(\Omega_{con})} &= \nu_{con}\int_{\Omega_{con}} B(x,t)B(x,t)^\top\nabla_x u(x,t)\cdot\nabla_x v(x)\,dx,\\ \langle \mathcal{B}u, v\rangle_{H^1(\Omega_{con})^\star, H^1(\Omega_{con})} &=\\ &-\int_{\partial\Omega_{con}}\gamma_0\Big(\nu(x,|B^\top\nabla_x\mathcal{L}_t u|)B(x,t)B(x,t)^\top\nabla_x\mathcal{L}_t u(x,t)\Big)\cdot n(x)\gamma_0 v(x)\,ds_x,\end{aligned}$$

for $u(\cdot,t), v \in H^1(\Omega_{con})$. Hence, we can write (4.61) shortly as

$$\sigma_{con} \int\limits_{\Omega_{con}} \frac{\partial}{\partial t}\overline{u}_c(x,t)v(x)\ dx + \langle \mathcal{A}\overline{u}_c + \mathcal{B}\overline{u}_c, v\rangle_{H^1(\Omega_{con})^\star,H^1(\Omega_{con})} = \widetilde{l}(\varphi(x,t),t)$$

for all $v \in H^1(\Omega_{con})$. We start to analyze the linear operator $\mathcal{A}$ and easily obtain that $\mathcal{A}$ is Lipschitz continuous, i.e. for all $u_1, u_2 \in H^1(\Omega_{con})$ it holds

$$\begin{aligned}\|\mathcal{A}u_1 - \mathcal{A}u_2\|_{H^1(\Omega_{con})^\star} &= \sup_{0\neq v\in H^1(\Omega_{con})} \frac{|\langle \mathcal{A}u_1 - \mathcal{A}u_2, v\rangle_{H^1(\Omega_{con})^\star,H^1(\Omega_{con})}|}{\|v\|_{H^1(\Omega_{con})}}\\ &\leq \sup_{0\neq v\in H^1(\Omega_{con})} \frac{\nu_{con}\overline{\gamma}_B\|\nabla_x(u_1-u_2)\|_{L^2(\Omega_{con})}\|\nabla_x v\|_{L^2(\Omega_{con})}}{\|v\|_{H^1(\Omega_{con})}}\\ &\leq \nu_{con}\overline{\gamma}_B\|u_1-u_2\|_{H^1(\Omega_{con})},\end{aligned}$$

where we have used (4.18) to bound B. Furthermore, the linear operator $\mathcal{A}$ is monotone, since for all $u_1, u_2 \in H^1(\Omega_{con})$ it holds

$$\langle \mathcal{A}u_1 - \mathcal{A}u_2, u_1-u_2\rangle_{H^1(\Omega_{con})^\star,H^1(\Omega_{con})} \geq \nu_{con}\underline{\gamma}_B\|\nabla_x(u_1-u_2)\|^2_{L^2(\Omega_{con})} \geq 0.$$

We now focus on the nonlinear operator $\mathcal{B}$, for which we fist introduce the linear extension operator $\mathcal{E} : H^1(\Omega_{con}) \to H^1(\Omega)$, such that $\|\mathcal{E}v\|_{H^1(\Omega)} \leq c_E\|v\|_{H^1(\Omega_{con})}$, cf. [1], in order to obtain when using integration by parts, that

$$\begin{aligned}\langle \mathcal{B}u, v\rangle_{H^1(\Omega_{con})^\star,H^1(\Omega_{con})} =&\\ &\int\limits_{\Omega\setminus\overline{\Omega_{con}}} \nu(x,|B^\top\nabla_x\mathcal{L}_t u|)B(x,t)B(x,t)^\top\nabla_x\mathcal{L}_t u(x,t)\cdot\nabla_x\mathcal{E}v(x)\ ds_x,\\ &\quad -\int\limits_{\Omega\setminus\overline{\Omega_{con}}} \mathrm{div}_x(\nu(x,|B(x,t)^\top\nabla_x\mathcal{L}_t u|)B(x,t)B(x,t)^\top\nabla_x\mathcal{L}_t u(x,t))\mathcal{E}v(x)\ dx\\ &= \int\limits_{\Omega\setminus\overline{\Omega_{con}}} \nu(x,|B^\top\nabla_x\mathcal{L}_t u|)B(x,t)B(x,t)^\top\nabla_x\mathcal{L}_t u(x,t)\cdot\nabla_x\mathcal{E}v(x)\ dx\\ &\qquad + \int\limits_{\Omega\setminus\overline{\Omega_{con}}} J_3(x,t)\mathcal{E}v(x)\ dx,\end{aligned}$$

for $u, v \in H^1(\Omega_{con})$, where $\mathcal{L}_t u$ satisfies the boundary value problem (4.62). Hence, for $u_1, u_2 \in H^1(\Omega_{con})$ satisfying (4.62), we have

$$\begin{aligned}\langle \mathcal{B}u_1 - \mathcal{B}u_2, v\rangle_{H^1(\Omega_{con})^\star,H^1(\Omega_{con})} =&\\ &\int\limits_{\Omega\setminus\overline{\Omega_{con}}} \nu(x,|B^\top\nabla_x\mathcal{L}_t u_1|)B(x,t)B(x,t)^\top\nabla_x\mathcal{L}_t u_1(x,t)\cdot\nabla_x\mathcal{E}v(x)\ dx\\ &\quad -\int\limits_{\Omega\setminus\overline{\Omega_{con}}} \nu(x,|B^\top\nabla_x\mathcal{L}_t u_2|)B(x,t)B(x,t)^\top\nabla_x\mathcal{L}_t u_2(x,t)\cdot\nabla_x\mathcal{E}v(x)\ dx,\end{aligned}$$

where the application of Lemma 4.5 to the operator $\mathcal{L}_t : H^1(\Omega_{con}) \to H^1(\Omega\backslash\overline{\Omega_{con}})$ gives

$$\begin{aligned}\|Bu_1 - Bu_2\|_{H^1(\Omega_{con})^\star} &= \sup_{v\in H^1(\Omega_{con})} \frac{|\langle \mathcal{B}u_1 - \mathcal{B}u_2, v\rangle_{H^1(\Omega_{con})^\star, H^1(\Omega_{con})}|}{\|v\|_{H^1(\Omega_{con})}} \\ &\leq 3\nu_0 c_E \overline{\gamma}_B \|\nabla_x \mathcal{L}_t u_1 - \nabla_x \mathcal{L}_t u_2\|_{L^2(\Omega\backslash\overline{\Omega_{con}})} \\ &\leq 3\nu_0 c_E \overline{\gamma}_B \|\mathcal{L}_t u_1 - \mathcal{L}_t u_2\|_{H^1(\Omega\backslash\overline{\Omega_{con}})}.\end{aligned}$$

According to Lemma 4.5, $\mathcal{L}_t u_1$ and $\mathcal{L}_t u_2$ are the unique solutions to (4.21) for the given boundary data u_1 and u_2, respectively, but the same right-hand side J_3, hence the continuity estimate (4.17) holds, and we deduce

$$\begin{aligned}\|Bu_1 - Bu_2\|_{H^1(\Omega_{con})^\star} &\leq 3\nu_0 c_E \overline{\gamma}_B \|\mathcal{L}_t u_1 - \mathcal{L}_t u_2\|_{H^1(\Omega\backslash\overline{\Omega_{con}})} \\ &\leq 3\nu_0 c_E \overline{\gamma}_B c_{\mathcal{L}_t} \|\gamma_0(u_1 - u_2)\|_{H^{1/2}(\partial\Omega_{con})} \\ &\leq 3\nu_0 c_E \overline{\gamma}_B c_{\mathcal{L}_t} c_{tr} \|u_1 - u_2\|_{H^1(\Omega_{con})},\end{aligned}$$

where the last estimate follows from the trace inequality, such that we conclude the Lipschitz continuity of the operator $\mathcal{B}$.

Moreover, for $u_1, u_2 \in H^1(\Omega_{con})$ satisfying (4.62) we obtain with the same calculations as before that

$$\begin{aligned}&\langle \mathcal{B}u_1 - \mathcal{B}u_2, u_1 - u_2\rangle_{H^1(\Omega_{con})^\star, H^1(\Omega_{con})} \\ &\quad = \int_{\Omega\backslash\overline{\Omega_{con}}} \nu(x, |U_1|) U_1(x,t) \cdot (U_1(x,t) - U_2(x,t))\, dx \\ &\qquad - \int_{\Omega\backslash\overline{\Omega_{con}}} \nu(x, |U_2|) U_2(x,t) \cdot (U_1(x,t) - U_2(x,t))\, dx,\end{aligned}$$

where $U_i = B^\top \nabla_x \mathcal{L}_t u_i$, for $i = 1, 2$. Using the same calculations as in the proof of Lemma 4.5, we deduce

$$\langle \mathcal{B}u_1 - \mathcal{B}u_2, u_1 - u_2\rangle_{H^1(\Omega_{con})^\star, H^1(\Omega_{con})} \geq \underline{\nu}\underline{\gamma}_B \|\nabla_x \mathcal{L}_t u_1 - \nabla_x \mathcal{L}_t u_2\|^2_{L^2(\Omega\backslash\overline{\Omega_{con}})}.$$

Due to Friedrichs's inequality (3.12), the norms $\|\nabla_x u\|_{L^2(\Omega\backslash\overline{\Omega_{con}})}$ and $\|u\|_{H^1(\Omega\backslash\overline{\Omega_{con}})}$ are equivalent on the space $H^1_{0,\partial\Omega}(\Omega\backslash\overline{\Omega_{con}}) \coloneqq \{u \in H^1(\Omega\backslash\overline{\Omega_{con}}) : \gamma_0 u = 0 \text{ on } \partial\Omega\}$, hence it follows that

$$\begin{aligned}\langle \mathcal{B}u_1 - \mathcal{B}u_2, u_1 - u_2\rangle_{H^1(\Omega_{con})^\star, H^1(\Omega_{con})} &\geq c\underline{\nu}\underline{\gamma}_B \|\mathcal{L}_t u_1 - \mathcal{L}_t u_2\|^2_{H^1(\Omega\backslash\overline{\Omega_{con}})} \\ &\geq c c_{tr}^2 \underline{\nu}\underline{\gamma}_B \|\gamma_0(u_1 - u_2)\|^2_{H^{1/2}(\partial\Omega_{con})},\end{aligned}$$

where the last estimate follows from the trace inequality.

Finally, the sum of both operators $\mathcal{A}+\mathcal{B}$ is Lipschitz continuous, i.e.

$$\|(\mathcal{A}+\mathcal{B})u_1-(\mathcal{A}+\mathcal{B})u_2\|_{H^1(\Omega_{con})^\star}\leq L\|u_1-u_2\|_{H^1(\Omega_{con})},$$

where $L=\overline{\gamma}_B\max(\nu_{con},3\nu_0 c_E c_{\mathcal{L}_t}c_{tr})$, and strongly monotone, i.e.

$$\begin{aligned}\langle(\mathcal{A}+\mathcal{B})u_1-(\mathcal{A}+\mathcal{B})u_2,u_1-u_2\rangle_{H^1(\Omega_{con})^\star,H^1(\Omega_{con})}&\\ \geq \nu_{con}\underline{\gamma}_B\|\nabla_x(u_1-u_2)\|^2_{L^2(\Omega_{con})}+cc_{tr}^2\underline{\nu}\underline{\gamma}_B\|\gamma_0(u_1-u_2)\|^2_{H^{1/2}(\partial\Omega_{con})}&\\ \geq C\|u_1-u_2\|^2_{H^1(\Omega_{con}),H^{1/2}(\partial\Omega_{con})}\geq \underline{c}_P^2C\|u_1-u_2\|^2_{H^1(\Omega_{con})}&\end{aligned}$$

with $C=\underline{\gamma}_B\min(\nu_{con},cc_{tr}^2\underline{\nu})$, where we have used the norm as defined in Lemma 4.7 and its application. Thus, it follows from Theorem 4.6 that the variational problem (4.61) has a unique solution $\overline{u}_c\in L^2(0,T;H^1(\Omega_{con}))$.

From here on, we proceed in the same way as in the proof of Theorem 4.8 considering the transported function $\overline{u}_c$ in order to introduce the solution $\overline{u}_{c,ext}(\cdot,t)=\mathcal{L}_t\overline{u}_c(\cdot,t)\in H^1(\Omega\backslash\overline{\Omega_{con}})$ for almost all $t\in[0,T]$ and to obtain the constructed solution $\overline{u}\in L^2(0,T;H_0^1(\Omega))$ of (4.60) defined as

$$\overline{u}(x,t)=\begin{cases}\overline{u}_c(x,t) & \text{for } x\in\Omega_{con},\\ \overline{u}_{c,ext}(x,t) & \text{for } x\in\Omega\backslash\overline{\Omega_{con}},\end{cases}$$

such that $\sigma\frac{\partial}{\partial t}u\in L^2(0,T;H^{-1}(\Omega))$. Finally, we define $u\in X$ as the transformed back function

$$u(y,t)=\overline{u}(\varphi^{-1}(x,t),t),\quad t\in[0,T],\ x\in\Omega,$$

which is a solution to (4.57), hence also to (4.40), for which the Lipschitz dependence on the data follows from the Lipschitz dependence of the solutions to the problems (4.61) and (4.62). This ends the proof. □

The problems that we have discussed in this chapter are elliptic-parabolic interface problems. At the interfaces the electric conductivity as well as the magnetic reluctivity are discontinuous. However, the corresponding jump conditions for the solution at the interfaces are implicitly given by the variational problem, which is subject of the next theorem.

THEOREM 4.17. *Let $J_3,M^\perp\in L^2(0,T;L^2(\Omega(t)))$. Then the corresponding solution $u(\cdot,t)$ of (4.58) is continuous across the interface $\Gamma_I(t)$, i.e. for all $t\in(0,T)$ and $x\in\Gamma_I(0)$, it holds*

$$u^-(\varphi(x,t),t)=u^+(\varphi(x,t),t),$$

so are also its normal flux, i.e. for all $t \in (0,T)$ *and* $x \in \Gamma_I(0)$*, it holds*

$$(\nu \nabla_x u(\varphi(x,t),t))^- \cdot n(\varphi(x,t)) = (\nu \nabla_x u(\varphi(x,t),t))^+ \cdot n(\varphi(x,t)),$$

and the time derivative, i.e. $t \in (0,T)$ *and* $x \in \Gamma_I(0)$*, it holds*

$$\frac{d}{dt} u^-(\varphi(x,t),t) = \frac{d}{dt} u^+(\varphi(x,t),t).$$

Proof. The proof is given in [26, Lemma 4.2]. □

REMARK 4.18. *Note that Theorem 4.17 is also applicable for all considered problems in this chapter, where the corresponding variational formulations can be similarly rewritten to an equivalent problem of the form* (4.58)*.*

Space-time finite element discretization

As in the linear case, we introduce the conforming finite-dimensional spaces $X_h \subset X$ and $Y_h \subset Y$, such that $X_h \subset Y_h$. Particularly, we even consider $X_h = Y_h$ as in (4.7) for our purpose. Hence, the discrete problem reads to find $u_h \in X_h$, such that

$$a(u_h, v_h) = l(v_h) \quad \text{for all } v_h \in Y_h, \tag{4.63}$$

where $a(\cdot,\cdot)$ and $l(\cdot)$ are defined as in (4.40). The existence of a unique solution $u_h \in X_h$ follows from Theorem 4.16, since the properties of $a(\cdot,\cdot)$ are inherited from the continuous problem. As in Section 4.1.3, we introduce the operator $A_e : Y_h \to Y_h^\star$, from which we derive the Newton operator A_e' as defined in (4.23). Using the finite element isomorphism (4.12), we obtain the equivalent problem (4.24), and we can apply Newton's method (4.25) with damping.

4.3.4 Numerical examples

In this section we provide some numerical results in order to illustrate the applicability and accuracy of the proposed method.

First, we again consider the mesh of the space-time cylinder Q from Figure 4.10, the manufactured solution

$$u(y,t) = (y-t)(1-y+t)t,$$

and the material parameters

$$\sigma(y) = \begin{cases} 1 & \text{for } y \in \Omega_{con}(t), \\ 0 & \text{for } y \in \Omega_{non}(t), \end{cases} \quad \text{and} \quad \nu(y) = \begin{cases} 2 & \text{for } y \in \Omega_{con}(t), \\ 1 + |\partial_y u|^2 & \text{for } y \in \Omega_{non}(t). \end{cases}$$

L	dofs	$\|\nabla_y(u-u_h)\|_{L^2(0,T,\Omega(t))}$	EOC
1	153	0.03552	
2	561	0.01792	0.987
3	2,145	0.00900	0.994
4	8,385	0.00451	0.997
5	33,153	0.00225	0.999
6	131,841	0.00113	1
7	525,825	0.00056	1
8	2,100,225	0.00028	1
9	8,394,753	0.00014	1

Table 4.14: The discretization error, which indicates linear convergence when using the parallel direct solver MUMPS on 16 cores for a uniform mesh refinement. In each refinement level, 5 Newton iterations were required.

Number of cores	1	2	4	8	16
MUMPS	115.81	84.78	67.03	54.78	50.59

Table 4.15: Computational times in seconds for solving the nonlinear problem (4.24) with MUMPS on a mesh with 525,313 nodes (degrees of freedom) and 262,144 elements. The solver required 5 Newton iterations.

Hence, we obtain for the right-hand side that $M^\perp = 0$ and

$$J_3(y,t) = \begin{cases} (y-t)(1-y+t)+4t & \text{for } y \in \Omega_{con}(t), \\ 2\Big(3(1-2y)^2t^3 + (12-24y)t^4 + 12t^5 + t\Big) & \text{for } y \in \Omega_{non}(t). \end{cases}$$

We apply Newton's method (4.25) to solve the nonlinear system (4.24), for which the parallel direct solver MUMPS is used to solve the linearized system (4.26). The error tolerance is 10^{-11} and in Table 4.14 we obtain a linear convergence behavior of the error for the spatial gradient of the solution in the $L^2(0,T,\Omega(t))$-norm. Furthermore, the computational times for solving the nonlinear problem (4.24) with respect to the number of cores are given in Table 4.15. Note that the measured times include the linearization of A in order to obtain A' in (4.26) and the converting of the data types between the software Netgen/NGSolve and PETSc in each Newton iteration.

The Permanent Magnet Synchronous Motor

Finally, we turn our focus to the rather complex geometry of the interior permanent magnet synchronous motor [77] from Figure 2.2, where both rotor and stator, denoted

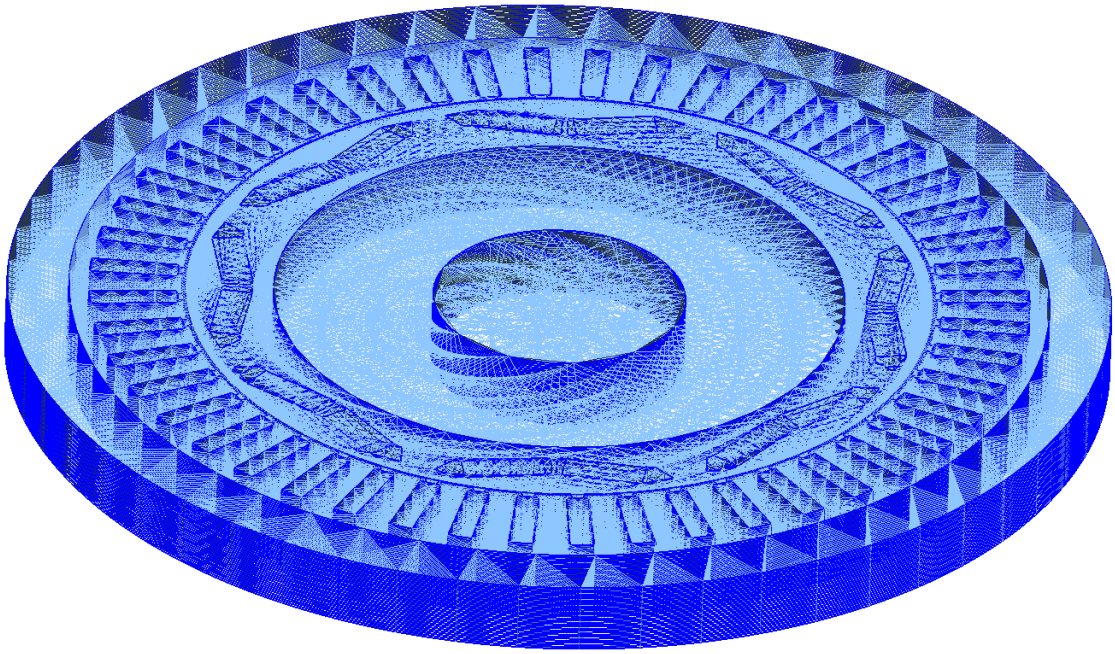

Figure 4.13: An unstructured mesh of the space-time cylinder Q, which is extruded vertically in time with 30 time slices considering a counterclockwise 90-degree rotational motion of $\Omega(0)$, and has 332,752 nodes and 1,976,347 elements.

by Ω_{fe}, are made of laminated steel sheets. There are 16 magnets arranged in a single V-shape constellation within the rotor and 48 coils within the stator right above the air gap. The thin air gap is separating the rotor and the stator, and there is an air hole in the middle of the motor, where the shaft is used to be. Air pockets are included around each pole of every permanent magnet. For the other domains we use the notations Ω_{cu} for the coils, Ω_m for the magnets and Ω_a for all air regions. The initial state of the motor $\Omega(0)$ is pulled up in time, where the rotation of the rotating parts, i.e. the rotor, the magnets and the air pockets around the magnets, is already considered within the mesh for the time span $(0, T)$ with $T = 0.015$ $[s]$ and a counterclockwise 90-degree rotational motion described by φ_{R_α} as in (3.8). Note that this corresponds to a rotational speed of 1000 revolutions per minute. Moreover, 30 time slices are inserted in order to have a good temporal resolution. The space-time mesh of the PMSM is completely unstructured within the time slices and consists of 332,752 nodes and 1,976,347 tetrahedral elements as visualized in Figure 4.13. The space-time mesh has different spatial resolutions, which has been chosen in advance. For instance, the mesh in the air gap and the regions around is finer than the other parts of the motor. Furthermore, the rotor and the stator are divided into a fine and

Material		$\sigma\ [\frac{A^2 \cdot s^2}{kg \cdot m^3}]$	$\nu\ [\frac{A \cdot m}{V \cdot s}]$
Air	Ω_a	0	$10^7/(4\pi)$
Coils	Ω_{cu}	0.0001	$10^7/(4\pi)$
Magnets	Ω_m	10^6	$10^7/(4.2\pi)$
Steel	Ω_{fe}	0	$\nu_{fe}(\lvert\nabla_x u\rvert)$

Table 4.16: The values for the electric conductivity σ and magnetic reluctivity ν in the different material regions.

coarse part, respectively, since it is not necessary to have a fine mesh everywhere in these regions. We refer to Figure 3.1 for the dimensions of the electric motor.

The values of the electric conductivity σ and the magnetic reluctivity ν for the different materials are given in Table 4.16, where the magnetic reluctivity ν is nonlinear in the ferromagnetic material, i.e. in the rotor and the stator. We describe the nonlinear behavior of the magnetic reluctivity ν_{fe} by the quadratic B-spline from Figure 2.3b, whose measured values are provided by Robert Bosch GmbH in Table 5.1. In order to avoid computational difficulties, we linearly extended the reluctivity spline ν_{fe} based on the last two measured values. Numerous thin copper wires are wounded around the coils, through which the current excitation is passed. The coils are grouped in 3 different phases U, V and W, which are excited with the same current strength but are shifted by 120 degrees. Each phase has another division into the regions Ω_{U^+}, Ω_{U^-}, Ω_{V^+}, Ω_{V^-} and Ω_{W^+}, Ω_{W^-}, denoting the direction of the current excitations, as depicted in Figure 4.14. In this expression, we can now define the impressed current density as

$$J_3(y,t) = J_3^+(y,t) + J_3^-(y,t),$$

where

$$J_3^+(y,t) = \begin{cases} J_U(t) & \text{for } y \in \Omega_{U^+}, \\ J_V(t) & \text{for } y \in \Omega_{V^+}, \\ J_W(t) & \text{for } y \in \Omega_{W^+}, \end{cases} \quad \text{and} \quad J_3^-(y,t) = \begin{cases} -J_U(t) & \text{for } y \in \Omega_{U^-}, \\ -J_V(t) & \text{for } y \in \Omega_{V^-}, \\ -J_W(t) & \text{for } y \in \Omega_{W^-}. \end{cases}$$

The single current densities for each phase are given as

$$\begin{aligned} J_U(t) &= j\ \sin\Big(4\alpha(t) + \psi\Big), \\ J_V(t) &= j\ \sin\Big(4\alpha(t) + \psi + \frac{4}{3}\pi\Big), \\ J_W(t) &= j\ \sin\Big(4\alpha(t) + \psi + \frac{2}{3}\pi\Big), \end{aligned}$$

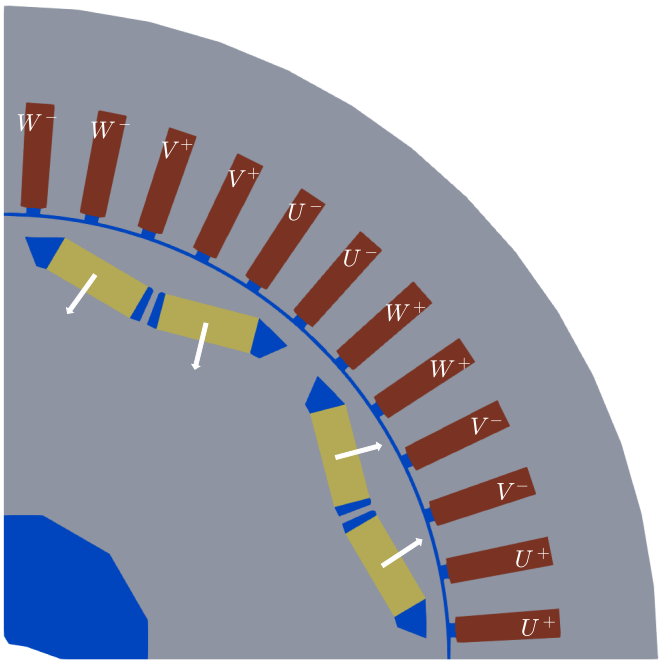

Figure 4.14: A part of the PMSM showing the different phases and directions of the current excitation, as well as the direction of the magnetic field exposed from the permanent magnets. This is repeated for the other four parts of the electric motor.

where $\alpha(t) = \frac{\pi}{2}\frac{t}{T}$ and $\psi = \frac{\pi}{18}$ is called the current angle. The amplitude j is given by $j = Ic/A_m$, where $I = 1555.64$ $[A]$ is the product of the current intensity and the number of windings per coil, $c = 2.75$ is the stacking factor and $A_m \approx 9.027 \cdot 10^{-5}$ $[m^2]$ is the area of one coil. Furthermore, this electric motor has 16 permanent magnets, whose magnetic field is described by $M = (M_1, M_2)^\top$, cf. Section 2.19. The direction of M is visualized in Figure 4.14 and its magnitude equals $|M| = \nu_m B_r$ $[\frac{A}{m}]$, where ν_m is the magnetic reluctivity for the magnets and $B_r = 1.216$ $[\frac{V \cdot s}{m^2}]$ is the magnetic remanence.

After specifying all parameters, we can solve the discrete variational formulation (4.63) by applying Newton's method (4.25) with damping. The derived linear system (4.26) is solved with the parallel direct solver MUMPS and the iterative solver GMRES with the BoomerAMG preconditioner as described in Section 3.6.1. We use a relative error tolerance of 10^{-11} for the stop criterion of Newton's method and a relative error tolerance of 10^{-5} for the parallel iterative solver GMRES. The computational times for solving the nonlinear problem (4.63) with respect to the number of cores are given in Table 4.17. Note that the measured times include the linearization of A in order to obtain A' in (4.26) and the converting of the data types between the software Netgen/NGSolve and PETSc in each Newton iteration. Figure 4.15

Number of cores	1	2	4	8	16
MUMPS	789.88	505.16	357.20	268.81	231.18
GMRES	2823.90	1469.55	791.94	425.10	251.07
iterations	321	340	315	323	318

Table 4.17: Computational times in seconds for solving the nonlinear system (4.24) with MUMPS and preconditioned GMRES with the BoomerAMG preconditioner. The solvers required 19 Newton iterations and the number of GMRES iterations gives the most needed iterations of all Newton steps.

Number of cores	1	2	4	8	16
MUMPS	609.31	403.39	303.98	228.48	196.84
GMRES	2122.03	1060.58	578.33	310.33	177.09
iterations	296	255	262	282	269

Table 4.18: Computational times in seconds for solving the nonlinear system (4.24) for the magnetostatic problem ($\sigma = 0$) with MUMPS and preconditioned GMRES with the BoomerAMG preconditioner. The solvers required 17 Newton iterations and the number of GMRES iterations gives the most needed iterations of all Newton steps.

displays the approximate solution u_h for different time points, for which we obtain correspondence between the rotation of the solution and the rotation of the rotor.

In many applications and experiments the magnetostatic problem (2.22) plays an important role. Therefore, we want to apply our space-time finite element method for this type of problems, for which we set the electric conductivity to zero in every region, cf. Section 2.2.3. The approximate solution u_h of the magnetostatic problem for different time points is depicted in Figure 4.16 and the computational times with respect to the number of cores are given in Table 4.18. Here we used the same relative error tolerances for Newton's method and the GMRES solver as above.

In context of electric motors, the torque is an important physical quantity that represents a valuable indicator of the motor's performance. The torque can be computed by the so-called Maxwell's stress tensor, see e.g. [9, Section 2.4]. In terms of Maxwell's stress tensor, the torque $T_c(t)$ at time $t \in [0, T]$ is obtained as [15, 51]

$$T_c(t) = L\nu_0 \int_{\Gamma_0} \nabla_y u(y,t)^\top Q(y) \cdot \nabla_y u(y,t) \, ds_y, \tag{4.64}$$

where $L = 0.1795$ $[m]$ is the length of the three-dimensional PMSM in the third spatial direction, ν_0 is the magnetic reluctivity in air, Γ_0 is a circular curve inside the

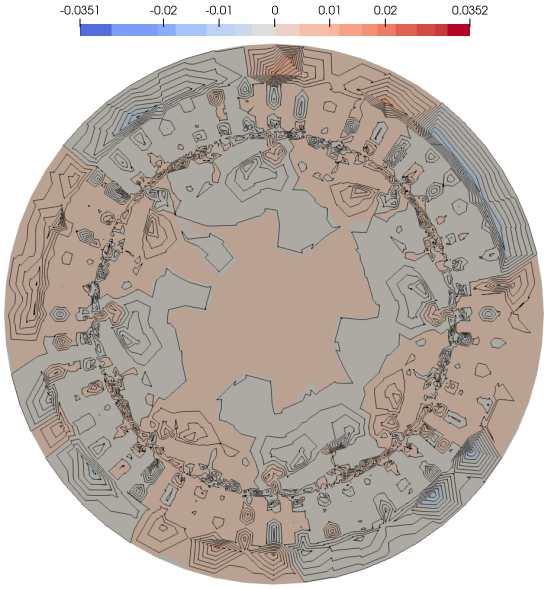

Solution u_h at time $t = 0.0[s]$.

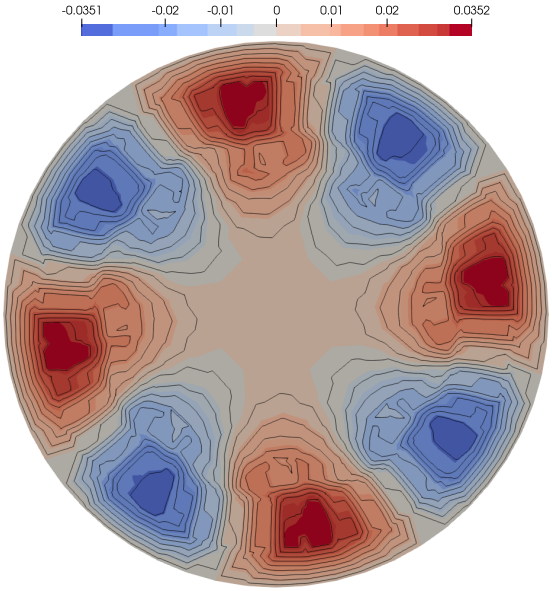

Solution u_h at time $t = 0.005[s]$.

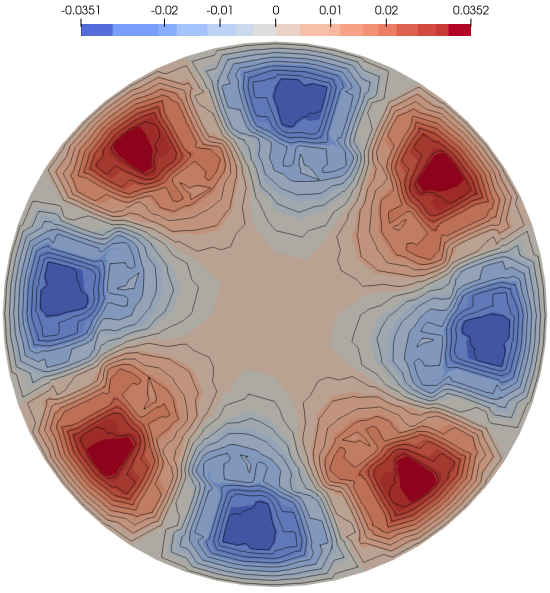

Solution u_h at time $t = 0.01[s]$.

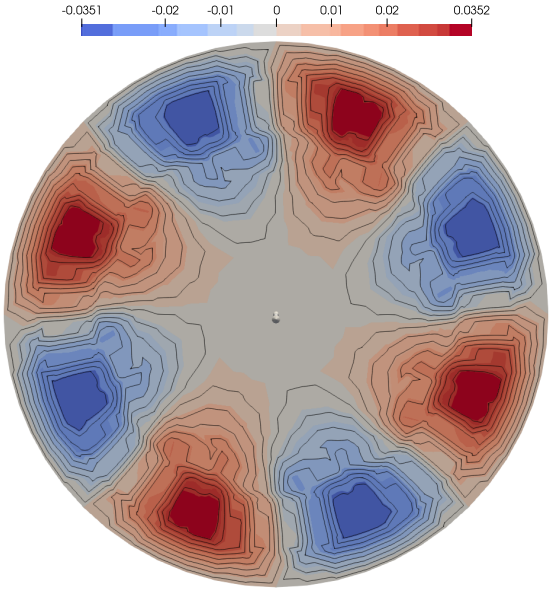

Solution u_h at time $t = 0.015[s]$.

Figure 4.15: The approximate solution u_h of (4.63) for different time points computed on the mesh from Figure 4.13.

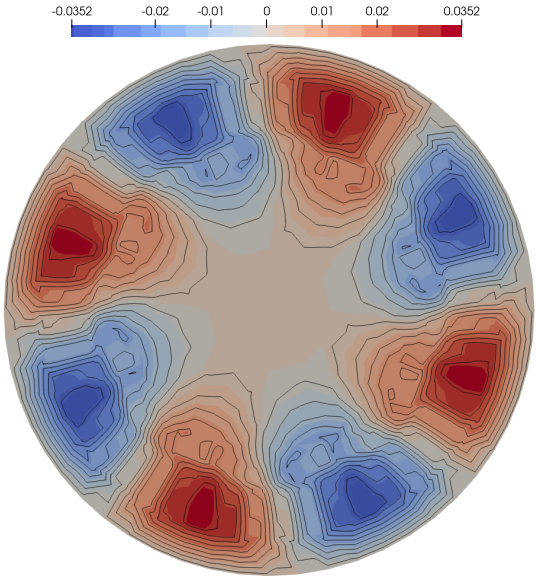

Solution u_h at time $t = 0.0[s]$.

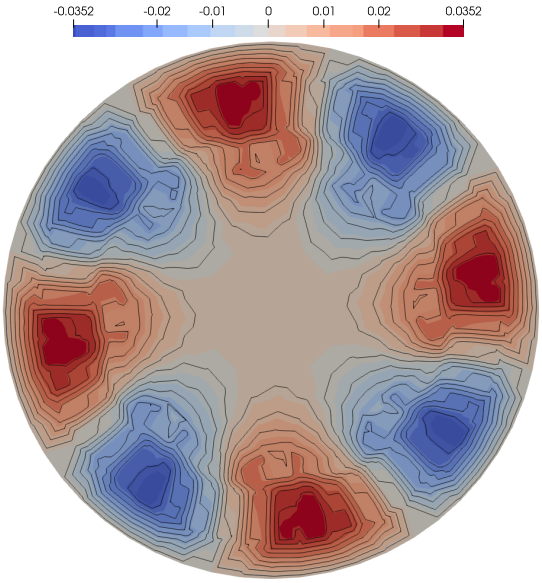

Solution u_h at time $t = 0.005[s]$.

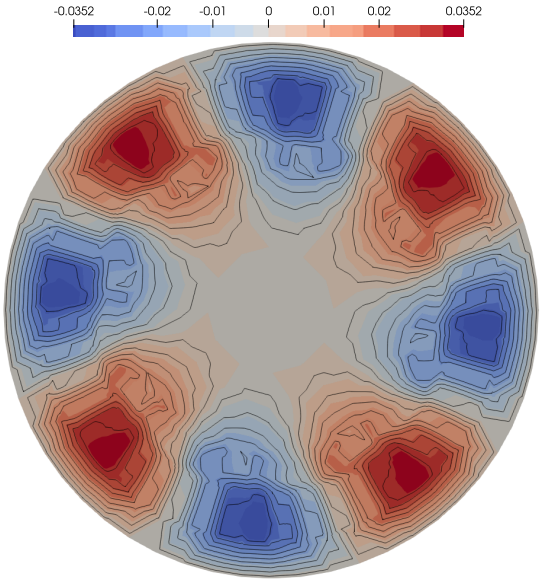

Solution u_h at time $t = 0.01[s]$.

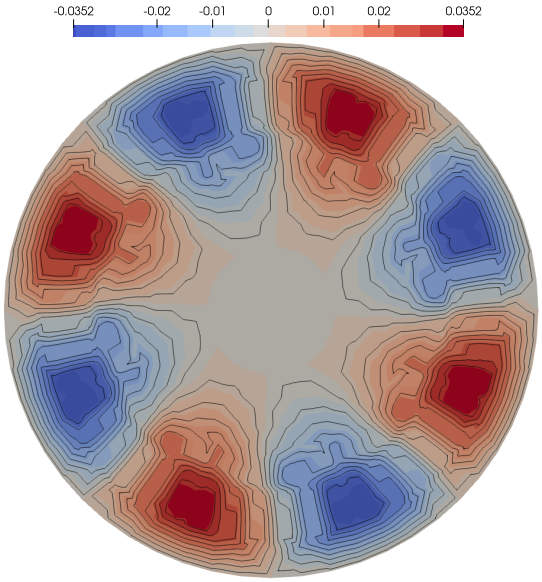

Solution u_h at time $t = 0.015[s]$.

Figure 4.16: The approximate solution u_h of the magnetostatic problem for different time points computed on the mesh from Figure 4.13.

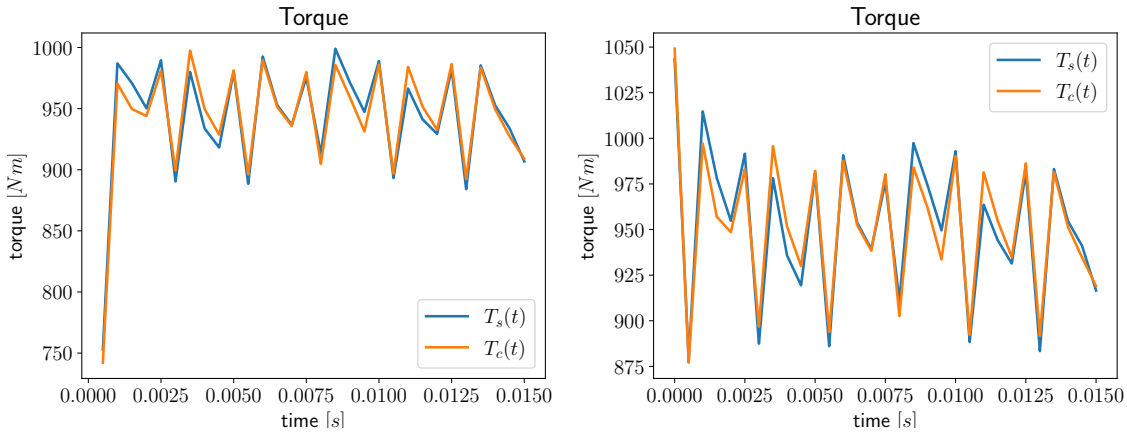

Figure 4.17: Left: The torques of the eddy current problem (4.63) computed by (4.64) and (4.65), respectively. The deviation of the curves is less than 2.3%. Right: The torques of the magnetostatic problem computed by (4.64) and (4.65), respectively. The deviation of the curves is less than 2.2%.

air gap and Q is a matrix defined by

$$Q(y) = Q(y_1, y_2) = \frac{1}{\sqrt{y_1^2 + y_2^2}} \begin{pmatrix} y_1 y_2 & \frac{y_2^2 - y_1^2}{2} \\ \frac{y_2^2 - y_1^2}{2} & -y_1 y_2 \end{pmatrix}.$$

On the other hand, as suggested by Arkkio [9, Section 2.4], Arrkio's method is another possibility to evaluate the torque $T_s(t)$ with the help of a surface integral, which is given as

$$T_s(t) = \frac{L\nu_0}{r_{out} - r_{in}} \int_S \nabla_y u(y,t)^\top Q(y) \cdot \nabla_y u(y,t)\, dy, \tag{4.65}$$

where S is an annulus with inner and outer radii $r_{in} = 78.8355$ $[mm]$ and $r_{out} = 79.0387$ $[mm]$ lying in the air gap between the rotor and the stator, and the other quantities are defined as in (4.64), see also [132]. Figure 4.17 shows the torques $T_c(t)$ and $T_s(t)$ evaluated at each time slice of the PMSM for the eddy current problem (4.40) and the magnetostatic problem, respectively, where the radius r_c of the curve for the computation of the torque $T_c(t)$ is chosen as $r_c = (r_{in} + r_{out})/2$. It turns out that both methods produce similar and acceptable results.

5 Conclusion and outlook

In this thesis we derived conforming space-time finite element methods on completely unstructured decompositions of space-time cylinders, considering both stationary but also moving domains. Treating time as an additional spatial component $x_{d+1} = t$, the movement of the body can be naturally captured by the mesh. Motivated by the application of space-time methods to rotating electric motors, we investigated the widely used eddy-current approximation derived from Maxwell's equations in the low-frequency regime. In fact, this approximation leads to an elliptic-parabolic interface problem when electrically conducting and non-conducting materials are involved, as is the case in electric motors. For this purpose, we began by analyzing the linear eddy current problem, formulating a space-time variational formulation in Bochner spaces as proposed in [144]. Using the Babuška-Nečas theory, we proved the unique solvability for both the continuous case and its Galerkin discretization in the space-time domain. While the proof in the continuous case requires an inf-sup stability condition for the uniqueness and a surjectivity condition for the existence of a solution, one of these conditions is sufficient to ensure a unique solution of the discretized variational formulation. Numerical examples validated the theoretical error estimates in the energy norm, using the space $S_h^1(\mathcal{T}_h)$ of piecewise linear and globally continuous functions with respect to some admissible and locally quasi-uniform decompositions $\mathcal{T}_h$ into shape regular simplicial finite elements.

We then extended the analysis to the nonlinear eddy current problem to describe the reluctivity in ferromagnetic materials. By applying Zarantonello's theorem and the principle of maximal monotone mappings, we established unique solvability. To demonstrate the effectiveness of our method, we presented a benchmark problem of a Switched Reluctance Motor. The results highlighted the accuracy of the space-time method, showing, on the one hand, agreement between the simulation and experimental measurements, and on the other hand its computational efficiency through a parallelization in space and time simultaneously.

In practice however, ferromagnetic materials exhibit hysteresis effects, which are usually complex to model. We adopted a specific hysteresis model proposed in [163] and derived the corresponding eddy current approximation and its variational formulation, resulting in a saddle-point system. Using our space-time approach, we solved this system, achieving results that closely matched observed hysteretic behavior. As before, parallel computing was used to solve now the entire system at once in space and time simultaneously.

Finally, we considered the eddy current problem posed on uniformly moving domains, for which the analysis is similar to the stationary case. The unique solvability were proven for both the linear and the nonlinear continuous case as well as their corresponding Galerkin discretizations. To showcase the applicability of the proposed method, we carried out a simulation of a rotating permanent magnet synchronous motor. Torque evaluations confirmed the method's accuracy, with simulation results aligning closely with practical observations.

There remain multiple paths for closer inspection and new discoveries in this field. A rather obvious extension involves the investigation of the eddy-current problem posed on spatially three-dimensional domains, resulting in four-dimensional space-time problems. However, the eddy current approximation in this spatial dimension leads to a curl-curl-formulation on related spaces [164], requiring more sophisticated analysis. On the other hand, the generation of four-dimensional meshes is not straight forward and many open-source mesh generating tools do not provide such functionalities. The authors of [115] and [134] address the methodology of generating such meshes, even for moving domains. Nevertheless, the resulting systems are extremely large, hence suitable parallel solvers are urgently necessary.

This highlights another area for future research. Although we have applied this approach to examples of practical interest, it is still a challenging task to improve parallel solvers in order to handle problems with much higher degrees of freedom, even for one and two-dimensional spatial domains. Furthermore, it is more involved to find suitable robust preconditioners for the iterative methods, especially when dealing with moving domains or interfaces.

Moreover, the numerical examples presented in this thesis were computed without incorporating any error estimators. Space-time methods, however, offer complete control over the discretization in spatial and temporal dimensions simultaneously, making space-time adaptivity a viable and promising approach [91]. The combination of parallelization and adaptivity will lead to efficient methods, opening the door to practical applications involving complex structures.

Finally, extending the eddy current problem to include hysteresis effects in moving domains is a compelling direction for future work. Such advances would further integrate space-time methods into practical applications, including the simulation of rotating electric motors like the PMSM. These developments have the potential to significantly enhance the applicability and performance of space-time finite element methods in complex, real-world scenarios.

Appendix

Number	$H := \|\mathbf{H}\|$ $[A/m]$	$B := \|\mathbf{B}\|$ $[T]$	Number	$H := \|\mathbf{H}\|$ $[A/m]$	$B := \|\mathbf{B}\|$ $[T]$
1	0	0	21	2000	1.35628106
2	10	0.07636101	22	2000	1.40054159
3	20	0.15180201	23	4000	1.43652212
4	30	0.22448302	24	5000	1.46790265
5	40	0.29440402	25	6000	1.49744319
6	50	0.36064503	26	7000	1.52514372
7	60	0.42228603	27	8000	1.55100425
8	70	0.47932704	28	9000	1.57594478
9	80	0.53268804	29	10000	1.59904531
10	90	0.58144905	30	20000	1.76197062
11	100	0.62653005	31	30000	1.83657593
12	200	0.91358011	32	40000	1.87070124
13	300	1.04791016	33	50000	1.89102655
14	400	1.12336021	34	60000	1.90583186
15	500	1.17213027	35	70000	1.91971717
16	600	1.20526032	36	80000	1.93268248
17	700	1.23103037	37	90000	1.94564779
18	800	1.25036042	38	100000	1.95861310
19	900	1.26601048	39	200000	2.08458619
20	1000	1.27982053	40	500000	2.46158548

Table 5.1: Measured values of the B-H-curve of a ferromagnetic material provided by Robert Bosch GmbH used to manufacture a PMSM.

References

[1] R. Adams and J. Fournier, *Sobolev Spaces*, Pure and Applied Mathematics, Elsevier, 2 ed., 2003.

[2] N. Allen and D. Rodger, *Description of team workshop problem 24: Nonlinear time-transient rotational test rig*, in Proc. of the TEAM Workshop in the 6th Round, 1996, pp. 57 – 60.

[3] A. Alonso Rodriguez and A. Valli, *Eddy Current Approximation of Maxwell Equations: Theory, Algorithms and Applications*, vol. 4, Springer Milano, 1 ed., 2014.

[4] P. Amestoy, A. Buttari, J.-Y. L'Excellent, and T. Mary, *Performance and scalability of the block low-rank multifrontal factorization on multicore architectures*, ACM Transactions on Mathematical Software, 45 (2019), pp. 2:1 – 2:26.

[5] P. Amestoy, I. S. Duff, J. Koster, and J.-Y. L'Excellent, *A fully asynchronous multifrontal solver using distributed dynamic scheduling*, SIAM Journal on Matrix Analysis and Applications, 23 (2001), pp. 15 – 41.

[6] R. Andreev, *Stability of sparse space–time finite element discretizations of linear parabolic evolution equations*, IMA Journal of Numerical Analysis, 33 (2012), pp. 242 – 260.

[7] F. Aràndiga, A. Baeza, and D. F. Yáñez, *Monotone cubic spline interpolation for functions with a strong gradient*, Applied Numerical Mathematics, 172 (2022), pp. 591 – 607.

[8] J. Argyris and D. Scharpf, *Finite elements in time and space*, Nuclear Engineering and Design, 10 (1969), pp. 456 – 464.

[9] A. Arkkio, *Analysis of Induction Motors Based on the Numerical Solution of the Magnetic Field and Circuit Equations: Dissertation*, Acta polytechnica Scandinavica: El, Finnish Acad. of Technic. Sciences, 1987.

[10] I. Babuška and A. K. Aziz, *The mathematical foundations of the finite element method with applications to partial differential equations*, Academic Press, New York, 1972.

[11] F. Bachinger, U. Langer, and J. Schöberl, *Numerical analysis of nonlinear multiharmonic eddy current problems*, Numerische Mathematik, 100 (2005), pp. 593 – 616.

[12] S. Badia, H. Dilip, and F. Verdugo, *Space-time unfitted finite element methods for time-dependent problems on moving domains*, Computers & Mathematics with Applications, 135 (2023), pp. 60 – 76.

[13] A. H. Baker, R. D. Falgout, T. V. Kolev, and U. M. Yang, *Multigrid smoothers for ultraparallel computing*, SIAM Journal on Scientific Computing, 33 (2011), pp. 2864 – 2887.

[14] S. Balay, W. D. Gropp, L. C. McInnes, and B. F. Smith, *Efficient management of parallelism in object oriented numerical software libraries*, in Modern Software Tools in Scientific Computing, E. Arge, A. M. Bruaset, and H. P. Langtangen, eds., Birkhäuser Press, 1997, pp. 163 – 202.

[15] J. Bastos and N. Sadowski, *Electromagnetic Modeling by Finite Element Methods*, Electrical and Computer Engineering, CRC Press, 2003.

[16] H. W. Beaty and J. L. Kirtley, *Electric Motor Handbook*, McGraw Hill Professional, 1 ed., 1998.

[17] T. Belytschko, W. Liu, B. Moran, and K. Elkhodary, *Nonlinear Finite Elements for Continua and Structures*, John Wiley & Sons, 2 ed., 2013.

[18] C. Bernardi, Y. Maday, and A. T. Patera, *Domain decomposition by the mortar element method*, in Asymptotic and Numerical Methods for Partial Differential Equations with Critical Parameters, H. G. Kaper, M. Garbey, and G. W. Pieper, eds., Springer Netherlands, Dordrecht, 1993, pp. 269 – 286.

[19] G. Bertotti, *Hysteresis in Magnetism: For Physicists, Materials Scientists, and Engineers*, Elsevier series in Electromagnetism, Elsevier Science, 1998.

[20] A. Binder, *Elektrische Maschinen und Antriebe*, Springer Berlin, Heidelberg, 1 ed., 2012.

[21] K. J. Binns, P. J. Lawrenson, and C. W. Trowbridge, *The Analytical and Numerical Solution of Electric and Magnetic Fields*, Wiley, 1993.

[22] D. Braess, *Finite Elemente: Theorie, schnelle Löser und Anwendungen in der Elastizitätstheorie*, Masterclass, Springer-Verlag Berlin Heidelberg, 5 ed., 2013.

[23] J. Brauer and F. Hirtenfelder, *Anisotropic materials in electromagnetic finite element analysis*, in 1991 International Conference on Computation in Electromagnetics, 1991, pp. 144 – 147.

[24] S. C. Brenner and L. R. Scott, *The Mathematical Theory of Finite Element Methods*, vol. 15 of Texts in Applied Mathematics, Springer New York, 3 ed., 2007.

[25] N. Burais and G. Grellet, *Numerical modelling of iron losses in ferromagnetic steel plate*, IEEE Transactions on Magnetics, 18 (1982), pp. 558 – 562.

[26] A. Cesarano, C. Dapogny, and P. Gangl, *Space-time shape optimization of rotating electric machines*, Mathematical Models and Methods in Applied Sciences, 34 (2024), pp. 2647 – 2708.

[27] J. Česenek and M. Feistauer, *Theory of the space-time discontinuous galerkin method for nonstationary parabolic problems with nonlinear convection and diffusion*, SIAM Journal on Numerical Analysis, 50 (2012), pp. 1181 – 1206.

[28] A. Chertov, *Units of Measurement of Physical Quantities. Translated by Scripta Technica, Inc*, Hayden Book Company, INC., 1964.

[29] P. Clément, *Approximation by finite element functions using local regularization*, R.A.I.R.O. Analyse Numérique, 9 (1975), pp. 77 – 84.

[30] COMSOL Multiphysics ™ v. 6.2. COMSOL AB, *AC/DC Module User's Guide*, 2023.

[31] R. Courant, *Variational methods for the solution of problems of equilibrium and vibrations*, Bulletin of the American Mathematical Society, 49 (1943), pp. 1 – 23.

[32] L. Dagum and R. Menon, *OpenMP: an industry standard api for shared-memory programming*, IEEE Computational Science and Engineering, 5 (1998), pp. 46 – 55.

[33] L. Dalcin and Y.-L. L. Fang, *mpi4py: Status update after 12 years of development*, Computing in Science & Engineering, 23 (2021), pp. 47 – 54.

[34] L. D. Dalcin, R. R. Paz, P. A. Kler, and A. Cosimo, *Parallel distributed computing using python*, Advances in Water Resources, 34 (2011), pp. 1124 – 1139. New Computational Methods and Software Tools.

[35] R. Dautray, A. Craig, M. Artola, M. Cessenat, J. Lions, and H. Lanchon, *Mathematical Analysis and Numerical Methods for Science and Technology: Volume 5 Evolution Problems I*, Mathematical Analysis and Numerical Methods for Science and Technology, Springer Berlin Heidelberg, 1999.

[36] L. Demkowicz, *Mathematical Theory of Finite Elements*, Computational Science and Engineering, Society for Industrial and Applied Mathematics, 2023.

[37] P. Deuflhard, *Newton Methods for Nonlinear Problems: Affine Invariance and Adaptive Algorithms*, vol. 35 of Springer Series in Computational Mathematics, Springer Berlin, Heidelberg, 1 ed., 2011.

[38] P. Deuflhard and F. Bornemann, *Numerische Mathematik II: Integration gewöhnlicher Differentialgleichungen*, De Gruyter Lehrbuch, Walter de Gruyter, 1994.

[39] M. Dobrowolski, *Angewandte Funktionalanalysis: Funktionalanalysis, Sobolev-Räume und elliptische Differentialgleichungen*, Masterclass, Springer Berlin Heidelberg, 2 ed., 2010.

[40] J. Donea, A. Huerta, J.-P. Ponthot, and A. Rodríguez-Ferran, *Arbitrary lagrangian–eulerian methods*, in Encyclopedia of Computational Mechanics, John Wiley & Sons, Ltd, 2004, ch. 14.

[41] C. Eck, H. Garcke, and P. Knabner, *Mathematische Modellierung*, Springer-Lehrbuch, Springer Spektrum Berlin, Heidelberg, 3 ed., 2017.

[42] H. Egger, M. Harutyunyan, R. Löscher, M. Merkel, and S. Schöps, *On torque computation in electric machine simulation by harmonic mortar methods*, Journal of Mathematics in Industry, 12 (2022).

[43] A. Einstein, *Zur elektrodynamik bewegter körper*, Annalen der Physik, 322 (1905), pp. 891 – 921.

[44] A. Ern and J.-L. Guermond, *Theory and Practice of Finite Elements*, vol. 159 of Applied Mathematical Sciences, Springer New York, 1 ed., 2004.

[45] L. Evans, *Partial Differential Equations*, vol. 19 of Graduate Studies in Mathematics, American Mathematical Society, 2 ed., 2010.

[46] R. D. Falgout and U. M. Yang, *hypre: A library of high performance preconditioners*, in Computational Science — ICCS 2002, P. M. A. Sloot, A. G. Hoekstra, C. J. K. Tan, and J. J. Dongarra, eds., Springer Berlin Heidelberg, 2002, pp. 632 – 641.

[47] Z. Ferkova, *Comparison between 2d and 3d modelling of induction machine using finite element method*, Advances in Electrical and Electronic Engineering, 13 (2015).

[48] A. E. Fitzgerald, J. Charles Kingsley, and S. D. Umans, *Electric Machinery*, McGraw-Hill, 6 ed., 2003.

[49] O. Forster, *Analysis 3: Maß- und Integrationstheorie, Integralsätze im $\mathbb{R}^n$ und Anwendungen*, Aufbaukurs Mathematik, Springer Spektrum Wiesbaden, 8 ed., 2017.

[50] V. François-Lavet, F. Henrotte, L. Stainier, L. Noels, and C. Geuzaine, *Vectorial incremental nonconservative consistent hysteresis model*, in Proceedings of the 5th International Conference on Advanded Computational Methods in Engineering (ACOMEN2011), 2011.

[51] E. Frank, *Free-form optimization of electric machines based on shape derivatives*, master's thesis, Johannes Kepler University Linz, 2010.

[52] F. N. Fritsch and R. E. Carlson, *Monotone piecewise cubic interpolation*, SIAM Journal on Numerical Analysis, 17 (1980), pp. 238 – 246.

[53] F. Frühauf, B. Gebauer, and O. Scherzer, *Detecting interfaces in a parabolic-elliptic problem from surface measurements*, SIAM Journal on Numerical Analysis, 45 (2007), pp. 810 – 836.

[54] E. Gabriel, G. E. Fagg, G. Bosilca, T. Angskun, J. J. Dongarra, J. M. Squyres, V. Sahay, P. Kambadur, B. Barrett, A. Lumsdaine, R. H. Castain, D. J. Daniel, R. L. Graham, and T. S. Woodall, *Open MPI: Goals, concept, and design of a next generation MPI implementation*, in Proceedings, 11th European PVM/MPI Users' Group Meeting, Budapest, 2004, pp. 97 – 104.

[55] M. J. Gander, *50 years of time parallel time integration*, in Multiple Shooting and Time Domain Decomposition Methods, T. Carraro, M. Geiger, S. Körkel, and R. Rannacher, eds., Cham, 2015, Springer International Publishing, pp. 69 – 113.

[56] M. J. Gander and M. Neumüller, *Analysis of a new space-time parallel multigrid algorithm for parabolic problems*, SIAM Journal on Scientific Computing, 38 (2016), pp. A2173 – A2208.

[57] P. Gangl, *Sensitivity-Based Topology and Shape Optimization with Application to Electrical Machines*, PhD thesis, Johannes Kepler University Linz, 2016.

[58] P. Gangl, S. Amstutz, and U. Langer, *Topology optimization of electric motor using topological derivative for nonlinear magnetostatics*, IEEE Transactions on Magnetics, 52 (2016), pp. 1 – 4.

[59] P. Gangl, M. Gobrial, and O. Steinbach, *A parallel space-time finite element method for the simulation of an electric motor*, in Domain Decomposition Methods in Science and Engineering XXVII, Z. Dostál, T. Kozubek, A. Klawonn, U. Langer, L. F. Pavarino, J. Šístek, and O. B. Widlund, eds., Springer Nature Switzerland, 2024, pp. 255 – 262.

[60] P. Gangl, M. Gobrial, and O. Steinbach, *A space-time finite element method for the eddy current approximation of rotating electric machines*, Computational Methods in Applied Mathematics, (2024).

[61] P. Gangl, S. Köthe, C. Mellak, A. Cesarano, and A. Mütze, *Multi-objective free-form shape optimization of a synchronous reluctance machine*, COMPEL - The international journal for computation and mathematics in electrical and electronic engineering, 41 (2022), pp. 1849 – 1864.

[62] P. Gangl and U. Langer, *Topology optimization of electric machines based on topological sensitivity analysis*, Computing and Visualization in Science, 15 (2012), pp. 345 – 354.

[63] P. Gangl, U. Langer, A. Laurain, H. Meftahi, and K. Sturm, *Shape optimization of an electric motor subject to nonlinear magnetostatics*, SIAM Journal on Scientific Computing, 37 (2015), pp. 1002 – 1025.

[64] C. Geuzaine and J.-F. Remacle, *Gmsh: A 3-d finite element mesh generator with built-in pre- and post-processing facilities*, International Journal for Numerical Methods in Engineering, 79 (2009), pp. 1309 – 1331.

[65] Z. Gmyrek, A. Boglietti, and A. Cavagnino, *Estimation of iron losses in induction motors: Calculation method, results, and analysis*, IEEE Transactions on Industrial Electronics, 57 (2010), pp. 161 – 171.

[66] W. Gropp, E. Lusk, and R. Thakur, *Using MPI-2: Advanced Features of the Message-Passing Interface*, The MIT Press, 1999.

[67] C. Grossmann, H.-G. Roos, and M. Stynes, *Numerical Treatment of Partial Differential Equations*, Universitext, Springer Berlin, Heidelberg, 1 ed., 2007.

[68] S. Gryś and M. Najgebauer, *An attempt of accuracy assessment of the hysteresis loop and power loss in magnetic materials during control measurements*, Measurement, 174 (2021), p. 108962.

[69] C. Hafner, *Numerische Berechnung elektromagnetischer Felder: Grundlagen, Methoden, Anwendungen*, Springer Berlin, Heidelberg, 1 ed., 1987.

[70] P. Hammond, *Applied Electromagnetism*, Pergamon Press Ltd., 1 ed., 1971.

[71] N. Hanappier, *Coupled electromagnetic-thermomechanical modeling of electric motors*, PhD thesis, Institut Polytechnique de Paris, 2021.

[72] P. Haupt, *Continuum Mechanics and Theory of Materials*, Advanced Texts in Physics, Springer Berlin, Heidelberg, 2 ed., 2002.

[73] B. Heise, *Analysis of a fully discrete finite element method for a nonlinear magnetic field problem*, SIAM Journal on Numerical Analysis, 31 (1994), pp. 745 – 759.

[74] F. Henrotte and K. Hameyer, *Computation of electromagnetic force densities: Maxwell stress tensor vs. virtual work principle* 1*, Journal of Computational and Applied Mathematics, 168 (2004), pp. 235 – 243.

[75] F. Henrotte, S. Steentjes, K. Hameyer, and C. Geuzaine, *Pragmatic two-step homogenisation technique for ferromagnetic laminated cores*, IET Science, Measurement & Technology, (2015), pp. 152 – 159.

[76] M. R. Hestenes and E. Stiefel, *Methods of conjugate gradients for solving linear systems*, Journal of research of the National Bureau of Standards, 49 (1952), pp. 409 – 435.

[77] J. Holley, *Stress-Constrained Topology Optimization with Application to the Design of Electrical Machines*, PhD thesis, Humboldt-Universität zu Berlin, Mathematisch-Naturwissenschaftliche Fakultät, 2023.

[78] A. Hughes, *Electric Motors and Drives: Fundamentals, Types and Applications*, Elsevier Ltd., 3 ed., 2006.

[79] N. Ida and J. P. A. Bastos, *Electromagnetics and Calculation of Fields (Lecture Notes in Statistics; 120)*, Springer New York, 2 ed., 1997.

[80] J. Jackson, *Classical Electrodynamics*, John Wiley, 3 ed., 1999.

[81] P. Jamet, *Galerkin-type approximations which are discontinuous in time for parabolic equations in a variable domain*, SIAM Journal on Numerical Analysis, 15 (1978), pp. 912 – 928.

[82] D. Jiles and D. Atherton, *Theory of ferromagnetic hysteresis*, Journal of Magnetism and Magnetic Materials, 61 (1986), pp. 48 – 60.

[83] M. Jung and U. Langer, *Methode der finiten Elemente für Ingenieure: Eine Einführung in die numerischen Grundlagen und Computersimulation*, Springer Vieweg Wiesbaden, 2 ed., 2013.

[84] B. Kaltenbacher, M. Kaltenbacher, and S. Reitzinger, *Identification of nonlinear B–H curves based on magnetic field computations and multigrid methods for ill-posed problems*, European Journal of Applied Mathematics, 14 (2003), pp. 15 – 38.

[85] M. Kaltenbacher, *Numerical Simulation of Mechatronic Sensors and Actuators*, Springer Berlin, Heidelberg, 3 ed., 2015.

[86] G. Karypis, *METIS and ParMETIS*, in Encyclopedia of Parallel Computing, D. Padua, ed., Springer US, Boston, MA, 2011, pp. 1117 – 1124.

[87] M. Kolmbauer, *The Multiharmonic Finite Element and Boundary Element Method for Simulation and Control of Eddy Current Problems*, PhD thesis, Johannes Kepler University Linz, 2012.

[88] D. Kopala, A. Ostaszewska-Liżewska, P. Råback, and R. Szewczyk, *Model of a 3d magnetic permeability tensor considering rotation and saturation states in materials with axial anisotropy*, Materials, 16 (2023).

[89] A. Kost, *Numerische Methoden in der Berechnung elektromagnetischer Felder*, Springer Berlin, Heidelberg, 1 ed., 1994.

[90] C. Köthe, *Pde-constrained shape optimization for coupled problems using space-time finite elements*, master's thesis, Graz University of Technology, 2020.

[91] C. Köthe, R. Löscher, and O. Steinbach, *Adaptive least-squares space-time finite element methods*. arXiv 2309.14300, 2023.

[92] F. Krall, *Analysis and implementation of algorithms for calculation of iron losses for fractional horsepower electric motors*, master's thesis, Graz University of Technology, 2017.

[93] L. Landau and E. Lifschitz, *Lehrbuch der theoretischen Physik: Klassiche Feldtheorie*, vol. 2, 12. überarbeitete Auflage, Akademie Verlag GmbH, Berlin, 1992.

[94] J. Lang, *Adaptive Multilevel Solution of Nonlinear Parabolic PDE Systems: Theory, Algorithm, and Applications*, vol. 16 of Lecture Notes in Computational Science and Engineering, Springer Berlin, Heidelberg, 1 ed., 2000.

[95] U. Langer and M. Neumüller, *Direct and iterative solvers*, in Computational Acoustics, M. Kaltenbacher, ed., Springer International Publishing, Cham, 2018, pp. 205 – 251.

[96] U. Langer and A. Schafelner, *Adaptive space-time finite element methods for non-autonomous parabolic problems with distributional sources*, Computational Methods in Applied Mathematics, 20 (2020), pp. 677 – 693.

[97] U. Langer, O. Steinbach, F. Tröltzsch, and H. Yang, *Unstructured space-time finite element methods for optimal control of parabolic equations*, SIAM Journal on Scientific Computing, 43 (2021), pp. A744 – A771.

[98] U. Langer, O. Steinbach, and H. Yang, *Robust space-time finite element methods for parabolic distributed optimal control problems with energy regularization*, Advances in Computational Mathematics, 50 (2024), pp. 24 – 50.

[99] L. P. Lebedev, I. I. Vorovich, and G. M. L. Gladwell, *Functional Analysis : Applications in Mechanics and Inverse Problems*, Solid Mechanics and its Applications, Springer Dordrecht, 2 ed., 2002.

[100] J. L. Lions, *Optimal Control of Systems Governed by Partial Differential Equations*, vol. 71 of Grundlehren der mathematischen Wissenschaften, Springer Berlin, Heidelberg, 1 ed., 1971.

[101] R. Löscher, *On unified frameworks for space-time optimal control and least squares problems*, PhD thesis, Graz University of Technology, 2023.

[102] C. Manni and P. Sablonnière, *Monotone interpolation of order 3 by C2 cubic splines*, IMA Journal of Numerical Analysis, 17 (1997), pp. 305 – 320.

[103] D. Marcsa and M. Kuczmann, *Comparison of the A^*-A and $T,\phi-\phi$ formulations for the 2-d analysis of solid-rotor induction machines*, Magnetics, IEEE Transactions on, 45 (2009), pp. 3329 – 3333.

[104] J. C. Maxwell, *A Treatise on Electricity and Magnetism*, vol. 1 of Cambridge Library Collection - Physical Sciences, Cambridge University Press, 1873.

[105] I. D. Mayergoyz, *Mathematical Models of Hysteresis and Their Applications*, Elsevier series in Electromagnetism, Elsevier, 1 ed., 2003.

[106] M. Merkel, P. Gangl, and S. Schöps, *Shape optimization of rotating electric machines using isogeometric analysis*, IEEE Transactions on Energy Conversion, 36 (2021), pp. 2683 – 2690.

[107] N. Meyers and J. Serrin, *$H = W.$*, Proceedings of the National Academy of Sciences of the United States of America, 51 (1964), pp. 1055 – 1056.

[108] N. Moës, J. Dolbow, and T. Belytschko, *A finite element method for crack growth without remeshing*, International Journal for Numerical Methods in Engineering, 46 (1999), pp. 131 – 150.

[109] C. Mollet, *Stability of Petrov-Galerkin discretizations: Application to the space-time weak formulation for parabolic evolution problems*, Computational Methods in Applied Mathematics, 14 (2014), pp. 231 – 255.

[110] Y. Mollet, J. J. C. Gyselinck, and R. V. Sabariego, *Influence of 2d and 3d meshes in fe computation of eddy-current losses in surface PMSMs*, 2017 International Conference on Optimization of Electrical and Electronic Equipment (OPTIM) & 2017 Intl Aegean Conference on Electrical Machines and Power Electronics (ACEMP), (2017), pp. 442 – 449.

[111] P. Monk, *Finite Element Methods for Maxwell's Equations*, Numerical Mathematics and Scientific Computation, Clarendon Press, 2003.

[112] F. Müller, G. Bavendiek, B. Schauerte, and K. Hameyer, *Measurement and simulation of a rotational single sheet tester*, Archives of Electrical Engineering, 68 (2019), pp. 173 – 183.

[113] S. Naik, B. Bag, and K. Chandrasekaran, *A 2d and 3d analysis on electromagnetic parameters of spoke-shape interior permanent magnet synchronous motor using FEM*, Periodica Polytechnica Electrical Engineering and Computer Science, 67 (2023), pp. 181 – 193.

[114] J. Nečas, *Sur une méthode pour résoudre les équations aux dérivées partielles du type elliptique, voisine de la variationnelle*, Annali della Scuola Normale Superiore di Pisa - Scienze Fisiche e Matematiche, 3e série, 16 (1962), pp. 305 – 326.

[115] M. Neumüller and E. Karabelas, *Generating admissible space-time meshes for moving domains in (d + 1) dimensions*, in Space-Time Methods: Applications to Partial Differential Equations, U. Langer and O. Steinbach, eds., De Gruyter, Berlin, Boston, 2019, ch. 6, pp. 185 – 206.

[116] M. Neumüller and O. Steinbach, *Refinement of flexible space-time finite element meshes and discontinuous galerkin methods*, Computing and Visualization in Science, 14 (2011), pp. 189 – 205.

[117] B. W. Ong and J. B. Schroder, *Applications of time parallelization*, Computing and Visualization in Science, 23 (2020).

[118] M. C. Pechlivanidou, I. D. Chasiotis, and Y. L. Karnavas, *A comparative study on 2d and 3d magnetic field analysis of permanent magnet synchronous motor using FEM simulations*, Journal of Electromagnetic Waves and Applications, 33 (2019), pp. 2215 – 2241.

[119] C. Pechstein, *Multigrid-Newton-methods for nonlinear magnetostatic problems*, master's thesis, Johannes Kepler University Linz, 2004.

[120] C. Pechstein and B. Jüttler, *Monotonicity-preserving interproximation of B–H-curves*, Journal of Computational and Applied Mathematics, 196 (2006), pp. 45–57.

[121] H. Prautzsch, W. Boehm, and M. Paluszny, *Bézier and B-Spline Techniques*, Mathematics and Visualization, Springer Berlin, Heidelberg, 1 ed., 2002.

[122] F. Preisach, *Über die magnetische Nachwirkung*, Zeitschrift für Physik, 94 (1935), pp. 277 – 302.

[123] F. Purnode, F. Henrotte, G. Louppe, and C. Geuzaine, *Neural network-based simulation of fields and losses in electrical machines with ferromagnetic laminated cores*, International Journal of Numerical Modelling: Electronic Networks, Devices and Fields, 37 (2024).

[124] P. Putek, P. Paplicki, and R. Palka, *Topology optimization of rotor poles in a permanent-magnet machine using level set method and continuum design sensitivity analysis*, COMPEL - The international journal for computation and mathematics in electrical and electronic engineering, 33 (2014).

[125] A. Quarteroni and A. Valli, *Theory and application of Steklov-Poincaré operators for boundary-value problems*, in Applied and Industrial Mathematics: Mathematics and Its Applications, R. Spigler, ed., vol. 56, Springer Netherlands, Dordrecht, 1991, pp. 179 – 203.

[126] A. Quarteroni and A. Valli, *Domain Decomposition Methods for Partial Differential Equations*, Oxford University Press, 1999.

[127] M. Rogowski, S. Aseeri, D. Keyes, and L. Dalcin, *mpi4py.futures: MPI-based asynchronous task execution for python*, IEEE Transactions on Parallel and Distributed Systems, 34 (2023), pp. 611 – 622.

[128] E. Rothe, *Zweidimensionale parabolische Randwertaufgaben als Grenzfall eindimensionaler Randwertaufgaben*, Mathematische Annalen, 102 (1930), pp. 650 – 670.

[129] J. W. Ruge and K. Stüben, *4. algebraic multigrid*, in Multigrid Methods, S. F. McCormick, ed., vol. 3 of Frontiers in Applied Mathematics, SIAM, Philadelphia, 1987, pp. 73 – 130.

[130] Y. Saad, *Iterative Methods for Sparse Linear Systems*, Society for Industrial and Applied Mathematics, 2 ed., 2003.

[131] Y. Saad and M. H. Schultz, *GMRES: A generalized minimal residual algorithm for solving nonsymmetric linear systems*, SIAM Journal on Scientific and Statistical Computing, 7 (1986), pp. 856 – 869.

[132] N. Sadowski, Y. Lefevre, M. Lajoie-Mazenc, and J. Cros, *Finite element torque calculation in electrical machines while considering the movement*, Magnetics, IEEE Transactions on, 28 (1992), pp. 1410 – 1413.

[133] R. Schaback and H. Wendland, *Numerische Mathematik*, Springer-Lehrbuch, Springer Berlin, Heidelberg, 5 ed., 2005.

[134] A. Schafelner, *Space-time Finite Element Methods*, PhD thesis, Johannes Kepler University Linz, 2021.

[135] O. Schenk and K. Gärtner, *PARDISO*, in Encyclopedia of Parallel Computing, D. Padua, ed., Springer US, Boston, MA, 2011, pp. 1458 – 1464.

[136] W. Schiesser, *The Numerical Method of Lines: Integration of Partial Differential Equations*, Elsevier Science, 1991.

[137] J. Schöberl, *C++11 implementation of finite elements in NGSolve*, Tech. Report 30, Institute of Analysis and Scientific Computing, TU Vienna, 2014.

[138] C. Schwab and R. Stevenson, *Space-time adaptive wavelet methods for parabolic evolution problems*, Mathematics of Computation, 78 (2009), pp. 1293 – 1318.

[139] L. R. Scott and S. Zhang, *Finite element interpolation of nonsmooth functions satisfying boundary conditions*, Mathematics of Computation, 54 (1990), pp. 483 – 493.

[140] R. Smirnov-Rueda, *On two complementary types of total time derivative in classical field theories and Maxwell's equations*, Foundations of Physics, 35 (2005), pp. 1695 – 1723.

[141] B. Smith, P. Bjorstad, and W. Gropp, *Domain Decomposition: Parallel Multilevel Methods for Elliptic Partial Differential Equations*, Cambridge University Press, 2004.

[142] C. W. Steele, *Numerical Computation of Electric and Magnetic Fields*, Springer New York, 1 ed., 1998.

[143] O. Steinbach, *Numerical Approximation Methods for Elliptic Boundary Value Problems: Finite and Boundary Elements*, Springer New York, 1 ed., 2007.

[144] O. Steinbach, *Space-time finite element methods for parabolic problems*, Computational Methods in Applied Mathematics, 15 (2015), pp. 551 – 566.

[145] O. Steinbach and H. Yang, *An algebraic multigrid method for an adaptive space-time finite element discretization*, in Large-Scale Scientific Computing, I. Lirkov and S. Margenov, eds., Cham, 2018, Springer International Publishing, pp. 66 – 73.

[146] O. Steinbach and H. Yang, *Comparison of algebraic multigrid methods for an adaptive space-time finite-element discretization of the heat equation in 3d and 4d*, Numerical Linear Algebra with Applications, 25 (2018), p. e2143.

[147] O. Steinbach and H. Yang, *Space-time finite element methods for parabolic evolution equations: discretization, a posteriori error estimation, adaptivity and*

solution, in Space-Time Methods: Applications to Partial Differential Equations, U. Langer and O. Steinbach, eds., De Gruyter, Berlin, 2019, ch. 7, pp. 207 – 248.

[148] O. Steinbach and M. Zank, *Coercive space-time finite element methods for initial boundary value problems*, Electronic Transactions on Numerical Analysis, 52 (2020), pp. 154 – 194.

[149] V. Thomée, *Galerkin Finite Element Methods for Parabolic Problems*, vol. 25 of Springer Series in Computational Mathematics, Springer Berlin, Heidelberg, 2 ed., 2006.

[150] M.-A. Tonnelat, *The Principles of Electromagnetic Theory and of Relativity*, Springer Dordrecht, 1 ed., 1966.

[151] A. Toselli and O. Widlund, *Domain Decomposition Methods—Algorithms and Theory*, vol. 34 of Springer Series in Computational Mathematics, Springer-Verlag, Berlin, 2005.

[152] I. Toulopoulos, *Numerical solutions of quasilinear parabolic problems by a continuous space-time finite element scheme*, SIAM Journal on Scientific Computing, 44 (2022), pp. A2944 – A2973.

[153] K. Urban and A. T. Patera, *An improved error bound for reduced basis approximation of linear parabolic problems*, Mathematics of Computation, 83 (2014), pp. 1599 – 1615.

[154] J. Van Bladel, *Electromagnetic Fields*, IEEE Press Series on Electromagnetic Wave Theory, Wiley, 2 ed., 2007.

[155] J. Van Bladel, *Relativity and Engineering*, Springer Series in Electronics and Photonics, Springer Berlin, Heidelberg, 1 ed., 2012.

[156] U. van Rienen, *Numerical Methods in Computational Electrodynamics: Linear Systems in Practical Applications*, Lecture Notes in Computational Science and Engineering, Springer Berlin, Heidelberg, 1 ed., 2000.

[157] A. Visintin, *Differential Models of Hysteresis*, Applied Mathematical Sciences, Springer Berlin, Heidelberg, 1 ed., 1994.

[158] Z. L. Wang, *The expanded maxwell's equations for a mechano-driven media system that moves with acceleration*, International Journal of Modern Physics B, 37 (2023), p. 2350159.

[159] T. Wildi, *Electrical Machines, Drives, and Power Systems*, Pearson Education, Inc., Upper Saddle River, 5 ed., 2002.

[160] S. Willerich, *Anwendung vektorieller Hysteresemodelle zur Charakterisierung ferromagnetischer Werkstoffe*, PhD thesis, Technical University Munich, 2021.

[161] J. Wloka, *Partielle Differentialgleichungen: Sobolevräume und Randwertaufgaben*, Mathematische Leitfäden, Vieweg+Teubner Verlag, 1982.

[162] X. Xiao, *Efficient vector hysteresis model for anisotropic ferromagnetic materials: a physical, thermodynamic approach*, vol. 58 of Aachener Schriftenreihe zur Elektromagnetischen Energiewandlung, Shaker Verlag, Düren, 2024.

[163] X. Xiao, F. Müller, G. Bavendiek, and K. Hameyer, *Analysis of vector hysteresis models in comparison to anhysteretic magnetization model*, Eur. Phys. J. Appl. Phys., 91 (2020).

[164] S. Zaglmayr, *High Order Finite Element Methods for Electromagnetic Field Computation*, PhD thesis, Johannes Kepler University Linz, 2006.

[165] M. Zank, *Inf-Sup Stable Space-Time Methods for Time-Dependent Partial Differential Equations*, vol. 36 of Monographic Series TU Graz / Computation in Engineering and Science, Verlag der Technischen Universität Graz, 2020.

[166] E. Zeidler, *Nonlinear Functional Analysis and Its Applications: II/ A: Linear Monotone Operators*, Springer New York, 1 ed., 1990.

[167] E. Zeidler, *Nonlinear Functional Analysis and Its Applications: II/ B: Nonlinear Monotone Operators*, Springer New York, 1 ed., 1990.

[168] S. Zhu, J. Lu, F. Zeng, and Z. Chu, *A method for measuring saturated B–H curves of silicon steel sheets*, in 2023 26th International Conference on Electrical Machines and Systems (ICEMS), 2023, pp. 1740 – 1745.

Monographic Series TU Graz
Computation in Engineering and Science

Vol. 1 Steffen Alvermann
Effective Viscoelastic Behavior of Cellular Auxetic Materials
2008
ISBN 978-3-902465-92-4

Vol. 2 Sendy Fransiscus Tantono
The Mechanical Behaviour of a Soilbag
under Vertical Compression
2008
ISBN 978-3-902465-97-9

Vol. 3 Thomas Rüberg
Non-conforming FEM/BEM Coupling in Time Domain
2008
ISBN 978-3-902465-98-6

Vol. 4 Dimitrios E. Kiousis
Biomechanical and Computational Modeling
of Atherosclerotic Arteries
2008
ISBN 978-3-85125-023-7

Vol. 5 Lars Kielhorn
A Time-Domain Symmetric Galerkin BEM
for Viscoelastodynamics
2009
ISBN 978-3-85125-042-8

Monographic Series TU Graz
Computation in Engineering and Science

Vol. 6 Gerhard Unger
Analysis of Boundary Element Methods for Laplacian Eigenvalue Problems
2009
ISBN 978-3-85125-081-7

Vol. 7 Gerhard Sommer
Mechanical Properties of Healthy and Diseased Human Arteries
2010
ISBN 978-3-85125-111-1

Vol. 8 Mathias Nenning
Infinite Elements for Elasto- and Poroelastodynamics
2010
ISBN 978-3-85125-130-2

Vol. 9 Thanh Xuan Phan
Boundary Element Methods for Boundary Control Problems
2011
ISBN 978-3-85125-149-4

Vol. 10 Loris Nagler
Simulation of Sound Transmission through Poroelastic Plate-like Structures
2011
ISBN 978-3-85125-153-1

Monographic Series TU Graz
Computation in Engineering and Science

Vol. 11 Markus Windisch
Boundary Element Tearing and Interconnecting Methods for Acoustic and Electromagnetic Scattering
2011
ISBN 978-3-85125-152-4

Vol. 12 Christian Walchshofer
Analysis of the Dynamics at the Base of a Lifted Strongly Buoyant Jet Flame Using Direct Numerical Simulation
2011
ISBN 978-3-85125-185-2

Vol. 13 Matthias Messner
Fast Boundary Element Methods in Acoustics
2012
ISBN 978-3-85125-202-6

Vol. 14 Peter Urthaler
Analysis of Boundary Element Methods for Wave Propagation in Porous Media
2012
ISBN 978-3-85125-216-3

Vol. 15 Peng Li
Boundary Element Method for Wave Propagation in Partially Saturated Poroelastic Continua
2012
ISBN 978-3-85125-236-1

Monographic Series TU Graz
Computation in Engineering and Science

Vol. 16 Andreas Jörg Schriefl
Quantification of Collagen Fiber Morphologies in Human Arterial Walls
2013
ISBN 978-3-85125-238-5

Vol. 17 Thomas S. E. Eriksson
Cardiovascular Mechanics
2013
ISBN 978-3-85125-277-4

Vol. 18 Jianhua Tong
Biomechanics of Abdominal Aortic Aneurysms
2013
ISBN 978-3-85125-279-8

Vol. 19 Jonathan Rohleder
Titchmarsh–Weyl Theory and Inverse Problems for Elliptic Differential Operators
2013
ISBN 978-3-85125-283-5

Vol. 20 Martin Neumüller
Space-Time Methods
2013
ISBN 978-3-85125-290-3

Monographic Series TU Graz
Computation in Engineering and Science

Vol. 21 Michael J. Unterberger
Microstructurally-Motivated Constitutive Modeling of Cross-Linked Filamentous Actin Networks
2013
ISBN 978-3-85125-303-0

Vol. 22 Vladimir Lotoreichik
Singular Values and Trace Formulae for Resolvent Power Differences of Self-Adjoint Elliptic Operators
2013
ISBN 978-3-85125-304-7

Vol. 23 Michael Meßner
A Fast Multipole Galerkin Boundary Element Method for the Transient Heat Equation
2014
ISBN 978-3-85125-350-4

Vol. 24 Lorenz Johannes John
Optimal Boundary Control in Energy Spaces
2014
ISBN 978-3-85125-373-3

Vol. 25 Hannah Weisbecker
Softening and Damage Behavior of Human Arteries
2014
ISBN 978-3-85125-370-2

Monographic Series TU Graz
Computation in Engineering and Science

Vol. 26 Bernhard Kager
Efficient Convolution Quadrature based Boundary Element Formulation for Time-Domain Elastodynamics
2015
ISBN 978-3-85125-382-5

Vol. 27 Christoph M. Augustin
Classical and All-floating FETI Methods with Applications to Biomechanical Models
2015
ISBN 978-3-85125-418-1

Vol. 28 Elias Karabelas
Space-Time Discontinuous Galerkin Methods for Cardiac Electromechanics
2016
ISBN 978-3-85125-461-7

Vol. 29 Thomas Traub
A Kernel Interpolation Based Fast Multipole Method for Elastodynamic Problems
2016
ISBN 978-3-85125-465-5

Vol. 30 Matthias Gsell
Mortar Domain Decomposition Methods for Quasilinear Problems and Applications
2017
ISBN 978-3-85125-522-5

Monographic Series TU Graz
Computation in Engineering and Science

Vol. 31 Christian Kühn
Schrödinger operators and singular infinite rank perturbations
2017
ISBN 978-3-85125-551-5

Vol. 32 Michael H. Gfrerer
Vibro-Acoustic Simulation of Poroelastic Shell Structures
2018
ISBN 978-3-85125-573-7

Vol. 33 Markus Holzmann
Spectral Analysis of Transmission and Boundary Value Problems for Dirac Operators
2018
ISBN 978-3-85125-642-0

Vol. 34 Osman Gültekin
Computational Inelasticity of Fibrous Biological Tissues with a Focus on Viscoelasticity, Damage and Rupture
2019
ISBN 978-3-85125-655-0

Vol. 35 Justyna Anna Niestrawska
Experimental and Computational Analyses of Pathological Soft Tissues – Towards a Better Understanding of the Pathogenesis of AAA
2019
ISBN 978-3-85125-678-9

Monographic Series TU Graz
Computation in Engineering and Science

Vol. 36 Marco Zank
Inf-Sup Stable Space-Time Methods for Time-Dependent Partial Differential Equations
2020
ISBN 978-3-85125-721-2

Vol. 37 Christoph Irrenfried
Convective turbulent near wall heat transfer at high Prandtl numbers
2020
ISBN 978-3-85125-724-3

Vol. 38 Christopher Albert
Hamiltonian Theory of Resonant Transport Regimes in Tokamaks with Perturbed Axisymmetry
2020
ISBN 978-3-85125-746-5

Vol. 39 Daniel Christopher Haspinger
Material Modeling and Simulation of Phenomena at the Nano, Micro and Macro Levels in Fibrous Soft Tissues of the Cardiovascular System
2021
ISBN 978-3-85125-802-8

Vol. 40 Markus Alfons Geith
Percutaneous Coronary Intervention
2021
ISBN 978-3-85125-801-1

Monographic Series TU Graz
Computation in Engineering and Science

Vol. 41 Dominik Pölz
Space-Time Boundary Elements for Retarded Potential Integral Equations
2021
ISBN 978-3-85125-811-0

Vol. 42 Douglas Ramalho Queiroz Pacheco
Stable and stabilised finite element methods for incompressible flows of generalised Newtonian fluids
2021
ISBN 978-3-85125-856-1

Vol. 43 Peter Schlosser
Superoscillations and their Schrödinger time evolution
2022
ISBN 978-3-85125-930-8

Vol. 44 Raphael Watschinger
Fast space-time boundary element methods for the heat equation
2023
ISBN 978-3-85125-949-0

Vol. 45 Ishan Gupta
Modelling Growth and Formation of Thrombus: A Multiphasic Approach
2023
ISBN 978-3-85125-964-3

Monographic Series TU Graz
Computation in Engineering and Science

Vol. 46 Mario Gobrial

Space-time Finite Element Methods

for the Eddy Current Problem and Applications

2025

ISBN 978-3-99161-048-9

Space-time Finite Element Methods
for the Eddy Current Problem and Applications

We formulate and analyze space-time finite element methods for the numerical simulation of the eddy current approximation in Bochner spaces. First, we examine the resulting elliptic-parabolic interface problem posed on electrically conducting and non-conducting stationary regions, providing the analysis of the unique solvability for the linear and nonlinear case. Furthermore, we address hysteresis effects in ferromagnetic materials by proposing a space-time finite element method tailored to a specific hysteretic material law. The investigation extends to moving bodies, analyzing the corresponding elliptic-parabolic interface problem. The Petrov-Galerkin space-time finite element discretization is formulated on completely unstructured decompositions of the space-time cylinder into simplicial elements, which allows for an adaptive resolution of the solution both in space and time. However, it requires the solution of the overall system of algebraic equations. While the use of parallel solution algorithms seems to be mandatory, this method also allows for a parallelization in space and time simultaneously. The numerical experiments confirm related a priori error estimates and demonstrate the applicability and accuracy of the proposed approach applied to realistic problems.

MONOGRAPHIC SERIES TU GRAZ
COMPUTATION IN ENGINEERING AND SCIENCE

Verlag der Technischen Universität Graz
www.tugraz-verlag.at

ISBN 978-3-99161-048-9
ISSN 1990-357X

ISBN 978-3-99161-048-9
9 783991 610489